This is to certify that the
thesis entitled

ORDER-TUNED VIBRATION ABSORBERS FOR SYSTEMS WITH CYCLIC SYMMETRY WITH APPLICATIONS TO TURBOMACHINERY

presented by

BRIAN JOHN OLSON

has been accepted towards fulfillment
of the requirements for the

PH.D. degree in MECHANICAL ENGINEERING

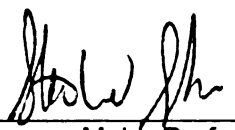

Major Professor's Signature

9/27/06

Date

ORDER-TUNED VIBRATION ABSORBERS FOR SYSTEMS WITH CYCLIC SYMMETRY WITH APPLICATIONS TO TURBOMACHINERY

By

Brian John Olson

A DISSERTATION

Submitted to
Michigan State University
in partial fulfillment of the requirements
for the degree of

DOCTOR OF PHILOSOPHY

Department of Mechanical Engineering

2006

ABSTRACT

ORDER-TUNED VIBRATION ABSORBERS FOR SYSTEMS WITH CYCLIC SYMMETRY WITH APPLICATIONS TO TURBOMACHINERY

By

Brian John Olson

This work investigates the performance of centrifugally-driven, order-tuned absorbers for vibration reduction in a class of systems with cyclic symmetry. The rotating flexible structures of interest are bladed disk assemblies, such as the fans, compressors and turbines in a jet engine, which consist of a nominally cyclic array of interconnected substructures. Under steady operation, these assemblies rotate at a constant speed and are subjected to traveling wave dynamic loading (the so-called engine order excitation), which is characterized by excitation frequencies that are proportional to the mean rotational speed of the rotor. Such excitations result in component vibrations and can lead to high cycle fatigue failure, noise, reduced performance, and other undesirable effects. Since order-tuned absorbers feature natural frequencies that scale directly with the rotor speed, they are ideally suited to address these vibrations. However, at the time of writing, there has been no systematic analytical treatment of absorber systems applied to cyclic rotating flexible structures under engine order excitation. This thesis reports the first such study.

The aim of this investigation is threefold: to quantify and understand the underlying linear resonance structure of a cyclically-coupled bladed disk assembly fitted with order-tuned absorbers; based on these findings, to design the absorbers to eliminate or otherwise reduce blade motions relative to the rotating hub; and to generalize the linear theory, methodology, and design to include the basic, first-order effects of nonlinearity.

The analysis is carried out assuming identical, identically-coupled substructures, which gives rise to a linearized model with block circulant matrices. A standard change of coordinates based on this cyclic structure essentially decouples the governing equations, and it gives rise to closed form expressions from which analytical results can be gleaned. The linear resonance structure is found to be surprisingly rich, a feature that arises from the order-nature of the absorbers. One of the main findings of the linear analysis, and indeed of this entire thesis, is the existence of a "no-resonance zone," that is, an entire spectrum of absorber designs for which there are no system resonances over the full range of possible rotor speeds. By designing the absorbers within this small, but finite spectrum, system resonances are avoided altogether and there is at least some level of robustness to parameter uncertainties.

In the presence of weak nonlinearity, which is introduced via the absorber path geometry, the underlying linear resonance structure is shown to qualitatively persist—including the no-resonance zone—provided that the excitation strength is sufficiently small. There does exist a nonlinear design strategy in which relative blade motions can be eliminated completely, but it depends on both the rotor speed and force amplitude. The design is thus effective for only a *single* set of operating conditions, which suggests that nonlinearity cannot be exploited to further improve absorber performance in the systems of interest. When nonlinearity cannot be avoided it is shown that softening characteristics are more desirable than hardening; the former simply sets an upper limit on the range of speeds over which the absorbers are effective while the latter may give rise to problematic resonances. Finally, for the weakly coupled and lightly damped systems under consideration, there may be a host of symmetry-breaking instabilities involving the desired traveling wave response. However, none could be identified. This is a very promising finding since bifurcations of this kind are highly undesirable from an applications viewpoint.

To my wife, Julie, my parents, and to the countless people who have supported me during this effort.

The theory of matrices exhibits much that is visually attractive. Thus, diagonal matrices, symmetric matrices, $(0,1)$ *matrices, and the like are attractive independently of their applications. In the same category are the circulants.*

– Philip J. Davis

ACKNOWLEDGMENTS

This thesis symbolizes the entirety of my journey in higher education, which has spanned over thirteen years of efforts and sacrifice, successes and failures, and uncountable life lessons. In bringing these pages to closure I can identify with a letter to Robert Hooke in February of 1676, in which Sir Isaac Newton wrote:

> "*If I have been able to see further, it was only because I stood on the shoulders of giants.*"

This effort would not have been possible without the encouragement and support of many individuals, to whom the following acknowledgments are dedicated.

First and foremost I wish to acknowledge my wife, Julie, for her continual patience, understanding and encouragement, my parents, whose support has been seemingly without bound, and my brother, Gregg, with whom I have enjoyed countless hours of engaging conversation.

I am particularly indebted to my advisor, colleague and friend, Steve Shaw, who has offered much guidance, insight and wisdom. It has been an absolute pleasure to know and work with him. Thanks are also due to my doctoral committee members Christophe Pierre (and also Matt Castanier), Alan Haddow, Brian Feeny, Cevat Gokcek, and Hassan Khalil.

To my esteemed colleagues—Jeff Rhoads, Pat Staron, Umar Farooq, Nyesunthi (Polarit) Apiwattanalunggarn, Gábor Csernák, and many more—your friendship and camaraderie have truly enriched my years as a student. I wish also to thank Richard Cohn and Jim Schramski.

In addition to my doctoral committee members, there have been many faculty and staff at Michigan State University to whom I owe many thanks: Craig Somerton, Manoochehr Koochesfahani, Ronald Rosenberg, Carol Bishop, Gaile Griffore, Craig Gunn, Aida Montalvo, Elaine Bailey, and Lindsay Niesen. I am grateful to the

many dedicated instructors at Northwestern Michigan College, including Jim "Chief Tormentor" Coughlin, Ken "Papa Bear" Stepnitz, Tony Jenkins, Steve Drake, and Ernie East, whose support and encouragement was pivotal in my early years as a student. Thanks also to Gábor Stépán from the Budapest University of Technology and Economics.

Finally, this work was supported by grant CMS-0408866 from the National Science Foundation. I would also like to thank Donald E. Knuth for creating the TEX system for typesetting [1], Leslie Lamport for extending this system to LATEX [2], and the many contributors to the LATEX 2_ε implementation, which was used to typeset this dissertation. I would not have had the patience to typeset this work using a WYSIWYG package.

TABLE OF CONTENTS

LIST OF TABLES

LIST OF FIGURES

SELECTED LIST OF OPERATORS

Relevant page numbers are given in the parentheses.

$\cdot$	Inner/dot product
$\oplus$	Direct sum (175)
$\otimes$	Direct/Kronecker product (176)
$\|\| \cdot \|\|$	Norm
$(\cdot)!$	Factorial
$\bar{(\cdot)}$	Complex conjugate
$(\cdot)^T$	Transpose
$(\cdot)^{\mathcal{H}} = \bar{(\cdot)}^T$	Conjugate/Hermitian transpose
$(\cdot)^{-1}$	Inverse
$\dot{(\cdot)} = \frac{d(\cdot)}{dt}$	Differentiation with respect to physical time t
$(\cdot)' = \frac{d(\cdot)}{d\tau}$	Differentiation with respect to dimensionless time τ
$\lambda(\cdot)$	Matrix spectrum
$\mathrm{circ}(\cdot)$	Circulant operator (13, 184)
$\mathrm{diag}(\cdot)$	Diagonal operator (176)
$\det(\cdot)$	Determinant
$\mathrm{Im}(\cdot)$	Imaginary part
$\log(\cdot)$	Logarithmic function to the base 10
$\mathrm{mod}(\cdot)$	Modulo
$\mathrm{Re}(\cdot)$	Real part
$\mathrm{tr}(\cdot)$	Trace

CHAPTER 1

Introduction

1.1 Motivation

The goal of this work is to investigate the performance of order-tuned absorbers for vibration reduction in (nearly) cyclic systems. The applications of interest are rotating flexible structures, and in particular turbine blades, bladed disks assemblies, blisks (integral disk/blade systems), and helicopter rotor blades. During steady operation these systems rotate at a constant speed and are subjected to traveling wave dynamic loading, which is characterized by excitation frequencies that are proportional to the mean rotational speed of the rotor. Such excitations result in component vibrations and can lead to high cycle fatigue (HCF) failure, noise, reduced performance, and other undesirable effects. This is an ideal setting for the use of centrifugally-driven, order-tuned vibration absorbers, yet their implementation to such systems has received little attention to date. Much is already known about the dynamic behavior of systems of vibration absorbers, and the same is true for systems with symmetries in general and for rotating flexible structures in particular. This work aims to apply the theory, methodology, and design of order-tuned absorbers to such systems.

We begin with a brief survey of order-tuned vibration absorbers in Section 1.2 and of systems with cyclic symmetry in Section 1.3. The application of vibration absorbers to rotating flexible structures is discussed in Section 1.4 and the chapter

closes in Section 1.5 with the main objectives and contributions of this work and an outline of the dissertation.

1.2 Order-Tuned Vibration Absorbers

Vibration absorbers were originally proposed by Frahm [4] in a United States patent in 1911, but it was Den Hartog [5, 6] who first carried out systematic studies on their characteristics and design, including an optimal choice of design parameters. They come in two basic varieties: *frequency-tuned* and *order-tuned*. In the former, the absorber is tuned to a given problematic frequency (typically near a resonance) and damping is added so that it performs effectively in the neighborhood of that frequency. Such absorbers rely on elastic elements to provide their restoring forces, and they are designed so that these forces counter the translational or rotational motion of the primary systems to which they are attached. In contrast, *order-tuned* vibration absorbers exploit the centrifugal field from rotation of the primary system [7, 8]. Since rotating flexible structures are dominated by forces that occur at orders of rotation (the so-called *traveling wave* or *engine order* excitations [9]), order-tuned absorbers are ideally suited for such applications.

A class of order-tuned absorbers that has enjoyed considerable attention in recent decades are centrifugal pendulum vibration absorbers, or CPVAs. They essentially consist of mass particles that ride along designer-specified paths relative to the primary system and their parameters are chosen such that they counteract the fluctuating loads applied to that system. Each employs the centrifugal field from rotation (rather than an elastic element) for its restoring force and this results in absorber natural frequencies that are proportional to the rotation rate, where the constant of proportionality is dictated by geometric parameters that are chosen by design. The selection of the absorber path shape and location relative to the center of rotation of the primary system prescribes its linear tuning order, as well as its nonlinear response

characteristics.

The dynamic performance, characteristics, and features of CPVAs are well-understood in typical situations, and there are numerous examples of their implementation. For example, they are widely-used for reducing torsional vibrations in rotating machinery, where they are attached directly to the rotor. CPVAs have been used in light aircraft engines [10] and helicopter rotors [11], and they are also finding new applications including diesel camshafts [12] and variable displacement automobile engines [13]. In nearly all applications, CPVAs employ circular paths due to the simplicity of their manufacture and also due to a lack of knowledge about noncircular paths.

Den Hartog described the basic features of CPVAs, including how one selects parameters for linear tuning, as well as a discussion of the frequency shifting that arises from nonlinear softening effects in circular-path absorbers (that is, the decrease in frequency as the amplitude of oscillation increases) [7]. He also suggested intentionally detuning (in fact, overtuning) the absorbers to avoid the jump instabilities associated with these nonlinear effects. This approach works well, but it comes at the expense of reduced absorber performance [14]. Newland carried out a systematic analysis of the nonlinear response of a CPVA and offered a strategy for selecting an appropriate level of detuning for circular path absorbers [15]. Extensive linear-based design guidelines exist for CPVAs applied to crankshafts of internal combustion engines [10].

Subsequent research on CPVAs focused on several issues, including the design of the absorber path for optimal performance and the response of CPVA systems composed of several absorbers fitted to a rotor. Research on CPVA paths begins with the analysis of Madden who suggested that a cycloidal path would avoid the nonlinear frequency shift that leads to jumps [16]. Denman carried out a systematic study of various paths and showed that a cycloidal path is slightly hardening whereas a particular epicycloidal path is neutral, that is, neither softening nor hardening

[17]. Further work showed that while the epicycloidal path leads to essentially linear absorber motions over all amplitude ranges, the corresponding torque applied to the primary system is not purely harmonic at the desired order, but contains higher order harmonics that arise from nonlinear kinematic effects [18]. An examination of general paths and their attendant torques led to the development of subharmonic pairs of epicycloidal absorbers that generate a purely harmonic torque [19–21].

When a rotor is fitted with multiple, identically-tuned CPVAs the absorbers are coupled through its inertia, and the coupling is inherently weak since the absorber inertia is much smaller than that of the rotor. Moreover, the absorbers are designed to be lightly damped and they are tuned (close to) the order of the excitation. These features give rise to a system of internally resonant, weakly coupled, and weakly damped oscillators—a situation ripe with instabilities and rich dynamics. Such features also lead to mathematical models with small nondimensional parameters that are amenable to analytical treatment using perturbation methods. Systematic investigations of nonlinear responses have been carried out using averaging and symmetric bifurcation theory for a range of path types [14, 22, 23]. It was shown that the desired synchronous response of the absorbers can undergo two basic types of instabilities. The first type maintains the symmetry of the response but results in jumps, just as in the case of a single absorber. For multiple absorbers, an additional instability can occur wherein the symmetry of the response is broken. This results in a rich bifurcation where multiple response branches arise, including some spatially localized responses [22, 24]. Similar analyses were carried out for CPVA systems composed of multiple subharmonic pairs [25]. The effects of small imperfections among the absorbers, which are inevitable due to manufacturing, in-service wear, and so on, were considered in the context of linear system models, where it was shown that these systems experience localized free modes of vibration, as well as localized responses to order excitation [26, 27].

Early experimental work on CPVAs focused on particular applications, for example, specific internal combustion engines. However, systematic experiments using a dedicated test rig have recently been carried out for both circular and epicycloidal path absorber systems [28–30]. These results confirm the linear and nonlinear behavior of CPVAs for these path types, and also demonstrate the rich behavior that occurs if absorbers are tuned too closely to the excitation order [29, 31]. In terms of applications, CPVAs show great promise for use in advanced internal combustion engines that offer increased fuel efficiency and reduced emissions [13].

Finally, impact dampers have recently attracted considerable attention in the jet engine community as an effective means of reducing blade vibration amplitudes. Such dampers typically consist of a single mass traveling back and forth in a cavity machined in a turbine blade, where energy dissipation occurs when the mass impacts the cavity walls. In this case, the impact damper is also designed to act as a tuned absorber, with both effects contributing to vibration reduction. Much of this work has been carried out experimentally for specific applications [32, 33], although there has been some systematic theoretical work as well [34]. Other impact damper designs are also being explored by industry, such as dry particle damping systems [35] that include a large number of tiny masses in a blade cavity, where energy dissipation is achieved from multiple impacts between the masses. Such designs have proven effective experimentally, although they suffer durability problems in the harsh jet engine environment (e.g., rotation, extreme temperatures, and so on).

1.3 Systems with Cyclic Symmetry

Many rotating flexible structures consist of an array of interconnected constituent parts (substructures) whose geometry and structural properties are rotationally periodic, and they are said to have *cyclic symmetry.* In a bladed disk, for example, the fundamental substructure is one blade plus the corresponding segment of the disk,

which is collectively referred to as a *sector*. The entire dynamics of these systems can be captured by analyzing a single sector, so long as one applies the appropriate phase conditions at the interfaces with adjacent sectors. This is a feature shared by all perfectly cyclic systems, and it offers a tremendous computational savings in their analysis.

The linear free response of a cyclic structure is characterized by identical motions of each sector, except for a fixed sector-to-sector phase difference, and hence the mode shapes are harmonic in the circumferential direction. For bladed disk assemblies, this leads to nodal lines across the disk called *nodal diameters*, and the system mode shapes are referred to as *nodal diameter modes*. An engine order excitation of order n will generally excite only the modes with n nodal diameters. Due to the cyclic symmetry of the system, most of the natural frequencies occur in repeated pairs and these correspond to traveling wave modes, where (in the absence of damping) the system kinetic energy remains fixed and is simply passed from one blade to another. The distinct frequencies correspond to standing wave modes, where the system kinetic energy varies sinusoidally [36]. If the sectors are only weakly coupled to one another, all of the system natural frequencies lie closely together, leading to a very rich structure with high modal density and high sensitivity to imperfections.

Generally, the blades on a turbomachinery rotor are meant to be identical. In practice, however, there are always small random uncertainties among the blades due to manufacturing tolerances, in-service wear, material imperfections, and so on. These small variations, referred to as *mistuning*, can lead to a confinement of vibration energy to a few blades or even a single blade, a phenomenon known as *localization* [37–40]. Due to this spacial confinement of energy, some of the blades may experience higher amplitudes than what is predicted from the ideal, perfectly periodic system [41–45]. Forced response amplifications of 200% or more can occur, resulting in high cycle fatigue and eventual failure. This is a major cost, safety, and readiness concern

for commercial and military jet engines alike [46].

The features of a typical cyclic system also lead to a rich variety of nonlinear dynamic behaviors. In particular, the repeated natural frequencies give rise to internal resonances when the systems are weakly damped and the excitation of interest is resonant. Additionally, there is the possibility of multiple interacting modes when the substructures are weakly coupled. These characteristics lead to situations ripe for instabilities, bifurcations, and a multitude of possible responses, just as in the case of torsional CPVAs. Previous research in this area has dealt with the modal interactions that arise from internal resonances [47–50] and nonlinear localization [51–54]. However, it is important to note that localization of responses can occur in perfectly tuned nonlinear system models, where the mistuning between subsystems arises from the frequency dependence on amplitudes, rather than from imperfections.

A recent line of particularly interesting research in cyclic systems has focused on the problem of how to design systems to reduce the harmful effects of localization. A promising idea is to introduce into the system intentional patterns of mistuning that can make the system robust with respect to the unavoidable imperfections. This has been quite successful, at least for linear system models [55–58].

1.4 Vibration Absorbers for Rotating Flexible Structures under Engine Order Excitation

Since order-tuned absorbers are designed to address system vibrations at a troublesome *order* (rather than a fixed frequency), it is natural to consider their use on rotating flexible structures subjected to engine order excitation. In this context, the desired system response is a traveling wave, where each sector behaves identically except for a fixed phase difference among nearest neighbors; any other response type implies decreased absorber performance. The ideal response is one in which the blades

remain stationary relative to the rotating hub and the absorbers respond in a traveling wave to identically counter the engine order (traveling wave) excitation of the blades.

Order-tuned absorbers have already been considered for helicopter rotor blades [59], for an ideal flexible beam [60], and for potential implementation in hollow turbine blades [61]. In addition, absorbers that employ order tuning at small amplitudes and that transition into impact absorbers at larger amplitudes have recently been experimentally [32, 33] and analytically [34] investigated. While these studies have been promising, they have been limited in several key ways: (1) each considered very specific applications; (2) the studies do not systematically address how to size and tune the absorbers for optimal performance over a wide range of operating conditions; and (3) all previous studies focused on the implementation of an absorber to an *individual* structural element (e.g., a single blade). In fact, these studies were limited to either theoretical results based on linear analyses or observations gleaned from experiments or simulations.

This thesis reports the first systematic analytical treatment of order-tuned vibration absorbers applied to a fully-coupled cyclic structure under engine order excitation, including detailed recommendations for both linear and nonlinear absorber design. In this way, it serves not only as the first study of its kind to unite the individually mature bodies of research on *absorber systems* and *cyclic systems*, but it also provides context and direction for what is sure to be a plentiful and rich course of ongoing theoretical and experimental work.

1.5 Dissertation Overview

The goal the investigation is threefold: (1) to quantify and understand the underlying linear resonance structure of a cyclically-coupled bladed disk assembly fitted with order-tuned absorbers; (2) based on these findings, to design the absorbers to

eliminate or otherwise reduce blade motions relative to the rotating hub; and (3) to generalize the linear theory, methodology, and design to include the basic, first-order effects of nonlinearity.

As we shall see, the underlying linear resonance structure of the cyclically coupled system fitted with absorbers is surprisingly rich, a feature that arises from the order-nature of the absorbers. This is manifested in the classical eigenvalue veering phenomenon and gives rise to an ideal absorber design (perfect absorber tuning) in which the absorber tuning order is set to identically match the engine order. In the absence of damping, the result is a total elimination of the blade motions relative to the rotating hub—independent of the rotor speed. One of the main findings of the linear analysis, and indeed of this entire thesis, is the existence of an entire spectrum of absorber designs for which there are no system resonances *over the full range of possible rotor speeds.* This corresponds to a continuous set of absorber *under*-tuning values, the so-called "no-resonance zone," where resonance is avoided altogether. By selecting a design within this small, but finite gap, there is at least some level of robustness to parameter uncertainties, but at the expense of residual (zero damping) or slightly increased (nonzero damping) blade motions.

Nonlinearity is introduced via the absorber paths and, for the desired traveling wave response, it gives rise to additional frequency response branches and resonances, but the fundamental linear resonance structure mentioned above is shown to qualitatively persist. There does exist a nonlinear tuning strategy that guarantees a branch of solutions corresponding to zero (or otherwise reduced) blade motions. However, unlike its linear counterpart, it is highly sensitive to parameter uncertainties. Even more importantly, the nonlinear tuning is shown to depend on both the rotor speed and force amplitude, and is thus effective only for a *single* set of operating conditions. These findings suggest that it is not practical to exploit nonlinearity to further improve the absorber performance in the cyclic systems under consideration. If nonlinearity

is inevitable, it is clearly shown that softening characteristics are more desirable than hardening; the former simply sets an upper limit on the range of rotor speeds over which the absorbers are effective, while the latter may give rise to problematic resonances (especially if the damping is light). Finally, for the weakly coupled and lightly damped systems under consideration, there may be a myriad of additional responses other than the desired traveling wave variety. However, based on a number of case studies and extensive numerical investigations, none could be identified. (Analytical local stability results for the fully-coupled nonlinear system are essentially intractable, even after a simplifying reduction of the Jacobian matrix is carried out.) This is, in fact, very good news from a practical viewpoint since a traveling wave response of the absorbers is desired.

The main body of the dissertation is organized as follows. Chapter 2 highlights relevant background topics and material, including some mathematical preliminaries, engine order excitation, vibration characteristics of cyclic systems, and frequency- and order-tuned vibration absorbers. A suitable mathematical model for a bladed disk assembly fitted with order-tuned vibration absorbers is developed in Chapter 3, from which a number of specific models to be systematically analyzed in the two subsequent chapters are gleaned. A linearized model is investigated in Chapter 4, which gives rise to a linear absorber tuning strategy, and these results are generalized in Chapter 5 to include the basic effects of nonlinearity. Finally, the dissertation closes with detailed recommendations for absorber design, a summary of contributions, and directions for future work in Chapter 6.

CHAPTER 2

Background

2.1 Introduction

This chapter highlights pertinent background material that will be useful in the analyses of subsequent chapters. Some mathematical preliminaries are considered first in Section 2.2, including the Kronecker product, the Fourier matrix, and the basic theory of circulants. These sections are quite brief and are meant only to highlight well-known, but fundamental results and properties. A more exhaustive treatment of the theory of circulants (including many proofs) is given in Appendix B, and Appendix A reviews some selected topics from linear algebra. A model for engine order excitation is subsequently developed in Section 2.3 and its traveling wave nature discussed. In order to characterize the basic free and forced response of cyclically-coupled systems under engine order excitation, a cyclic chain of linear oscillators is investigated in Section 2.4. Finally, the theory of frequency- and order-tuned vibration absorbers is given in Section 2.5, and the chapter closes in Section 2.6 with some concluding remarks.

2.2 Mathematical Preliminaries

We make frequent use of the theory of circulant matrices throughout this work. Their basic properties are outlined in this section, along with some other relevant mathemat-

ical preliminaries. The Kronecker product is defined first in Section 2.2.1, followed by the Fourier matrix in Section 2.2.2. Circulant and block circulant matrices are defined in Section 2.2.3, and it is shown how to diagonalize such matrices in Section 2.2.4. These sections are meant as a quick reference and correspondingly the treatment is brief and proofs are omitted. A more detailed account of the theory of circulants is given in Appendix B, which was distilled from the classical text by Davis [62] and the work by Óttarsson [36], and some selected topics from linear algebra are given in Appendix A.

2.2.1 The Kronecker Product

Let $\mathbf{A} \in \mathbb{C}^{m\times n}$ and $\mathbf{B} \in \mathbb{C}^{p\times q}$. Then the Kronecker (direct) product of $\mathbf{A}$ and $\mathbf{B}$ is the $mp \times nq$ matrix

$$\mathbf{A} \otimes \mathbf{B} = \begin{bmatrix} a_{11}\mathbf{B} & a_{12}\mathbf{B} & \cdots & a_{1n}\mathbf{B} \\ a_{21}\mathbf{B} & a_{22}\mathbf{B} & \cdots & a_{2n}\mathbf{B} \\ \vdots & \vdots & \ddots & \vdots \\ a_{m1}\mathbf{B} & a_{m2}\mathbf{B} & \cdots & a_{mn}\mathbf{B} \end{bmatrix}. \tag{2.1}$$

Some selected useful properties of the Kronecker product are as follows.

1. If $\mathbf{A}$, $\mathbf{B}$, $\mathbf{C}$, and $\mathbf{D}$ are square matrices such that $\mathbf{AC}$ and $\mathbf{BD}$ exist, then $(\mathbf{A} \otimes \mathbf{B})(\mathbf{C} \otimes \mathbf{D}) = (\mathbf{AC}) \otimes (\mathbf{BD})$.
2. If $\mathbf{A}$ and $\mathbf{B}$ are invertible matrices, then $(\mathbf{A} \otimes \mathbf{B})^{-1} = \mathbf{A}^{-1} \otimes \mathbf{B}^{-1}$.
3. If $\mathbf{A}$ and $\mathbf{B}$ are square matrices, then $(\mathbf{A} \otimes \mathbf{B})^{\mathcal{H}} = \mathbf{A}^{\mathcal{H}} \otimes \mathbf{B}^{\mathcal{H}}$.

Here, $(\cdot)^{\mathcal{H}} = (\bar{\cdot})^T$ denotes the *Hermitian operator*, or conjugate transpose.

2.2.2 The Fourier Matrix

Let $j = \sqrt{-1}$ and $\mathcal{N} = \{1, 2, \ldots, N\}$. Then the $N \times N$ complex Fourier matrix is defined as

$$\mathbf{E} = \mathbf{E}_N = [e_{ik}]; \quad e_{ik} = \frac{1}{\sqrt{N}} w^{(i-1)(k-1)} = \frac{1}{\sqrt{N}} e^{j(k-1)\varphi_i}, \qquad i, k \in \mathcal{N} \tag{2.2}$$

where $w = w_N = e^{\frac{2j\pi}{N}}$ is the primitive N^{th} root of unity (see Section B.4.1 of Appendix B) and

$$\varphi_i = \frac{2\pi(i-1)}{N}, \qquad i \in \mathcal{N} \tag{2.3}$$

is the angle subtended from the positive real axis in the complex plane to the i^{th} power of w_N. (See Figure B.1 on page 191.) When the dimension of $\mathbf{E}_N$ is clear, the subscript N will be omitted. It is shown in Section 2.2.4 that all circulant matrices share the same linearly independent eigenvectors

$$\left.\begin{aligned} \mathbf{e}_i &= \frac{1}{\sqrt{N}}\left(1, w^{(i-1)}, w^{2(i-1)}, \ldots, w^{(N-1)(i-1)}\right)^T \\ &= \frac{1}{\sqrt{N}}\left(1, e^{j\varphi_i}, e^{j2\varphi_i}, \ldots, e^{j(N-1)\varphi_i}\right)^T \end{aligned}\right\}, \qquad i \in \mathcal{N} \tag{2.4}$$

which compose the N columns (or rows) of $\mathbf{E}$, that is, $\mathbf{E} = [\mathbf{e}_1, \mathbf{e}_2, \ldots, \mathbf{e}_N]$. An important property of the Fourier matrix is that it is unitary and, therefore,

$$\mathbf{E}^{\mathcal{H}}\mathbf{E} = \mathbf{E}\mathbf{E}^{\mathcal{H}} = \mathbf{I}, \tag{2.5}$$

where $\mathbf{I}$ is the identity matrix. Finally, the matrices $\mathbf{E}^{\mathcal{H}}$, $\mathbf{E}\otimes\mathbf{I}$, and $(\mathbf{E}\otimes\mathbf{I})^{\mathcal{H}} = \mathbf{E}^{\mathcal{H}}\otimes\mathbf{I}$ are also unitary.

2.2.3 Circulant Matrices

An $N \times N$ *circulant matrix* (or *circulant* for short) is formed from an N-vector by cyclically permuting its entries and is of the form

$$\mathbf{C} = \begin{bmatrix} c_1 & c_2 & \cdots & c_N \\ c_N & c_1 & \cdots & c_{N-1} \\ \vdots & \vdots & \ddots & \vdots \\ c_2 & c_3 & \cdots & c_1 \end{bmatrix}. \tag{2.6}$$

Thus a circulant matrix is defined completely by an ordered set of *generating elements* $c_1, c_2, \ldots, c_N$. It is convenient to define the *circulant operator* circ $(\cdot)$ that takes as its argument these generating elements and results in the array given by Equation (2.6), that is,

$$\mathbf{C} = \text{circ}\,(c_1, c_2, \ldots, c_N)\,. \tag{2.7}$$

The set of all such matrices will be designated by $\mathscr{C}_N$. An $NM \times NM$ *block circulant* matrix is defined similarly to Equation (2.6) and has the representation given by Equation (2.7), where each entry c_k is replaced by the $M \times M$ matrix $\mathbf{C}_k$ for each $k \in \mathcal{N}$. The ordered set of matrices $\mathbf{C}_1, \mathbf{C}_2, \ldots, \mathbf{C}_N$ are called its *generating matrices.* The set of all $NM \times NM$ block circulant matrices with $M \times M$ blocks, which is sometimes called a block circulant of type (M, N), will be denoted by $\mathscr{BC}_{M,N}$. Finally, if a matrix is both circulant and symmetric it can be written as

$$\mathbf{C} = \begin{cases} \text{circ}\left(c_1, c_2, \ldots, c_{\frac{N}{2}}, c_{\frac{N+2}{2}}, c_{\frac{N}{2}}, \ldots, c_3, c_2\right), & N \text{ even} \\ \text{circ}\left(c_1, c_2, \ldots, c_{\frac{N-1}{2}}, c_{\frac{N+1}{2}}, c_{\frac{N+1}{2}}, c_{\frac{N-1}{2}}, \ldots, c_3, c_2\right), & N \text{ odd} \end{cases} \tag{2.8}$$

and necessarily has repeated generating elements; only $(N+2)/2$ are distinct if N is even and $(N+1)/2$ are distinct if N is odd. The set of all $N \times N$ *symmetric circulants* is denoted by $\mathscr{SC}_N$. An $NM \times NM$ *block circulant, block symmetric* matrix is obtained by replacing each c_k in Equation (2.8) with $\mathbf{C}_k$ for each $k \in \mathcal{N}$. The set of all $NM \times NM$ block circulant, block symmetric matrices with $M \times M$ blocks will be denoted by $\mathscr{BCBS}_{M,N}$.

2.2.4 Diagonalization of Circulants

A matrix $\mathbf{C} \in \mathscr{C}_N$ with generating elements $c_1, c_2, \ldots, c_N$ can be diagonalized via the unitary (similarity) transformation

$$\mathbf{E}_N^{\mathcal{H}} \mathbf{C} \mathbf{E}_N = \begin{bmatrix} \lambda_1 & & & 0 \\ & \lambda_2 & & \\ & & \ddots & \\ 0 & & & \lambda_N \end{bmatrix}, \tag{2.9}$$

where

$$\lambda_i = \sum_{k=1}^{N} c_k w^{(k-1)(i-1)}, \qquad i \in \mathcal{N}. \tag{2.10}$$

As a consequence, *all* circulant matrices share the same eigenvectors, which are given by Equation (2.4). Their eigenvalues are given by Equation (2.10) and depend only on

the generating elements. Similarly, a matrix $\mathbf{C} \in \mathscr{BC}_{M,N}$ can be block diagonalized via the unitary transformation[1]

$$(\mathbf{E}_N^{\mathcal{H}} \otimes \mathbf{I}_M)\mathbf{C}(\mathbf{E}_N \otimes \mathbf{I}_M) = \begin{bmatrix} \mathbf{\Lambda}_1 & & & \mathbf{0} \\ & \mathbf{\Lambda}_2 & & \\ & & \ddots & \\ \mathbf{0} & & & \mathbf{\Lambda}_N \end{bmatrix}, \tag{2.11}$$

where $\mathbf{0}$ and $\mathbf{I}_M$ are the $M \times M$ zero and identity matrices, respectively, and

$$\mathbf{\Lambda}_i = \sum_{k=1}^{N} \mathbf{C}_k w^{(k-1)(i-1)}, \qquad i \in \mathcal{N} \tag{2.12}$$

which depends only on the generating matrices $\mathbf{C}_1, \mathbf{C}_2, \ldots, \mathbf{C}_N$. Since Equation (2.11) is a unitary transformation it preserves the eigenvalues of $\mathbf{C}$. Hence its eigenvalues are the eigenvalues of the N matrices $\mathbf{\Lambda}_i \in \mathbb{C}^{M \times M}$. If $\mathbf{v}_i$ is an eigenvector of $\mathbf{\Lambda}_i$ then the corresponding eigenvector of $\mathbf{C}$ is $\mathbf{u}_i = \mathbf{e}_i \otimes \mathbf{v}_i$.

2.3 Engine Order Excitation

2.3.1 Mathematical Model

Ideally, the steady axial gas pressure in a jet engine might vary with radius but is otherwise uniform in the circumferential direction, thus resulting in an identical force field on each blade in a particular fan, compressor, or turbine within the engine. In practice, however, flow entering an engine inlet invariably meets static obstructions, such as struts, stator vanes, etc., in addition to rotating bladed disk assemblies in its path to the exhaust. Even in steady operation, therefore, the flow slightly upstream of these bladed assemblies is non-uniform in pressure, temperature, and so on. This results in a static pressure (effective force) field on the blades that varies circumferentially, an example of which is shown in Figure 2.1.

Consider, for example, an engine in steady operation with n evenly-spaced struts slightly upstream (or downstream) of a bladed assembly. As explained in [9] these

[1]Note that $(\mathbf{E}_N \otimes \mathbf{I}_M)^{\mathcal{H}} = (\mathbf{E}_N^{\mathcal{H}} \otimes \mathbf{I}_M)$, which follows from Property 3 of Section 2.2.1.

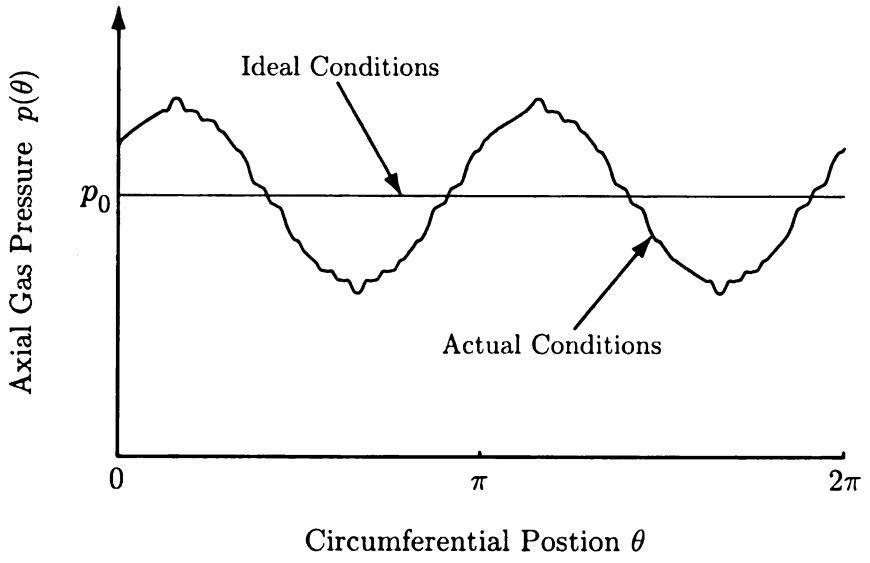

Figure 2.1. The the axial gas pressure $p(\theta)$: ideal and (example) actual conditions.

obstructions produce a circumferential variation upon the mean axial gas pressure that is essentially proportional to $\cos n\theta$, where θ is an angular position. Thus a blade rotating through this static pressure field experiences a force proportional to $\cos n\Omega t$, where Ω is the constant angular speed of the bladed disk assembly and t is time. An adjacent blade experiences the same force, but at a constant fraction of time later. This type of excitation is defined as *engine order excitation* and n is said to be the *order* of the excitation.

To be more precise, the axial gas pressure of a steady flow through a jet engine may be described by a function $p(\theta) = p(\theta + 2\pi)$, where θ is an angular coordinate measured relative to a fixed origin on the machine. That is, the pressure field is rotationally periodic and can therefore be expanded in a Fourier series with terms of the form $p_o \cos n\theta$. Then if the angular position of the i^{th} blade relative to the same origin is defined by

$$\theta_i(t) = \Omega t + \frac{2\pi}{N}(i-1), \qquad i \in \mathcal{N}$$

where N is the total number of blades and $\mathcal{N} = \{1, 2, \ldots, N\}$ is the set of blade, or *sector* numbers, it follows that the total effective force exerted on blade i due to the

n^{th} harmonic of the pressure field $p(\theta)$ can be captured by

$$F\cos\big(n\Omega t + 2\pi\tfrac{n}{N}(i-1)\big)\,, \qquad i \in \mathcal{N}. \tag{2.13}$$

Upon complexifying this gives rise to

$$F_i(t) = Fe^{j\phi_i}e^{jn\Omega t}, \qquad i \in \mathcal{N} \tag{2.14}$$

which is a model for the n^{th} predominant component of the excitation. It has period $T = 2\pi/n\Omega$, strength F, and is said to have angular speed Ω. The so-called *inter-blade phase angle* is defined by

$$\phi_i = \phi_i^{(n)} = 2\pi\frac{n}{N}(i-1) = n\varphi_i, \qquad i \in \mathcal{N} \tag{2.15}$$

where $n \in \mathbb{Z}_+$ is the *order* of the excitation and φ_i is the angle subtended from blade 1 to blade i and is defined by Equation (2.3). Equation (2.14) is defined as n^{th} engine order (e.o.) excitation (n e.o. excitation) or *traveling wave* excitation and is used to model the dynamic loading on models of bladed disk assemblies throughout this work. The traveling wave characteristics of this type of excitation are considered next.

2.3.2 Traveling Wave Characteristics

Equation (2.14) is a function of continuous time t and it is discretized in space via the index i. This gives rise to two interpretations of engine order excitation relative to the rotating hub (one discrete and the other continuous) and these can be visualized in Figure 2.2, which shows a dissection of the excitation amplitudes along time and sector axes. In the first and usual sense, Equation (2.14) is a *discrete temporal* variation of the dynamic loading applied to individual blades. That is, under an engine order n excitation each sector is harmonically forced with strength F and frequency $n\Omega$, but with a fixed phase difference relative to its nearest neighbors. Physically, one can think of this as placing N different observers at the discrete sectors and having the i^{th}

observer record the excitation strength applied to sector i as a function of time. Their recorded time traces would resemble those shown in Figure 2.2a. In the second and more general sense, Equation (2.14) can be viewed as a *continuous spatial* variation of the excitation strength relative to the rotating hub (along the sector axis) that evolves with increasing time, i.e., it is a propagating waveform or *traveling wave.* If a single observer was placed on the rotating hub and recorded the strength of this traveling wave as a function of i (taken here to be *continuous*), it would resemble the curve shown in Figure 2.2b. In this context, the instantaneous loading applied to individual blades is obtained by essentially "sampling" the continuous traveling wave at each sector $i \in \mathcal{N}$ and, as time evolves, these sampled points define N time-profiles of the force amplitudes, which is equivalent to the discrete temporal interpretation described above. However, the latter interpretation illuminates some important traveling wave characteristics of the engine order excitation that are otherwise difficult to explain, and in what follows these are systematically described.

To explain the traveling wave mathematically, it is convenient to define

$$\Phi_k(\chi) = \cos\Big(\tfrac{2\pi(k-1)}{N}\chi\Big) = \cos(\varphi_k\chi), \tag{2.16}$$

which is a cosinusoidal waveform with wavelength $2\pi/\varphi_k$. Then for $i \in \mathcal{N}$ Equation (2.14) can be written (in real form) as

$$F_i(t) = F\cos\big(\varphi_{n+1}(i-1) + n\Omega t\big), \tag{2.17a}$$

$$= F\Phi_{n+1}(i - 1 + Ct), \tag{2.17b}$$

which is a harmonic function with a wavelength of $2\pi/\varphi_{n+1} = N/n$ *sectors* (φ_{n+1} is the wave number) and angular frequency $n\Omega$. Equation (2.17b) shows that it is a traveling wave (TW) in the negative i-direction (descending blade number) with speed $C = n\Omega/\varphi_{n+1} = N\Omega/2\pi$, measured in *sectors per second.* An example plot of this continuous backward traveling wave (BTW) is shown in Figure 2.2b and, as described above, the applied loads can be obtained from this figure by continuously

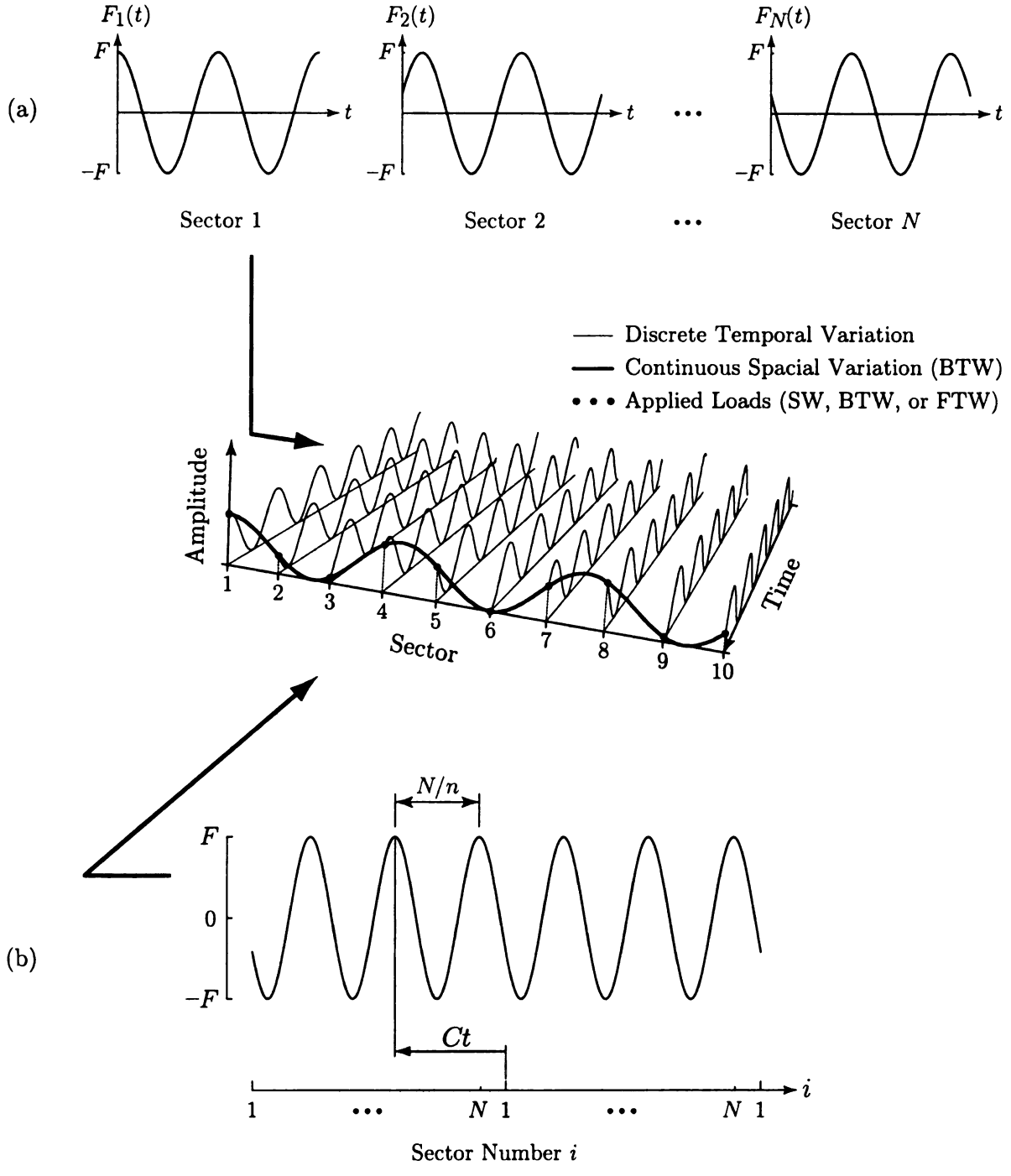

Figure 2.2. An example illustration of the *discrete temporal* and *continuous spatial* variations of the traveling wave excitation defined by Equation (2.14) (in real form): (a) the discrete dynamic loads with amplitude F and period $T = 2\pi/n\Omega$ applied to each sector; and (b) the continuous BTW excitation with wavelength N/n and speed $C = N\Omega/2\pi$ relative to the rotating hub.

"sampling" the waveform at the discrete sector numbers as time evolves. Then the engine order excitation *applied to the individual blades* consists of a wave composed of these N discrete points, examples of which are shown in Figure 2.3 a-d. Interestingly, this gives rise to discrete SW or even forward traveling wave (FTW) applied dynamic loads (depending on the value of n relative to N) even though Equation (2.17) is strictly a backward traveling waveform relative to the rotating hub. These additional possibilities arise due to aliasing of the "sampled points" just as it occurs in elementary signal processing theory [63, 64]. Before characterizing the traveling and standing waveforms it is shown that one need only consider engine orders $n \in \mathcal{N}$.

The traveling wave nature of the discrete applied loads (i.e., SW, BTW, or FTW) depends only on the value of n relative to N. To see this, let

$$\bar{n} = n \bmod N \in \mathcal{N}, \qquad n \in \mathbb{Z}_+ \tag{2.18}$$

and assume $n = \bar{n} + mN$ for some integer m. Then one can write $\Phi_{\bar{n}+mN+1}(\chi) = \Phi_{\bar{n}+1}(\chi)$ and it follows that if $n = \bar{n}$ corresponds to a SW, BTW, or FTW then so does $\bar{n} + mN$ for any $m \in \mathbb{Z}_+$. In this sense, the traveling wave nature of the applied dynamic loads is seen to alias relative to N. These features are characterized next for engine orders $n \in \mathcal{N}$, where it is understood that the results can be applied to any $n > N$ simply by taking n modulo N (where appropriate).

For the special case when $n = N$ the rotating blades become entrained with the excitation since $\phi_i^{(N)} = 2\pi n(i-1)$ with $i, n \in \mathbb{Z}_+$ and hence each is forced with the same strength *and* phase. As illustrated in Figure 2.3d, this is effectively a SW excitation where each blade is harmonically forced according to $F_i(t) = F\cos n\Omega t$. Entrainment also occurs when $n = N/2$ if N is even, in which case $\phi_i^{(N/2)} = \pi n(i-1)$, where $(i-1)$ is odd (resp. even) for even (resp. odd) sector numbers $i \in \mathcal{N}$. Accordingly, all blades with odd sector numbers are driven by $F_i(t) = F\cos n\Omega t$, as are the blades with even sector numbers, but with a 180-degree phase shift. As shown in Figure 2.3b, this amounts to the same standing wave excitation as the $n = N$ case,

Table 2.1. Sets of engine orders $n \,(\mathrm{mod}\, N) \in \mathcal{N} = \mathcal{N}_{\mathrm{SW}}^{\mathrm{O,E}} \bigcup \mathcal{N}_{\mathrm{BTW}}^{\mathrm{O,E}} \bigcup \mathcal{N}_{\mathrm{FTW}}^{\mathrm{O,E}}$ corresponding to backward traveling wave (BTW), forward traveling wave (FTW), and standing wave (SW) dynamics loads applied to the blades for (a) odd N and (b) even N. These can be visualized in Figure 2.3*i-ii*.

(a) Odd N	(b) Even N
$\mathcal{N}_{\mathrm{BTW}}^{\mathrm{O}} = \left\{ n \in \mathbb{Z}_+ \,:\, 1 \leq n \leq \frac{N-1}{2} \right\}$	$\mathcal{N}_{\mathrm{BTW}}^{\mathrm{E}} = \left\{ n \in \mathbb{Z}_+ \,:\, 1 \leq n \leq \frac{N-2}{2} \right\}$
$\mathcal{N}_{\mathrm{FTW}}^{\mathrm{O}} = \left\{ n \in \mathbb{Z}_+ \,:\, \frac{N+1}{2} \leq n \leq N-1 \right\}$	$\mathcal{N}_{\mathrm{FTW}}^{\mathrm{E}} = \left\{ n \in \mathbb{Z}_+ \,:\, \frac{N+2}{2} \leq n \leq N-1 \right\}$
$\mathcal{N}_{\mathrm{SW}}^{\mathrm{O}} = \{N\}$	$\mathcal{N}_{\mathrm{SW}}^{\mathrm{E}} = \left\{ \frac{N}{2}, N \right\}$

except for a phase reversal in the excitation among adjacent blades. The engine orders corresponding to SW excitations for odd and even N are denoted by the sets $\mathcal{N}_{\mathrm{SW}}^{\mathrm{O,E}} \subset \mathcal{N}$, which are defined in Table 2.1 and all other values of $n \in \mathcal{N}$ correspond to traveling waves. Engine orders $n \in \mathcal{N}_{\mathrm{BTW}}^{\mathrm{O,E}}$ (resp. $n \in \mathcal{N}_{\mathrm{FTW}}^{\mathrm{O,E}}$) correspond to BTW (resp. FTW) excitation, an example of which is shown in Figure 2.3a (resp. Figure 2.3c), where $\mathcal{N}_{\mathrm{BTW}}^{\mathrm{O,E}}$ and $\mathcal{N}_{\mathrm{FTW}}^{\mathrm{O,E}}$ are also defined in Table 2.1. These sets can be visualized in Figure 2.3 *i-ii* for odd and even N.

2.4 Vibration Characteristics of Cyclic Systems

The basic free vibration characteristics of cyclic systems are discussed next, in addition to forced vibration under the engine order excitation described in Section 2.3. A prototypical linear model is introduced in Section 2.4.1, which consists of a cyclic array of N identical, identically coupled oscillators, each with a single degree of freedom (DOF). Its forced response is considered in Section 2.4.2, including a decoupling strategy based on the cyclic symmetry of the system. The details of its free response are given in Section 2.4.3 and in Section 2.4.4, which discuss the eigenfrequency characteristics and normal modes of vibration, respectively. Finally, conditions for resonance are given in Section 2.4.5, along with a description of the underlying linear resonance structure in terms of the engine order and angular speed of the excitation.

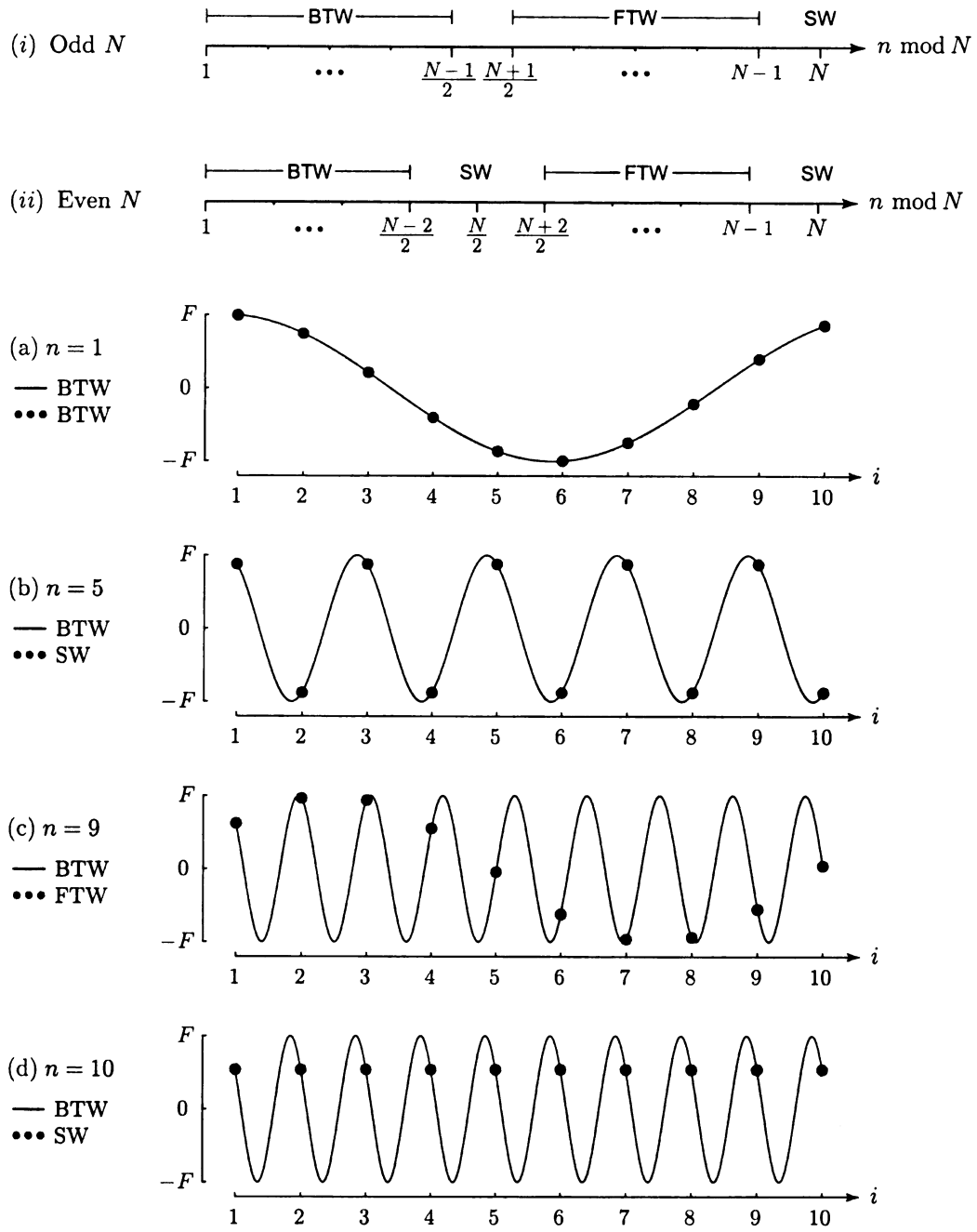

Figure 2.3. Engine orders n mod N corresponding to BTW, FTW and SW applied dynamic loading for (i) odd N and (ii) even N (see also Table 2.1); example plots of applied dynamic loading (represented by the dots) for a model with $N = 10$ sectors and with (a) $n = 1$ (BTW), (b) $n = 5$ (SW), (c) $n = 9$ (FTW), and (d) $n = 10$ (SW). The BTW engine order excitation is represented by the solid lines.

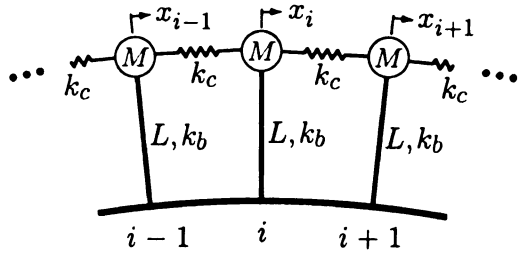

Figure 2.4. A prototypical linear cyclic system with cyclic boundary conditions $x_0 = x_N$ and $x_{N+1} = x_1$.

2.4.1 A Prototypical Model

The undamped cyclic system to be considered is shown schematically in Figure 2.4. It consists of a cyclic chain of N single-DOF oscillators each of mass M, the dynamics of which are captured by the transverse displacements x_i, and these are uniformly attached around the circumference of a (nonrotating) rigid hub via linear elastic elements of stiffness k_b and effective length L. Adjacent masses are elastically coupled via linear springs, each with stiffness k_c. It is assumed that the elastic elements are unstressed when the oscillators are in a purely radial configuration, that is, when $x_i = 0$ for each $i \in \mathcal{N}$. An individual oscillator, together with the nearest-forward-neighbor elastic coupling, forms one fundamental *sector* and there are N such sectors in the overall system. Finally, the system is subjected to engine order excitation of order $n \in \mathbb{Z}_+$ and angular speed Ω, which can be modeled by Equation (2.14).

The linear equation of motion for sector i is obtained in the usual manner. It is divided through by the inertia term ML and time is rescaled according to $\tau = \omega_o t$, where $\omega_o = \sqrt{k_b/M}$ is the undamped natural frequency of a single isolated sector. Then if $q_i = x_i/L$ the dynamics of the i^{th} sector are governed by

$$q_i'' + q_i + \nu^2(-q_{i-1} + 2q_i - q_{i+1}) = f e^{j\phi_i} e^{jn\sigma\tau}, \qquad i \in \mathcal{N} \tag{2.19}$$

where $\nu = \sqrt{k_c/k_b}$ is a nondimensional coupling strength and $(\,\cdot\,)' = d(\,\cdot\,)/d\tau$. The dimensionless angular speed and strength of the engine order excitation are denoted by $\sigma = \Omega/\omega_o$ and $f = F/Lk_b$, respectively, n is its order, and ϕ_i is the interblade

phase angle defined by Equation (2.15). In Equation (2.19) it is understood that

$$q_0 = q_N \qquad \text{and} \qquad q_{N+1} = q_1, \tag{2.20}$$

which implies that the N^{th} oscillator is coupled to the first.

By stacking the N coordinates q_i into the configuration vector $\mathbf{q} = (q_1, q_2, \ldots, q_N)^T$, the governing equation of motion for the overall N–DOF system takes the form

$$\mathbf{q}'' + \mathbf{K}\mathbf{q} = \mathbf{f}e^{jn\sigma\tau}, \qquad i \in \mathcal{N} \tag{2.21}$$

where $\mathbf{f} = (fe^{j\phi_1}, fe^{j\phi_2}, \ldots, fe^{j\phi_N})^T$ is the system forcing vector, which accounts for the constant phase difference in the dynamic loading from one sector to the next. The $N \times N$ matrix

$$\mathbf{K} = \begin{bmatrix} 1+2\nu^2 & -\nu^2 & 0 & \ldots & 0 & -\nu^2 \\ -\nu^2 & 1+2\nu^2 & -\nu^2 & \ldots & 0 & 0 \\ 0 & -\nu^2 & 1+2\nu^2 & \ldots & 0 & 0 \\ \vdots & \vdots & \vdots & \ddots & \vdots & \vdots \\ 0 & 0 & 0 & \ldots & 1+2\nu^2 & -\nu^2 \\ -\nu^2 & 0 & 0 & \ldots & -\nu^2 & 1+2\nu^2 \end{bmatrix} \tag{2.22}$$

reflects the nondimensional stiffness of each sector relative to the hub (additive unity along its diagonal) and also the inter-sector coupling (ν^2 along the super- and sub-diagonal). The elements $-\nu^2$ appearing in the $(1, N)$ and $(N, 1)$ positions of $\mathbf{K}$ are due to the cyclic boundary conditions given by Equation (2.20), and in particular the $q_{i\pm1}$ terms in Equation (2.19). (In their absence, the system represents a finite chain of N oscillators.) Thus, in addition to being symmetric, Equation (2.22) is also a circulant and can be written as[2]

$$\mathbf{K} = \text{circ}\left(1+2\nu^2, -\nu^2, 0, \ldots, 0, -\nu^2\right) \in \mathscr{SC}_N, \tag{2.23}$$

[2]This is a property shared by *all* linear(ized), perfectly cyclic systems with N sectors, a single–DOF per sector, and nearest-neighbor coupling. In the more general case of multi–DOF per sector, the system matrices are block circulant (and also block symmetric) and hence belong to $\mathscr{BCBS}_{M,N}$, where M is the number of DOF per sector.

where the circ $(\cdot)$ operation is defined in Section 2.2.3. In the absence of coupling (that is, if $\nu = 0$) $\mathbf{K}$ is diagonal and Equation (2.21) represents a decoupled set of N harmonically forced, single–DOF oscillators.

The forced response of Equation (2.21) under engine order excitation is considered next with emphasis on a modal analysis whereby the fully coupled system (that is, one in which $\nu \neq 0$) is reduced to a set of N single–DOF oscillators, only one of which is (harmonically) excited. Such an analysis illuminates the basic vibration characteristics of linear cyclic systems, including their eigenfrequency and resonance structures. The approach taken here, and a generalization in which each sector has many DOF, is applied to the linear system in Chapter 4 and also in Chapter 5 to handle (block) reduction of the Jacobian matrices.

2.4.2 Forced Response Under Engine Order Excitation

The steady-state response of Equation (2.21) can be obtained using standard techniques [65] and, for non-resonant forcing, it is given by

$$\mathbf{q}^{\mathrm{ss}}(\tau) = \left(\mathbf{K} - n^2\sigma^2\mathbf{I}\right)^{-1}\mathbf{f}\, e^{jn\sigma\tau}, \tag{2.24}$$

where $\mathbf{I}$ is the $N \times N$ identity matrix. However, this requires inversion of the impedance matrix $\mathbf{K} - n^2\sigma^2\mathbf{I}$, which can be computationally expensive for a large number of sectors, and it offers little insight into the basic vibration characteristics. In what follows, a transformation based on the cyclic symmetry of the system is exploited to fully decouple the single, N–DOF system to a set of N, single–DOF oscillators from which the steady-state response can easily be obtained. The procedure is similar to the usual modal analysis from elementary vibration theory. However, a key difference is that the transformation matrix (and hence the system mode shapes) is known *a priori* and, since the transformation is unitary (thus preserving the system eigenvalues), the natural frequencies can be obtained *after* the transformation is carried out. Moreover, due to orthogonality conditions between the normal modes

and forcing vector, the steady-state response of the overall system reduces to finding the forced response of a *single* harmonically-forced, single–DOF oscillator in modal space, which offers a clear advantage over the solution to Equation (2.24).

It was shown in Section 2.3.2 that an engine order excitation can be regarded as traveling wave dynamic loading, and it is therefore reasonable to expect steady-state solutions of the same type. We begin with a simple way to show the existence of such a response, and then systematically describe it based on the results of the aforementioned modal analysis.

Existence of a Traveling Wave Response

Since the excitation is a traveling wave it is natural to search for traveling wave steady-state solutions of the same form, that is,

$$q_i^{\mathrm{ss}}(\tau) = Ae^{j\phi_i}e^{jn\sigma\tau} \tag{2.25}$$

for each $i \in \mathcal{N}$. Equation (2.25) assumes that each sector responds with the same amplitude A, but with a constant phase difference relative to its nearest neighbors, and together all N such solutions form a traveling wave response among the sectors. (In real form, Equation (2.25) can be written as $q_i^{\mathrm{ss}}(\tau) = A\Phi_{n+1}(i - 1 + C\tau)$, where $\Phi(\,\cdot\,)$ is defined by Equation (2.16) and $C = n\sigma/\varphi_{n+1}$ is the wave speed of the engine order excitation.) By mapping this trial solution into Equation (2.19) and dividing through by the common term $e^{j\phi_i}e^{jn\sigma\tau}$ one obtains

$$-(n\sigma)^2 A + A + \nu^2\left(-Ae^{-j\varphi_{n+1}} + 2A - Ae^{j\varphi_{n+1}}\right) = f, \tag{2.26}$$

where the identity

$$\phi_{i\pm1} - \phi_i = \pm\varphi_{n+1} \tag{2.27}$$

has been employed. Upon simplification, the amplitude A is found to be

$$A = \frac{f}{1 + 2\nu^2(1 - \cos\varphi_{n+1}) - (n\sigma)^2}, \tag{2.28}$$

from which it follows that $\bar{\omega}_{n+1} = \sqrt{1 + 2\nu^2(1 - \cos\varphi_{n+1})}$ is one of the N natural frequencies of the coupled system, and it corresponds to mode $p = n + 1$.[3]

Equation (2.28) highlights a fundamental result when a linear cyclic system with nearest-neighbor elastic coupling is subjected to engine order excitation of order n: mode $n + 1$ is excited. The reason for this is not clear from this approach, but it can be described systematically via a modal analysis that considers the fully coupled system.

Modal Analysis

It is well-known that circulant matrices, such as the stiffness matrix defined by Equation (2.23), can be diagonalized via a similarity transformation involving the Fourier matrix, and in what follows this property is exploited to fully decouple the governing equations of motion given by Equation (2.21). The theory is due to P.J. Davis (1979) and is exhaustively developed in his seminal work, *Circulant Matrices* [62]. A detailed development of the pertinent theory is given in Appendix B (and summarized without proofs in Section 2.2) in a way that should be familiar to the vibrations engineer.

Diagonalization can be achieved by employing Equation (2.9), and in particular Theorem B.7 on page 197. To this end, the change of coordinates[4]

$$\mathbf{q}(\tau) = \mathbf{E}\mathbf{u}(\tau) = \sum_{k=1}^{N} \mathbf{e}_k u_k(\tau) \qquad \text{or} \qquad q_p(\tau) = \mathbf{e}_p^T \mathbf{u}(\tau), \qquad p \in \mathcal{N} \tag{2.29}$$

is introduced, where $\mathbf{E}$ is the $N \times N$ complex Fourier matrix and $\mathbf{e}_p$ (given by Equation (2.4)) is its p^{th} column, $(\cdot)^T$ denotes transposition, and $\mathbf{u} = (u_1, u_2, \ldots, u_N)^T$ is a vector of modal, or *cyclic* coordinates. Substituting Equation (2.29) into Equation (2.21) and multiplying from the left by $\mathbf{E}^{\mathcal{H}}$ yields

$$\mathbf{E}^{\mathcal{H}}\mathbf{E}\mathbf{u}'' + \mathbf{E}^{\mathcal{H}}\mathbf{K}\mathbf{E}\mathbf{u} = \mathbf{E}^{\mathcal{H}}\mathbf{f}e^{jn\sigma\tau}. \tag{2.30}$$

[3]Strictly speaking, the excited mode is $p = n \bmod N + 1$, which will be shown in the next section.

[4]The index p corresponds to the p^{th} mode of vibration and shall be referred to as the *mode number*.

Since $\mathbf{E}^{\mathcal{H}}\mathbf{E} = \mathbf{I}$ from Equation (2.5) (that is, $\mathbf{E}$ is unitary, which is proved in Section B.4.2) and in light of Equation (2.9), it follows that

$$\begin{bmatrix} u_1'' \\ u_2'' \\ \vdots \\ u_N'' \end{bmatrix} + \begin{bmatrix} \bar{\omega}_1^2 & & & 0 \\ & \bar{\omega}_2^2 & & \\ & & \ddots & \\ 0 & & & \bar{\omega}_N^2 \end{bmatrix} \begin{bmatrix} u_1 \\ u_2 \\ \vdots \\ u_N \end{bmatrix} = \begin{bmatrix} \mathbf{e}_1^{\mathcal{H}}\mathbf{f} \\ \mathbf{e}_2^{\mathcal{H}}\mathbf{f} \\ \vdots \\ \mathbf{e}_N^{\mathcal{H}}\mathbf{f} \end{bmatrix} e^{jn\sigma\tau}, \tag{2.31}$$

where the p^{th} scalar element of the $N \times 1$ modal forcing vector $\mathbf{E}^{\mathcal{H}}\mathbf{f}$ is $\mathbf{e}_p^{\mathcal{H}}\mathbf{f}$. Equation (2.29) is a unitary (similarity) transformation and hence the system natural frequencies are preserved, which is guaranteed by Theorem A.1 on page 180. For each $p \in \mathcal{N}$ they follow from Equation (2.10) and are given implicitly by

$$\begin{aligned} \bar{\omega}_p^2 \equiv \left(\frac{\omega_p}{\omega_o}\right)^2 &= 1 + 2\nu^2 - \nu^2 w^{(p-1)} + 0 + \ldots + 0 - \nu^2 w^{(N-1)(p-1)} \\ &= 1 + 2\nu^2 - \nu^2\left(w^{(p-1)} + w^{(N-1)(p-1)}\right) \\ &= 1 + 2\nu^2(1 - \cos\varphi_p), \end{aligned} \tag{2.32}$$

where $w = e^{\frac{2j\pi}{N}}$ is the primitive N^{th} root of unity (see Section B.4.1) and the identity $w^{(p-1)} + w^{(N-1)(p-1)} = 2\cos\varphi_p$ has been employed. The overbar indicates that the frequencies are in dimensionless form.

Equation (2.31) is a decoupled set of N, single–DOF harmonically forced modal oscillators and, in the steady-state, the p^{th} modal response is

$$u_p^{\text{ss}}(\tau) = \frac{\mathbf{e}_p^{\mathcal{H}}\mathbf{f}}{\bar{\omega}_p^2 - (n\sigma)^2}\, e^{jn\sigma\tau}, \qquad p \in \mathcal{N}. \tag{2.33}$$

The steady state response of sector i (in physical coordinates) can be obtained from the transformation given by Equation (2.29) and is given by $q_i^{\text{ss}}(\tau) = \mathbf{e}_i^T\mathbf{u}^{\text{ss}}(\tau)$, or

$$\begin{aligned} q_i^{\text{ss}}(\tau) &= \sum_{k=1}^{N} \frac{1}{\sqrt{N}} e^{j(i-1)\varphi_k} u_k^{\text{ss}}(\tau) \\ &= \frac{1}{\sqrt{N}} \sum_{k=1}^{N} \frac{\mathbf{e}_k^{\mathcal{H}}\mathbf{f}}{\bar{\omega}_k^2 - (n\sigma)^2}\, e^{j(i-1)\varphi_k} e^{jn\sigma\tau}, \qquad i \in \mathcal{N} \end{aligned} \tag{2.34}$$

which reflects that the total system response is simply a superposition of individual modal responses. Depending on the details of the modal forcing terms $\mathbf{e}_p^{\mathcal{H}}\mathbf{f}$ Equation (2.34) shows that there are N *possible* resonances, and these arise if the excitation frequency matches a system natural frequency. However, only a single mode survives under an engine order excitation of order n, which is clear by applying Theorem B.3 on page 192. Then the p^{th} modal forcing term reduces to

$$\begin{aligned}\mathbf{e}_p^{\mathcal{H}}\mathbf{f} &= \sum_{k=1}^{N} \frac{1}{\sqrt{N}} \bar{w}^{(k-1)(p-1)} f w^{n(k-1)} \\ &= \frac{f}{\sqrt{N}} \sum_{k=1}^{N} w^{(k-1)(n+1-p)} \\ &= \begin{cases} \sqrt{N} f, & n+1-p = mN \\ 0, & \text{otherwise} \end{cases}\end{aligned} \tag{2.35}$$

(m is an *arbitrary* integer), which shows that the force vector $\mathbf{f}$ is mutually orthogonal to all but one of the modal vectors $\mathbf{e}_p$, that is, only a *single* mode is excited. Therefore, given an engine order $n \in \mathbb{Z}_+$ and since $p \in \mathcal{N}$, the excited mode is

$$p = n \bmod N + 1. \tag{2.36}$$

Finally, since $(i-1)\varphi_{n+1} = \phi_i$, Equation (2.34) can be written as

$$q_i^{\text{ss}}(\tau) = \frac{f}{\bar{\omega}_{n+1}^2 - (n\sigma)^2} e^{j\phi_i} e^{jn\sigma\tau}, \qquad i \in \mathcal{N} \tag{2.37}$$

which is recognized to be in agreement with the results of the previous section.

Indeed, the process described above is significantly more laborious than the direct approach of the previous section, but many general features can be gleaned from the analysis. The eigenfrequency characteristics are described next, followed by a description of the normal modes in Section 2.4.4, and the system resonance structure is detailed in Section 2.4.5.

2.4.3 Eigenfrequency Characteristics

The dimensionless natural frequencies follow from Equation (2.32) and are given by

$$\bar{\omega}_p = \frac{\omega_p}{\omega_o} = \sqrt{1 + 2\nu^2(1 - \cos\varphi_p)}, \qquad p \in \mathcal{N} \tag{2.38}$$

which clearly exhibit the effect of the coupling. For $\nu = 0$ we recover $\bar{\omega}_p = 1$, or $\omega_p = \omega_o$ in dimensional form, which was used to nondimensionalize the model in Section 2.4.1. In this case the sectors are dynamically isolated and each has the same natural frequency. For nonzero coupling ($\nu \neq 0$) it is clear that there will be repeated natural frequencies, a degeneracy that is due to the circulant structure of $\mathbf{K}$. This is manifested in the cyclic term

$$\cos\varphi_p = \cos\left(\tfrac{2\pi(p-1)}{N}\right) = \mathrm{Re}\left(w_N^{p-1}\right), \tag{2.39}$$

which can be obtained by projecting the powers of the N^{th} roots of unity onto the real axis. (See Figure B.1 on page 191.) Multiplicity of the eigenfrequencies can also be visualized in Figure 2.5, which shows the dimensionless natural frequencies in terms of the diametral components (that is, the number of *nodal diameters*) in their attendant mode shapes versus the mode number p for weak and strong coupling and for odd and even N. These cyclic features are now described in terms of mode numbers in the sets $\mathcal{P}_{\mathrm{BTW}}^{\mathrm{O,E}}$, $\mathcal{P}_{\mathrm{FTW}}^{\mathrm{O,E}}$, and $\mathcal{P}_{\mathrm{SW}}^{\mathrm{O,E}}$, which are defined in Table 2.2. A description of the BTW, FTW, and SW designations of these sets is deferred to the next section.

The natural frequency corresponding to mode $p = 1 \in \mathcal{P}_{\mathrm{SW}}^{\mathrm{O,E}}$ (zero harmonic of Equation (2.39)) is distinct, but the remaining natural frequencies appear in repeated pairs, except for the case of even N, in which case the $p = (N+2)/2 \in \mathcal{P}_{\mathrm{SW}}^{\mathrm{E}}$ frequency ($N/2$ harmonic) is also distinct. There are $(N-1)/2$ such pairs if N is odd, and these correspond to mode numbers in $\mathcal{P}_{\mathrm{BTW}}^{\mathrm{O}}$ and $\mathcal{P}_{\mathrm{FTW}}^{\mathrm{O}}$, respectively. For even N there are $(N-2)/2$ repeated natural frequencies corresponding to mode numbers in $\mathcal{P}_{\mathrm{E}}^{\mathrm{BTW}}$ and $\mathcal{P}_{\mathrm{E}}^{\mathrm{FTW}}$. Finally, if $k \in \mathcal{P}_{\mathrm{BTW}}^{\mathrm{O,E}}$ then the mode number of the corresponding repeated eigenfrequency is $N + 2 - k \in \mathcal{P}_{\mathrm{FTW}}^{\mathrm{O,E}}$.

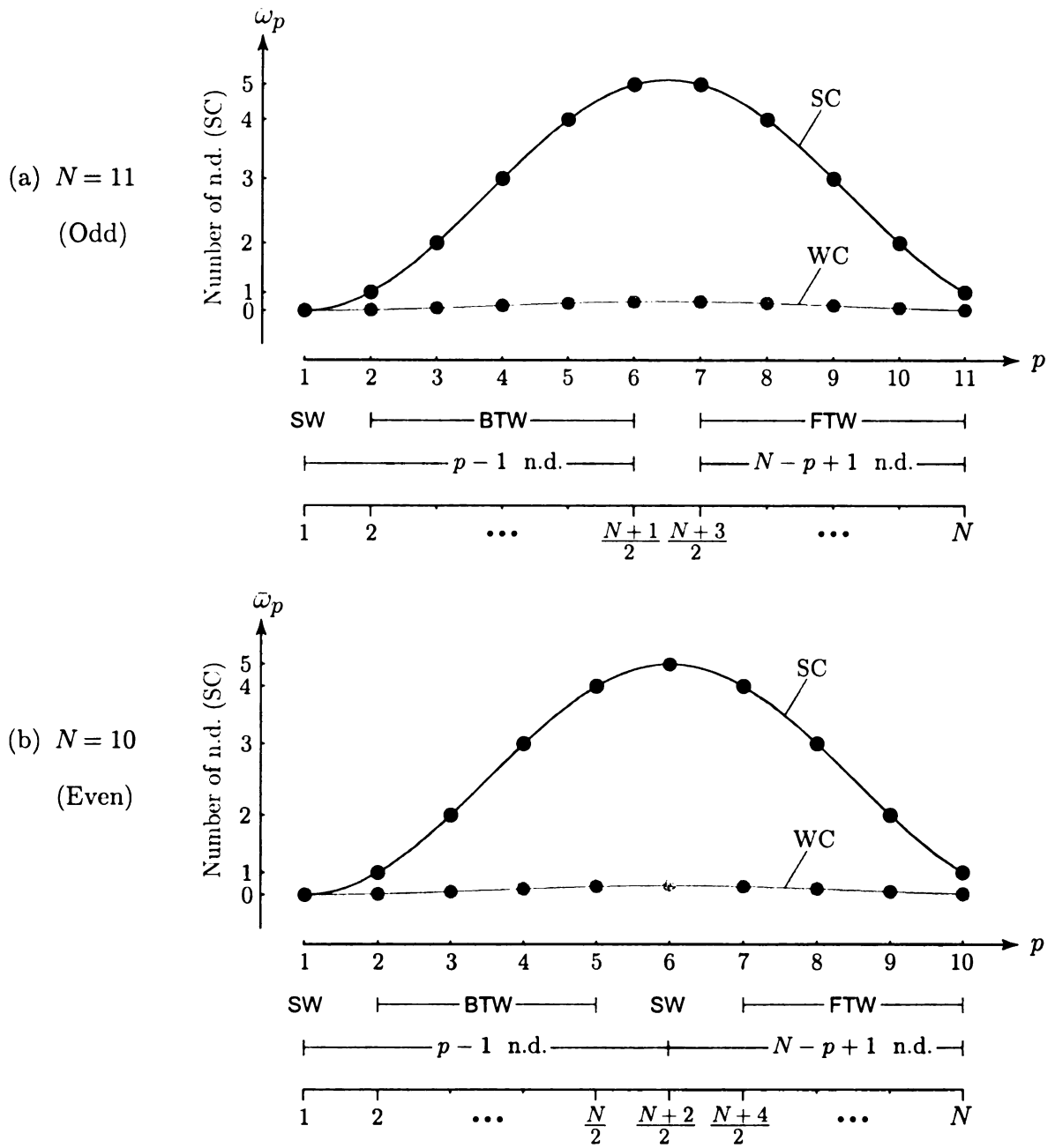

Figure 2.5. Dimensionless natural frequencies $\bar{\omega}_p$ in terms of the number of nodal diameters (n.d.) versus mode number p for weak coupling (WC) and strong coupling (SC): (a) $N = 11$ (odd) and (b) $N = 10$ (even). Also indicated below each figure is, for general N, the number of n.d. at each value of p and also the mode numbers corresponding to standing waves (SW), backward traveling waves (BTW), and forward traveling waves (FTW).

Table 2.2. Sets of mode numbers $p \in \mathcal{N} = \mathcal{P}^{\text{O,E}}_{\text{SW}} \bigcup \mathcal{P}^{\text{O,E}}_{\text{BTW}} \bigcup \mathcal{P}^{\text{O,E}}_{\text{FTW}}$ corresponding to standing wave (SW), backward traveling wave (BTW), and forward traveling wave (FTW) normal modes of free vibration for (a) odd N and (b) even N.

(a) Odd N	(b) Even N
$\mathcal{P}^{\text{O}}_{\text{SW}} = \{1\}$	$\mathcal{P}^{\text{E}}_{\text{SW}} = \left\{1, \frac{N+2}{2}\right\}$
$\mathcal{P}^{\text{O}}_{\text{BTW}} = \left\{p \in \mathbb{Z}_+ : 2 \leq n \leq \frac{N+1}{2}\right\}$	$\mathcal{P}^{\text{E}}_{\text{BTW}} = \left\{p \in \mathbb{Z}_+ : 2 \leq n \leq \frac{N}{2}\right\}$
$\mathcal{P}^{\text{O}}_{\text{FTW}} = \left\{p \in \mathbb{Z}_+ : \frac{N+3}{2} \leq n \leq N\right\}$	$\mathcal{P}^{\text{E}}_{\text{FTW}} = \left\{p \in \mathbb{Z}_+ : \frac{N+4}{2} \leq n \leq N\right\}$

The normal modes of vibration are described next, and it will be shown that each can be categorized as a SW, BTW, or FTW.

2.4.4 Normal Modes of Vibration

In Section 2.4.2 it was shown that Equation (2.21) can be decoupled via a unitary (similarity) transformation involving the Fourier matrix $\mathbf{E} = [\mathbf{e}_1, \mathbf{e}_2, \ldots, \mathbf{e}_N]$ and as a consequence $\mathbf{e}_p$ is the p^{th} normal mode of vibration corresponding to the natural frequency $\bar{\omega}_p$. In what follows these mode shapes are characterized by investigating the free response of the sysem, and it is shown that they are of the SW, BTW, or FTW variety.

The free response of the system in its p^{th} mode of vibration can be described by $\mathbf{q}^{(p)}(\tau) = a_p \mathbf{e}_p e^{j\bar{\omega}_p \tau}$, where a_p is a modal amplitude and the natural frequency $\bar{\omega}_p$ is defined by Equation (2.38). (There will generally be a phase angle as well, which is omitted since its presence does not affect the arguments to follow.) Noting that element i of $\mathbf{e}_p$ can be written as $w^{(p-1)(i-1)} = e^{j\varphi_p(i-1)}$ and for $i, p \in \mathcal{N}$ the free response of sector i can be written (in real form) as

$$q_i^{(p)}(\tau) = a_p \cos\left(\varphi_p(i-1) + \bar{\omega}_p \tau\right), \tag{2.40a}$$

$$= a_p \Phi_p(i - 1 + C_p \tau), \tag{2.40b}$$

where $C_p = \bar{\omega}_p / \varphi_p$ and the function $\Phi_k(\chi)$ is defined by Equation (2.16). Equa-

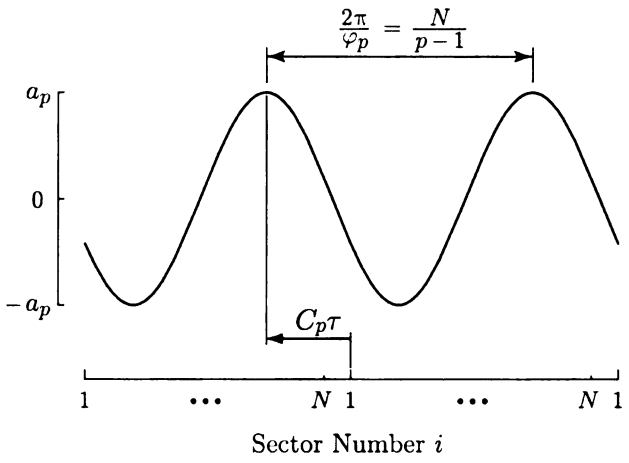

Figure 2.6. A backward traveling wave $a_p\Phi_p(i-1+C_p\tau) = a_p\cos(\varphi_p(i-1)+\bar{\omega}_p\tau)$ with amplitude a_p, wavelength $2\pi/\varphi_p = N/(p-1)$, and speed $C_p = \bar{\omega}_p/\varphi_p$.

tion (2.40) is a function of continuous time τ and it is discretized according to the sector number i. In this way, it is endowed with the same *discrete temporal* and *continuous spatial* duality that was described in Section 2.3.2 in the context of traveling wave dynamic loading (engine order excitation). That is, it can be regarded as (1) the time-response of individual (discrete) sectors, or (2) a continuous spacial variation of displacements among the sectors that evolves with increasing time (i.e., a traveling wave). The propagating waveform is strictly a BTW in the negative i-direction (descending sector number) with wavelength $2\pi/\varphi_p = N/(p-1)$ and speed C_p, an illustration of which is shown in Figure 2.6. However, depending on the value of p, this gives rise to SW, BTW, or FTW mode shapes, a property that follows analogously from the features described in Figure 2.3.

For the special case of $p = 1$ it is clear from Equation (2.40a) that each sector behaves identically with the same amplitude and the same phase since $\varphi_1 = 0$. An additional special case occurs when $p = (N+2)/2$ if N is even. Then $\varphi_{(N+2)/2} = \pi$ and each sector has the same amplitude but adjacent sectors oscillate with a 180-degree phase difference. Hence the vibration modes $p \in \mathcal{P}_{\text{SW}}^{\text{O,E}}$ correspond to SW mode shapes whose characteristics can be visualized in Figure 2.3b and Figure 2.3d

by replacing the amplitude F with a_p. The remaining mode shapes correspond to repeated natural frequencies and are either BTWs or FTWs. In particular, the normal modes $p \in \mathcal{P}_{\text{BTW}}^{\text{O,E}}$ (resp. $p \in \mathcal{P}_{\text{FTW}}^{\text{O,E}}$) are backward (resp. forward) traveling waves and can be visualized in Figure 2.3a (resp. Figure 2.3c). If mode $k \in \mathcal{P}_{\text{BTW}}^{\text{O,E}}$ is a BTW corresponding to a natural frequency $\bar{\omega}_k$, then the attendant FTW mode is $N+2-k \in \mathcal{P}_{\text{FTW}}^{\text{O,E}}$ corresponding to $\bar{\omega}_{N+2-k} = \bar{\omega}_k$.

Figure 2.7 illustrates the normal modes of free vibration for a model with $N = 100$ sectors. In this figure, the extent of the radial lines represents sector displacements; those appearing outside (resp. inside) the hub are to be interpreted as being positively (resp. negatively) displaced relative to their zero positions. Modes 1 and 51 are SWs and modes 2–50 (resp. 52–100) consist of backward (resp. forward) traveling waves. Finally, the number of nodal diameters can be clearly identified in Figure 2.7. For example, modes 4 and 98 feature 3 n.d.

2.4.5 Resonance Structure

In general, there may be a system resonance whenever the excitation frequency matches a natural frequency, that is, if $n\sigma = \bar{\omega}_p$ or $n\Omega = \omega_p$ in dimensional form. These *possible* resonances can be conveniently identified in a *Campbell diagram*, an example of which is shown in Figure 2.8a for a model with $N = 10$, $\nu = 0.5$, and for engine orders $n \in \mathcal{N}$. (The general case of $n \in \mathbb{Z}_+$ is considered below.) In this figure, the natural frequencies are plotted in terms of the dimensionless rotor speed and several *engine order lines* $n\sigma$ are superimposed. Possible resonances correspond to intersections of the order lines and eigenfrequency loci, and there are $(N+2)/2$ (resp. $(N+1)/2$) such possibilities for each engine order when N is odd (resp. even). In light of Equation (2.35), however, there is only a *single* resonance associated with each n under the traveling wave dynamic loading of Section 2.3 and it corresponds to the mode number given by Equation (2.36). These are indicated by black dots in

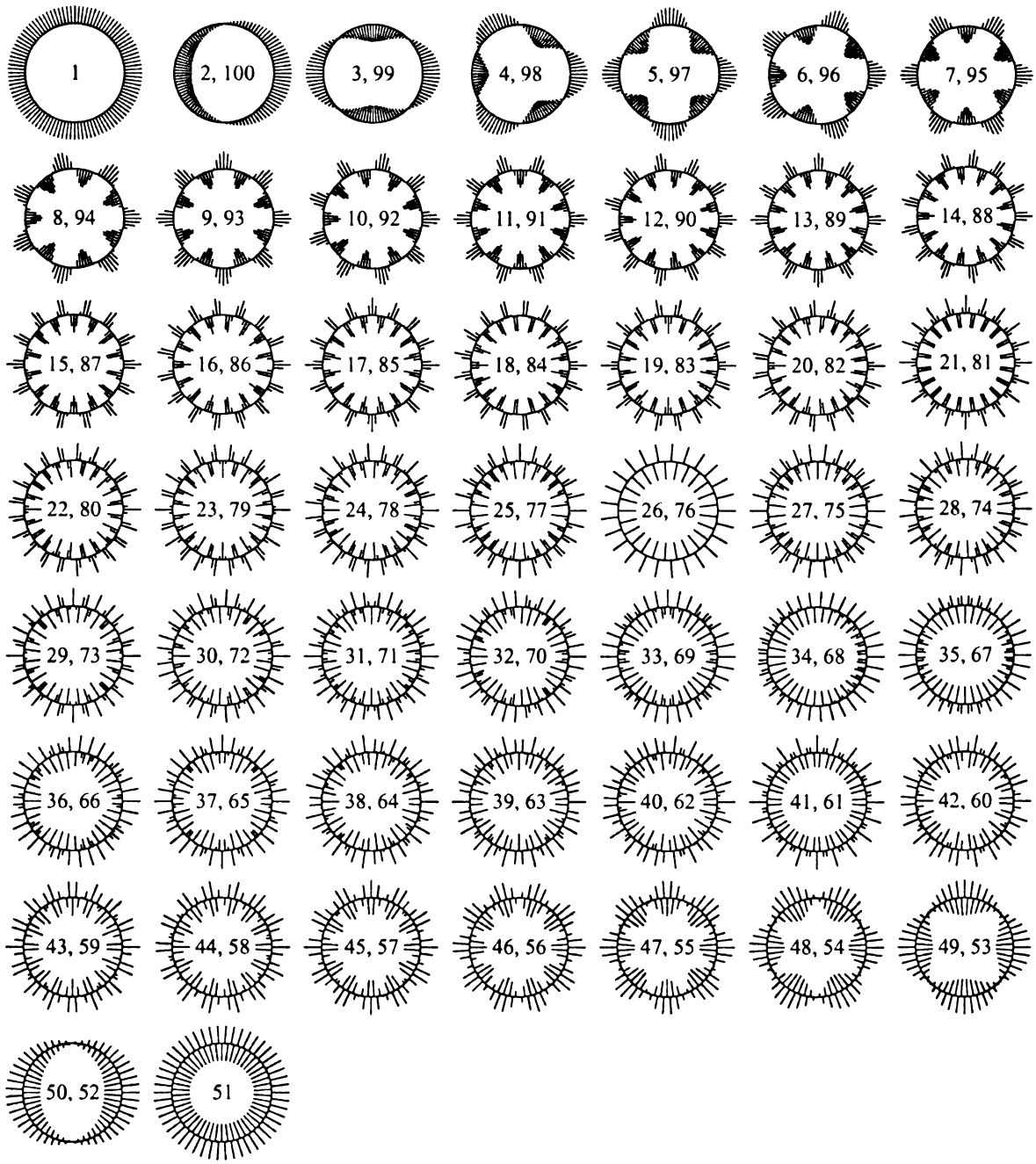

Figure 2.7. Normal modes of free vibration for a model with $N = 100$ sectors. Mode 1 consists of a SW, in which each sector oscillates with the same amplitude *and* phase. Mode 51 also corresponds to a SW, but neighboring oscillators oscillate exactly 180 degrees out of phase. Modes 2–50 (resp. 52–100) consist of BTWs (resp. FTWs).

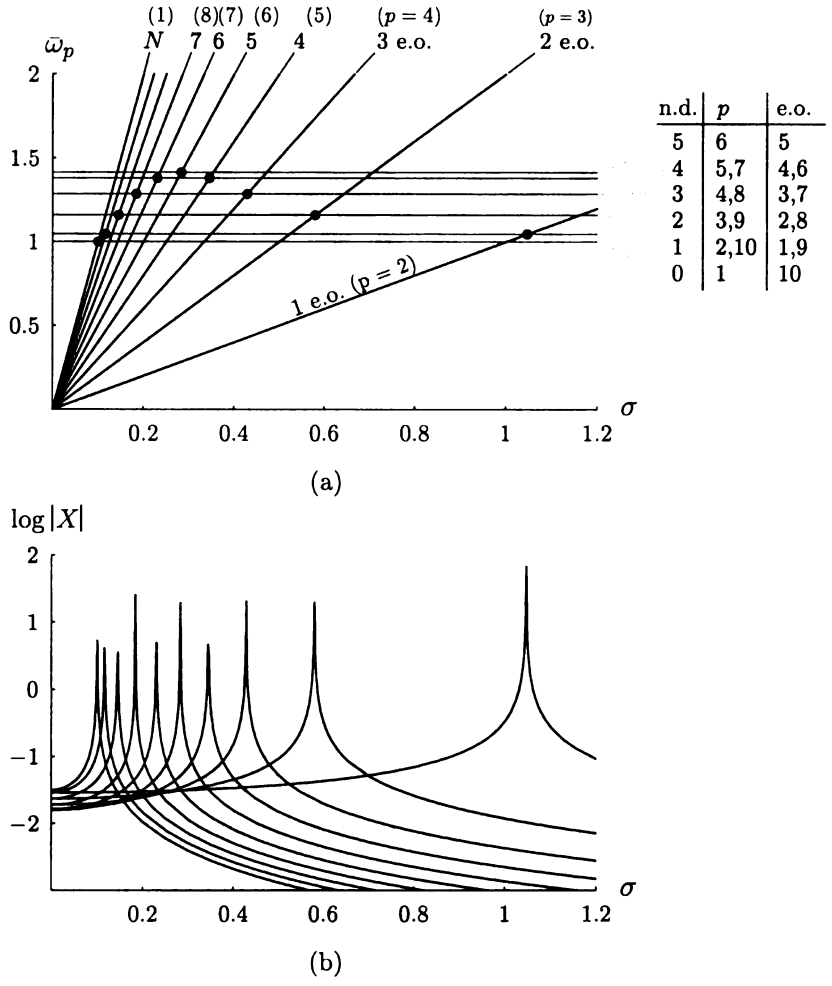

n.d.	p	e.o.
5	6	5
4	5,7	4,6
3	4,8	3,7
2	3,9	2,8
1	2,10	1,9
0	1	10

Figure 2.8. (a) Campbell diagram and (b) corresponding frequency response curves for $N = 10$, $\nu = 0.5$, $f = 0.01$, and $n = 1, \ldots, N$.

Figure 2.8a and the corresponding frequency response curves are shown in Figure 2.8b for a model with $f = 0.01$. For example, a 3 e.o. (resp. 7 e.o.) excitation gives rise to a resonance of the 4^{th} (resp. 8^{th}) mode, which is a BTW (resp. FTW) with 3 nodal diameters. (The TW and n.d. designations can be verified in Figure 2.5.)

The basic resonance structure shown in Figure 2.8a for $n = 1, \ldots, N$ essentially aliases relative to the total number of sectors, in the sense that the excited modes for $n = mN+1, \ldots, (m+1)N$ with $m \in \mathbb{Z}_+$ are the *same* as those for $n = 1, \ldots, N$. This

Table 2.3. Condition on the engine order $n \in \mathbb{Z}_+$ to excite mode $p \in \mathcal{N}$ for $N = 10$.

Excited Mode	Conditions on Engine Order n
1	$mN = 10, 20, 30, \ldots$
2	$1 + mN = 1, 11, 21, \ldots$
3	$2 + mN = 2, 12, 22, \ldots$
$\vdots$	$\vdots$
$N - 1$	$N - 2 + mN = 8, 18, 28, \ldots$
N	$N - 1 + mN = 9, 19, 29, \ldots$

follows from the orthogonality condition given by Equation (2.35) and is manifested in Equation (2.36), which gives a relationship for the excited mode in terms of the engine order n and total number of sectors N. Since $n > 0$ by assumption (see Section 2.3) the first mode ($p = 1$) is excited when $n = mN = 10, 20, 30, \ldots$, the second mode ($p = 2$) is excited when $n = 1 + mN = 1, 11, 21, \ldots$, and so on. Table 2.3 summarizes these conditions for a model with $N = 10$ sectors and the corresponding resonance structure for $n = N, \ldots, 20N$ is shown in Figure 2.9a. Each collection of resonance points $n = mN + 1, \ldots, (m+1)N$ is qualitatively the same in structure. However, for $m > 1$ the resonances become increasingly clustered, which is shown in Figure 2.9b for $n = N, \ldots, 2N$ and in Figure 2.9c for $n = 2N, \ldots, 3N$. In terms of the sets defined in Table 2.1 and Table 2.2, an engine order $n \bmod N \in \mathcal{N}_{\mathrm{SW}}^{\mathrm{O,E}}$ excites a SW mode $p \in \mathcal{P}_{\mathrm{SW}}^{\mathrm{O,E}}$. Similarly, an engine order $n \bmod N \in \mathcal{N}_{\mathrm{FTW}}^{\mathrm{O,E}}$ (resp. $n \bmod N \in \mathcal{N}_{\mathrm{FTW}}^{\mathrm{O,E}}$) excites a FTW (resp. BTW) mode $p \in \mathcal{P}_{\mathrm{FTW}}^{\mathrm{O,E}}$ (resp. $p \in \mathcal{P}_{\mathrm{BTW}}^{\mathrm{O,E}}$).

2.5 Vibration Absorbers

2.5.1 Introduction

When an engineering structure experiences unwanted levels of vibration due to periodic excitations acting on its constituent parts it may be impractical (or even impos-

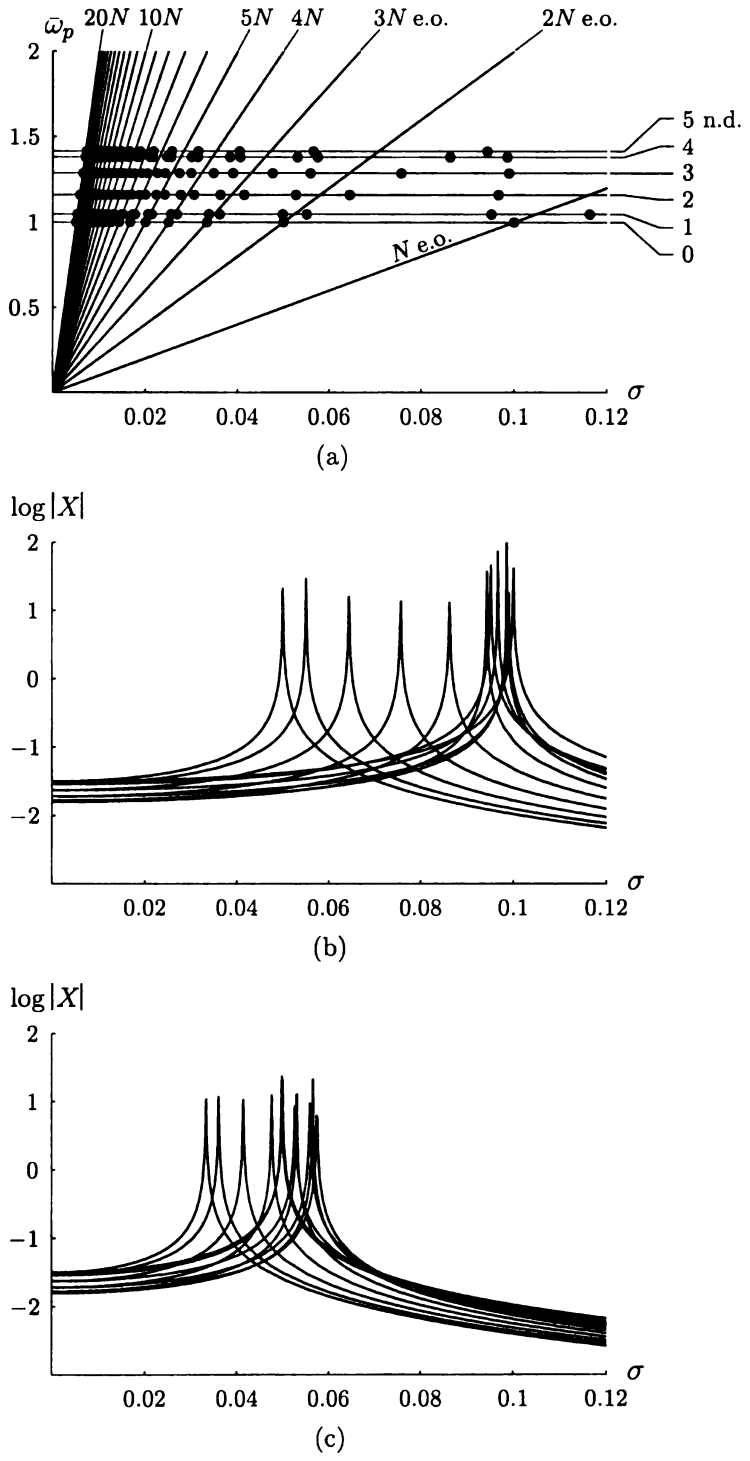

Figure 2.9. (a) Campbell diagram for $N = 10$, $\nu = 0.5$, $f = 0.01$, and $n = 1, \ldots, 20N$ and the corresponding frequency response curves for (b) $n = N, \ldots, 2N$ and (c) $n = 2N, \ldots, 3N$.

sible) to change the makeup of the system to improve its vibratory characteristics, or to change or eliminate the source of the excitation. In these cases tuned vibration absorbers offer a possible solution.

The notion of a vibration absorber was introduced by Frahm [4] in a United States patent in 1911, but it was Den Hartog [5, 6] who first carried out systematic studies on tuned absorbers, including an optimal choice of parameters. Tuned vibration absorbers are auxiliary components that are attached to a primary system to eliminate, or otherwise reduce its steady-state motions. This is done through a particular choice of absorber parameters, typically by setting the natural frequency of the absorber close to the most problematic harmonic of the excitation. The absorber is said to be *exactly tuned* if these frequencies match identically; otherwise, the absorber is said to be *detuned.*

We shall discuss two varieties of vibration absorbers: the classical *frequency-tuned* dynamic vibration absorber (DVA) in Section 2.5.2 and the *order-tuned* centrifugal pendulum vibration absorber (CPVA) in Section 2.5.3. The DVA, which is shown in Figure 2.10a, relies on an elastic element for its restoring force, whereas the CPVA, examples of which are shown in Figure 2.10b (circular path) and Figure 2.10c (general path), employ the centrifugal field due to rotation of the primary system. Order-tuned absorbers play a key role in this dissertation.

2.5.2 The Frequency-Tuned Dynamic Vibration Absorber

Here we highlight the classical theory of the frequency-tuned DVA due to Den Hartog [6]. Consider the 2–DOF system shown in Figure 2.10a. It consists of a primary system (M, C, K) that is harmonically excited by $f(t) = f_o e^{j\omega t}$, where f_o is the strength of the excitation and ω is its (constant) frequency, t is time, and $j = \sqrt{-1}$. When this primary system is isolated (i.e., when the absorber is not attached) it has a resonance at $\omega_N = \sqrt{K/M}$ (its undamped natural frequency), which is indicated

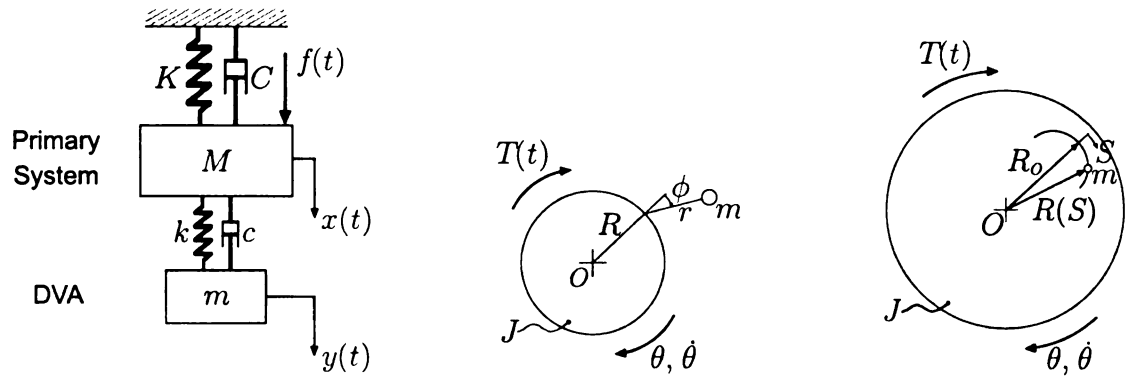

(a) DVA (b) Circular Path CPVA (c) General Path CPVA

Figure 2.10. Tuned vibration absorbers: (a) DVA; (b) Circular Path CPVA; (c) General Path CPVA.

by the dashed lines in Figure 2.11. A DVA subsystem (m, c, k) is attached to M and its parameters are chosen to attenuate the vibratory response of the primary system near $\omega = \omega_N$. The undamped natural frequency of the *isolated* DVA is denoted by $\omega_n = k/m$.

The governing equations of motion for the composite system in Figure 2.10a are given by

$$\mathbf{M}\ddot{\mathbf{x}} + \mathbf{C}\dot{\mathbf{x}} + \mathbf{K}\mathbf{x} = \mathbf{f}e^{j\omega t}, \tag{2.41}$$

where $\mathbf{x} = (x, y)^T$ and $\mathbf{f} = (f_o, 0)^T$ are displacement and forcing vectors and

$$\mathbf{M} = \begin{bmatrix} M & 0 \\ 0 & m \end{bmatrix}, \qquad \mathbf{C} = \begin{bmatrix} C+c & -c \\ -c & c \end{bmatrix}, \qquad \mathbf{K} = \begin{bmatrix} K+k & -k \\ -k & k \end{bmatrix},$$

are the mass, damping, and stiffness matrices. Assuming harmonic motion, the steady-state solution to Equation (2.41) follows in the usual way and, for non-resonant forcing, is given by

$$\begin{bmatrix} x(t) \\ y(t) \end{bmatrix} = \begin{bmatrix} X \\ Y \end{bmatrix} e^{j\omega t}, \tag{2.42}$$

where

$$\left.\begin{aligned} X &= \frac{f_o\left(k - m\omega^2 + j\omega c\right)}{\Gamma} \\ Y &= \frac{f_o\left(k + j\omega c\right)}{\Gamma} \end{aligned}\right\} \tag{2.43}$$

are the steady-state amplitudes of the primary and absorber systems, respectively, and

$$\Gamma = \Big(K + k - m\omega^2 + j(C + c)\omega\Big)\Big(k - m\omega^2 + jc\omega\Big) - (k + jc\omega)^2 . \tag{2.44}$$

We first consider a tuning strategy for the undamped DVA, that is, for $c = 0$. It will be shown that the undamped absorber can be designed to completely eliminate the steady-state motions of M—independent of C—but that the resulting design is not robust to frequency drift. It is then shown how this situation can be improved by including damping in the absorber model.

Absorber Tuning: Undamped DVA

In the absence of absorber damping ($c = 0$), the condition $\omega^2 = k/m$ is sufficient to eliminate steady-state motions of M, which is clear from the first element of Equation (2.43). Since we are interested in improving the response of the primary system near its resonance $\omega \cong \omega_N = \sqrt{K/M}$, the absorber should be designed such that

$$\omega^2 = \omega_N^2 = \omega_n^2 \qquad \text{or} \qquad \omega^2 = \frac{K}{M} = \frac{k}{m}, \tag{2.45}$$

which is the *absorber tuning*. That is, the absorber is designed such that its natural frequency matches that of the isolated primary system. This is accomplished by choosing the absorber parameters m and k such that Equation (2.45) is satisfied.

If the undamped absorber is tuned according to Equation (2.45), then

$$\left.\begin{aligned} X &= 0 \\ Y &= -f_o/k \end{aligned}\right\} \tag{2.46}$$

(independent of C) and the steady-state motions of the primary system are completely eliminated. Under this tuning strategy the absorber oscillates out of phase with respect to the excitation, which is clear from the sign of Y, and it exerts at all times a force equal in magnitude to the applied force $f(t)$. The resulting frequency response of the primary system is given by the solid lines in Figure 2.11.

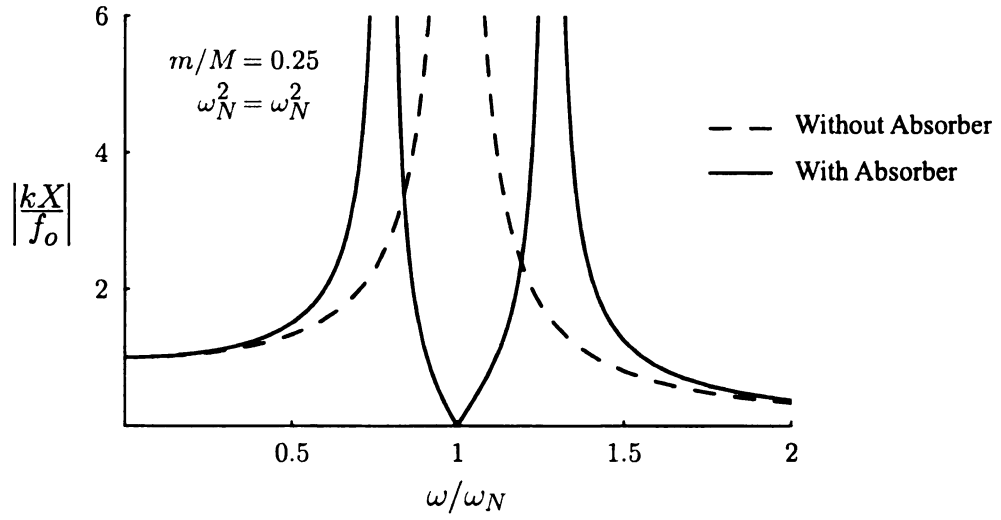

Figure 2.11. Dimensionless amplitude of the primary system versus dimensionless excitation frequency: effect of an undamped vibration absorber ($c = 0$) on the response of the undamped primary system ($C = 0$).

From a design standpoint, there are two different ways to acheive the absorber tuning:

1. If the allowable amplitude Y is prescribed, set $k = |-f_o/Y| = f_o/Y$ (from Eq. (2.46)). Then the required absorber mass follows from Eq. (2.45) and is given by $m = k/\omega_N^2 = \left(\frac{k}{K}\right)M$.

2. If the absorber mass m is prescribed, set $k = m\omega_N^2 = \left(\frac{m}{M}\right)K$ (from Eq. (2.45)). Then the resulting absorber amplitude is Y and is given by Eq. (2.46).

In the first strategy the absorber is assumed to have a limited space in which to operate and the designer is not at liberty to arbitrarily choose its mass. Conversely, if the absorber mass is specified (typically it is made as small as possible), then the corresponding absorber amplitude is automatically prescribed.

Absorber Tuning: Damped DVA

The undamped DVA just described is successful in that it removes the original resonance peak in the response of the primary system, but it does so at the expense of an additional resonance, which is shown in Figure 2.11. This may be undesirable

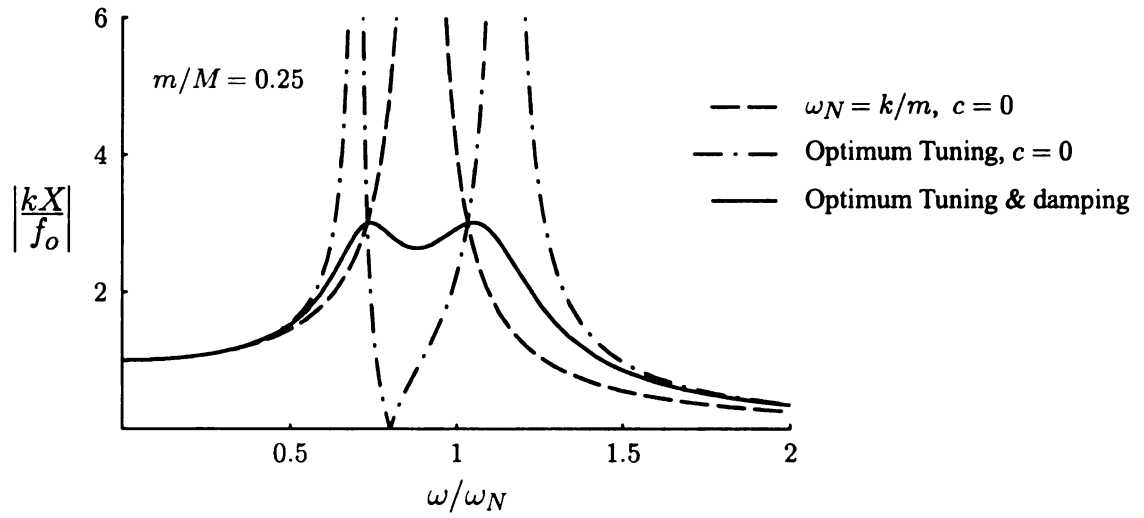

Figure 2.12. Dimensionless amplitude of the primary system versus dimensionless excitation frequency: effect of a damped vibration absorber ($c \neq 0$) on the response of the undamped primary system ($C = 0$).

for a machine that must pass through the first resonance in order to reach its steady-state operating speed, and also if it exhibits significant frequency drift under normal operation. The composite system can be made robust to these situations by including damping in the absorber model. The basic idea is to first optimally detune the absorber away from the perfect tuning given by Equation (2.45), which assures that the two points shared by all frequency response curves of the composite system have the same ordinate value. Then the absorber damping is adjusted to optimize the two resonance peaks. Den Hartog [6] was the first to propose such an optimization scheme, and the reader is referred to his work for details.[5] See [67–69] for additional work related to the optimum design of damped vibration absorbers. An example plot of an optimally tuned system with a damped DVA is shown in Figure 2.12.

[5]The reader should note that Equation (3.24) on page 96 of [6] has a typographical error. The damping terms should be $(2(c/c_c)g)^2$, not $(2(c/c_c)gf)^2$. This equation is correctly reported in [66].

2.5.3 The Order-Tuned Centrifugal Pendulum Vibration Absorber

The classical frequency-tuned DVA of Section 2.5.2 is effective only at a particular frequency and it works well for systems with steady operating speeds. However, absorbers of this type are not suitable for many systems with rotating assemblies, such as an automobile or jet engine, which are characterized by varying speeds and forces that occur at orders of rotation [7]. Here we briefly highlight the essential features of a centrifugal pendulum vibration absorber (CPVA) and indicate how it can be tuned to a given *order* of rotation, rather than to a fixed frequency, and is hence effective at *all* speeds.

The system shown in Figure 2.10b on page 40 captures the essential features of a typical CPVA. It consists of a rigid rotor (primary system) with polar moment of inertia J and radius R, which rotates about a fixed axis at O. The primary system is harmonically excited by a torque of the form $T(t) = T_o + \tilde{T}e^{jn\Omega t}$, where $\tilde{T}$ is the strength of the fluctuating excitation, n is its order, t is time, Ω is the speed of the rotor, and T_o is the mean torque. A pendulum absorber of length r and mass m is attached to the periphery of the rotor and its parameters are chosen to reduce the torsional oscillations of the primary system.

An analysis similar to the one carried out in Section 2.5.2 for the frequency-tuned DVA shows that the steady-state torsional oscillations of the rotor can be eliminated completely by setting the undamped natural frequency of the absorber to that of the excitation. A key difference, however, is that the absorber's natural frequency is *proportional to the rotor speed* [70]. That is,

$$\omega_n = \sqrt{\frac{R}{r}}\,\Omega \equiv \tilde{n}\Omega, \tag{2.47}$$

where $\tilde{n} = \sqrt{R/r}$ is defined as the *linear tuning order* of the absorber. This gives rise to a tuning condition $n = \tilde{n}$ (the so-called *order-tuning*) which is *independent* of the rotor speed. In this way, the absorber tuning is effective over the full range of

possible rotor speeds.

Similar statements can be made for the more general, arbitrary-path absorber system shown in Figure 2.10c, which has been exhaustively studied by Shaw and coworkers. The reader is referred to a wealth of existing literature for the theoretical details [14, 18, 20–23, 25, 27, 71, 72] and experimental validation [28–30, 73–75].

2.6 Concluding Remarks

An overview of relevant theoretical background has been given, including some mathematical preliminaries, a detailed account of engine order excitation and its application to a prototypical cyclic system, and on the basic operation and features of frequency- and order-tuned vibration absorbers.

Key mathematical concepts were briefly stated in Section 2.2, including the Kronecker product, the Fourier matrix, circulant matrices, and the diagonalization of circulants. This was done in a way that elicits ease of reference; a much more detailed account of the required mathematical machinery is given in Appendix A and Appendix B, including many of the proofs.

A mathematical model for engine order excitation was developed in Section 2.3. It was described in terms of a *discrete temporal* variation of dynamic loading applied to individual blades as well as a *continuous spatial* variation of the excitation strength relative to the rotating hub, and the former was subsequently categorized as a BTW, SW, or FTW. The essence of these two interpretations of the excitation is captured in Figure 2.2.

A detailed account of the vibration characteristics of a generic linear cyclic system, with nearest-neighbor elastic coupling, under engine order excitation was given in Section 2.4, including a description of its rich eigenfrequency and resonance structures for large engine orders. The essence of these features are captured in Figure 2.8 and Figure 2.9.

Finally, the basic theory of frequency-tuned dynamic vibration absorbers was highlighted in Section 2.5 and this was compared to that of order-tuned absorbers. A key feature in the latter is that the absorbers are tuned to a given order of rotation, rather than to a fixed frequency.

Mathematical models are developed next for arbitrary-path, order-tuned absorbers fitted to a bladed disk assembly under engine order excitation.

CHAPTER 3

Mathematical Models

3.1 Introduction

A general mathematical model is developed for the bladed disk assemblies of interest fitted with arbitrary-path, order-tuned vibration absorbers, from which a number of specific models to be considered in subsequent chapters are distilled. The chapter begins with a brief overview of typical modeling approaches in Section 3.2, including motivation for the simplified lumped-parameter blade models to be employed. The geometry of an arbitrary absorber path is then described in Section 3.3, which forms a kinematic model for a general-path absorber, and the desired model for a nominally-cyclic bladed disk assembly fitted with such absorbers is formulated in Section 3.4. This general model forms the basis for all of the analysis to follow, and a number of simplifications and reductions are carried out to put it in a more tractable form. Specifically, the equations of motion for the case of circular-path absorbers with motion-limiting stops are derived in Section 3.5, and these are subsequently linearized for small blade and absorber motions and cast into a form that is employed in Chapter 4. Reduction of the full nonlinear equations of motion via scaling and averaging is deferred to Chapter 5, where the nonlinear system dynamics are estimated for the case of a single isolated blade/absorber and for the cyclically-coupled system with identical sectors. In these nonlinear models a specific two-parameter family of

paths is employed, which is derived in Section 3.4.4. Finally, blade and absorber damping levels are estimated in Section 3.6 and a summary of the models is given in Section 3.7.

3.2 Modeling Approach

3.2.1 Absorber and Blade Models

For the applications of interest an absorber realization may consist of a spherical mass that rolls on a machined path (or more generally a surface) relative to the primary system, in this case a blade [76]. By ignoring the effects of rotational inertia, it can be modeled by a mass particle that translates along a prescribed curvilinear path relative to the blade. (Realistic absorber masses are very small relative to those of the blades due to strict limitations on rattling space.) If in addition the absorber path is circular, then it can be modeled by a simple pendulum attached to the primary structure.

Accurate modeling of the bladed disk assemblies of interest, a typical representation of which is shown in Figure 3.1a, can be significantly more complicated due to their complex geometries. The blades are characterized by significant transverse curvature (camber), in addition to variations in thickness, width, and curvature along their chordwise lengths. They are generally attached at their roots to the periphery of a circular disk by means of, for example, a dovetail joint and the composite assembly forms one stage in a turbomachine [77]. As our understanding of the dynamics of such bladed disk assemblies has improved, so too has the level of sophistication of the attendant modeling and analysis techniques. Typical models generally fall into three basic categories and they are briefly presented below in order of increasing complexity, both in terms of the dynamic phenomena that they are able to capture and in the corresponding analysis.

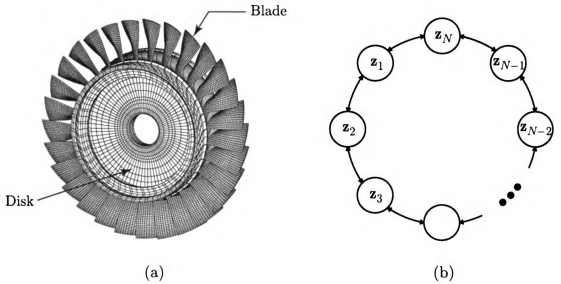

Figure 3.1. (a) Finite element model of a bladed disk assembly (reproduced with permission from [3]); (b) General cyclic system with N identical cells and nearest-neighbor coupling.

The first and undisputedly simplest models assume lumped parameters and essentially consist of a cyclic chain of nominally identical oscillators [36, 47, 58, 78–80]. (See Figure 3.1b.) The analysis involved with such models is relatively simple, especially if one assumes that each sector is identical, i.e., that the structure is perfectly cyclic.[1] Then the fully coupled system can be reduced to a set of reduced-order models via a transformation based on its cyclic symmetry, similarly to the way it was done in Section 2.4.2. This often offers significant insight into the overall system behavior, even if a very small number of DOF is employed. While these models are very attractive due to their simplicity and are able capture some very rich dynamics of cyclically-symmetric structures, they do have serious limitations. Clearly, one cannot expect to capture all of the complicated mode shapes of the actual system, such as plate- or shell-type modes of the hub. Moreover, parameter identification can be extremely difficult if it is desired to use such models to predict specific behavior in an actual

[1]Such a structure is said to be perfectly *tuned*. When there are small differences among the sectors, due to material tolerances, in-service wear, and so on, the structure is said to be *mistuned*. This designation is not to be confused with intentional under- or over-tuning of the absorbers, which is referred to as *detuning*. (See Section 4.4.)

structural system [36].

The second type of models employ distributed-parameter elements and are therefore able to satisfactorily capture more complicated normal modes, including those that involve flexure of the rotating hub, but at the expense of a significantly more involved analysis [9, 81, 82]. For example, the transverse blade vibrations may be captured by cantilevered beams, provided that the disk is sufficiently stiff and the blades are sufficiently long relative to the hub dimensions (large aspect ratio). Classical beam theory breaks down for smaller aspect ratios but can be replaced by a more general shell theory. Again, while such an approach offers higher-fidelity modeling, it is accompanied by more difficult and expensive analyses by means of, for example, Rayleigh/Ritz/Galerkin methods, variational techniques, transfer matrices, finite elements, and numerical methods [77].

Finally, the third modeling approach involves a full finite element representation of a real bladed disk assembly [3, 83–86], such as the compressor stage shown in Figure 3.1a. A finite element model is typically generated for only one sector and, assuming that all sectors are identical, cyclic symmetry can be used to calculate the free and forced response much more efficiently than by modeling the entire system. While this approach offers the highest-fidelity modeling, the computation involved can be prohibitively high. This is especially true for large industrial stages with complicated geometry or if mistuning is included, which causes possibly drastic changes in the dynamics due to a disruption of the cyclic symmetry. Many realizations of randomly mistuned rotors must be run in order to accurately assess the full statistics of the blade response. This is generally not feasible due to the size of an industrial finite element model of a bladed disk, which can run into the millions of DOF. However, advanced reduced-order modeling techniques have been developed by Pierre *et al.* and others since the 1990s [85–89], which offer a more tractable finite element analysis.

3.2.2 Motivation for Lumped-Parameter Blade Models

The aim of this dissertation is to investigate the performance of centrifugally-driven, *order-tuned absorbers* to attenuate vibrations in *cyclic rotating flexible structures* subjected to traveling-wave dynamic loading. These two classes of systems are special cases of *systems of vibration absorbers* and *nominally cyclic systems*, respectively, both of which have been extensively studied in many contexts and, taken individually, each forms a very mature body of research. However, at the time of writing there have been no systematic analytical treatments of vibration absorbers *applied to* nominally cyclic systems, and it is thus appropriate to begin such an effort with simplified, lumped-parameter models. In what follows, a number of such models are developed, the analysis of which forms the remainder of this thesis. The applications of interest are rotating flexible structures—bladed disk assemblies in particular—and the work is carried out in this context, though the methodology and results should also be applicable to address vibration issues in other systems with nominal cyclicity.

A kinematic model for the absorbers is developed first by quantifying the geometry of an arbitrary path.

3.3 The Geometry of an Arbitrary Absorber Path

This section describes in general terms the geometry of the absorber paths, which prescribe their positions relative to the primary systems, or blades. Key results are relationships among the path variables, which are described in Section 3.3.1 and an expression for the tangent angle of each path, which is given in Section 3.3.2. These are employed in Section 3.4, where the equations of motion for a bladed disk assembly fitted with general-path absorbers are derived.

Consider the i^{th} general path shown in Figure 3.2. It can be described relative to a basepoint O by the radius vector $\mathbf{R}_i(S_i) = R_i(S_i)\hat{\mathbf{e}}_i^R$, where S_i is the arc length

along the path relative to an origin at its vertex V. The angle subtended by S_i is denoted by $\vartheta_i(S_i)$ and the distance from the basepoint to the path vertex is given by $R_i(0) = R_{oi} = \alpha_i L_i + d_i$, where α_i and L_i are defined in Section 3.4 and d_i is the local radius of curvature at V. Physically, the absorbers may have rattling space limits, which are denoted by $\pm S_{oi}$, and in such cases their displacements are restricted such that $|S_i| \leq S_{oi}$. The path could also be described in terms of the length ρ_i and angle ψ_i. A circular path is obtained by restricting $\rho_i = d_i = \text{constant}$, which is indicated by the dashed lines in Figure 3.2. Finally, the paths are generally assumed to be symmetric about their vertices at $S_i = 0$ implying that $R_i(S_i) = R_i(-S_i)$, i.e., that each $R_i(S_i)$ is an *even* function in S_i. However, this assumption is formally introduced in later developments when specific paths are chosen for the analysis. In what follows, there are no assumptions built into the absorber paths other than their gross placement relative to the blades.

Relationships between the path variables R_i, S_i, and ϑ_i are derived next and the angle ς_i between the radius and tangent unit vectors $\hat{\mathbf{e}}_i^R$ and $\hat{\mathbf{e}}_i^S$ is subsequently quantified. We draw liberally from the development in [90].

3.3.1 Fundamental Relationship Between Path Variables

Let P be an arbitrary position along the general path corresponding to $R_i, S_i, \vartheta_i > 0$ and let Q correspond to $R_i + \delta R_i$, $S_i + \delta S_i$, and $\vartheta_i + \delta\vartheta_i$, where $\delta R_i, \delta S_i, \delta\vartheta_i > 0$ are small additional increments. Then relationships between the path variables can be obtained by considering the triangle PQM in Figure 3.2. If $\delta c_i = \mathsf{PQ}$, it follows from $(\mathsf{PQ})^2 = (\mathsf{PM})^2 + (\mathsf{MQ})^2$ that

$$\left(\frac{\delta c_i}{\delta\vartheta_i}\right)^2 = \left(R_i \frac{\sin\delta\vartheta_i}{\delta\vartheta_i}\right)^2 + \left(\frac{\delta R_i}{\delta\vartheta_i} + R_i \sin(\delta\vartheta_i/2)\frac{\sin(\delta\vartheta_i/2)}{\delta\vartheta_i/2}\right)^2,$$

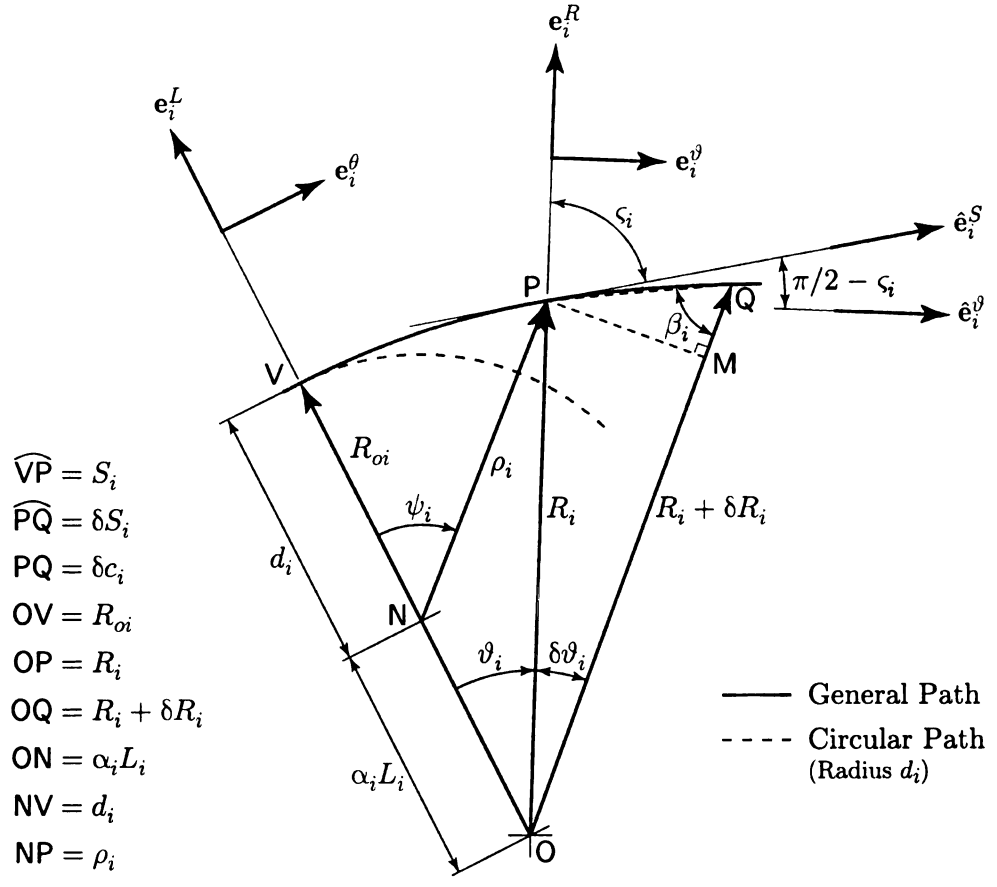

Figure 3.2. Geometry of a general absorber path.

where we have divided through by $(\delta\vartheta_i)^2$. Then

$$\left(\frac{\delta S_i}{\delta\vartheta_i}\right)^2 = \left(\frac{\delta S_i}{\delta c_i}\frac{\delta c_i}{\delta\vartheta_i}\right)^2$$
$$= \left(\frac{\delta S_i}{\delta c_i}\right)^2\left[\left(R_i\frac{\sin\delta\vartheta_i}{\delta\vartheta_i}\right)^2 + \left(\frac{\delta R_i}{\delta\vartheta_i} + R_i\sin(\delta\vartheta_i/2)\frac{\sin(\delta\vartheta_i/2)}{\delta\vartheta_i/2}\right)^2\right].$$

In the limit as $\mathsf{Q} \to \mathsf{P}$ (that is, $\delta\vartheta_i \to 0$) it follows that

$$\left(\frac{dS_i}{d\vartheta_i}\right)^2 = (1)^2\left[(R_i(1))^2 + \left(\frac{dR_i}{d\vartheta_i} + R_i(0)(1)\right)^2\right],$$

or

$$(dS_i)^2 = (R_i d\vartheta_i)^2 + (dR_i)^2. \tag{3.1}$$

Equation (3.1) gives the fundamental relationship between the path variables S_i, R_i, and ϑ_i. By dividing through by $(d\vartheta_i)^2$ and $(dS_i)^2$ the equivalent expressions

$$\frac{dS_i}{d\vartheta_i} = \sqrt{R_i^2 + \left(\frac{dR_i}{d\vartheta_i}\right)^2}, \tag{3.2a}$$

$$\Gamma_i \equiv R_i\frac{d\vartheta_i}{dS_i} = \sqrt{1 - \left(\frac{dR_i}{dS_i}\right)^2}, \tag{3.2b}$$

easily follow, which are employed in the next section and elsewhere in the thesis. In light of their frequent appearance in the subsequent analysis, the expressions appearing in Equation (3.2b) are denoted by Γ_i. Then the angle subtended by S_i is given by the integral

$$\vartheta_i(S_i) = \int_0^{S_i}\frac{\Gamma_i(\chi)}{R_i(\chi)}d\chi. \tag{3.3}$$

Next the angle between the unit vectors $\hat{\mathbf{e}}_i^R$ and $\hat{\mathbf{e}}_i^S$ is quantified.

3.3.2 Angle Between Radius Vector and Tangent

In Figure 3.2 consider the ratio

$$\tan\beta_i = \frac{\mathsf{MP}}{\mathsf{MQ}} = \frac{R_i\sin\delta\vartheta_i}{\delta R_i + 2R_i\sin^2(\delta\vartheta_i/2)} = \frac{R_i\frac{\sin\delta\vartheta_i}{\delta\vartheta_i}}{\frac{\delta R_i}{\delta\vartheta_i} + 2R_i\sin(\delta\vartheta_i/2)\frac{\sin(\delta\vartheta_i/2)}{\delta\vartheta_i/2}}, \tag{3.4}$$

where $\mathsf{MP} = R_i \sin \delta\vartheta_i$ has been employed and also

$$\begin{aligned}
\mathsf{MQ} &= \mathsf{OQ} - \mathsf{OM} \\
&= R_i + \delta R_i - R_i \cos \delta\vartheta_i \\
&= \delta R_i + R_i(1 - \cos \delta\vartheta_i) \\
&= \delta R_i + 2R_i \sin^2(\delta\vartheta_i/2).
\end{aligned}$$

In the limit as $\mathsf{Q} \to \mathsf{P}$ (that is, $\delta\vartheta_i \to 0$), $\beta_i \to \varsigma_i$ and it follows from Equation (3.4) that

$$\begin{aligned}
\tan \varsigma_i &= \lim_{\delta\vartheta_i \to 0} \tan \beta_i \\
&= \frac{R_i(1)}{\frac{dR_i}{d\vartheta_i} + 2R_i(0)(1)} \\
&= R_i \frac{d\vartheta_i}{dR_i},
\end{aligned} \tag{3.5}$$

which is an expression for ς_i in terms of R_i and ϑ_i. Expressions for $\sin \varsigma_i$ and $\cos \varsigma_i$, which will be needed in subsequent sections, can be obtained as follows. Consider

$$\begin{aligned}
\frac{dS_i}{dR_i} = \frac{dS_i}{d\vartheta_i}\frac{d\vartheta_i}{dR_i} &= \sqrt{R_i^2 + \left(\frac{dR_i}{d\vartheta_i}\right)^2}\,\frac{d\vartheta_i}{dR_i} && \text{(from Eqn. (3.2a))} \\
&= \sqrt{R_i^2\left(\frac{d\vartheta_i}{dR_i}\right)^2 + \left(\frac{dR_i}{d\vartheta_i}\frac{d\vartheta_i}{dR_i}\right)^2} \\
&= \sqrt{1 + \left(R_i\frac{d\vartheta_i}{dR_i}\right)^2} \\
&= \sqrt{1 + \tan^2 \varsigma_i} && \text{(from Eqn. (3.5))} \\
&= \sec \varsigma_i = 1/\cos \varsigma_i.
\end{aligned}$$

From this result, together with Equation (3.5), it follows that

$$\sin \varsigma_i = \tan \varsigma_i \cos \varsigma_i = R_i \frac{d\vartheta_i}{dR_i}\frac{dR_i}{dS_i} = R_i \frac{d\vartheta_i}{dS_i}. \tag{3.6}$$

To summarize, and in light of Equation (3.2b),

$$\Gamma_i = \sin\varsigma_i = R_i \frac{d\vartheta_i}{dS_i} = \sqrt{1 - \left(\frac{dR_i}{dS_i}\right)^2}, \tag{3.7a}$$

$$\cos\varsigma_i = \frac{dR_i}{dS_i}, \tag{3.7b}$$

$$\tan\varsigma_i = R_i \frac{d\vartheta_i}{dR_i}, \tag{3.7c}$$

which relate the path variables R_i, S_i, and ϑ_i to the angle ς_i between the unit vectors $\hat{\mathbf{e}}_i^R$ and $\hat{\mathbf{e}}_i^S$.

We now turn to a derivation of the governing equations of motion for a bladed disk assembly fitted with general-path absorbers, from which a number of specific models are distilled.

3.4 Bladed Disk Assembly Fitted with General-Path Absorbers

In this section an idealized mathematical model of a bladed disk assembly under engine order excitation is systematically developed. Each blade on the rotating assembly is fitted with a centrifugally-driven, order-tuned vibration absorber and the governing nonlinear equations of motion for the overall coupled system are derived. The analysis to follow in subsequent chapters is carried out for the case of perfect symmetry among the sectors, implying identical blade and absorber models, and for a specific family of absorber paths. However, the equations of motion are derived for the general case of nominal cyclicity and arbitrary-path absorbers, a model that is amenable to ongoing work on, for example, the effects of parameter mistuning and it allows for the eventual investigation of various path geometries. The model is described in Section 3.4.1, followed by the development of the system kinetic and potential energy in Section 3.4.2. The general nonlinear equations of motion are subsequently derived in Section 3.4.3 by employing the method of Lagrange and a particular two-parameter

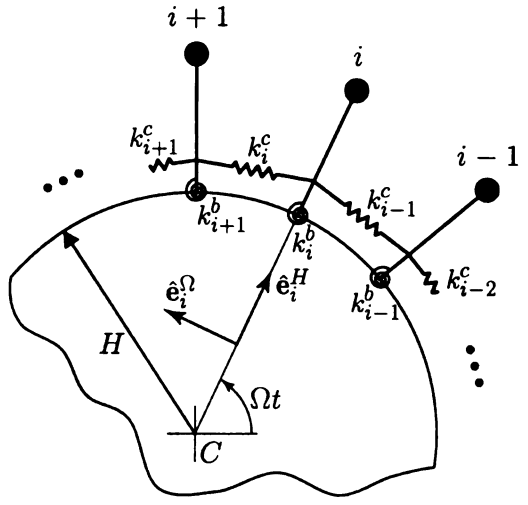

Figure 3.3. Lumped parameter model of a rotating bladed disk assembly.

family of paths, which are employed in Chapter 5, is described in Section 3.4.4.

3.4.1 Lumped-Parameter Model

An idealized, lumped-parameter model of a rotating bladed disk assembly is shown schematically in Figure 3.3. It consists of a nominally-cyclic array of N blades, and each is modeled by a simple pendulum of length L_i and mass M_i. These are uniformly attached around the periphery of a rigid disk of radius H, which rotates at a constant speed Ω about a fixed axis through C. The single-mode flexural stiffness of blade i (the i^{th} primary system) is modeled with a linear torsional spring of stiffness k_i^b, and the elastic inter-blade coupling (due to shrouds, aerodynamic effects, and so on) is captured by linear springs of stiffness k_i^c. As indicated in the sector model shown in Figure 3.4, the coupling springs connect adjacent blades at a distance b (radially along the blade lengths) relative to their attachment points to the rotor. It is assumed that the springs are unstressed when the blades are in a purely radial configuration, that is, when $\theta_i = 0$ for each $i \in \mathcal{N}$.

The blades are fitted with nominally identical vibration absorbers, which essentially consist of particle masses m_i (typically each $m_i \ll M_i$) riding on user-specified

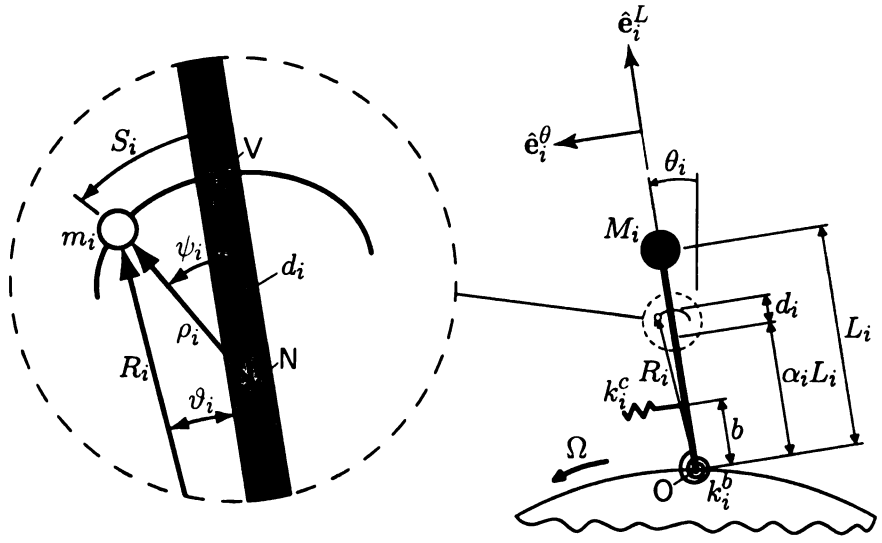

Figure 3.4. Sector model of a bladed disk assembly fitted with a general-path absorber. The mathematical details of the absorber path are given in Section 3.3.

paths. In what follows the equations of motion are derived for arbitrary paths, and then specific paths are chosen for the analyses in subsequent chapters. Figure 3.4 shows a schematic of the i^{th} blade fitted with a general-path absorber, which together with a portion of the rigid disk composes the i^{th} fundamental sector. If we require that point O in Figure 3.2 coincides with the attachment point of blade i to the rotor, and that the unit vectors $\hat{\mathbf{e}}_i^L$ and $\hat{\mathbf{e}}_i^\theta$ are aligned and rotate with the blade as shown in Figure 3.4, then the mathematical details for the i^{th} absorber path are given in Section 3.3. Loosely speaking, the absorbers are said to be "centered" a distance $\alpha_i L_i$ radially along the blade pendulums. Then α_i is the dimensionless distance from the blade base point O to the absorber "attachment" or "base" point N.

There are a number of ways to model the system damping, but in light of the inherently small levels encountered in practice the details are not crucial. (It is acknowledged, however, that modeling and quantifying these details in actual structural systems and absorber implementations can be quite challenging.) For the purposes of this study it will suffice to employ simple linear viscous damping models; the blade and inter-blade damping is captured by linear torsional and translational dampers

(not shown in Figure 3.3 or Figure 3.4) with constants c_i^b and c_i^c, respectively. The effective *translational* absorber damping constant is denoted by $c_i^{\bar{a}}$, where a bar has been added to the superscript $\bar{a}$ to distinguish it from the *torsional* damping constant c_i^a to be employed in the linearized model in Section 3.5. Further comments on damping are given in Section 3.6, including estimates of realistic damping constants and an approximate (resp. exact) relationship between $c_i^{\bar{a}}$ and c_i^a for the case of general (resp. circular) paths.

Finally, the primary systems (blades) are harmonically excited in the transverse sense by engine order excitation of order n and the model described in Section 2.3, that is, Equation (2.14) is adopted for this purpose. Consideration of all possible engine orders can be somewhat cumbersome, since one must not only distinguish between odd and even n in the analysis, but also how certain order-dependent features alias relative to N [91–94]. These additional complications were revealed in the analysis of the generic cyclic system in Section 2.4. In order to eliminate some of these details, and to focus on a particular absorber tuning strategy, the engine order is restricted such that $0 < n < N$ throughout the remainder of this work, though it is possible for $n \geq N$ in practice. This does not qualitatively affect the approach nor the conclusions.[2] The case of noninteger $n \in \mathbb{R}_+$ is non-physical for bladed disk assemblies under engine order excitation, but it is of academic interest and may be possible in other systems. This situation and its implications in cyclic systems is treated briefly in Appendix C.

[2]The reader should note that the effect of large engine orders, specifically those greater than N, can be directly inferred from the results of Section 2.4.

3.4.2 Kinetic and Potential Energy

The total system kinetic energy is that of the N blades and their attendant absorbers and is given by

$$T = \frac{1}{2}\sum_{p=1}^{N} M_p \|\mathbf{u}_p\|^2 + \frac{1}{2}\sum_{p=1}^{N} m_p \|\mathbf{v}_p\|^2, \tag{3.8}$$

where $\|\cdot\|$ denotes the vector norm and

$$\left.\begin{aligned} \mathbf{u}_i &= H\Omega\,\hat{\mathbf{e}}_i^{\Omega} + L_i(\Omega+\dot{\theta}_i)\hat{\mathbf{e}}_i^{\theta} \\ \mathbf{v}_i &= H\Omega\,\hat{\mathbf{e}}_i^{\Omega} + R_i(\Omega+\dot{\theta}_i)\hat{\mathbf{e}}_i^{\vartheta} + \dot{S}_i\hat{\mathbf{e}}_i^{S} \end{aligned}\right\}, \qquad i \in \mathcal{N}$$

are the absolute velocities of the i^{th} blade and absorber masses, respectively. The unit vectors $\hat{\mathbf{e}}_i^{\Omega}$ and $\hat{\mathbf{e}}_i^{\theta}$ are mutually orthogonal, as are the vectors $\hat{\mathbf{e}}_i^{\vartheta}$ and $\hat{\mathbf{e}}_i^{S}$, and these are defined in Figure 3.2 and Figure 3.3. (See also Figure 3.4.) Physically, $H\Omega\,\hat{\mathbf{e}}_i^{\Omega}$ is the velocity of the i^{th} blade basepoint relative to the hub center C and $L_i(\Omega+\dot{\theta}_i)\hat{\mathbf{e}}_i^{\theta}$ (resp. $R_i(\Omega+\dot{\theta}_i)\hat{\mathbf{e}}_i^{\vartheta} + \dot{S}_i\hat{\mathbf{e}}_i^{S}$) is the velocity of the i^{th} blade mass M_i (resp. absorber mass m_i) relative to O. The corresponding speeds are given by

$$\|\mathbf{u}_i\| = H^2\Omega^2 + L_i^2\big(\Omega+\dot{\theta}_i\big)^2 + 2L_iH\Omega\big(\Omega+\dot{\theta}_i\big)\cos\theta_i, \qquad i \in \mathcal{N}$$

$$\begin{aligned} \|\mathbf{v}_i\| = {} & H^2\Omega^2 + R_i^2\big(\Omega+\dot{\theta}_i\big)^2 + \dot{S}_i^2 \\ & + 2H\Omega R_i\big(\Omega+\dot{\theta}_i\big)\cos(\theta_i+\vartheta_i) \\ & + 2H\Omega\dot{S}_i\left(\Gamma_i\cos(\theta_i+\vartheta_i) + \frac{dR_i}{dS_i}\sin(\theta_i+\vartheta_i)\right) \\ & + 2R_i\big(\Omega_i+\dot{\theta}_i\big)\Gamma_i, \qquad i \in \mathcal{N} \end{aligned}$$

where the inner products

$$\left.\begin{aligned} \hat{\mathbf{e}}_i^{\Omega}\cdot\hat{\mathbf{e}}_i^{\theta} &= \cos\theta_i \\ \hat{\mathbf{e}}_i^{\Omega}\cdot\hat{\mathbf{e}}_i^{\vartheta} &= \cos(\theta_i+\vartheta_i) \\ \hat{\mathbf{e}}_i^{\Omega}\cdot\hat{\mathbf{e}}_i^{S} &= \Gamma_i\cos(\theta_i+\vartheta_i) + \frac{dR_i}{dS_i}\sin(\theta_i+\vartheta_i) \\ \hat{\mathbf{e}}_i^{\vartheta}\cdot\hat{\mathbf{e}}_i^{S} &= \Gamma_i \end{aligned}\right\}, \qquad i \in \mathcal{N}$$

have been employed, as well as the expressions given in Equation (3.7).

Ignoring gravitational effects, the system potential energy arises only from the flexural stiffness of the blades (linear torsional springs) and elastic coupling (linear coupling springs) among the sectors. It is given by

$$V = \frac{1}{2}\sum_{p=1}^{N} k_p^b \theta_p^2 + \frac{1}{2}\sum_{p=1}^{N} k_p^c b^2 (\theta_{p+1} - \theta_p)^2, \tag{3.9}$$

where $\theta_{N+1} = \theta_1$. The coupling elements k_i^c are meant to capture only the basic pliancy between adjacent blades and hence their nonlinear kinematic contributions have been neglected in Equation (3.9). This approximation is done independently of any assumptions on the blade amplitudes and does not imply small (linearized) blade motions.

Next the governing nonlinear equations of motion are derived.

3.4.3 Equations of Motion

DIMENSIONAL FORM

The equations of motion are derived by employing Lagrange's method with the generalized coordinates $q_i^{(\mathrm{a})} = S_i$ and $q_i^{(\mathrm{b})} = \theta_i$ for each $i \in \mathcal{N}$. They follow from

$$\frac{d}{dt}\left(\frac{\partial T}{\partial \dot{q}_i^{(k)}}\right) + \frac{\partial V}{\partial q_i^{(k)}} - \frac{\partial T}{\partial q_i^{(k)}} = Q_i^{(k)}, \qquad i \in \mathcal{N}, \quad k = \mathrm{a}, \mathrm{b} \tag{3.10}$$

where the kinetic and potential energy terms T and V are defined by Equation (3.8) and Equation (3.9). The i^{th} set of generalized forces arise from the engine order excitation and linear viscous damping. They are

$$\left.\begin{aligned} Q_i^{(\mathrm{a})} &= -c_i^{\bar{a}} \dot{S}_i \\ Q_i^{(\mathrm{b})} &= -c_i^b \dot{\theta}_i - c_{i-1}^c b\left(\dot{\theta}_i - \dot{\theta}_{i-1}\right) - c_i^c b\left(\dot{\theta}_i - \dot{\theta}_{i+1}\right) \\ &\quad + c_i^{\bar{a}} R_i \Gamma_i \dot{S}_i + F_o L_i e^{j\phi_i} e^{jn\Omega t} \end{aligned}\right\}, \qquad i \in \mathcal{N} \tag{3.11}$$

where F_o and n are the strength and order of the excitation. Then the governing equations of motion for the i^{th} sector follow from Equation (3.10) and take the form

$$m_i\ddot{S}_i + m_iR_i\Gamma_i\ddot{\theta}_i + c_i^{\bar{a}}\dot{S}_i - m_iR_i\frac{dR_i}{dS_i}\left(\Omega+\dot{\theta}_i\right)^2 + m_iH\Omega^2\left(\Gamma_i\sin(\theta_i+\vartheta_i) - \frac{dR_i}{dS_i}\cos(\theta_i+\vartheta_i)\right) = 0, \qquad i\in\mathcal{N} \quad (3.12a)$$

$$M_iL_i^2\ddot{\theta}_i + c_i^b\dot{\theta}_i - c_i^{\bar{a}}R_i\Gamma_i\dot{S}_i + k_i^b\theta_i + M_iL_iH\Omega^2\sin\theta_i + m_i\left[\begin{array}{l} R_i^2\ddot{\theta}_i + R_i\Gamma_i\ddot{S}_i + 2R_i\frac{dR_i}{dS_i}\dot{S}_i\left(\Omega+\dot{\theta}_i\right) \\ \qquad + \frac{d(R_i\Gamma_i)}{dS_i}\dot{S}_i^2 + H\Omega^2R_i\sin(\theta_i+\vartheta_i)\end{array}\right] + c_{i-1}^c b\left(\dot{\theta}_i-\dot{\theta}_{i-1}\right) + c_i^c b\left(\dot{\theta}_i-\dot{\theta}_{i+1}\right) + k_{i-1}^c b^2(\theta_i-\theta_{i-1}) + k_i^c b^2(\theta_i-\theta_{i+1}) = F_oL_ie^{j\phi_i}e^{jn\Omega t}, \quad i\in\mathcal{N} \quad (3.12b)$$

which describe the absorber and blade dynamics, respectively. The subscripts on the blade angles are taken mod N here and in all subsequent sections such that $\theta_{N+1} = \theta_1$ and $\theta_0 = \theta_N$, which are cyclic boundary conditions implying that the N^{th} blade is coupled to the first.

Dimensionless Form

It is desirable to work with a dimensionless form of the governing equations. This is done by restricting $L_i = L$, $M_i = M$, and $k_i^b = k_b$ for all $i \in \mathcal{N}$ and rescaling time according to $\tau = \omega_o t$, where

$$\omega_o = \sqrt{\frac{k_b/L^2}{M}} \quad (3.13)$$

is the undamped natural frequency of a single isolated blade (without an absorber) with zero coupling ($k_i^c = 0$) and zero rotor speed ($\Omega = 0$). Then if $s_i = S_i/L$ and $r_i = R_i/L$ denote the i^{th} nondimensional arc and radial lengths, respectively, a dimensionless form of the equations of motion follows by dividing Equation (3.12a) (resp. Equation (3.12b)) through by the inertia term $ML\omega_o^2$ (resp. $ML^2\omega_o^2$). They

are

$$\mu_i s_i'' + \mu_i r_i \Gamma_i \theta_i'' + \xi_i^{\bar{a}} s_i' - \mu_i r_i \frac{dr_i}{ds_i}(\sigma + \theta_i')^2 + \mu_i \delta\sigma^2 \left(\Gamma_i \sin(\theta_i + \vartheta_i) - \frac{dr_i}{ds_i} \cos(\theta_i + \vartheta_i) \right) = 0, \qquad i \in \mathcal{N} \tag{3.14a}$$

$$\theta_i'' + \xi_i^b \theta_i' - \xi_i^{\bar{a}} r_i \Gamma_i s_i' + \theta_i + \delta\sigma^2 \sin\theta_i + \mu_i \left[\begin{array}{l} r_i^2 \theta_i'' + r_i \Gamma_i s_i'' + 2 r_i \dfrac{dr_i}{ds_i} s_i'(\sigma + \theta_i') \\ \qquad + \dfrac{d(r_i \Gamma_i)}{ds_i} s_i' s_i' + \delta\sigma^2 r_i \sin(\theta_i + \vartheta_i) \end{array} \right] + \xi_{i-1}^c (\theta_i' - \theta_{i-1}') + \xi_i^c (\theta_i' - \theta_{i+1}') + \nu_{i-1}^2 (\theta_i - \theta_{i-1}) + \nu_i^2 (\theta_i - \theta_{i+1}) = F e^{j\phi_i} e^{jn\sigma\tau}, \qquad i \in \mathcal{N} \tag{3.14b}$$

where $(\,\cdot\,)' = d(\,\cdot\,)/d\tau$ and it follows from Equation (3.3) and Equation (3.7a) that

$$\vartheta_i(s_i) = \int_0^{s_i} \frac{\Gamma_i(\chi)}{r_i(\chi)} d\chi, \tag{3.15}$$

$$\Gamma_i(s_i) = \sqrt{1 - \left(\frac{dr_i}{ds_i} \right)^2}. \tag{3.16}$$

The dimensionless parameters appearing in Equation (3.14) are defined in Table 3.1 and the nondimensional distance from the blade basepoint O to the path vertex V is denoted by $r_{oi} \equiv r_i(0) = \alpha_i + \gamma_i$ (dimensionally $R_{oi} = \alpha_i L + d_i$). It should be noted that actual selection of parameter values is application-specific. The reader is referred to [34] for an example discussion on how to map physical experimental parameters onto these nondimensional parameters.

There are no assumptions pertaining to the absorber paths in the nonlinear models described above, other than their gross placement relative to the blades. In the next section a specific two-parameter family of paths is derived and these are used to investigate the basic effects of nonlinearity on the absorber performance. The equations of motion are derived for the case of circular absorber paths in Section 3.5.

Table 3.1. Selected list of dimensionless variables and parameters.

Parameter	Description
$F = F_o L/k_b$	Strength of the engine order excitation (nonlinear models)
$f = F_o L/k_b\psi_o$	Strength of the engine order excitation (linearized model)
$r_{oi} = r_i(0) = \alpha_i + \gamma_i$	Radial length from blade base point O to path vertex V
$r_i = R_i/L$	Radial length from blade base point O to i^{th} absorber at P
$s_i = S_i/L$	Arc length from path vertex V to i^{th} absorber mass at P
$x_i = \theta_i/\psi_o$	Normalized blade angle
$y_i = \psi_i/\psi_o$	Normalized absorber angle (circular path)
α_i	Distance from blade base point O to absorber base point N
$\upsilon = \nu\sqrt{\frac{k_b/L^2}{k_c}}$	Distance from blade base to coupling spring attachment pt.
$\gamma_i = d_i/L$	Length of i^{th} absorber pendulum (circular path)
$\delta = H/L$	Radius of the rotor disk
$\mu_i = m_i/M$	i^{th} absorber mass
$\nu_i = \omega_i^c/\omega_o = \sqrt{\frac{k_i^c}{k_b/b^2}}$	Strength of coupling between blade i and blade $i+1$
$\phi_i = 2\pi\frac{n}{N}(i-1)$	i^{th} inter-blade phase angle
$\varphi_i = \frac{2\pi(i-1)}{N}$	Angle subtended from sector 1 to sector i
$\tau = \omega_o t$	Time
ϑ_i	Angle subtended by S_i
$\xi_i^a = \frac{c_i^a/L^2}{\sqrt{(k_b/L^2)M}}$	i^{th} absorber (torsional) damping constant
$\xi_i^{\bar{a}} = \frac{c_i^{\bar{a}}/L^2}{\sqrt{(k_b/L^2)M}}$	i^{th} absorber (effective translational) damping constant
$\xi_i^b = \frac{c_i^b/L^2}{\sqrt{(k_b/L^2)M}}$	i^{th} blade damping constant
$\xi_i^c = \left(\frac{b}{L}\right)^2\frac{c_i^c}{\sqrt{(k_b/L^2)M}}$	i^{th} coupling damping constant
$\sigma = \Omega/\omega_o$	Angular speed of the rotor

3.4.4 A Generalized Two-Parameter Family of Paths

In what follows, a two-parameter family of paths is derived in terms of linear and nonlinear tuning parameters, which will serve as the fundamental absorber design variables in the subsequent chapters. The basic idea is to assume an expanded form of each absorber position relative to its basepoint, which is captured by the radial lengths $r_i(s_i)$. In doing so, only even terms are included such that the paths are symmetric about their vertices. The expansions are introduced to the full nonlinear equations of motion and, by restricting zero blade motions relative to the rotating hub and appropriately truncating nonlinear terms, a set of well-known nonlinear systems results. These reduced systems depend only on the absorber dynamics and they motivate the selection of two tuning parameters. The first parameter sets the linear absorber tuning order (a topic that is more fully described in Chapter 4) by setting the path curvature at its vertex. The second parameter prescribes the nonlinear tuning by varying the curvature along the path, and can be thought of as the strength of the path nonlinearity. Proper selection of this parameter is motivated in Chapter 5.

In what follows, each absorber path is assumed to be identical and identically fitted to the blades by imposing $\alpha_i = \alpha$ and $\gamma_i = \gamma$ for all $i \in \mathcal{N}$. Then

$$r_{oi} \equiv r_o = \alpha + \gamma, \qquad \forall\, i \in \mathcal{N} \tag{3.17}$$

represents the dimensionless distance from the blade basepoint to the path vertex. By restricting $\theta_i = \theta_i' = \theta_i'' = 0$, Equation (3.14a) reduce to

$$s_i'' - 4\sigma^2 r_i \frac{dr_i}{ds_i} + \delta\sigma^2\left(\Gamma_i \sin\vartheta_i - \frac{dr_i}{ds_i}\cos\vartheta_i\right) = 0, \qquad i \in \mathcal{N} \tag{3.18}$$

which describes the nonlinear absorber dynamics for the desired case of zero blade motions relative to the rotating hub. Next the dimensionless radial length $r_i(s_i)$ is expanded according to

$$r_i^2(s_i) = b_0 + b_2 s_i^2 + b_4 s_i^4 + \mathcal{O}(s_i^6), \tag{3.19}$$

where only even terms are considered since $r_i(-s_i) = r_i(s_i)$ is even by assumption. Each has the same constant coefficients, implying that all of the paths are identical. Since $r_o = \alpha+\gamma = r_i(0) = \sqrt{b_0}$ the first parameter in Equation (3.19) is automatically prescribed and is given by $b_0 = r_o^2 = (\alpha+\gamma)^2$, and the remaining parameters b_2 and b_4 are to be specified. Substituting Equation (3.19) into Equation (3.18) and expanding in s_i yields

$$s_i'' + \tilde{n}^2\sigma^2 s_i + \eta\sigma^2 s_i^3 + \mathcal{O}(s_i^5) = 0, \tag{3.20}$$

where

$$\left.\begin{aligned} \tilde{n} &= \sqrt{-b_2 - \left(\frac{b_2-1}{\sqrt{b_0}}\right)\delta} \\ \eta &= -2b_4 - \left(\frac{(b_2-1)^2 + 12b_0b_4}{6b_0\sqrt{b_0}}\right)\delta \end{aligned}\right\} \tag{3.21}$$

are defined to be the *linear absorber tuning order* and the *nonlinear absorber tuning parameter*, respectively.

Equation (3.20) is recognized to be a standard undamped and unforced Duffing oscillator, a comprehensive treatment of which can be found in most texts on nonlinear systems [95–97]. For small amplitudes the nonlinear term can be neglected and the oscillator exhibits free harmonic motions with frequency $\tilde{n}\sigma$. It is well-known that linear tuning of the centrifugally-driven absorbers under consideration can be accomplished by setting the absorber tuning order $\tilde{n}$, which depends on the absorber placement and system geometry, relative to the order of the excitation n [10]. When these match identically, and in the absence of damping, a complete elimination of vibrations of the primary system is possible, which is shown systematically in Chapter 4 for the models described above. For larger motions the nonlinearity in Equation (3.20) becomes important and the oscillations become amplitude-dependent. In the context of absorber path design, therefore, the nonlinear tuning parameter η is used to modify the absorber behavior without compromising the small-motion linear tuning $\tilde{n} \approx n$. When $\eta > 0$ the response is hardening, and it is softening for $\eta < 0$. Finally, the

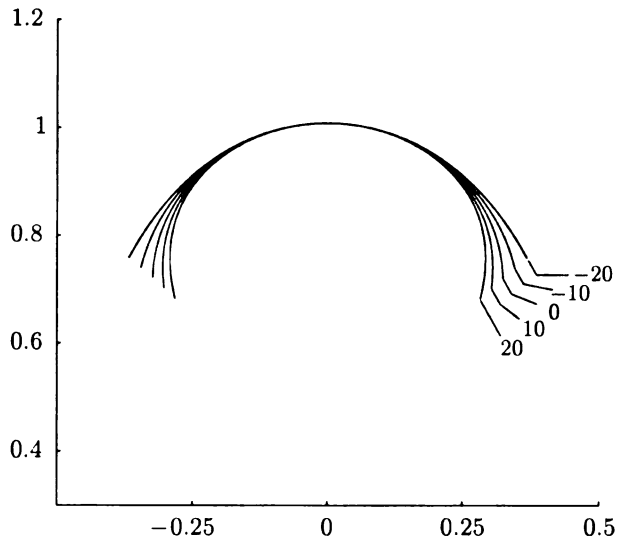

Figure 3.5. A generalized family of absorber paths defined by Equation (3.19) for $\alpha = 0.84$, $\delta = 0.67$, $\tilde{n} = 3$ ($\gamma = 0.168$ and $r_o = 1.008$), $-0.47 \leq s_i \leq 0.47$, and for a range of nonlinear tuning from softening to hardening: $\eta = -20, -10, 0, 10, 20$.

coefficient terms in front of δ in Equation (3.21) appear since the absorber paths are measured from the base of the blade, and not from the center of the rotor as it is done in the CPVA work by Shaw and coworkers [14].

The remaining expansion coefficients b_2 and b_4 can be obtained from Equation (3.21) in terms of the system geometry and the linear and nonlinear tuning parameters $\tilde{n}$ and η. To summarize,

$$\left.\begin{aligned} b_0 &= r_o^2 \\ b_2 &= \frac{\delta - \tilde{n}^2 r_o}{\delta + r_o} \\ b_4 &= -\frac{\delta(1+\tilde{n}^2)^2}{12(\delta + r_o)^3} - \frac{r_o}{2(\delta + r_o)}\eta \end{aligned}\right\}, \tag{3.22}$$

where r_o is defined by Equation (3.17). An example plot of the generalized family of absorber paths defined by Equation (3.19) is shown in Figure 3.5 for a particular blade geometry and absorber design and for a range of nonlinear tuning from softening to hardening.

Next we consider a special case of the equations of motion in which circular-path

absorbers are employed.

3.5 Bladed Disk Assembly Fitted with Circular-Path Absorbers

In what follows, the nonlinear equations of motion for a nominally cyclic bladed disk assembly fitted with circular-path absorbers are deduced from the general system given by Equation (3.12). These are linearized for small blade/absorber motions in Section 3.5.2 and subsequently modified to account for physical rattling space limitations of the absorbers. The resulting mathematical model is employed in the linear analysis of Chapter 4.

3.5.1 Equations of Motion

Consider the sector model shown in Figure 3.6, which features the same pendulum-like blade model described in Section 3.4. In this case the blades are fitted with *circular-path* absorber pendulums of mass m_i and radius d_i, the motions of which are described by the angles ψ_i. (The angles ψ_i^o correspond to motion-limiting stops, which are incorporated into the equations of motion in the next section.) The governing equations of motion for the overall system could be derived from this model in the usual manner via the method of Lagrange. However, it will be more convenient to deduce them from the general results of Section 3.4 by restricting the arbitrary path shown in Figure 3.2 to be circular.

By restricting each $\rho_i = d_i$ to be constant the general path shown in Figure 3.2 (solid line) reduces to a circular path (dashed line). Then $S_i = d_i\psi_i$ for all $i \in \mathcal{N}$ and

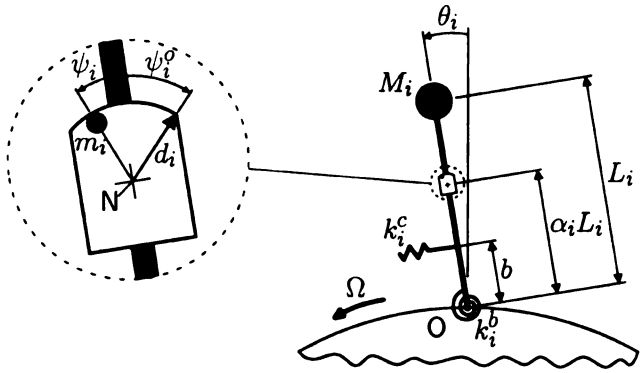

Figure 3.6. Sector model for a bladed disk assembly fitted with circular-path absorbers with limited rattling space.

it can be shown that

$$\left.\begin{aligned} R_i^2 &= \alpha_i^2 L_i^2 + d_i^2 + 2 d_i \alpha_i L_i \cos\psi_i \\ R_i \sin\vartheta_i &= d_i \sin\psi_i \\ R_i \cos\vartheta_i &= \alpha_i L_i + d_i \cos\psi_i \\ R_i \Gamma_i &= \alpha_i L_i \cos\psi_i + d_i \\ \frac{d(R_i\Gamma_i)}{dS_i} &= -\frac{\alpha_i L_i \sin\psi_i}{d_i} \\ R_i \frac{dR_i}{dS_i} &= -\alpha_i L_i \sin\psi_i \end{aligned}\right\}, \qquad i \in \mathcal{N} \tag{3.23}$$

which relate the general-path variables R_i, S_i, and ϑ_i to the circular-path angle ψ_i. The expressions given in Equation (3.23) can be employed to deduce the circular-path equations of motion term-by-term from Equation (3.12), the results of which are summarized in Table 3.2. For the proposed circular-path model it is natural to express the absorber damping in terms of a *torsional* viscous damping constant instead of the effective *translational* representation of Section 3.4. The generalized forces are re-formulated to account for this and are given by

$$\left.\begin{aligned} Q_i^{(\mathrm{a})} &= -c_i^a \dot{\psi}_i \\ Q_i^{(\mathrm{b})} &= -c_i^b \dot{\theta}_i - c_{i-1}^c b\big(\dot{\theta}_i - \dot{\theta}_{i-1}\big) - c_i^c b\big(\dot{\theta}_i - \dot{\theta}_{i+1}\big) \\ &\qquad + c_i^a \dot{\psi}_i + F_o L_i e^{j\phi_i} e^{jn\Omega t} \end{aligned}\right\}, \qquad i \in \mathcal{N} \tag{3.24}$$

where c_i^a is the torsional damping constant for the i^{th} absorber and is not to be confused with $c_i^{\bar{a}}$. (These are implicitly related in Section 3.6.) The desired equations of motion follow from Equation (3.12) by performing the substitutions given in Table 3.2 and by employing the re-formulated generalized forces given by Equation (3.24). For $i \in \mathcal{N}$ they are

$$m_i d_i^2 \left(\ddot{\theta}_i + \ddot{\psi}_i\right) + c_i^a \dot{\psi}_i + m_i d_i H \Omega^2 \sin(\theta_i + \psi_i) + m_i d_i \alpha_i L_i \ddot{\theta}_i \cos\psi_i + m_i d_i \alpha_i L_i \left(\Omega + \dot{\theta}_i\right)^2 \sin\psi_i = 0, \tag{3.25a}$$

$$\begin{aligned} M_i L_i^2 \ddot{\theta}_i + c_i^b \dot{\theta}_i - c_i^a \dot{\psi}_i + k_i^b \theta_i + M_i L_i H \Omega^2 \sin\theta_i \\ + m_i \left[\begin{array}{l} \alpha_i^2 L_i^2 \ddot{\theta}_i + d_i^2 \left(\ddot{\theta}_i + \ddot{\psi}_i\right) \\ \quad + d_i \alpha_i L_i \left(\ddot{\psi}_i + 2\ddot{\theta}_i\right) \cos\psi_i \\ \quad - d_i \alpha_i L_i \left(\dot{\psi}_i^2 + 2(\Omega + \dot{\theta}_i)\dot{\psi}_i\right) \sin\psi_i \\ \quad + H\Omega^2 (\alpha_i L_i \sin\theta_i + d_i \sin(\theta_i + \psi_i)) \end{array} \right] \\ + c_{i-1}^c b \left(\dot{\theta}_i - \dot{\theta}_{i-1}\right) + c_i^c b \left(\dot{\theta}_i - \dot{\theta}_{i+1}\right) \\ + k_{i-1}^c b^2 (\theta_i - \theta_{i-1}) + k_i^c b^2 (\theta_i - \theta_{i+1}) = F_o L_i e^{j\phi_i} e^{jn\Omega t}. \end{aligned} \tag{3.25b}$$

In the next section these are linearized for small blade/absorber motions and are modified to account for limited absorber amplitudes imposed by the geometry of the blades.

3.5.2 Linearized Model with Restrictions on the Absorber Amplitudes

In any realistic physical implementation the absorber amplitudes will be restricted by the blade geometry and this is captured by the motion-limiting stops in Figure 3.6, where ψ_i^o represents the limiting angle of the i^{th} absorber. Impacts occur whenever $|\psi_i| = \psi_i^o$, the dynamics of which have been investigated in [34, 98] for the case of a single isolated blade/absorber combination. This feature is included for generality but will not be directly exploited in the analysis of Chapter 4, where it is assumed that $|\psi_i| < \psi_i^o$ throughout.

Table 3.2. Selected terms in the general-path equations of motion given by Equation (3.12) and their counterparts for the case of circular-path absorbers.

General Path Term	Circular Path Term
$m_i\ddot{S}_i$	$m_i d_i\ddot{\psi}_i$
$m_i R_i\Gamma_i\ddot{\theta}_i$	$m_i(\alpha_i L_i\cos\psi_i + d_i)\ddot{\theta}_i$
$-m_i R_i\frac{dR_i}{dS_i}(\Omega+\dot{\theta}_i)^2$	$m_i\alpha_i L_i(\Omega+\dot{\theta}_i)^2\sin\psi_i$
$m_i H\Omega^2\Big(\Gamma_i\sin(\theta_i+\vartheta_i) - \frac{dR_i}{dS_i}\cos(\theta_i+\vartheta_i)\Big)$	$m_i H\Omega^2\sin(\theta_i+\psi_i)$
$m_i R_i^2\ddot{\theta}_i$	$m_i(\alpha_i^2 L_i^2 + d_i^2 + 2d_i\alpha_i L_i\cos\psi_i)\ddot{\theta}_i$
$m_i R_i\Gamma_i\ddot{S}_i$	$m_i d_i(d_i + \alpha_i L_i\cos\psi_i)\ddot{\psi}_i$
$2m_i R_i\frac{dR_i}{dS_i}\dot{S}_i(\Omega+\dot{\theta}_i)$	$-2m_i d_i\alpha_i L_i(\Omega+\dot{\theta}_i)\dot{\psi}_i\sin\psi_i$
$m_i\frac{d(R_i\Gamma_i)}{dS_i}\dot{S}_i^2$	$-m_i d_i\alpha_i L_i\dot{\psi}_i^2\sin\psi_i$
$m_i H\Omega^2 R_i\sin(\theta_i+\vartheta_i)$	$m_i H\Omega^2(\alpha_i L_i\sin\theta_i + d_i\sin(\theta_i+\psi_i))$

Equation (3.25) is linearized for small blade and absorber motions and is made dimensionless in the same way as it was done in Section 3.4.3. The absorber and blade motions are subsequently scaled according to $x_i = \theta_i/\psi_o$ and $y_i = \psi_i/\psi_o$, where each $\psi_i^o = \psi_o$ has been assumed to be identical, and thus impacts correspond to $|y_i| = 1$. Then by dividing through by ψ_o the dynamics of the i^{th} sector are governed by

$$\mu_i\gamma_i^2(x_i'' + y_i'') + \xi_i^a y_i' + \mu_i\gamma_i\delta\sigma^2(x_i+y_i) + \mu_i\gamma_i\alpha_i(x_i'' + \sigma^2 y_i) = 0, \quad i\in\mathcal{N} \tag{3.26a}$$

$$\begin{aligned} &x_i'' + \xi_i^b x_i' - \xi_i^a y_i' + x_i + \delta\sigma^2 x_i \\ &\quad + \mu_i\begin{bmatrix} \alpha_i^2 x_i'' + \gamma_i^2(x_i''+y_i'') + \alpha_i\gamma_i(y_i''+2x_i'') \\ +\alpha_i\delta\sigma^2 x_i + \gamma_i\delta\sigma^2(x_i+y_i)\end{bmatrix} \\ &\quad + \xi_{i-1}^c(x_i' - x_{i-1}') + \xi_i^c(x_i' - x_{i+1}') \\ &\quad + \nu_{i-1}^2(x_i - x_{i-1}) + \nu_i^2(x_i - x_{i+1}) = f e^{j\phi_i}e^{jn\sigma\tau}, \qquad i\in\mathcal{N} \end{aligned} \tag{3.26b}$$

where the dimensionless parameters are defined in Table 3.1. Equation (3.26) forms the basis for the linear analysis of Chapter 4.

Estimates for the blade and absorber damping constants are developed next in addition to a relationship between the nondimensional torsional and effective transla-

tional absorber damping constants ξ_a and $\xi_{\bar{a}}$.

3.6 Estimates of the Dimensionless Damping Constants

As a guide to sensical parameter selection in numerical simulations, approximate expressions for the blade and absorber damping constants ξ_b and ξ_a are formulated in terms of their respective damping ratios. These can be obtained by considering the free vibration of an isolated blade/absorber combination when the absorber is locked in place and from the free response of an absorber when the blade is locked relative to the rotating disk. The linearized model of Section 3.5.2 is used for this purpose. A relationship between the *torsional* absorber damping constant ξ_a and the effective *translational* damping constant $\xi_{\bar{a}}$ is also derived. In all of what follows identical sectors are assumed.

Consider the special case when the absorbers are locked in their zero positions relative to the blades. In the absence of coupling (i.e., only an isolated sector is considered) the corresponding linearized equation of motion follows from Equation (3.26b) by setting $y = y' = y'' = 0$ and it can be expressed as

$$(1 + \mu(\alpha + \gamma)^2)x'' + \xi_b x' + (1 + (1 + \mu(\alpha + \gamma))\delta\sigma^2)x = fe^{jn\sigma\tau}. \tag{3.27}$$

In practice the absorber-to-blade mass ratio is very small and centrifugal stiffening has a negligible effect on the blade natural frequencies. By restricting $\mu = 0$ and $\sigma = 0$ it thus follows from Equation (3.27) that

$$\xi_b \cong 2\rho_b, \tag{3.28}$$

where ρ_b is the blade damping ratio. Damping levels in the blades can be 0.1% or less relative to critical, which gives rise to the approximation $\xi_b \cong 0.002$.

A similar calculation can be carried out for the absorbers. When the blades are locked in their zero positions relative to the rotating disk the absorbers become

dynamically isolated and their linearized dynamics are governed by

$$\mu\gamma^2 y'' + \xi_a y' + \mu\gamma(\alpha + \delta)\sigma^2 y = 0, \tag{3.29}$$

which follows from Equation (3.26a) with $x = x' = x'' = 0$. By employing the equivalent mass, damping, and stiffness terms in Equation (3.29), one can obtain

$$\xi_a = 2\mu\gamma^2\tilde{n}\sigma\rho_a, \tag{3.30}$$

where $\tilde{n} = \sqrt{(\alpha + \delta)/\gamma}$ is the linear absorber tuning order (this is discussed more fully in Chapter 4) and ρ_a is the absorber damping ratio. As discussed in the forthcoming chapters, we will be interested in the system dynamics for absorber tuning $\tilde{n}$ close to the engine order n and also near resonance conditions, which correspond approximately to $\sigma = 1/\sqrt{n^2 - \delta} \cong 1/n$. Under these conditions $\tilde{n}\sigma \cong 1$ and Equation (3.30) can be approximated by

$$\xi_a \cong 2\mu\gamma^2\rho_a. \tag{3.31}$$

Given the absorber mass, pendulum length (circular path) and critical damping level, Equation (3.31) can be employed to approximate the torsional damping constant ξ_a.

The damping constants ξ_a and $\xi_{\bar{a}}$ can be (approximately) related by comparing the absorber damping term in Equation (3.14a) (nonlinear system with general-path absorbers) to that in Equation (3.26a) (linearized system with circular-path absorbers). By multiplying the latter through by the stopper angle ψ_o and dividing by γ (this makes it possible to compare the equations directly) the absorber damping term for the linearized system can be written as $\xi_a\psi_i'/\gamma = \xi_a s_i'/\gamma^2$, where $s_i = \gamma\psi_i$ has been employed, and the corresponding damping term for the nonlinear system is $\xi_{\bar{a}} s_i'$. An exact (resp. approximate) relationship between the torsional and effective translational absorber damping constants for a circular (resp. general) path can be obtained by equating these expressions and is given by

$$\xi_a = \gamma^2\xi_{\bar{a}}, \tag{3.32}$$

(a)

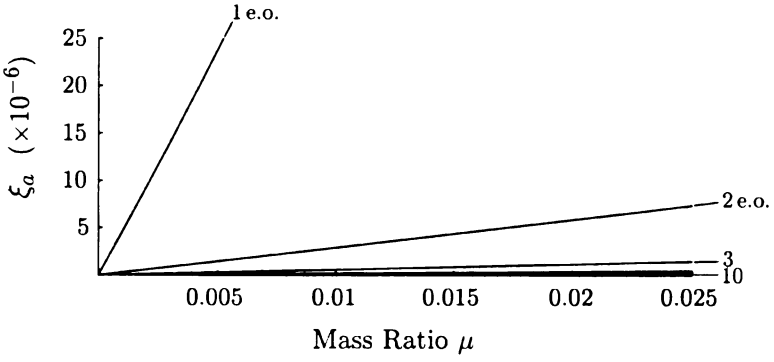

(b)

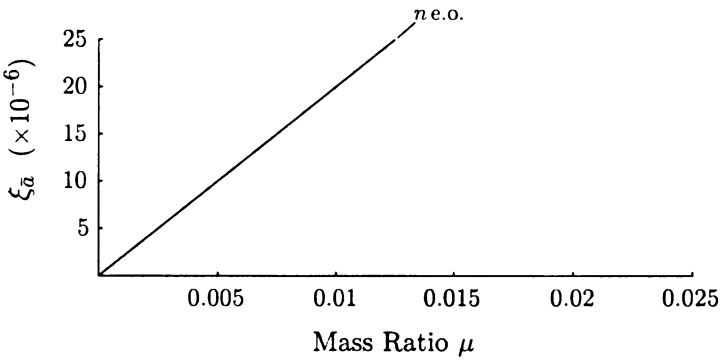

Figure 3.7. Approximate (a) torsional and (b) translational absorber damping constant versus mass ratio μ based on Equation (3.31) and Equation (3.33) for $\rho_a = 0.005$, $\alpha = 0.84$, $\delta = 0.67$, and engine orders (e.o.) $n = 1, \ldots, 10$.

where γ is the dimensionless length of the absorber pendulum (resp. the dimensionless curvature of the absorber path at its vertex). When the path is general Equation (3.32) gives a reasonable relationship between the absorber damping constants, depending on the strength of the path nonlinearity η and the amplitude of the absorber motions. For linear absorber tuning $\tilde{n} \approx n$ and for rotor speeds close to resonance

$$\xi_{\bar{a}} \cong 2\mu\rho_a, \tag{3.33}$$

which follows from Equation (3.32) together with Equation (3.31).

Figure 3.7 shows example plots of ξ_a and $\xi_{\bar{a}}$ in terms of the mass ratio μ for an absorber damping ratio $\rho_a = 0.001$ and for various engine orders. These charts can be used to obtain an appropriate order of magnitude for the damping constants to

be used for the frequency response loci and in numerical simulations. In Chapter 5 the frequency response curves are generated for a model with $\alpha = 0.84$, $\delta = 0.67$, $\mu = 0.0035$, $n = 3$, and $\rho_a = 0.005$, which gives rise to $\xi_{\bar{a}} \cong 2 \times 10^{-6}$. The values $\xi_b = 2 \times 10^{-3}$ and $\xi_{\bar{a}} = 2 \times 10^{-6}$ are used when damping is included, and also in the simulations.

3.7 Concluding Remarks

A lumpted-parameter mathematical model of a bladed disk assembly fitted with centrifugally-driven, general-path vibration absorbers has been systematically developed, which serves as the basis for all of the analysis to follow. We shall be interested in three specific cases of this general nonlinear system:

1. The linearized system with motion-limiting stops, which is given by Equation (3.26);
2. The fully nonlinear system given by Equation (3.14) with *zero inter-blade coupling* ($\nu = 0$), together with the two-parameter family of paths defined by Equation (3.19); and
3. The fully-coupled nonlinear system ($\nu \neq 0$) given by Equation (3.14), together with the two-parameter family of paths defined by Equation (3.19).

These three systems are systematically analyzed in the next two chapters, and throughout the remainder of this work they shall be referred to as (1) the *coupled linear* or *linearized system*, (2) the *isolated nonlinear system*, and (3) the *coupled nonlinear system*.

We begin in the next chapter with an analysis based on the coupled linearized system.

CHAPTER 4

Forced Response of the Coupled Linear System

4.1 Introduction

In this chapter the fundamental linearized dynamics of a cyclically-coupled bladed disk assembly fitted with circular-path vibration absorbers are investigate in detail. The aim is twofold: to quantify and understand the underlying linear resonance structure of the coupled linear system under engine order excitation and, based on these findings, to design the absorbers to eliminate or otherwise reduce blade motions relative to the rotating hub. (The basic effects of nonlinearity are investigated in Chapter 5 for an isolated blade/absorber combination and also for the fully coupled cyclic system.) An auxiliary, but very important topic includes a decoupling strategy based on the cyclic symmetry of the system whereby the fully-coupled linear model can be simplified to a set of reduced-order models, from which analytical results easily follow. The analysis is based on the well-known theory of circulants, which is summarized in Section 2.2 and covered in detail in Appendix B, and it is also employed in Chapter 5 to handle block diagonalization of Jacobian matrices.

As we shall see, the underlying linear resonance structure is surprisingly subtle and complicated, a feature that arises from the order-nature of the absorbers. However,

the (block) decoupled models to be formulated give rise to a set of tractable analytical expressions for the system eigenfrequencies which, when represented in a Campbell diagram, clarify the nature of the resonance structure for various absorber designs and for *any* number of sectors, engine order, or coupling strength. A particular absorber design strategy is motivated from these eigenfrequency versus rotor speed plots in terms of a detuning parameter, which essentially assigns the absorber tuning order (which depends on the system geometry) relative to the order of the excitation. It will be shown that ideal (exact) tuning, where the absorber tuning order is chosen to identically match the excitation order, completely eliminates the system resonances and (in the absence of damping) results in zero-amplitude steady-state blade motions over all rotor speeds. Such a tuning scheme, however, is susceptible to the effects of parameter uncertainties. An important contribution of this chapter is that, in addition to the exact tuning, there exists a *range* of absorber undertuning values for which there are no system resonances—independent of the rotor speed. Therefore, a practical tuning strategy involves intentionally detuning the absorbers within this "no-resonance zone." The approach offers a more robust design against system resonances, but at the expense of some residual steady-state blade vibrations.

The chapter is organized as follows. The linearized system to be considered is described in Section 4.2, where the dimensionless equations of motion are formulated for a single sector and subsequently for the overall coupled system. Two special cases of these governing equations are considered: the case when the blades (resp. absorbers) are locked in their zero positions relative to the rotating hub (resp. blades) in Section 4.2.3 (resp. Section 4.2.4). The former motivates the absorber tuning order, which is employed in subsequent sections to tune the absorbers to a given order of the excitation, and the latter is investigated in detail in Section 4.3.1, with the aim of providing a benchmark against which the effectiveness of the absorbers can be evaluated. The forced response of the general system is detailed in Section 4.3.2, and

an absorber tuning strategy is motivated in Section 4.4. The effects of damping are briefly considered in Section 4.5, and the chapter closes with some concluding remarks Section 4.6.

4.2 Mathematical Model

The bladed disk model to be considered is shown in Figure 4.1a in dimensionless form. It consists of a rotationally periodic array of N identical, identically-coupled sector models, one of which is depicted in Figure 4.1b. The disk has radius δ and it rotates at a fixed speed σ about an axis through C. Each blade is modeled by a simple pendulum of unity mass and length, the dynamics of which are captured by the normalized angles x_i. (See Table 3.1 on page 64.) The blades are attached to the rotating disk via linear torsional springs with unity stiffness and adjacent blades are elastically coupled by linear springs with stiffness ν. It is assumed that the springs are unstretched when the blades are in a purely radial configuration, that is, when each $x_i = 0$. As shown in the inset of Figure 4.1b each blade is fitted with a pendulum-like, circular-path absorber with radius γ and mass μ at an effective distance α along the blade length. The absorber dynamics are captured by the normalized pendulum angles y_i and they are limited according to $|y_i| \leq 1$ by stops, which represents the rattling space limits imposed by the blade geometry.[1] Linear viscous damping is also included (but not indicated in the figure). Blade and inter-blade damping is captured by linear torsional and translational dampers with constants ξ_b and ξ_c, respectively, and the absorber damping is captured by a torsional damper with constant ξ_a. Finally, the system is subjected to the traveling wave dynamic loading described in Section 2.3, and Equation (2.14) is employed for this purpose. Throughout the remainder of this thesis it is assumed that $0 < n < N$ for simplicity. This does not, however, affect the

[1]This feature is included for generality, but in all of what follows it is assumed that $|y_i| < 1$, i.e., that impacts do not occur. The impacting dynamics for this system are investigate in [34] for an isolated blade/absorber combination.

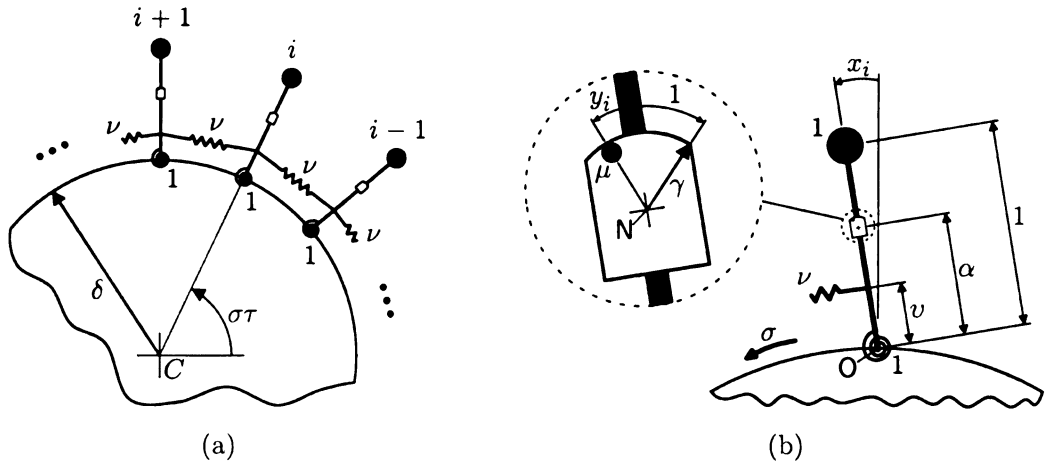

Figure 4.1. (a) Model of bladed disk assembly and (b) sector model.

results; they can be generalized to account for $n \geq N$ according to the discussions in Section 2.3 and also Section 2.4.

Next a mathematical model that describes the linear dynamics of the i^{th} sector is described. The overall system is composed of N such models, and these are cast in a matrix-vector form with block circulant coefficient matrices in Section 4.2.2.

4.2.1 Sector Model

The governing equations of motion for the i^{th} 2-DOF sector follow from Equation (3.25) of Chapter 3. They are

$$\mu\gamma^2(x_i'' + y_i'') + \xi_a y_i' + \mu\gamma\delta\sigma^2(x_i + y_i) + \mu\gamma\alpha(x_i'' + \sigma^2 y_i) = 0, \qquad i \in \mathcal{N} \tag{4.1a}$$

$$\begin{aligned} & x_i'' + \xi_b x_i' - \xi_a y_i' + x_i + \delta\sigma^2 x_i \\ & \quad + \mu \begin{bmatrix} \alpha^2 x_i'' + \gamma^2(x_i'' + y_i'') + \alpha\gamma(y_i'' + 2x_i'') \\ \qquad + \alpha\delta\sigma^2 x_i + \gamma\delta\sigma^2(x_i + y_i) \end{bmatrix} \\ & \quad + \xi_c(-x_{i-1}' + 2x_i' - x_{i+1}') \\ & \quad + \nu^2(-x_{i-1} + 2x_i - x_{i+1}) = f e^{j\phi_i} e^{jn\sigma\tau}, \qquad i \in \mathcal{N} \end{aligned} \tag{4.1b}$$

where the dimensionless parameters are defined in Table 3.1 on page 64. In Equation (4.1) the parameter subscripts have been dropped since the sectors are assumed to be identical and identically coupled, and the remaining subscripts i are taken mod N such that $x_{N+1} = x_1$ and $x_0 = x_N$. In matrix-vector form, Equation (4.1) becomes

$$\left.\begin{aligned}\mathbf{M}\mathbf{z}_i'' + \mathbf{C}\mathbf{z}_i' + \mathbf{K}\mathbf{z}_i + \mathbf{C}_c(-\mathbf{z}_{i-1}' + 2\mathbf{z}_i' - \mathbf{z}_{i+1}') \\ + \mathbf{K}_c(-\mathbf{z}_{i-1} + 2\mathbf{z}_i - \mathbf{z}_{i+1}) = \mathbf{f}e^{j\phi_i}e^{jn\sigma\tau}\end{aligned}\right\}, \qquad i \in \mathcal{N} \quad (4.2)$$

where the vector

$$\mathbf{z}_i = \begin{bmatrix} x_i \\ y_i \end{bmatrix} = \begin{bmatrix} \theta_i/\psi_o \\ \psi_i/\psi_o \end{bmatrix} \quad (4.3)$$

captures the sector dynamics and the elements of the sector mass, damping, and stiffness matrices are given in Table 4.1. The matrices

$$\mathbf{C}_c = \begin{bmatrix} \xi_c & 0 \\ 0 & 0 \end{bmatrix}, \quad \mathbf{K}_c = \begin{bmatrix} \nu^2 & 0 \\ 0 & 0 \end{bmatrix}, \quad (4.4)$$

capture the inter-blade coupling and vanish when $\xi_c = 0$ and $\nu = 0$, respectively, in which case Equation (4.2) describes the forced motion of N isolated blade/absorber systems. (Equation (4.2) is studied in detail in [34, 98] for the case when $N = 1$, $\mathbf{K}_c = \mathbf{0}$, and $\mathbf{C}_c = \mathbf{0}$, including the impact dynamics that occur when $|y_i| = 1$, that is, $|\psi_i| = \psi_o$.) The sector forcing vector is given by

$$\mathbf{f} = \begin{bmatrix} f \\ 0 \end{bmatrix}, \quad (4.5)$$

where f is defined in Table 3.1. Finally, the parameter $\omega_c = \frac{b}{L}\sqrt{k_c/M}$ (see ν in Table 3.1) is the undamped natural frequency of a single isolated blade (with no absorber) with $k_b = 0$ and $\Omega = 0$ and with a single coupling stiffness element k_c connected to an adjacent, stationary blade.

Table 4.1. Elements of the sector mass, damping, and stiffness matrices **M**, **C**, and **K**.

$M_{11} = 1 + \mu(\alpha+\gamma)^2$	$C_{11} = \xi_b$	$K_{11} = 1 + (1 + \mu(\alpha+\gamma))\,\delta\sigma^2$
$M_{12} = \mu\gamma(\alpha+\gamma)$	$C_{12} = -\xi_a$	$K_{12} = \mu\gamma\delta\sigma^2$
$M_{21} = M_{12}$	$C_{21} = 0$	$K_{21} = K_{12}$
$M_{22} = \mu\gamma^2$	$C_{22} = \xi_a$	$K_{22} = \mu\gamma\,(\alpha+\delta)\,\sigma^2$

4.2.2 System Model

By stacking each $\mathbf{z}_i$ into the configuration vector $\mathbf{q} = (\mathbf{z}_1, \mathbf{z}_2, \ldots, \mathbf{z}_N)^T$, the governing matrix equation of motion for the overall $2N$–DOF system takes the form

$$\hat{\mathbf{M}}\mathbf{q}'' + \hat{\mathbf{C}}\mathbf{q}' + \hat{\mathbf{K}}\mathbf{q} = \hat{\mathbf{f}}e^{jn\sigma\tau}, \tag{4.6}$$

where $\hat{\mathbf{M}}$ is block diagonal with diagonal blocks $\mathbf{M}$ and $\hat{\mathbf{K}} \in \mathscr{BCBS}_{2,N}$ has generating matrices $\mathbf{K} + 2\mathbf{K}_c, -\mathbf{K}_c, \mathbf{0}, \ldots, \mathbf{0}, -\mathbf{K}_c$. The matrix $\hat{\mathbf{C}} \in \mathscr{BCBS}_{2,N}$ is similarly defined by replacing $\mathbf{K}$ with $\mathbf{C}$ and $\mathbf{K}_c$ with $\mathbf{C}_c$ in $\hat{\mathbf{K}}$. In terms of the circulant operator the system mass, damping, and stiffness matrices are given by

$$\left.\begin{aligned} \hat{\mathbf{M}} &= \operatorname{circ}(\mathbf{M}, \mathbf{0}, \mathbf{0}, \ldots, \mathbf{0}, \mathbf{0}) = \operatorname*{diag}_{i\in\mathcal{N}}(\mathbf{M}) \\ \hat{\mathbf{C}} &= \operatorname{circ}(\mathbf{C} + 2\mathbf{C}_c, -\mathbf{C}_c, \mathbf{0}, \ldots, \mathbf{0}, -\mathbf{C}_c) \\ \hat{\mathbf{K}} &= \operatorname{circ}(\mathbf{K} + 2\mathbf{K}_c, -\mathbf{K}_c, \mathbf{0}, \ldots, \mathbf{0}, -\mathbf{K}_c) \end{aligned}\right\}, \tag{4.7}$$

where the circ $(\cdot)$ operation is defined in Section 2.2 and also in Appendix B.[2] Finally, the system forcing vector is

$$\hat{\mathbf{f}} = \left(\mathbf{f}e^{j\phi_1}, \mathbf{f}e^{j\phi_2}, \ldots, \mathbf{f}e^{j\phi_N}\right)^T, \tag{4.8}$$

where $\mathbf{f}$ is given by Equation (4.5) and ϕ_i is defined by Equation (2.15).

[2]See [62] for a comprehensive treatment of circulant matrices and their properties. A brief review of such matrices is given in Section 2.2 on page 11 and a more exhaustive treatment of the theory, including many proofs, is given in Appendix B. In all of what follows and whenever reference is made to Section 2.2 it is understood that, in most cases, more details can be found in Appendix B.

4.2.3 Special Case: The Blades Locked

Consider the special case when the blades are locked in their zero positions relative to the rotating disk. This leads to a system of dynamically isolated absorbers that oscillate freely under the influence of centrifugal effects. The governing equations follow from Equation (4.2) by setting $x_i = x_i' = x_i'' \equiv 0$, and are given by

$$M_{22} y_i'' + C_{22} y_i' + K_{22} y_i = 0, \qquad i \in \mathcal{N} \tag{4.9}$$

where the mass, damping, and stiffness terms M_{22}, C_{22}, and K_{22} are defined in Table 4.1. Equation (4.9) is a set of N uncoupled and unforced single-DOF harmonic oscillators. Their dimensionless undamped natural frequencies are given by

$$\bar{\omega}_{22} \equiv \frac{\omega_{22}}{\omega_o} = \sqrt{\frac{\alpha + \delta}{\gamma}}\, \sigma \equiv \tilde{n}\sigma, \tag{4.10}$$

or $\omega_{22} = \tilde{n}\Omega$ in dimensional form, where ω_o is defined by Equation (3.13) and

$$\tilde{n} = \sqrt{\frac{\alpha + \delta}{\gamma}} \tag{4.11}$$

is defined to be the *absorber tuning order*. Since the absorbers are restrained only through centrifugal effects, $\bar{\omega}_{22}$ scales directly with σ [32, 61]. This feature is exploited in Section 4.4 to tune the absorbers to a given *order* of the excitation, rather than to a fixed *frequency*, as is done in the classical sense [99]. The tuning parameter $\tilde{n}$ is used for this purpose and is determined by selecting the dimensionless curvature of the pendulum absorber γ (dimensionally d) and the distance of its effective attachment point from the center of rotation of the rotor, that is, $\alpha + \delta$ (dimensionally $\alpha L + H$).

4.2.4 Special Case: The Absorbers Locked

Here we consider a model in which the absorbers are locked in their zero positions relative to the blades. By setting $y_i = y_i' = y_i'' \equiv 0$, the equations of motion for the

i^{th} sector follow from Equation (4.2) and are given by

$$\left.\begin{aligned} M_{11}x_i'' + C_{11}x_i' + K_{11}x_i + \xi_c(-x_{i-1}' + 2x_i' - x_{i+1}') \\ + \nu^2(-x_{i-1} + 2x_i - x_{i+1}) = fe^{j\phi_i}e^{jn\sigma\tau} \end{aligned}\right\}, \qquad i \in \mathcal{N} \tag{4.12}$$

where ξ_c, ν, and f are defined in Table 3.1 and also $x_{N+1} = x_1$ and $x_0 = x_N$. The governing matrix equation of motion for the overall N-DOF system is given by

$$\hat{\mathbf{M}}_{11}\mathbf{x}'' + \hat{\mathbf{C}}_{11}\mathbf{x}' + \hat{\mathbf{K}}_{11}\mathbf{x} = \hat{\mathbf{f}}_{11}e^{jn\sigma\tau}, \tag{4.13}$$

where $\mathbf{x} = (x_1, x_2, \ldots, x_N)^T$ is a configuration vector and

$$\hat{\mathbf{f}}_{11} = \left(fe^{j\phi_1}, fe^{j\phi_2}, \ldots, fe^{j\phi_N}\right)^T \tag{4.14}$$

is the system forcing vector. The system matrices are both symmetric and circulant, and they can be represented by

$$\left.\begin{aligned} \hat{\mathbf{M}}_{11} &= \operatorname{circ}(M_{11}, 0, 0, \ldots, 0, 0) = \operatorname*{diag}_{i\in\mathcal{N}}(M_{11}) \\ \hat{\mathbf{C}}_{11} &= \operatorname{circ}(C_{11} + 2\xi_c, -\xi_c, 0, \ldots, 0, -\xi_c) \\ \hat{\mathbf{K}}_{11} &= \operatorname{circ}\left(K_{11} + 2\nu^2, -\nu^2, 0, \ldots, 0, -\nu^2\right) \end{aligned}\right\}. \tag{4.15}$$

In the absence of coupling, that is, when $\nu = \xi_c \equiv 0$, the system matrices given by Equation (4.15) are all diagonal, and Equation (4.13) is a decoupled set of N harmonically forced, single-DOF oscillators.

We now detail the steady-state forced response of Equation (4.13) (with the absorbers locked) and, subsequently, that of Equation (4.6) (with the absorbers free to move). In both cases a coordinate transformation is employed in order to significantly uncouple the governing matrix equations.

4.3 Forced Response

The forced response of the overall system is governed by Equation (4.6), which can be handled using standard techniques [65]. Its solution in the steady-state follows in

the usual way and is given by

$$\mathbf{q}^{\mathrm{ss}}(\tau) = \hat{\mathbf{Z}}^{-1}\hat{\mathbf{f}}e^{jn\sigma\tau}, \tag{4.16}$$

where $\hat{\mathbf{Z}} = \hat{\mathbf{K}} - n^2\sigma^2\hat{\mathbf{M}} + jn\sigma\hat{\mathbf{C}}$ is the system impedance matrix of dimension $2N \times 2N$. However, Equation (4.16) does not offer any insight into the design and effectiveness of the proposed vibration absorbers, and it also requires computation of $\hat{\mathbf{Z}}^{-1}$, which can be quite involved for many bladed disk models. We thus turn to a decoupling strategy that exploits the system symmetry and it is systematically shown how to reduce the governing matrix equation of motion to a set of reduced-order models.

It is well-known that, due to its cyclic symmetry (and in particular due to the circulant structure of the system matrices [62]), Equation (4.6) can be decoupled via a modal (unitary) transformation to a set of N reduced-order models, each with two DOF [36, 92, 100–102]. (The reduced-order models have the same number of DOF as an individual sector, in this case two.) Similar statements can be made for Equation (4.13), which captures the system dynamics for the special case when the absorbers are locked in their zero positions relative to the blades. Since the system matrices are circulant for this special case, one can fully decouple the N–DOF model to a set of N, single–DOF systems. A special feature of the uncoupled systems described above is that only mode $n + 1$ is excited, provided that n is an integer (as shown subsequently). Hence the steady-state response of the overall $2N$–DOF (resp. N–DOF) system described above reduces to the solution of a single, harmonically forced, 2–DOF (resp. single–DOF) system.

In order to provide a benchmark against which the effectiveness of the absorbers can be evaluated, we first consider the forced response of the system when the absorbers are locked relative to the blades. It should be noted that the corresponding analysis could be obtained directly from the more general analysis of Section 4.3.2. However, it is instructive to introduce the modal transformation in this simpler setting, which clearly demonstrates the essential features of the approach. The forced

response of the general system, where the absorbers are free to move, is investigated in Section 4.3.2 and employs the same methodology. An absorber tuning strategy is motivated in Section 4.4 based on these results.

4.3.1 Response with the Absorbers Locked

The purpose of this section is twofold: to demonstrate the essential features of the analysis, a generalization of which is employed in Section 4.3.2 for the case when the absorbers are free to move, and to review some of the vibration characteristics of linear cyclic systems. Some specific topics include: decoupling the equations of motion; orthogonality of the modal forcing vector; the steady-state system response; characteristics of the natural frequencies and attendant normal modes (see [9, 92, 94] for further characteristics); and conditions for resonance. The results will also be useful for comparisons when evaluating the effectiveness of the absorbers in subsequent sections. The reader who is familiar with these topics can proceed, with minimal loss of continuity, to Section 4.3.2.

Modal Analysis

Consider the forced response of the system in Figure 4.1a for the special case when the absorbers are locked in their zero positions relative to the blades. Due to the cyclicity of the model and the corresponding circulant structure of the system matrices given by Equation (4.15), one can employ a standard unitary (similarity) transformation to decouple the governing equations of motion. In particular, we wish to apply the result given by Equation (2.9) of Section 2.2.4 to each of the system matrices. This

can be achieved by introducing the change of coordinates[3,4]

$$\mathbf{x} = \mathbf{E}\tilde{\mathbf{x}}, \qquad \text{or} \qquad x_p = \mathbf{e}_p^T \tilde{\mathbf{x}}, \qquad p \in \mathcal{N} \tag{4.17}$$

where $\mathbf{E}$ is the $N \times N$ complex Fourier matrix and $\mathbf{e}_p$ is its p^{th} column (these are defined by Equation (2.2) and Equation (2.4)), and $\tilde{\mathbf{x}} = (\tilde{x}_1, \tilde{x}_2, \ldots, \tilde{x}_N)^T$ is a vector of modal, or *cyclic* coordinates. Substituting Equation (4.17) into Equation (4.13), multiplying from the left by the unitary matrix $\mathbf{E}^{\mathcal{H}}$, and invoking Equation (2.9) yields a system of N decoupled scalar equations. They are

$$\tilde{M}_{11}^{(p)} \tilde{x}_p'' + \tilde{C}_{11}^{(p)} \tilde{x}_p' + \tilde{K}_{11}^{(p)} \tilde{x}_p = \mathbf{e}_p^{\mathcal{H}} \hat{\mathbf{f}}_{11} e^{jn\sigma\tau}, \qquad p \in \mathcal{N} \tag{4.18}$$

where $(\cdot)^{\mathcal{H}} = (\bar{\cdot})^T$ denotes the conjugate transpose and $\mathbf{e}_p^{\mathcal{H}} \hat{\mathbf{f}}_{11}$ is the p^{th} element of $\mathbf{E}^{\mathcal{H}} \hat{\mathbf{f}}_{11}$, and is discussed subsequently. The modal mass, damping, and stiffness terms follow from Equation (2.10) and are given by

$$\left.\begin{aligned} \tilde{M}_{11}^{(p)} &= M_{11} \\ \tilde{C}_{11}^{(p)} &= C_{11} + 2\xi_c(1 - \cos\varphi_p) \\ \tilde{K}_{11}^{(p)} &= K_{11} + 2\nu^2(1 - \cos\varphi_p) \end{aligned}\right\}, \qquad p \in \mathcal{N} \tag{4.19}$$

where φ_p is defined by Equation (2.3) and the elements M_{11}, C_{11}, and K_{11} are defined in Table 4.1. Note that the identity $w^{(p-1)} + w^{(N-1)(p-1)} = 2\cos\varphi_p$ has been employed, where $w_N = w = e^{\frac{2j\pi}{N}}$ is the primitive N^{th} root of unity.[5] The transformation of the single N–DOF system given by Equation (4.13) to the system of N decoupled single–DOF systems given by Equation (4.18) is illustrated in Figure 4.2.

Assuming harmonic motion, the p^{th} steady-state modal response follows easily

[3]The reader who is not familiar with transformations of this type should regard Equation (4.17) as the usual modal transformation employed in elementary linear vibration theory. (See Figure 4.2.) The columns $\mathbf{e}_i$ of the fourier matrix $\mathbf{E}$ are, in fact, the eigenvectors of *any* circulant matrix, and hence they define the system mode shapes for *all* linear cyclic systems with a single DOF per sector.

[4]The index p corresponds to the p^{th} mode of vibration and shall be referred to as the *mode number.*

[5]See Section B.4.1 of Appendix B for a derivation of the N^{th} roots of unity. The distinct N^{th} roots are plotted in Figure B.1 on page 191 for $N = 1, \ldots, 9$.

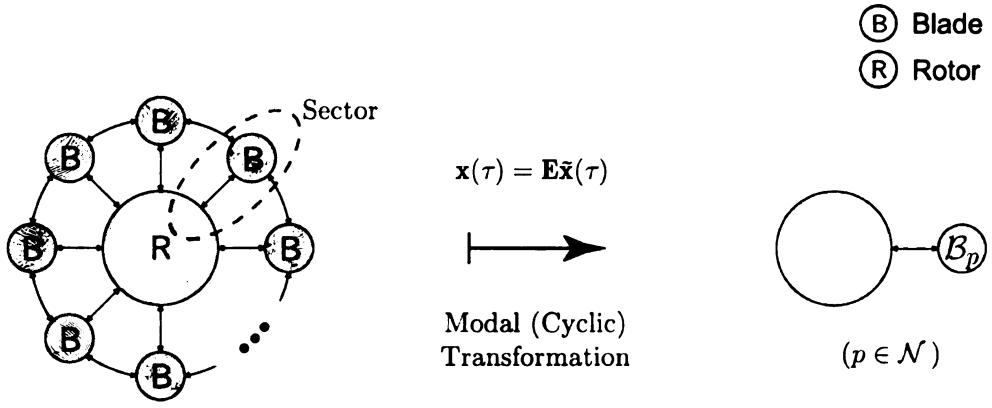

(a) A Single Coupled N–DOF System in Physical Space

(b) N Decoupled 1–DOF Systems in Modal Space

Figure 4.2. The topology of a bladed disk assembly in (a) physical space and (b) modal space. The modal transformation $\mathbf{x}(\tau) = \mathbf{E}\tilde{\mathbf{x}}(\tau)$ reduces the cyclic array of N single–DOF coupled models B, which together form a N–DOF coupled system, to a set of N single–DOF decoupled models $\mathcal{B}_p$.

from Equation (4.18) and is given by

$$\tilde{x}_p^{ss}(\tau) = \frac{1}{\tilde{\Gamma}_{11}^{(p)}} \mathbf{e}_p^{\mathcal{H}} \hat{\mathbf{f}}_{11} e^{jn\sigma\tau}, \qquad p \in \mathcal{N} \tag{4.20}$$

where

$$\tilde{\Gamma}_{11}^{(p)} = \tilde{K}_{11}^{(p)} - n^2\sigma^2 \tilde{M}_{11}^{(p)} + jn\sigma\tilde{C}_{11}^{(p)}, \qquad p \in \mathcal{N}. \tag{4.21}$$

Under the assumption that $0 < n < N$ is an integer, the p^{th} modal forcing term simplifies considerably and is given by [36, 92]

$$\begin{aligned} \mathbf{e}_p^{\mathcal{H}} \hat{\mathbf{f}}_{11} &= \frac{f}{\sqrt{N}} \sum_{k=1}^{N} w^{(k-1)(n+1-p)} \\ &= \begin{cases} \sqrt{N} f, & p = n+1 \\ 0, & \text{otherwise} \end{cases} \end{aligned} \tag{4.22}$$

which follows from Theorem B.3 on page 192. Equation (4.22) shows that only mode

$n+1$ is excited and, therefore,[6]

$$\tilde{x}_{n+1}^{\mathrm{ss}}(\tau) = \frac{\sqrt{N}f}{\tilde{\Gamma}_{11}^{(n+1)}} e^{jn\sigma\tau} \tag{4.23}$$

is the only non-zero modal response in the steady-state. The response of sector i (in physical coordinates) follows from the transformation given by Equation (4.17) and is given by $x_i^{\mathrm{ss}} = \mathbf{e}_i^T \tilde{\mathbf{x}}^{\mathrm{ss}}$, or

$$x_i^{\mathrm{ss}}(\tau) = X e^{j\phi_i} e^{jn\sigma\tau}, \qquad i \in \mathcal{N} \tag{4.24}$$

where $\tilde{\mathbf{x}}^{\mathrm{ss}}(\tau) = \left(0, \ldots, 0, \tilde{x}_{n+1}^{\mathrm{ss}}(\tau), 0, \ldots, 0\right)^T$ and $w^{n(i-1)} = e^{j\phi_i}$ have been employed and $X = f/\tilde{\Gamma}_{11}^{(n+1)}$ is the steady-state amplitude of the blades. Equation (4.24) shows that each blade behaves identically except for a constant phase shift from one sector to another, which is captured by the inter-blade phase angle ϕ_i. This approach offers a significant computational advantage over the brute force solution of the full N-DOF system, and it is employed in Section 4.3.2 for the general case when the absorbers are free to move.

Eigenfrequency Characteristics and Conditions for Resonance

Since the transformation given by Equation (4.17) is unitary, the (dimensionless) natural frequencies $\bar{\omega}_{11}^{(p)}$ are preserved and they follow in the usual way from $\tilde{K}_{11}^{(i)}$ and $\tilde{M}_{11}^{(i)}$. In terms of the parameters defined in Table 3.1, they are given by

$$\bar{\omega}_{11}^{(p)} \equiv \frac{\omega_{11}^{(p)}}{\omega_o} = \sqrt{\frac{1 + \delta\sigma^2(1 + \mu(\alpha+\gamma)) + 2\nu^2\left(1 - \cos\varphi_p\right)}{1 + \mu\left(\alpha+\gamma\right)^2}}, \qquad i \in \mathcal{N} \tag{4.25}$$

where ω_o is given by Equation (3.13) and φ_p is defined by Equation (2.3). For zero inter-blade coupling ($\nu = 0$) all of the natural frequencies are identical, and they

[6]It is customary in the rotordynamics literature to designate the system modes in terms of their "diamatral components," or number of "nodal diamters." (These can be clearly visualized in the modal configurations shown in Figure 2.7 on page 35.) Specifically, if $0 < n \leq N/2$ (or $0 < n \leq (N-1)/2$ if N is odd) then an n e.o excitation can only excite modes with n nodal diameters. However, such a designation is slightly more cumbersome if one considers larger values of n (in this chapter and the next we consider $0 < n < N$) and hence we shall say instead that an engine order n excites only mode $p = n + 1$.

increase with increasing rotor speed σ due to centrifugal effects. The presence of the absorber masses ($\mu \neq 0$) slightly lowers the natural frequencies. For very small absorber masses relative to the mass of the blades, that is, $0 < \mu \ll 1$, the natural frequencies can be approximated by

$$\bar{\omega}_{11}^{(p)} \cong \sqrt{1 + \delta\sigma^2 + 2\nu^2(1 - \cos\varphi_p)}, \qquad i \in \mathcal{N} \tag{4.26}$$

which clearly exhibits the effects of centrifugal stiffening and coupling. Finally, if $\mu = \nu = \sigma \equiv 0$ we recover $\bar{\omega}_{11}^{(p)} = 1$, or $\omega_{11}^{(p)} = \omega_o$, which was used in Section 4.2.1 to nondimensionalize the model. By comparing Equation (4.26) to Equation (2.38), it is clear that the eigenfrequency characteristics discussed in Section 2.4.3 apply here as well.

In the turbomachinery literature it is common to plot the natural frequencies in terms of the "diametral components," that is, the number of "nodal diameters" (n.d.) in their attendant mode shapes [103]. (These can be visualized in Figure 2.7 on page 35.) However, in light of the crucial role centrifugal stiffening plays in the absorber performance (this is investigated in detail in Section 4.4), we shall opt instead for an interference, or *Campbell diagram* representation of the natural frequencies. Such a diagram is shown in Figure 4.3a for $N = 10$ blades and for a particular sector model. In this figure, the natural frequency loci are plotted in terms of the dimensionless rotor speed, and they are seen to increase for increasing σ due to centrifugal effects. The diametral component of each frequency locus is also indicated.

In general, there may be a system resonance whenever $n\sigma = \bar{\omega}_{11}^{(p)}(\sigma)$ or, equivalently, $n\Omega = \omega_{11}^{(p)}(\Omega)$, and these *possible* resonances can be identified in a Campbell diagram by the intersections of the natural frequency loci with an engine order line $n\sigma$. (An example of such a frequency versus rotor speed diagram is shown in Figure 4.3a, where several order lines are indicated.) Such resonances can arise, for example, from excitations with multiple dominant orders, mistuning [9], nonlinear effects, or non-integer n. (Appendix C briefly discusses the case of $n \in \mathbb{R}_+$.) However, for linear

Table 4.2. Data to accompany Fig. 4.3 and Figs. 4.5–4.7 for a model with $N = 10$, $n = 3$, $\alpha = 0.84$, $\delta = 0.67$, $\mu = 0.015$, and $\xi_a = \xi_b = \xi_c = 0$. Then $\beta_{\text{cr}} = -0.00701$ (from Equation (D.2) of Appendix D) and $\beta_{\text{cr}}^{\text{app}} = -0.00706$ (from Equation (4.46) of Section 4.4.2).

Figure	Tuning	β	γ	$\tilde{n}$	$\hat{n}$	$\hat{n}_{\text{app}}$	ν	σ_{res}
4.3	–	–	0.169	–	–	–	0.50	0.442
4.5a	Over	+0.15	0.127	3.45	3.473	3.487	0.01	0.338
4.5b	Over	+0.15	0.127	3.45	3.473	3.487	0.25	0.364
4.5c	Over	+0.15	0.127	3.45	3.473	3.487	0.50	0.443
4.6a	Under	−0.07	0.194	2.790	2.811	2.820	0.50	0.468
4.6b	Over	+0.07	0.147	3.210	3.232	3.244	0.50	0.423
4.7a	Under	−0.00351	0.169	2.989	3.011	3.021	0.50	–
4.7b	Exact	0	0.168	3	3.021	3.032	0.50	–

cyclic systems, and in the absence of parameter mistuning, an integer engine order $1 \leq n < N$ excites only mode $p = n + 1$, which is clear from Equation (4.22). (See Section 2.4.5 for a description of the resonance structure for the case when $n \geq N$.) For a given engine order, the corresponding *actual* resonance, that is, the value of σ for which

$$n\sigma = \bar{\omega}_{11}^{(n+1)}(\sigma), \qquad \text{or, equivalently} \qquad n\Omega = \omega_{11}^{(n+1)}(\Omega) \tag{4.27}$$

is indicated by a circle in Figure 4.3a for each of the engine orders considered, and the corresponding frequency response curves are shown in Figure 4.3b for $f = 0.01$ and $\xi_b = \xi_c = 0$. The resonant frequency for the $n = 3$ case is indicated in Table 4.2, along with other data corresponding to Figures 4.5–4.7; these are explained in Section 4.3.2 and Section 4.4.2.

4.3.2 Response with the Absorbers Free

We now turn to the forced dynamics of the overall $2N$-DOF system, which are governed by Equation (4.6), and employ an approach similar to that of Section 4.3.1. In

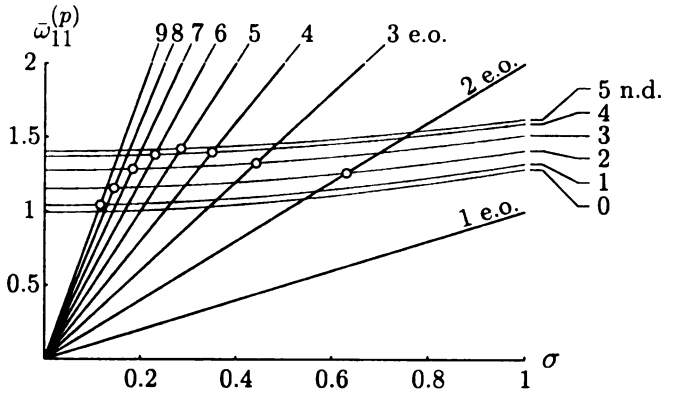

(a) Campbell Diagram

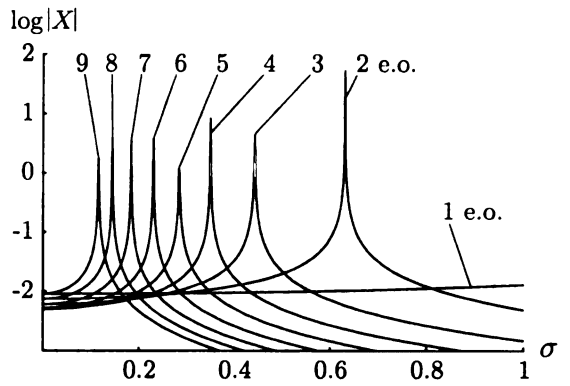

(b) Frequency Response Curves

Figure 4.3. (a) Campbell diagram for $N = 10$, $\alpha = 0.84$, $\delta = 0.67$, $\gamma = 0.169$, $\mu = 0.015$, $\nu = 0.5$, and engine orders (e.o.) $n = 1, 2, \ldots, N-1$ and (b) the corresponding frequency response curves with $f = 0.01$, and $\xi_b = \xi_c = 0$.

the present case the system matrices $\tilde{\mathbf{M}}$, $\tilde{\mathbf{C}}$, and $\tilde{\mathbf{K}}$ are *block* circulant, and one can (block) decouple these equations to a set of N, 2–DOF forced oscillators by employing the result given by Equation (2.11) on page 15.[7]

Modal Analysis

We introduce the change of coordinates

$$\mathbf{q} = (\mathbf{E} \otimes \mathbf{I})\mathbf{u}, \qquad \text{or} \qquad \mathbf{z}_p = (\mathbf{e}_p^T \otimes \mathbf{I})\mathbf{u}, \qquad p \in \mathcal{N} \tag{4.28}$$

where $\mathbf{E}$ is the $N \times N$ complex Fourier matrix and $\mathbf{e}_p$ is its p^{th} column, $\otimes$ is the Kronecker product (these are defined in Section 2.2.2 and Section 2.2.1), $\mathbf{I}$ is the 2×2 identity matrix (the dimension of $\mathbf{I}$ corresponds to the number of DOF in each sector), and $\mathbf{u} = (\mathbf{u}_1, \mathbf{u}_2, \ldots, \mathbf{u}_N)^T$ is a vector of modal, or *cyclic coordinates* with each $\mathbf{u}_p = (\tilde{x}_p, \tilde{y}_p)^T$. Substituting Equation (4.28) into Equation (4.6) and multiplying from the left by the unitary matrix $(\mathbf{E} \otimes \mathbf{I})^{\mathcal{H}} = (\mathbf{E}^{\mathcal{H}} \otimes \mathbf{I})$ yields a system of N block decoupled equations, each with two DOF. They are given by

$$\tilde{\mathbf{M}}_p \mathbf{u}_p'' + \tilde{\mathbf{C}}_p \mathbf{u}_p' + \tilde{\mathbf{K}}_p \mathbf{u}_p = (\mathbf{e}_p^{\mathcal{H}} \otimes \mathbf{I})\hat{\mathbf{f}} e^{jn\sigma\tau}, \qquad p \in \mathcal{N} \tag{4.29}$$

where $(\mathbf{e}_p^{\mathcal{H}} \otimes \mathbf{I})\hat{\mathbf{f}}$ is the p^{th} 2×1 block of $(\mathbf{E}^{\mathcal{H}} \otimes \mathbf{I})\hat{\mathbf{f}}$. Figure 4.4 illustrates the transformation of the single $2N$–DOF system given by Equation (4.6) to a system of N block decoupled 2–DOF forced oscillators given by Equation (4.29).

The 2×2 mass, damping, and stiffness matrices associated with the p^{th} mode follow from Equation (2.12) of Section 2.2.4 and are given by

$$\left.\begin{aligned} \tilde{\mathbf{M}}_p &= \mathbf{M} \\ \tilde{\mathbf{C}}_p &= \mathbf{C} + 2\mathbf{C}_c(1 - \cos\varphi_p) \\ \tilde{\mathbf{K}}_p &= \mathbf{K} + 2\mathbf{K}_c(1 - \cos\varphi_p) \end{aligned}\right\}, \qquad p \in \mathcal{N} \tag{4.30}$$

where φ_p is defined by Equation (2.3), the elements of $\mathbf{M}$, $\mathbf{C}$, and $\mathbf{K}$ are defined in Table 4.1 and their attendant parameters are given in Table 3.1, and the coupling

[7]The number of DOF in each decoupled system is that of an individual sector, in this case two.

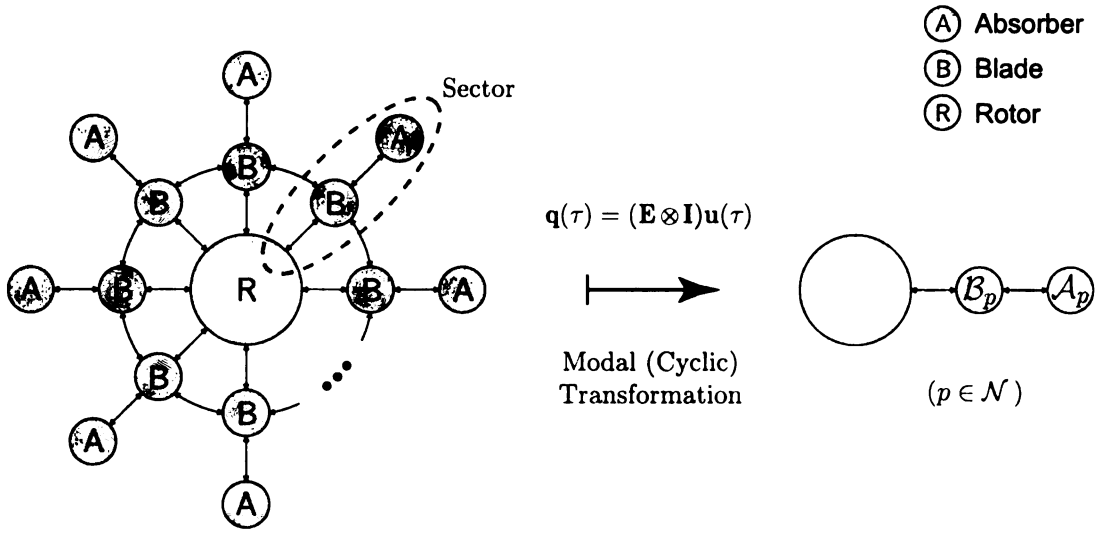

(a) A Single Coupled $2N$–DOF System (b) N Decoupled 2–DOF Systems

Figure 4.4. The topology of a bladed disk assembly fitted with absorbers in (a) physical space and (b) modal space. The modal transformation $\mathbf{q}(\tau) = (\mathbf{E} \otimes \mathbf{I})\mathbf{u}(\tau)$ reduces the cyclic array of N, 2–DOF sector models (B, A), which together form a $2N$–DOF coupled system, to a set of N, 2–DOF block decoupled models $(\mathcal{B}_p, \mathcal{A}_p)$.

matrices $\mathbf{C}_c$ and $\mathbf{K}_c$ are defined by Equation (4.4). In light of Equation (4.22), the p^{th} modal forcing vector takes the form

$$(\mathbf{e}_p^{\mathcal{H}} \otimes \mathbf{I})\hat{\mathbf{f}} = \begin{bmatrix} \mathbf{e}_p^{\mathcal{H}} \hat{\mathbf{f}}_{11} \\ 0 \end{bmatrix} = \begin{cases} \sqrt{N}\,\mathbf{f}, & p = n+1 \\ \mathbf{0}, & \text{otherwise} \end{cases} \tag{4.31}$$

where $\hat{\mathbf{f}}_{11}$ is the system forcing vector for the case when the absorbers are locked in their zero positions relative to the blades, $\mathbf{f} = (f, 0)^T$ is the sector forcing vector, and $\mathbf{0} = (0, 0)^T$. Since only mode $p = n+1$ is excited, $\mathbf{u}_{n+1}(\tau)$ is the only nonzero modal response in the steady-state.

Assuming harmonic motion, and in light of Equation (4.31), the p^{th} steady-state modal response follows easily from Equation (4.29) and is given by

$$\mathbf{u}_p^{\text{ss}}(\tau) = \begin{cases} \sqrt{N}\,\tilde{\mathbf{Z}}_{n+1}^{-1}\,\mathbf{f} e^{jn\sigma\tau}, & p = n+1 \\ \mathbf{0}, & \text{otherwise} \end{cases} \tag{4.32}$$

where

$$\tilde{\mathbf{Z}}_p = \tilde{\mathbf{K}}_p - n^2\sigma^2\tilde{\mathbf{M}}_p + jn\sigma\tilde{\mathbf{C}}_p, \qquad p \in \mathcal{N} \tag{4.33}$$

is the p^{th} modal impedance matrix. The response of sector i (in physical coordinates) follows from the transformation given by Equation (4.28) with $\mathbf{u}^{\text{ss}}(\tau) = (\mathbf{0}, \ldots, \mathbf{0}, \mathbf{u}^{\text{ss}}_{n+1}(\tau), \mathbf{0}, \ldots, \mathbf{0})^T$ and is given by

$$\mathbf{z}^{\text{ss}}_i(\tau) = \tilde{\mathbf{Z}}^{-1}_{n+1}\mathbf{f}\, e^{j\phi_i} e^{jn\sigma\tau}, \qquad i \in \mathcal{N} \tag{4.34}$$

where $w^{n(i-1)} = e^{j\phi_i}$ has been employed. From Equation (4.34) it is clear that each blade/absorber combination behaves identically except for a constant phase shift from one sector to another, which is captured by the inter-blade phase angle ϕ_i. This approach offers a significant computational advantage over the brute-force solution to the full $2N$–DOF system, as given by Equation (4.16).

Eigenfrequency Structure and Conditions for Resonance

The $2N$ dimensionless natural frequencies of the system are defined implicitly by the characteristic polynomial

$$\det\left(\hat{\mathbf{K}} - \bar{\omega}^2\hat{\mathbf{M}}\right) = 0,$$

the solution of which can be quite involved for any reasonable bladed disk model. This effort can be significantly reduced, however, by instead using the modal matrices defined by Equation (4.30). We recall that each $\tilde{\mathbf{M}}_p$ and $\tilde{\mathbf{K}}_p$ follow from a unitary (similarity) transformation of $\hat{\mathbf{M}}$ and $\hat{\mathbf{K}}$ and hence the system natural frequencies are preserved. These eigenfrequencies follow from the N, second-order characteristic polynomials $\det\left(\tilde{\mathbf{K}}_p - \bar{\omega}^2\tilde{\mathbf{M}}_p\right) = 0$, or

$$\det\left(\mathbf{K} - \bar{\omega}^2\mathbf{M} + 2\mathbf{K}_c(1 - \cos\varphi_p)\right) = 0, \qquad p \in \mathcal{N} \tag{4.35}$$

where the sector mass, stiffness, and coupling matrices are defined in Table 4.1 and by Equation (4.4). Equation (4.35) features the same cyclic term, i.e., Equation (2.39),

that was encountered in Section 2.4.3 and we thus expect similar eigenfrequency characteristics to the ones described there and also in Sectioni 4.3.1. If P is the number of DOF in an individual sector (in the present study $P = 2$), then there are P natural frequencies $\bar{\omega}^{(p)}$ corresponding to each $p \in \mathcal{N}$. There are, in this case, N such groups of $P = 2$ natural frequencies of the overall system. The multiplicity of these *groups* of natural frequencies is identical to that of the *individual* eigenfrequencies described in Section 2.4.3.

If $\mathbf{v}_p$ is an eigenvector of the p^{th} decoupled modal system, then the corresponding normal mode of the overall system is $\mathbf{e}_p \otimes \mathbf{v}_p$, where $\mathbf{e}_p$ is the p^{th} modal vector for the case when the absorbers are locked relative to the blades.[8] With the exception of the $p = 1$ mode, $\mathbf{v}_p$ is influenced by the overall system configuration, and in particular by its elastic coupling, which is clear by inspection of the modal stiffness matrices $\tilde{\mathbf{K}}_p$. In a particular mode of vibration, the blade and absorber in each sector oscillate either in phase or out of phase relative to one another with amplitudes that depend on the strength and nature of the inter-sector coupling, and these features are captured by $\mathbf{v}_p$. The dynamics of each sector are identical, except for a constant difference in phase from one sector to another, and this is captured by $\mathbf{e}_p$. Hence the modal configuration of the overall system is described by a composite of these two vectors, which is mathematically given by $\mathbf{e}_p \otimes \mathbf{v}_p$.

The $2N$ dimensionless natural frequencies $\bar{\omega}_{1,2}^{(p)}$ $(p \in \mathcal{N})$ are plotted in Figure 4.5 in terms of the rotor speed σ for $N = 10$, $n = 3$, for a particular sector model, and for various levels of the inter-blade coupling ν. (The natural frequencies $\bar{\omega}_{11}^{(p)}$ and $\bar{\omega}_{22}$ are also shown for reasons discussed below. Also, for quick reference here and in subsequent chapters, Table 4.3 gives a selected list of commonly used undamped natural frequencies.) In these Campbell diagrams, the N natural frequencies $\bar{\omega}_1^{(p)}$

[8]When the absorbers are locked each of the the system matrices is a circulant. Since *all* circulant matrices share the same linearly independent eigenvectors, which are the columns of the Fourier matrix, the system normal modes are $\mathbf{e}_p$ with $p \in \mathcal{N}$.

Table 4.3. Selected list of dimensionless undamped natural frequencies.

Freq.	Eqn.	Description
$\bar{\omega}_1^{(p)}$	(4.35)	Of the coupled system corresponding to in-phase modes
$\bar{\omega}_2^{(p)}$	(4.35)	Of the coupled system corresponding to out-of-phase modes
$\bar{\omega}_{11}^{(p)}$	(4.25)	Of the coupled system if the absorbers are locked relative to the blades
$\bar{\omega}_{11}$	–	Of an isolated blade without an absorber
$\bar{\omega}_{22}$	(4.10)	Of each absorber if the blades are locked relative to the rotating hub

branching from $\sigma = 0$ (since N is even there are $(N-2)/2 = 4$ repeated pairs) correspond to in-phase modes, wherein the absorber/blade combination in a particular sector oscillates in phase. The remaining N natural frequencies $\bar{\omega}_2^{(p)}$ have the same number of repeated pairs and correspond to out-of-phase modes. As shown in Figure 4.5a, the frequencies $\bar{\omega}_1^{(p)}$ and also $\bar{\omega}_2^{(p)}$ are nearly coincident when the inter-blade coupling is weak, that is, when ν is small and they spread out for increasing ν, which is shown in Figure 4.5b and Figure 4.5c. In the absence of inter-blade coupling, $\bar{\omega}_1^{(p)}$ are identically coincident (as are $\bar{\omega}_2^{(p)}$) and there are exactly $P = 2$ distinct natural frequencies, each with multiplicity N.

The frequency loci in Figure 4.5 exhibit the classical eigenvalue veering phenomenon, or mutual repulsion of the eigenfrequencies [104, 105], which arises due to small the dynamic coupling (via the absorber mass) between the blades and absorbers. To see this, we focus on Figure 4.5a, where the sets of frequencies $\bar{\omega}_1^{(p)}$ and $\bar{\omega}_2^{(p)}$ are mutually nearly coincident. This plot also shows the natural frequencies $\bar{\omega}_{11}^{(p)}$ (resp. $\bar{\omega}_{22}$), corresponding to the case when the absorbers (resp. blades) are locked relative to the blades (resp. rotor). As the rotor speed σ is increased from zero, the natural frequencies $\bar{\omega}_1^{(p)}$ (resp. $\bar{\omega}_2^{(p)}$) initially lie close to $\bar{\omega}_{22} = \tilde{n}\sigma$ (resp. $\bar{\omega}_{11}^{(p)}$), where the absorber tuning order $\tilde{n}$ is defined by Equation (4.11). (For zero rotor speed $\bar{\omega}_1^{(p)}$ and $\bar{\omega}_{22}$ are, in fact, coincident and each has the same initial slope of $\tilde{n}$.) They

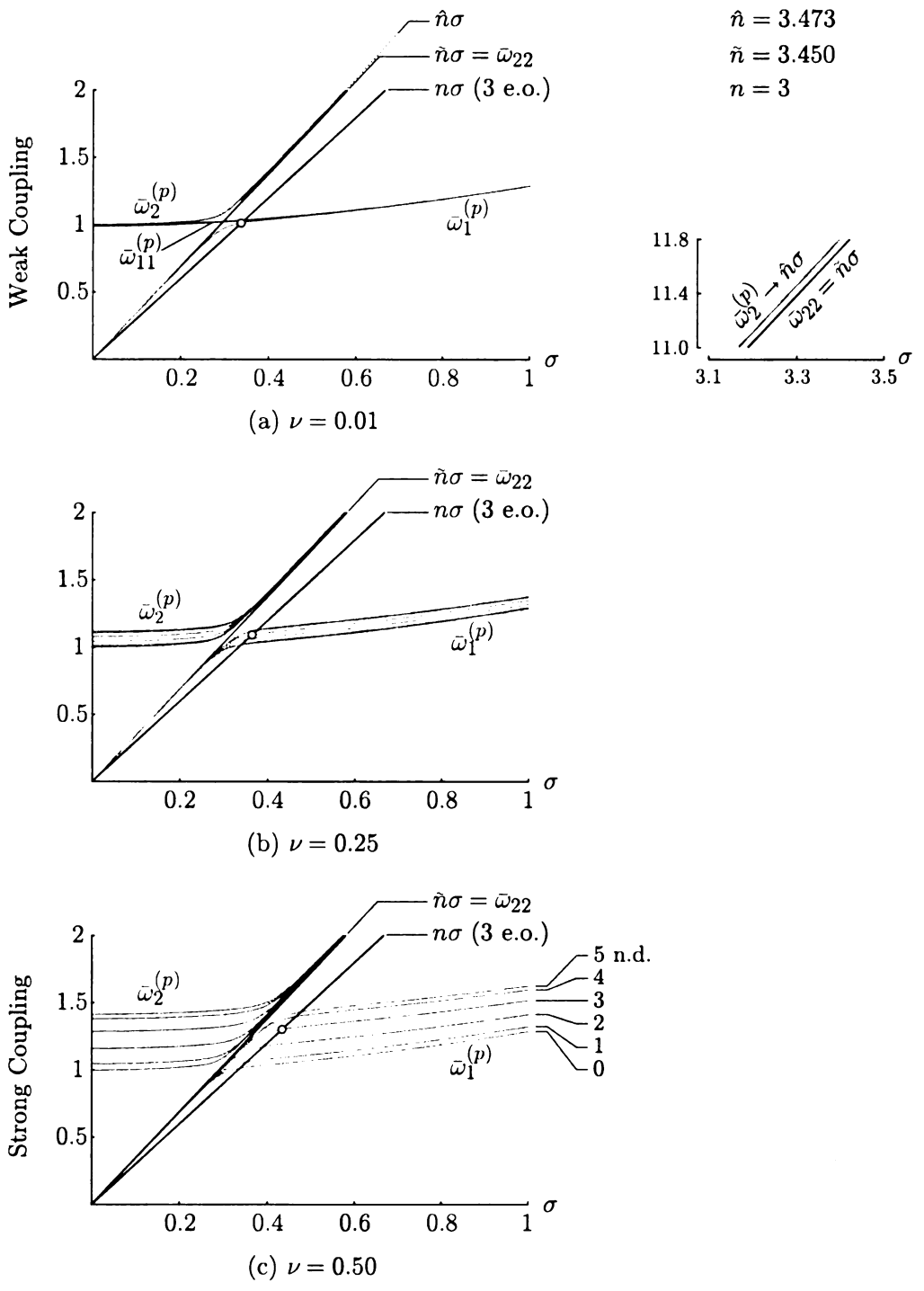

Figure 4.5. Campbell diagrams showing the engine order (e.o.) line $n\sigma$ and the dimensionless natural frequencies $\bar{\omega}_{11}^{(p)}$, $\bar{\omega}_{22} = \tilde{n}\sigma$, and $\bar{\omega}_{1,2}^{(p)}$ versus the dimensionless rotor speed σ for $N = 10$, $n = 3$, $\alpha = 0.84$, $\gamma = 0.127$, $\delta = 0.67$, and $\mu = 0.015$ with: (a) $\nu = 0.01$; (b) $\nu = 0.25$; (c) $\nu = 0.5$.

exhibit veering near the intersections of $\bar{\omega}_{11}^{(p)}$ and $\bar{\omega}_{22}$, and for large rotor speeds the eigenfrequencies $\bar{\omega}_1^{(p)}$ asymptotically approach $\bar{\omega}_{11}^{(p)}$ for each $p \in \mathcal{N}$. However, the frequencies $\bar{\omega}_2^{(p)}$ nearly track $\bar{\omega}_{22} = \tilde{n}\sigma$ as σ becomes increasingly large, but with a slight offset in slope. This is shown in the inset of Figure 4.5a. In fact, it can be shown that

$$\bar{\omega}_2^{(p)} \to \hat{n}\sigma \quad \text{as} \quad \sigma \to \infty, \tag{4.36}$$

where the *critical absorber tuning order* $\hat{n}(\tilde{n}) > \tilde{n}$ is defined by Equation (D.1) in Appendix D. This is a crucial observation, one that is exploited in the absorber tuning of Section 4.4. Finally, note that there is a fixed relationship between $\tilde{n}$ and $\hat{n}$, which is nearly linear for $\tilde{n} > 1$. Once the absorber mass μ and its tuning order $\tilde{n}$ are prescribed, then the critical tuning order is automatically set and can be approximated by

$$\hat{n}_{\text{app}} = (1 + \alpha^2\mu)\,\tilde{n}, \tag{4.37}$$

which works quite well for $\tilde{n} > 1$ and for reasonable choices of α and μ.

Possible resonances can be identified in Figure 4.5 by the intersections of the eigenfrequency loci $\bar{\omega}_{1,2}^{(p)}(\sigma)$ with the order line $n\sigma$, and they correspond to rotor speeds $\sigma = \sigma_{\text{res}}$ for which $n\sigma = \bar{\omega}_{1,2}^{(p)}(\sigma)$. However, it was shown in Section 4.3.2 that only mode $n+1$ is excited in the steady-state, and hence there is a system resonance only when

$$n\sigma = \bar{\omega}_{1,2}^{(n+1)}(\sigma), \qquad \text{or, equivalently} \qquad n\Omega = \omega_{1,2}^{(n+1)}(\Omega) \tag{4.38}$$

is satisfied. These resonances are indicated by circles in Figure 4.5 and they are summarized in Table 4.2 on page 90 along with other relevant data. The main objective of this chapter is to select the absorber parameters to avoid such resonances over a range of rotor operating speeds; this is the subject of the next section.

As a final note, the inter-blade coupling ν can be quite small—on the order of 1% or less—but much larger values are also possible. Aerodynamic coupling also exists

and can be significant in terms of both stiffness and damping. In order to show clearly which modes are excited, and also the effects of absorber (de)tuning, a rather large (possibly unrealistic) value of the coupling will be employed in the ensuing numerical analysis; this does not qualitatively affect the approach nor the conclusions.

4.4 Absorber Tuning

Absorber tuning refers to a particular choice of absorber parameters to attenuate, as much as possible, the response of the primary systems (blades) over a range of operating speeds, and in particular near resonance. This is done by prescribing the dimensionless parameters μ, γ, and α, which in turn specify the absorber mass m, the radius r of its path, and it's placement along the blades, respectively. It is shown in Section 4.4.1 that, in the absence of damping, there exists an absorber tuning such that full annihilation of the blade vibrations is possible, although this may require large-amplitude vibrations of the absorbers. This tuning is accomplished by matching the order of the isolated absorbers to that of the excitation, just as it is done with frequencies in the classical dynamic vibration absorber [99], and also with orders for the centrifugal pendulum vibration absorber [7]. (See Section 2.5.) In the presence of small absorber damping, however, it becomes impossible to eliminate the blade vibrations completely, a topic that is briefly addressed in Section 4.5. The effects of *detuning* the absorbers relative to the excitation order is explored in Section 4.4.2.[9] It is shown that overtuning the absorbers results in only one system resonance over all possible rotation speeds, even though there are two DOF per sector and there are N such sectors, and the same is true for most values of undertuning. However, there exists a small region of absorber undertuning, bounded on one side by the exact

[9]In this work *detuning* means that all absorbers are identically over- or under-tuned relative to n. This is not to be confused with *mistuning*, which refers to small random uncertainties in the system parameters. In the turbomachinery literature, detuning and mistuning are often used interchangeably, but they must be clearly distinguished in this investigation.

tuning (zero detuning), for which there are no system resonances. This *no-resonance gap* motivates a particular tuning strategy, which offers a significant reduction of the blade amplitudes, and it is robust to random perturbations of the system model.

Consider again the Campbell diagrams in Figure 4.5. Whereas n is fixed for a particular engine order excitation, the tuning order $\tilde{n}$ depends on the model parameters α, δ, and γ (these are prescribed by design), and the additional choice for the dimensionless absorber mass μ sets the critical tuning order $\hat{n}(\tilde{n})$. The tuning strategy employed here is to simply choose these parameters to optimally orient the line $\tilde{n}\sigma$ (and hence $\hat{n}\sigma$) relative to $n\sigma$ in the frequency-σ plane. This in turn sets the asymptotic behavior of the system natural frequencies $\bar{\omega}_{1,2}^{(p)}$ and hence prescribes the system resonance structure. It is clear that by choosing $\tilde{n}\sigma = n\sigma$ (this corresponds to zero detuning) there will be no crossings of the order line $n\sigma$ and the natural frequency loci $\bar{\omega}_{1,2}^{(p)}(\sigma)$, and hence there will be no system resonances over the full range of possible rotor speeds. However, slight errors in this tuning can introduce a resonance, and therefore such a design is not robust. One can more generally avoid resonances by choosing parameters such that $\tilde{n} \leq n < \hat{n}(\tilde{n})$. This is clear from the large-σ asymptotic behavior of $\bar{\omega}_2^{(p)}$, and specifically from the inset of Figure 4.5a. The existence of this finite, but narrow, tuning range allows one to design an absorber system with some level of robustness to parameter uncertainties.

The arguments described above are developed in detail in the next section using the steady-state system response of Section 4.3.2, and in the context of absorber detuning in Section 4.4.2.

4.4.1 Exact Tuning

It is customary to introduce the tuning order $\tilde{n}$ as one of the absorber parameters, and this is done in the present study via the substitution

$$\gamma = \frac{\alpha + \delta}{\tilde{n}^2}, \tag{4.39}$$

thereby replacing γ with $\tilde{n}$ in the formulation. With zero system damping, i.e., $\xi_a = \xi_b = \xi_c = 0$, and after some simplification, the steady-state response described by Equation (4.34) can be reduced to

$$\begin{bmatrix} x_i^{ss}(\tau) \\ y_i^{ss}(\tau) \end{bmatrix} = \begin{bmatrix} X \\ Y \end{bmatrix} e^{j\phi_i} e^{jn\sigma\tau}, \qquad i \in \mathcal{N} \tag{4.40}$$

where

$$\left.\begin{aligned} X &= \frac{f\tilde{n}^2(n^2-\tilde{n}^2)}{\Gamma} \\ Y &= -\frac{f\tilde{n}^2\left(\frac{\delta}{\alpha}(n^2-\tilde{n}^2)+n^2(1+\tilde{n}^2)\right)}{\left(1+\frac{\delta}{\alpha}\right)\Gamma} \end{aligned}\right\} \tag{4.41}$$

are the blade and absorber steady-state response amplitudes and

$$\begin{aligned} \Gamma = {} & \mu\alpha^2(1+\tilde{n}^2)^2n^2\sigma^2 + \tilde{n}^2(n^2-\tilde{n}^2) \\ & + (n^2-\tilde{n}^2)\left(\mu\alpha\delta(1+\tilde{n}^2) - \tilde{n}^2(n^2-\delta)\right)\sigma^2 \\ & + 2\nu^2\tilde{n}^2(n^2-\tilde{n}^2)(1-\cos\varphi_{n+1}), \end{aligned}$$

where φ_i is defined by Equation (2.3). The ideal, or *exact* absorber tuning follows by inspection of the first entry of Equation (4.41) and is given by

$$\tilde{n} = n, \qquad \text{or} \qquad \bar{\omega}_{22} = \tilde{n}\sigma = n\sigma. \tag{4.42}$$

If the system is tuned according to Equation (4.42) the blade and absorber amplitudes reduce to

$$\left.\begin{aligned} X &= 0 \\ Y &= -\frac{fn^2}{\mu\alpha^2\left(1+\frac{\delta}{\alpha}\right)(1+n^2)\sigma^2} \end{aligned}\right\}, \qquad (\tilde{n}=n) \tag{4.43}$$

which shows that the blade vibrations can be eliminated completely. In this case the absorber amplitudes are inversely proportional to the mass ratio μ and also to $\alpha(\alpha+\delta)$. It is therefore desirable to make the absorber masses large relative to the blade mass and to place them as close to the end of the blades as possible. In practice,

however, there are limits on the size and makeup of the absorber masses (typically μ is very small, on the order of 10^{-2} to 10^{-3}) and on their placement relative to the blades. The negative sign in Y implies that the absorbers oscillate out of phase with respect to the excitation. Physically, this means the absorbers exert forces on the blades that identically counter the action of the applied loading for all time and for all rotor speeds.[10]

4.4.2 Absorber Detuning and the No-Resonance Zone

By implementing the absorber tuning given by Equation (4.42) one is simply setting the natural frequency of the isolated absorbers to the excitation frequency, that is, $\bar{\omega}_{22} = \tilde{n}\sigma = n\sigma$, and the absorbers are said to be *exactly tuned*. Again, we emphasize that the said tuning is valid at all rotation speeds, a feature that is made possible by the structure of $\bar{\omega}_{22}(\sigma) = \tilde{n}\sigma$. However, any perturbation of the model or absorber parameters, due to in-service wear, environmental effects, and so on, will invariably destroy the exact tuning. To account for such effects, and to allow for intentionally detuned designs, we let

$$\tilde{n} = n(1 + \beta), \tag{4.44}$$

where β is a detuning parameter. Perfect, or exact tuning corresponds to $\beta = 0$, while undertuning (resp. overtuning) corresponds to $\beta < 0$ (resp. $\beta > 0$).

Figure 4.6 and Figure 4.7 depict the blade/absorber frequency response amplitude curves and also the natural frequency loci for a set of four representative detuning values. (The corresponding tuning orders, detuning data, and the resonant rotor speeds are given in Table 4.2 on page 90.) In these plots we take $f = 0.01$ and use the parameters employed in Figure 4.5c. The solid lines in the blade and absorber response curves show the response amplitudes as a function of rotor speed. The dashed lines correspond to the blade/absorber amplitudes when the absorbers are

[10] These results remain valid even for varying rotor speeds, that is, $\sigma = \sigma(\tau)$, so long as the variations occur on a much longer time scale than the dynamics of the blades and absorbers.

locked in their zero positions relative to the blades; these curves are used for reference to assess the dynamic effects of the absorbers.

Overtuning the absorbers (i.e., setting $\beta > 0$) increases the slope $\tilde{n}$ of $\bar{\omega}_{22}(\sigma) = \tilde{n}\sigma$ relative to the engine order n in the frequency-σ planes, and it is clear from Figure 4.6b that a resonance of the in-phase mode corresponding to $\bar{\omega}_1^{(n+1)}$ is guaranteed. For sufficiently large undertuning such that $\beta < \beta_{\rm cr} < 0$ (with $\beta_{\rm cr}$ defined below), the out-of-phase mode corresponding to $\bar{\omega}_2^{(n+1)}$ is excited near resonance; an example of this situation is shown in Figure 4.6a for $\beta = -0.07$. One of the more interesting findings of this chapter is that there are no system resonances for absorber tuning values that satisfy

$$\beta_{\rm cr} < \beta \leq 0, \tag{4.45}$$

where $\beta_{\rm cr}$ is the *critical absorber undertuning* and is given implicitly by Equation (D.2) of Appendix D. Zero (resp. critical) detuning, that is, $\beta = 0$ (resp. $\beta = \beta_{\rm cr}$), corresponds to $\tilde{n} = n$ (resp. $\hat{n} = n$). An example tuning within the *no-resonance gap* defined by Equation (4.45) is shown in Figure 4.7a for $\beta = \beta_{\rm cr}/2 = -0.00351$, where $\beta_{\rm cr} = -0.00701$, and the perfectly tuned case is shown in Figure 4.7b. These cases clearly demonstrate the effectiveness of properly tuned absorbers. The resonance that occurred at $\sigma_{\rm res} = 0.442$ when the absorbers are locked is completely eliminated, and the response amplitudes of the blades are significantly reduced (or eliminated completely) over the full range of possible rotor speeds.

Another way to visualize the no-resonance gap defined by Equation (4.45) is to construct a plot of the rotor speeds corresponding to (possible) resonance(s) versus the absorber detuning parameter β. Such a plot is shown in Figure 4.8 for the same parameters used in Figures 4.5-4.7. In this diagram, the no-resonance gap is identified by the shaded region between the dotted lines corresponding to $\beta = 0$ (zero detuning) and $\beta = \beta_{\rm cr}$ (critical detuning), where $\beta_{\rm cr} = -0.00701$ for this case.

The extent of the no-resonance gap depends on the absorber parameters and the

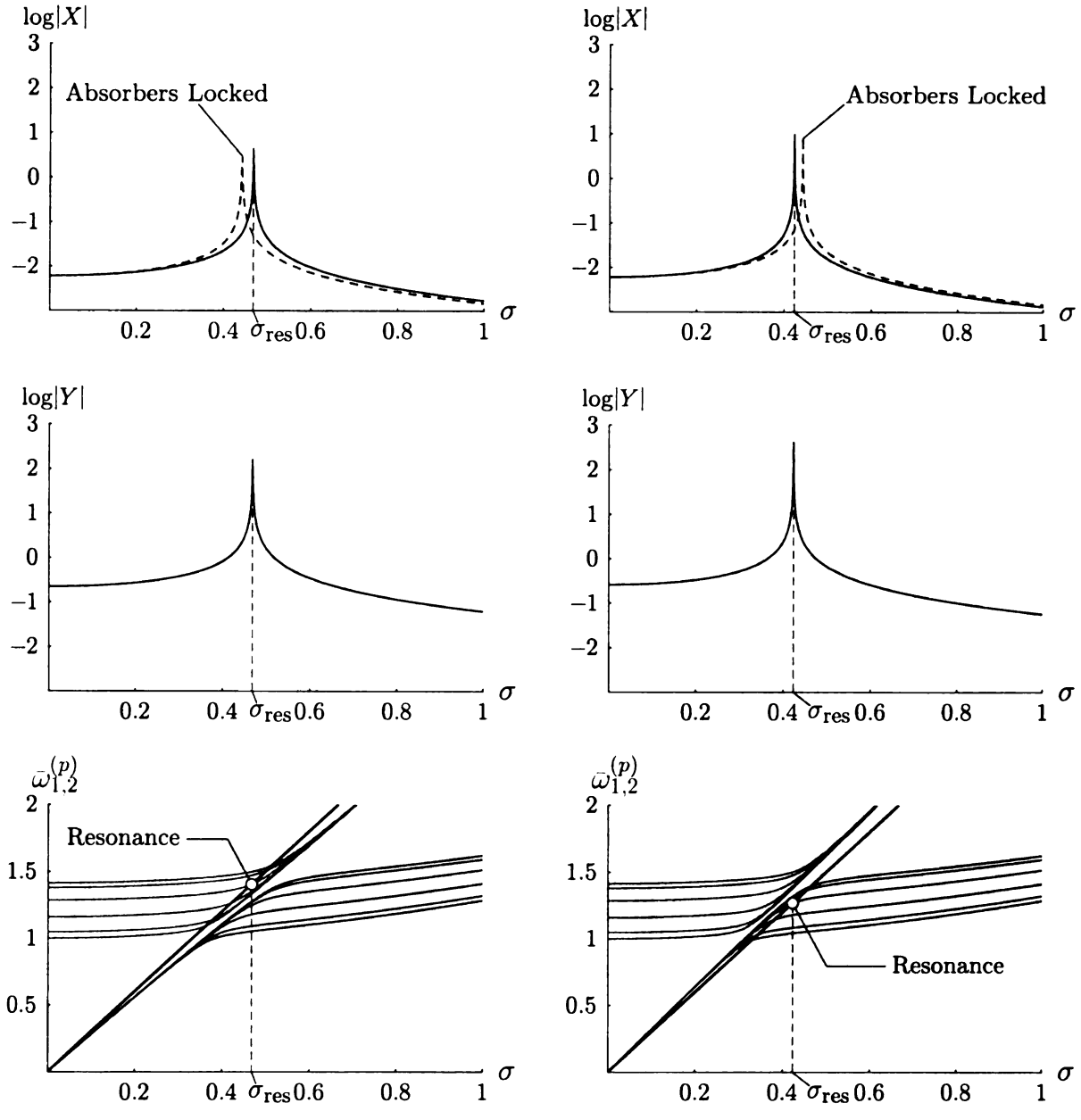

Figure 4.6. Absorber and blade frequency response curves and Campbell diagrams for $N = 10$, $n = 3$, $\alpha = 0.84$, $\delta = 0.67$, $\mu = 0.015$, $\nu = 0.5$, $f = 0.01$, and zero damping: (a) $\beta = -0.07$ (undertuned); (b) $\beta = +0.07$ (overtuned); (– –) frequency response with the absorbers locked. See Table 4.2 on page 90 for the corresponding tuning order data and resonant rotor speeds σ_{res}.

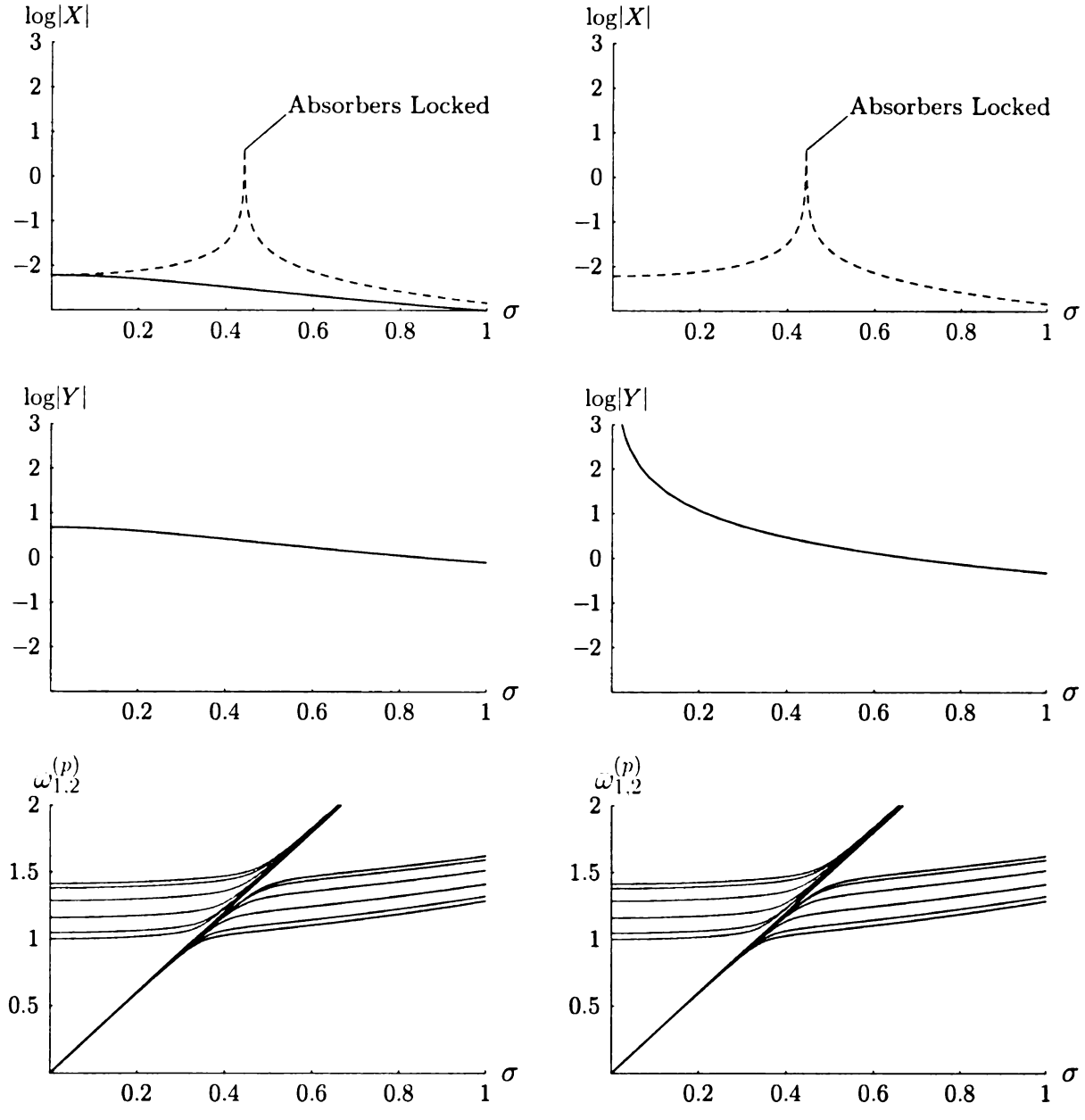

Figure 4.7. Absorber and blade frequency response curves and Campbell diagrams for $N = 10$, $n = 3$, $\alpha = 0.84$, $\delta = 0.67$, $\mu = 0.015$, $\nu = 0.5$, $f = 0.01$, and zero damping: (a) $\beta = \beta_{cr}/2 = -0.00351$ (slightly undertuned); (b) $\beta = 0$ (zero, or perfect tuning); (– –) frequency response with the absorbers locked. The critical absorber detuning is $\beta_{cr} = -0.00701$. See Table 4.2 on page 90 for the corresponding tuning order data and resonant rotor speeds σ_{res}.

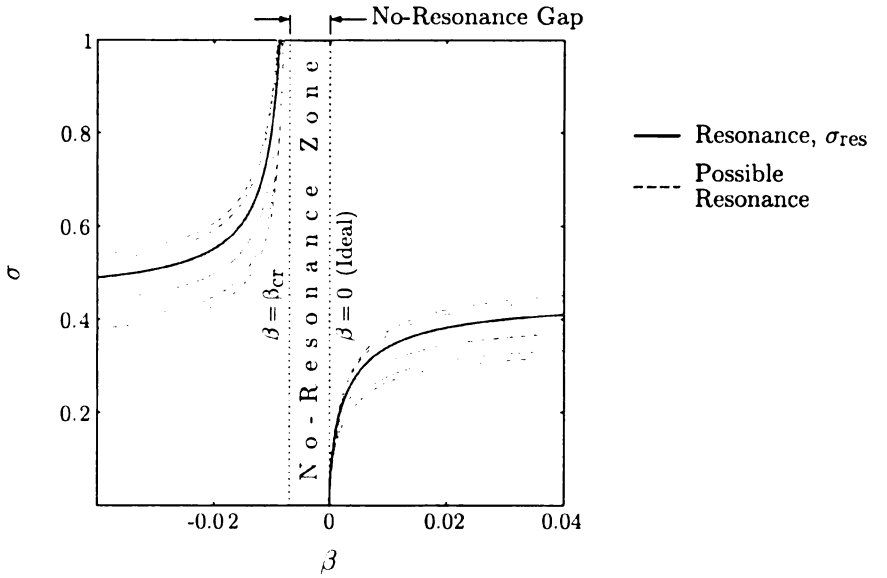

Figure 4.8. Rotor speeds σ_{res} corresponding to resonance (—) and possible resonant speeds (– –) in terms of the absorber detuning β for $N = 10$, $n = 3$, $\alpha = 0.84$, $\delta = 0.67$, $\mu = 0.015$, and $\nu = 0.50$. The no-resonance gap is defined by $\beta_{\text{cr}} < \beta \leq 0$, where $\beta_{\text{cr}} = -0.00701$.

engine order, but is *independent* of the inter-blade coupling ν. The sensitivity of the gap to variations in these parameters is indicated in Figure 4.9, which follows from Equation (D.2) in Appendix D. (A simpler approximate expression, which works quite well over a wide range of parameters, is described below.) In all cases, the sensitivity is most pronounced for small engine orders and it decreases for increasing n. As shown in Figure 4.9a (resp. Figure 4.9b) the critical detuning β_{cr} exhibits near-linear (resp. -quadratic) behavior in terms of μ (resp. α), and by inspection of Figure 4.9c it is nearly independent of δ for most engine orders ($n > 2$). Note that β_{cr} vanishes (implying that the no-resonance gap vanishes) in the absence of the absorbers ($\mu = 0$) or when the absorbers are attached to the periphery of the rotor ($\alpha = 0$). This is consistent with intuition since zero-mass absorbers cannot provide the required loads to counter the action of the excitation on the blades. Also, if the absorber and blade pendulum attachment points coincide on the circumference of the rigid rotor, their dynamics become independent. It is clear, therefore, that

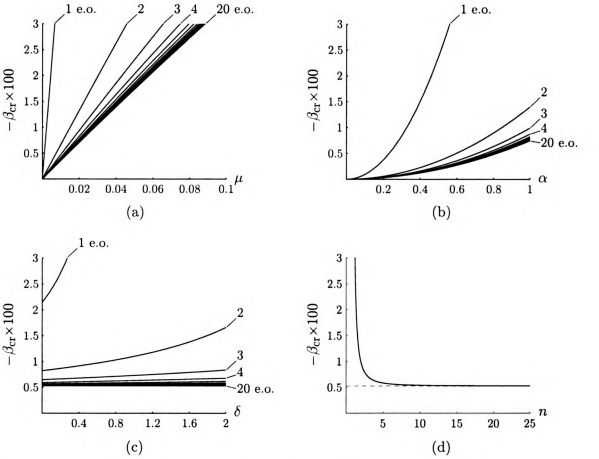

Figure 4.9. Critical undertuning $-\beta_{cr} \times 100$ of the absorbers versus (a) the dimensionless absorber mass μ (with $\alpha = 0.84$ and $\delta = 0.67$), (b) the dimensionless distance from blade base to absorber base point α (with $\delta = 0.67$ and $\mu = 0.015$), (c) the dimensionless radius of rotor disk δ (with $\alpha = 0.84$ and $\mu = 0.015$), and (d) the engine order n (with $\alpha = 0.84$, $\delta = 0.67$, and $\mu = 0.015$). The dashed line in (d) corresponds to the large-n approximation of β_{cr} given by Equation (D.3) in Appendix D.

both μ (absorber mass) and α (absorber placement relative to its attendant blade) are coupling parameters in the sense that their departure from zero implies dynamic coupling between the blades and absorbers.

The parameter trends described above, and in particular those shown in Figure 4.9a and Figure 4.9b, motivate a two-parameter expansion of the critical detuning β_{cr} about $(\mu, \sigma) = (0, 0)$. This results in the simple approximation

$$\beta_{cr}^{app} = -\frac{(n^2+1)^2}{2n^2(n^2-\delta)}\,\mu\alpha^2 + \mathcal{O}(\mu^2, \alpha^3), \tag{4.46}$$

which works quite well over a large range of realistic parameter values. More importantly, Equation (4.46) clearly shows that the extent of the no-resonance zone depends primarily on the absorber mass and its placement along the blade. It can be widened by increasing either μ or α. For any engine order $n > 2$, Equation (4.46) also shows that β_{cr} is essentially independent of the rotor diameter, which is consistent with the exact curves shown in Figure 4.9.

Based on the above analysis it is reasonable to choose $\beta = \beta_{\text{cr}}/2$, which is simply the average of the exact and critical detuning. Then Equation (4.44) becomes

$$\tilde{n} = n\left(1 + \frac{\beta_{\text{cr}}}{2}\right) \tag{4.47}$$

and the engine order n is very close to (but not exactly) the average of $\hat{n}(\tilde{n})$ and $\tilde{n}$. Such a tuning strategy, which was used in the example shown in Figure 4.7a, guarantees (in the absence of damping) no system resonances and it offers good robustness to parameter and model uncertainties.

The effects of system damping are investigated next.

4.5 The Effects of Damping

When an undamped absorber is exactly-tuned according to Equation (4.42), its action identically counters that of the engine order excitation on the blade to which it is attached. This results in a full elimination of blade motions *independent* of the blade and inter-blade damping levels. However, any level of absorber damping (or detuning) will give rise to residual blade motions, in which case coupling and blade damping levels will also affect the response. The aim of this section is to numerically characterize the effects of damping on absorber performance, particularly within the no-resonance zone described in Section 4.4.2. It is shown that the no-resonance gap persists in the presence of sufficiently small absorber damping and that it is essentially unaffected by realistic blade and inter-blade damping levels. We begin by describing

the effects of the absorber damping for tuning values *outside* the no-resonance zone.

To understand the effects of absorber damping on the overall system dynamics, it is instructive to consider two extremes: when the absorbers are free and undamped and when they are locked relative to the blades, which correspond to the limiting cases of $\xi_a = 0$ and $\xi_a \to \infty$, respectively. When the absorbers are free, undamped, and tuned outside of the no-resonance zone (and in the absence of blade and inter-blade damping) there is a single resonance at $\sigma = \sigma_{\text{res}}$, which corresponds to the intersection of the engine order line $n\sigma$ with $\bar{\omega}_1^{(n+1)}$ or $\bar{\omega}_2^{(n+1)}$, and it is defined implicitly by Equation (4.38). For infinite absorber damping the absorbers are essentially locked relative to the blades and hence each blade/absorber combination has the same amplitude, that is, $|x_i(\tau)| = |y_i(\tau)|$ for $i \in \mathcal{N}$. In this case there is also a single resonance (denoted in this section by $\sigma = \sigma_L$), which is defined implicitly by Equation (4.27). An example of σ_{res} and σ_L is shown in Figure 4.10a and the corresponding frequency response curves are depicted in Figure 4.10b-c. There must be a continuous spectrum of frequency responses between the $\xi_a = 0$ and $\xi_a \to \infty$ extremes, which is characterized by a resonance shift toward σ_L. This is shown in Figure 4.11 for the same parameter values used in Figure 4.10 with $\xi_b = \xi_c = 0$ and for various levels of the absorber damping ξ_a. As the absorber damping is increased from zero, the resonance point shifts (in this case to the right) toward σ_L, and the peak blade/absorber amplitudes initially decreases, which is shown in Figure 4.11a-d. By further increasing ξ_a the resonance point continues to evolve toward σ_L and the peak amplitudes begin to increase, which is shown in Figure 4.11e-f. Finally, in the limit as $\xi_a \to \infty$ the frequency response becomes essentially identical to the locked absorber case. This is shown in Figure 4.11g.

A qualitatively similar trend can be observed when the absorbers are tuned *within* the no-resonance zone, except that there are no system resonances for the limiting case of $\xi_a = 0$, and hence if ξ_a is sufficiently small. This is shown in Figure 4.12a-d

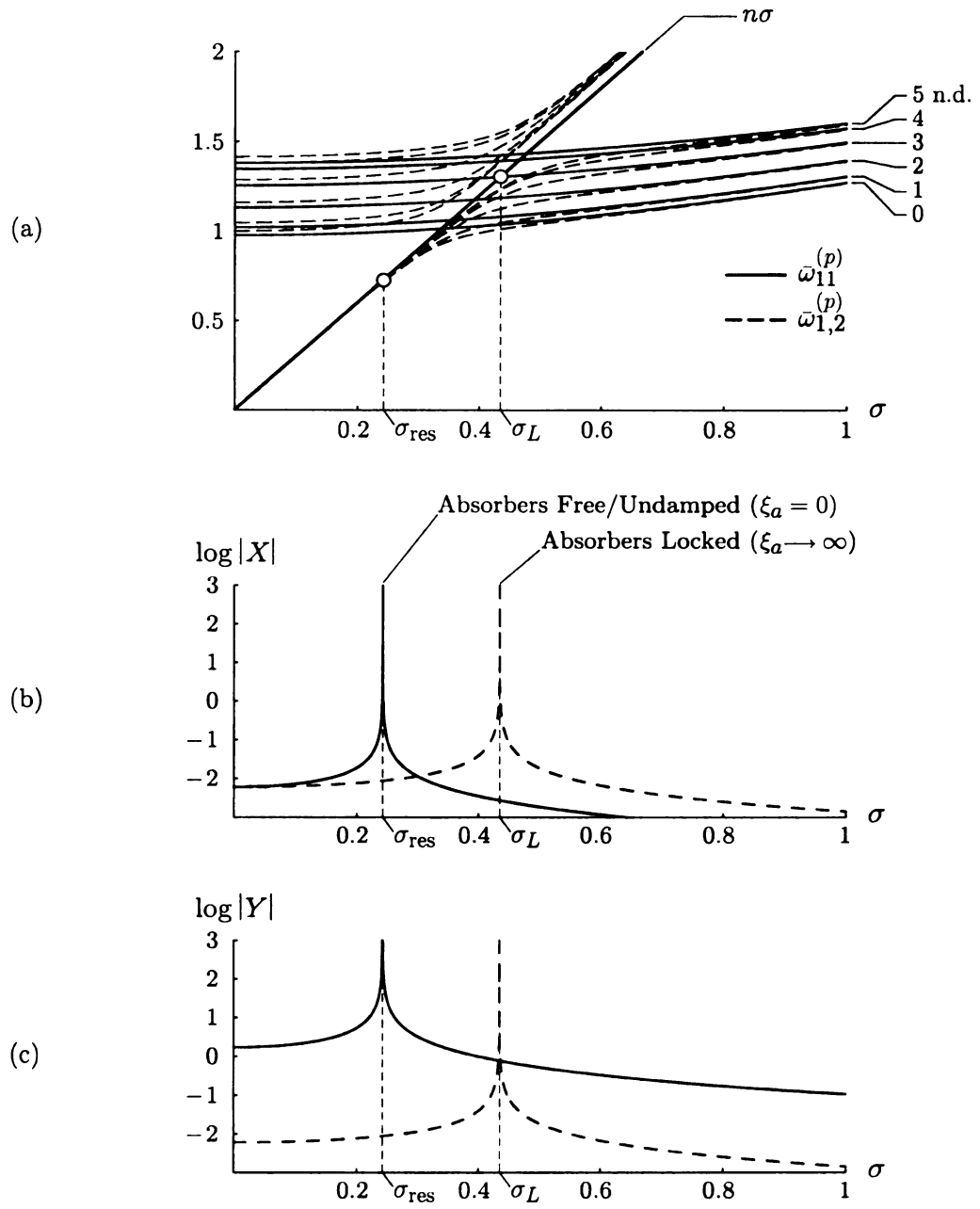

Figure 4.10. (a) Campbell diagram showing the resonant rotor speeds σ_{res} and σ_L and the corresponding (b) blade and (c) absorber frequency response curves for a model with $N = 10$, $n = 3$, $\alpha = 0.84$, $\beta = 0.01$, $\delta = 0.67$, $\mu = 0.05$, $\nu = 0.5$, $f = 0.01$, and $\xi_b = \xi_c = 0$.

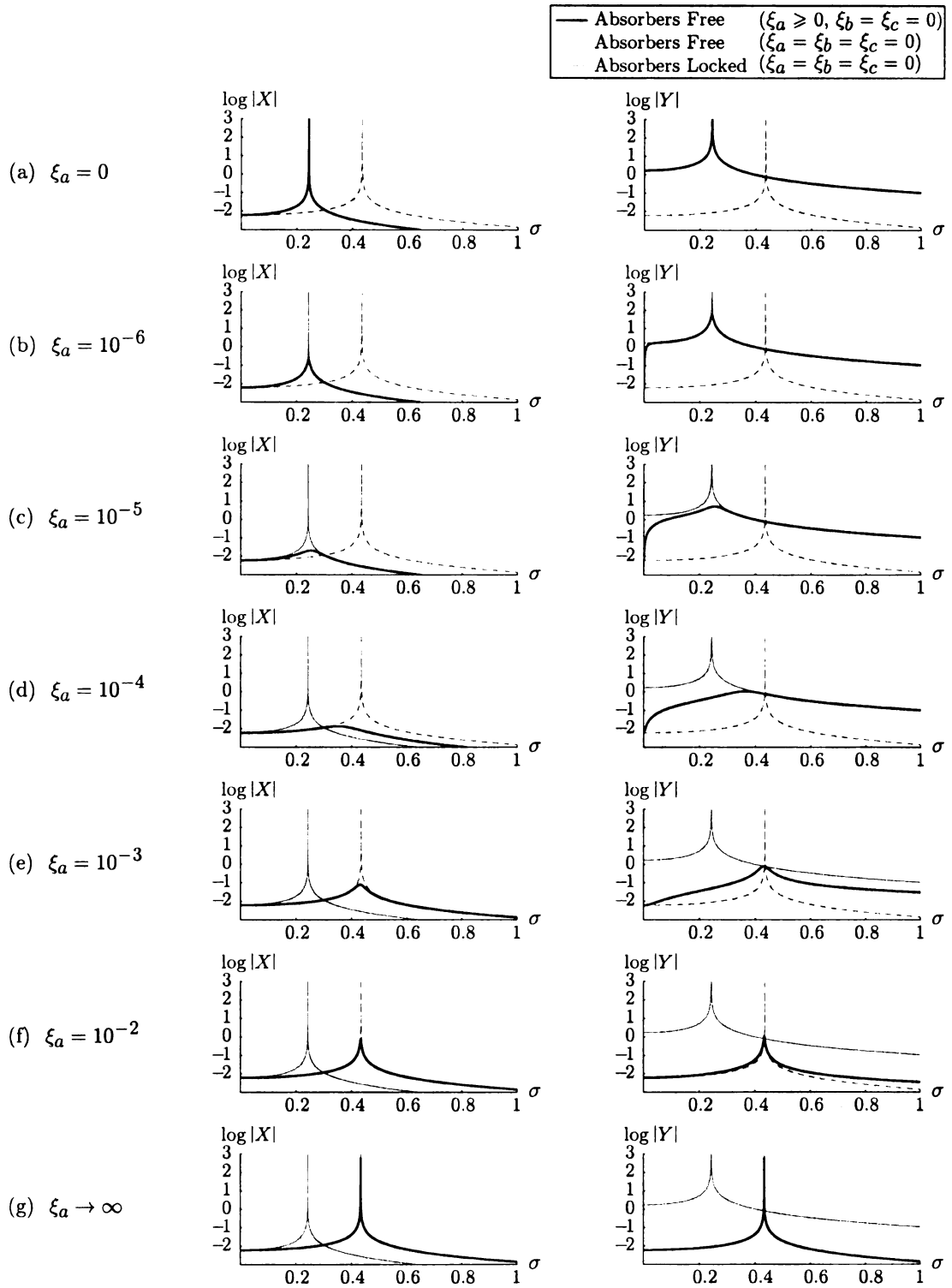

Figure 4.11. Blade and absorber (free and locked) frequency response curves for overtuned absorbers ($\beta = 0.01$), for the same parameter values used in Figure 4.10, and for various levels of the absorber damping ξ_a.

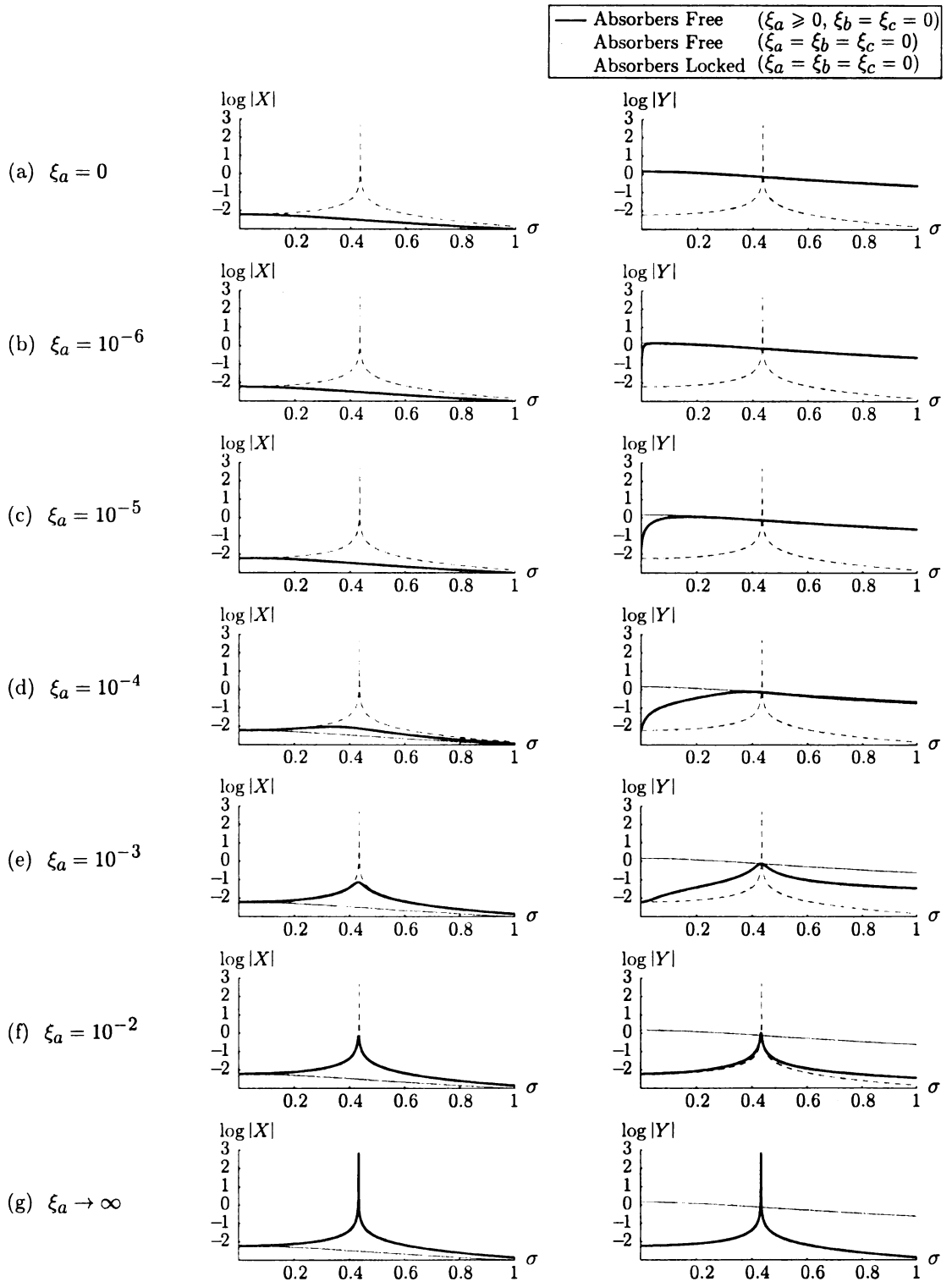

Figure 4.12. Blade and absorber (free and locked) frequency response curves for absorbers tuned within the no-resonance zone ($\beta = \beta_{cr}/2 = -0.00351$), for the same parameter values used in Figure 4.10, and for various levels of the absorber damping ξ_a.

for $\beta = \beta_{\rm cr}/2$, $\xi_b = \xi_c = 0$, and for various levels of the absorber damping ξ_a. A system resonance is born if the absorber damping is sufficiently increased, which is shown in Figure 4.12e-g. In these cases the absorber's performance is so severely degraded by the presence of damping that they are no longer effective in attenuating blade motions, even with proper tuning. However, for reasonable absorber damping levels there are no system resonances over the full range of rotor speeds, and in this sense the no-resonance zone is seen to persist for sufficiently small ξ_a. Figure 4.12b shows a representative set of frequency response curves for a typical level of absorber damping.

Finally, it can be shown that the blade and inter-blade damping has a much less dramatic effect on the system dynamics. By increasing either ξ_b or ξ_c the blade and absorber amplitudes are simply reduced and, for absorber tuning outside of the resonance zone, there is generically no significant shift in the resonance point. Physically, this is a sensical result; the presence of blade or inter-blade damping actually *helps* the absorbers achieve attenuation of blade motions, whereas an increase in ξ_a does the exact opposite.

4.6 Concluding Remarks

An implementation of order-tuned vibration absorbers to a linearized, cyclically symmetric bladed disk assembly has been investigated. A standard change of coordinates based on the cyclic symmetry of the system was employed to reduce the governing $2N$ equations of motion to a set of N, reduced-order equations, from which an absorber tuning strategy was formulated. One of the main findings of this chapter, and indeed of this entire thesis, is the existence of a no-resonance zone, that is, a range of absorber undertuning values for which there are no system resonances *over the full range of possible rotor speeds.* By tuning each absorber within this generally small (but finite) range, resonance can be avoided altogether and there is at least some level

of robustness to parameter uncertainty. The extent of this no-resonace gap depends primarily on the mass of the absorber to that of the blade and on its placement along the blade length, especially for larger engine orders. The gap can be widened by increasing the absorber mass and/or by placing it further away from the root of the blade, effectively strengthening its dynamic potential to suppress blade motions.

These fundamental results are now generalized in the next chapter to include first-order nonlinear effects.

CHAPTER 5

Forced Response of the Nonlinear System

5.1 Introduction

The linear results of Chapter 4 are now generalized to include the basic first-order effects of nonlinearity, which is introduced via the absorber path geometry. Together with the linear design recommendations of Section 4.4, the aim of this chapter is to possibly exploit nonlinearity to further improve the absorber performance, particularly for linear tuning within the no-resonance zone. It is therefore of particular importance to determine if the no-resonance zone persists under increasing absorber path nonlinearity. Also, it is well known that for the lightly damped and weakly coupled cyclic systems under consideration, there may be a host of solution types other than the desired traveling wave response [106–108] in which all sectors behave identically except for a constant shift in phase among adjacent sectors. If nonlinearity is to be exploited, or if it is otherwise present and unavoidable in the sector models, these additional instabilities (if they exist) must be addressed as a part of the design process.

It is convenient to employ the generalized, two-parameter familiy of paths that were developed in Section 3.4.4 to introduce the nonlinearity. These allow the final path design to be specified *directly* by choosing a linear tuning order $\tilde{n}$ (this was carried out in Section 4.4 in terms of the linear order detuning β) and a *nonlinear*

tuning parameter η. According to the linear theory there is a continuous spectrum of (under)tuning values for which there are no system resonances over the full range of possible rotor speeds. Proper linear design therefore involves tuning the absorbers within this no-resonance zone. The path parameter η acts essentially as the strength of the path nonlinearity, which has a continuous range from softening ($\eta < 0$) to hardening ($\eta > 0$). Its selection forms the main focus of this chapter.

The nonlinear sector models from Section 3.4 are employed, along with the two-parameter family of paths described above. These are systematically reduced via scaling and averaging to a set of nonlinear *averaged sector models*, which forms a basis for the analytical and numerical investigations that follow. In addition to the desired traveling wave response, the averaged models are general enough to capture solutions with slowly-varying amplitudes and phases in *individual* sectors. However, we focus only on traveling wave responses, where *all* of the sectors behave identically but with a fixed phase difference among adjacent sectors, and on instabilities of this response, which would result in bifurcations to other response types. The analysis is carried out first for the *isolated* nonlinear system, consisting of a single linear blade and nonlinear absorber. This allows for a complete description of the effects of nonlinearity on the sector dynamics without additional complicating features due to inter-sector coupling. When coupling is present, and under a traveling wave response, the nonlinear system qualitatively features these same dynamics on a *sector-to-sector* basis, but there may also exist bifurcations to non-traveling wave motions in addition to the usual jump bifurcations associated with the isolated sector. In fact, it is shown that the multi-sector traveling wave response corresponds directly to an equivalent single sector model whose natural frequency is shifted by a specific amount that depends on the coupling and the mode being excited.

It is shown that the underlying linear resonance structure—and hence the no-resonance gap and desired linear absorber tuning—qualitatively persists in the pres-

ence of nonlinearity, provided that the excitation and path nonlinearity are sufficiently small. Moreover, given *any* linear tuning strategy and for zero damping, there exists a nonlinear tuning that guarantees a branch of solutions for which there are zero blade motions relative to the rotating hub. However, for proper linear undertuning this gives rise to an undesirable hardening path with potentially problematic auxiliary resonances and it is highly susceptible to parameter uncertainty. Even more importantly, the nonlinear tuning criterion depends on the rotor speed as well as the strength of the excitation and is thus effective near a *single* operating condition, much like the frequency-tuned DVA of Section 2.5.2. These findings suggest that it is impossible to exploit nonlinearity to further improve the absorber performance, and it is therefore desirable to maintain nearly-linear absorber motions. Should nonlinearity be unavoidable, the results clearly show that softening characteristics are more desirable than hardening, where the former simply sets an upper limit on permissible rotor speeds and the latter involves potentially problematic auxiliary resonances at low rotor speeds, particularly for light damping. Finally, when inter-sector coupling is included, no instabilities to non-traveling wave motions could be identified. In this way, the analysis of an *individual* sector offers global qualitative results that are applicable to the fully coupled system, including stability.

The chapter is organized as follows. A mathematical formulation is carried out in Section 5.2, beginning with a description of the governing nonlinear equations of motion in Section 5.2.1. These are scaled in Section 5.2.2, the underlying linear resonance structure is shown to persist under the scaling in Section 5.2.3, and the method of averaging is employed in Section 5.2.4. This gives rise to simplified approximate sector models that form the basis for all of the analysis that follows. Existence of the desired traveling wave response is discussed in Section 5.3 in terms of stationary points of the averaged system, and its local stability is subsequently addressed. Features of the forced response of the isolated nonlinear system are highlighted in

Section 5.4 with an emphasis on the blade and absorber frequency response and also criteria for zero blade amplitudes. Finally, the forced response of the fully coupled nonlinear system is considered in Section 5.5 with the goal of quantifying possible instabilities to non-traveling wave responses, and the chapter closes in Section 5.6 with some concluding remarks.

5.2 Formulation

In what follows the nonlinear equations of motion given by Equation (3.14), together with the generalized family of paths described in Section 3.4.4, are systematically reduced via scaling and averaging to a model that is amenable to the tools from nonlinear dynamics. As with the analysis of Chapter 4, this is carried out under the assumption of identical, identically-coupled sectors. The governing equations of motion are briefly reviewed in Section 5.2.1 and they are scaled in Section 5.2.2 to capture first-order nonlinearity via the absorber paths. In Section 5.2.3 a comparison is made between the scaled sector models and the linearized sector models of Chapter 4, and it is shown that the linear resonance structure qualitatively persists under the scaling. Finally, averaging is carried out in Section 5.2.4 in both polar and Cartesian forms. The resulting averaged sector models form the basis for all of the analysis that follows.

5.2.1 Equations of Motion

The cyclically-coupled model to be considered features the same lumped-parameter arrangement for the bladed disk assembly that was employed in Chapter 4, which is shown in Figure 5.1a (see Section 4.2 on page 78 or Table 3.1 on page 64 for a description of it parameters), and the circular-path kinematic model for the absorbers is replaced by the more general, arbitrary-path description of Section 3.3. This is shown in the sector model in Figure 5.1b, where μ is the i^{th} dimensionless absorber

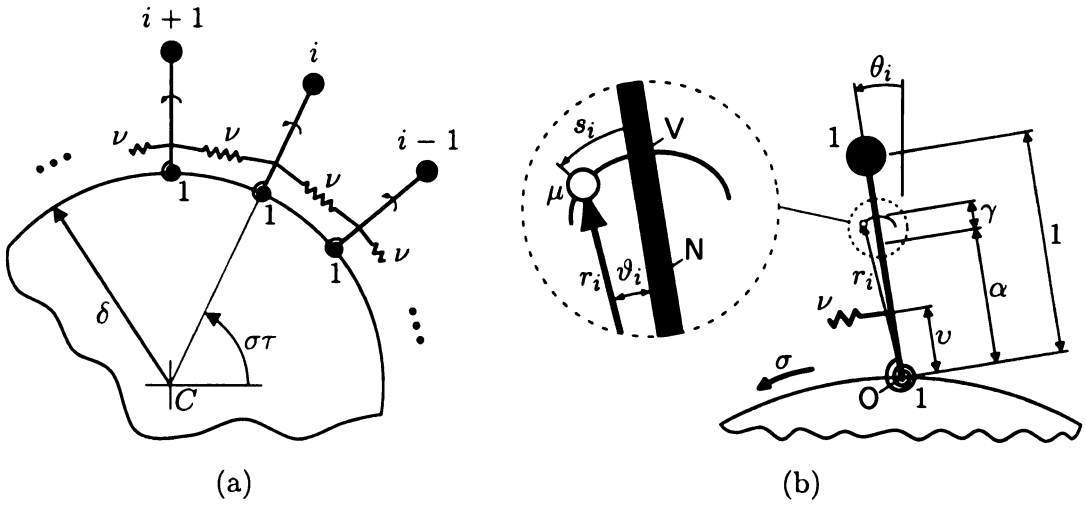

Figure 5.1. (a) Model of bladed disk assembly and (b) sector model.

mass, s_i is its nondimensional displacement along the arbitrary path, which subtends an angle $\vartheta_i(s_i)$ relative to the vertex at V, and $r_i(s_i)$ is the dimensionless radius length to the absorber relative to the blade basepoint O. Relationships between these fundamental path variables were derived in Section 3.3.1.

The equations of motion for the i^{th} sector follow from the development in Section 3.4 and they are given by

$$\mu s_i'' + \mu r_i \Gamma_i \theta_i'' + \xi_{\bar{a}} s_i' - \mu r_i \frac{dr_i}{ds_i}(\sigma + \theta_i')^2 + \mu\delta\sigma^2\left(\Gamma_i \sin(\theta_i + \vartheta_i) - \frac{dr_i}{ds_i}\cos(\theta_i + \vartheta_i)\right) = 0, \qquad i \in \mathcal{N} \tag{5.1a}$$

$$\theta_i'' + \xi_b \theta_i' - \xi_{\bar{a}} r_i \Gamma_i s_i' + \theta_i + \delta\sigma^2 \sin\theta_i + \mu\left[\begin{array}{l} r_i^2\theta_i'' + r_i\Gamma_i s_i'' + 2r_i\dfrac{dr_i}{ds_i}s_i'(\sigma + \theta_i') \\ \qquad + \dfrac{d(r_i\Gamma_i)}{ds_i}s_i' s_i' + \delta\sigma^2 r_i \sin(\theta_i + \vartheta_i) \end{array}\right] + \nu^2(-\theta_{i-1} + 2\theta_i - \theta_{i+1}) = F\cos(n\sigma\tau + \phi_i), \qquad i \in \mathcal{N} \tag{5.1b}$$

where the coupling damping ξ_c has been ignored, the functions $\Gamma_i = \Gamma_i(s)$ and $\vartheta_i = \vartheta_i(s)$ are defined by Equation (3.15) and Equation (3.16), respectively, and the subscripts i have been dropped from the system parameters (these are defined in

Table 3.1 on page 64) since the sectors are taken to be identical. The absorber paths are assumed to be of the form given by Equation (3.19) on page 65, where

$$\left.\begin{aligned} b_0 &= \left(\frac{\alpha(\tilde{n}^2+1)+\delta}{\tilde{n}^2}\right)^2 \\ b_2 &= -\frac{\alpha\tilde{n}^2}{\alpha+\delta} \\ b_4 &= -\frac{\delta\tilde{n}^6}{12(\alpha+\delta)^3(\tilde{n}^2+1)} - \frac{\alpha(\tilde{n}^2+1)+\delta}{2(\alpha+\delta)(\tilde{n}^2+1)}\eta \end{aligned}\right\} \tag{5.2}$$

are the path coefficients if γ is written in terms of the absorber tuning order according to Equation (4.39) of Chapter 4. In this representation, each path depends only on the linear and nonlinear tuning parameters $\tilde{n} = \sqrt{\frac{\alpha+\delta}{\gamma}}$ and η. Once these are set by design, and given the disk radius δ, then α and γ are automatically prescribed (these represent the effective placement of the absorbers along the blade lengths and the curvature at their vertices).

Next the full nonlinear system given by Equation (5.1) is systematically reduced to a set of weakly nonlinear oscillators, and perturbation techniques are subsequently carried out on these reduced equations.

5.2.2 Scaling

In any realistic physical implementation, the absorber masses will be much smaller than that of the blades, primarily due to stringent restrictions on the absorber rattling space and therefore on its dimensions and mass. It is thus reasonable to take

$$\mu = \varepsilon^m$$

as the basis for the scaling, where $0 < \varepsilon \ll 1$ is a small dimensionless parameter and the constant m is to be determined. The blade and absorber dynamics are assumed to scale with ε according to

$$\theta_i = \varepsilon^k \hat{\theta}_i \qquad \text{and} \qquad s_i = \varepsilon^\ell \hat{s}_i$$

for each $i \in \mathcal{N}$ in a manner that is to be determined. Blade damping levels relative to critical are often 0.01% or less and, in order to achieve the desired order tuning, absorber damping is generally made as small as possible. As discussed in Section 3.6, the corresponding dimensionless blade and (effective *translational*) absorber damping constants are on the order of 10^{-3} and 10^{-6}, respectively, and they are scaled according to

$$\xi_b = \varepsilon^p \hat{\xi}_b \qquad \text{and} \qquad \xi_{\bar{a}} = \varepsilon^q \hat{\xi}_{\bar{a}}.$$

It is additionally assumed that the inter-blade elastic coupling is weak, that is,

$$\nu^2 = \varepsilon^n \hat{\nu}^2,$$

which together with the assumption of light damping allows for the investigation of a host of possible instabilities, bifurcations, and multiple interacting modes.[1] Finally, weak forcing is assumed, that is,

$$F = \varepsilon^r \hat{f},$$

since the nonlinear dynamics near resonance are of interest.

The scaling parameters m, k, l, p, q, n, and r are chosen such that, to leading order ($\varepsilon = 0$), a simplified and solvable system is obtained, one that is used as the basis for the method of averaging. In order to investigate the potentially rich dynamics when the system is weakly coupled and lightly damped, the scaling is chosen so that the nonlinearity, damping, and coupling all appear at $\mathcal{O}(\varepsilon)$ and it should preserve, as much as possible, the linear resonance structure described in Chapter 4. To this end, a suitable choice for the scaling parameters is found to be

$$m = 2, \quad k = \tfrac{3}{2}, \quad l = \tfrac{1}{2}, \quad p = 3, \quad q = 1, \quad n = 1, \quad r = \tfrac{5}{2}. \tag{5.3}$$

[1]When the coupling is strong (which can occur in shrouded assemblies or via other coupling mechanisms) and for sufficiently weak forcing, there exists the possibility of only two interacting modes, the analysis of which is left for future work.

Upon substitution and simplification the i^{th} scaled sector model becomes

$$\hat{\theta}_i'' + \bar{\omega}_{11}^2\hat{\theta}_i + \varepsilon\hat{\nu}^2\big(-\hat{\theta}_{i-1} + 2\hat{\theta}_i - \hat{\theta}_{i+1}\big)$$
$$= \varepsilon\big(-r_o\hat{s}_i'' - \delta\sigma^2\hat{s}_i - \hat{\xi}_b\hat{\theta}_i' + \hat{f}\cos(n\sigma\tau + \phi_i)\big) + \mathcal{O}(\varepsilon^{3/2}), \tag{5.4a}$$

$$\hat{s}_i'' + \bar{\omega}_{22}^2\hat{s}_i = \varepsilon\big(-r_o\hat{\theta}_i'' - \delta\sigma^2\hat{\theta}_i - \hat{\xi}_{\bar{a}}\hat{s}_i' - \eta\sigma^2\hat{s}_i^3\big) + \mathcal{O}(\varepsilon^{3/2}), \tag{5.4b}$$

where the frequencies $\bar{\omega}_{11} = \sqrt{1+\delta\sigma^2}$ and $\bar{\omega}_{22} = \tilde{n}\sigma$ are summarized in Table 4.3 on page 96 and r_o is defined by Equation (3.17) (where γ is eliminated according to Equation (4.39)).

When $\varepsilon = 0$, Equation (5.4) reduces to a pair of *decoupled*, undamped, and unforced linear oscillators. The first oscillator describes the free vibration of an isolated blade *without* an absorber, while the second captures the dynamics of each absorber if the blades are locked relative to the rotating hub, which was discussed in Section 4.2.3. The general case of small $\varepsilon \neq 0$ is simply a perturbation of these uncoupled systems; Equation (5.4a) is a *linear*, weakly forced oscillator that approximates the motions of blade $i \in \mathcal{N}$ while Equation (5.4b), which captures the i^{th} absorber dynamics, is unforced and weakly nonlinear due to the cubic absorber path term. These oscillators are weakly coupled due to the assumptions of small μ (representing the blade-to-absorber coupling) and small inter-blade stiffness coupling.

Absorber design is carried out by choosing the linear absorber tuning order $\tilde{n}$ (the proper selection of which was discussed in Section 4.4) *and* the nonlinear tuning parameter η, both of which appear only in the i^{th} absorber equation, that is, Equation (5.4b). This in turn prescribes the absorber paths by setting the constants b_0, b_2, and b_4 in Equation (5.2) and it fixes the effects of the absorbers on the blade dynamics via the first two (inertia and stiffness) terms in the parentheses on the right hand side of Equation (5.4a).

Before proceeding with a further reduction of Equation (5.4) via averaging, it should be verified that the scaled sector models suitably capture the underlying linear

resonance structure that was described in Chapter 4. This is done in the next section, where it is shown that the no-resonance zone qualitatively persists under the scaling.

5.2.3 Linear Resonance Structure of the Scaled System

If the scaling in Section 5.2.2 is applied to the i^{th} linearized sector model defined by Equation (4.1), and if the assumption of motion-limiting stops is removed by multiplying through by the stopper angle ψ_o, then it can be directly compared to the i^{th} scaled sector model given by Equation (5.4) with $\eta = 0$. These two systems (in this section we refer to them as the *linearized* model and *scaled* model for simplicity) match identically if $\mu = 0$ in M_{11} and K_{11} (see Table 4.1 on page 81), which simply ignores the contribution of the absorber inertia in those terms. In this way, the scaling is seen to essentially linearize the blade dynamics (with an accompanying additional loss of some dynamic coupling terms involving μ) while at the same time capturing the basic first-order effects of the absorber path nonlinearity.

Since $\mu = \varepsilon^2$ will generally be small, it is expected that the linear resonance structure qualitatively persists under the scaling of the previous section. This is verified in Figure 5.2a which shows example plots of the rotor speeds σ_{res} corresponding to resonance for the linearized (solid lines) and scaled (dashed lines) systems described above versus the linear absorber detuning parameter β for zero damping and for various values of μ. (Table 5.1 lists the corresponding values of ε, β_{cr}, and λ_{cr} for the various mass ratios.) To simplify matters, the curves are shown for the special case of a single isolated blade/absorber combination, that is, for $\nu = 0$ (this is equivalent to considering only the possible resonance corresponding to $p = 1$), but this does not preclude a direct comparison of the two models for accuracy. It is clear that the linear resonance structures of the two systems are in good agreement for sufficiently small mass ratios, and both feature the no-resonance gap. As μ increases, so too does the percent error in σ_{res} between the linearized and scaled systems, which is shown

Table 5.1. Data to accompany Figure 5.2.

μ	ε	β_{cr} ($\times 10^3$)	λ_{cr}	μ	ε	β_{cr} ($\times 10^3$)	λ_{cr}
0	0	0	–	0.005	0.0707	−2.348	−0.597
0.001	0.0316	−0.470	−0.268	0.010	0.1000	−4.685	−0.841
0.002	0.0447	−0.940	−0.378	0.015	0.1225	−7.012	−1.027
0.003	0.0548	−1.410	−0.463	0.020	0.1414	−9.329	−1.182
0.004	0.0632	−1.879	−0.534	0.025	0.1581	−11.637	−1.317

in Figure 5.2b. For reasonable mass ratios, however, the error is seen to be small over a wide range of detuning values, except near the critical detuning $\beta = \beta_{cr}$ where the error becomes unbounded (implying that the scaled system predicts a slightly larger no-resonance gap). The scaled model increasingly overestimates β_{cr} by a finite amount,[2] but otherwise satisfactorily captures the underlying linear resonance structure.

Next the nonlinear scaled sector models of the previous section are further reduced via the method of averaging. The perturbation analysis simply casts them into a standard and tractable form, from which blade and absorber amplitudes can be estimated.

5.2.4 Averaging

In what follows averaging is carried out on the scaled sector models of Section (5.2.2). This is done first in the standard polar form and the results are subsequently converted to cartesian coordinates. Both forms are used in the analysis, either explicitly or implicitely—whichever is most convenient.

[2]This could be obtained by deriving the counterpart to β_{cr} for the scaled system (see Equation (D.2) of Appendix D) and comparing the two critical detuning values.

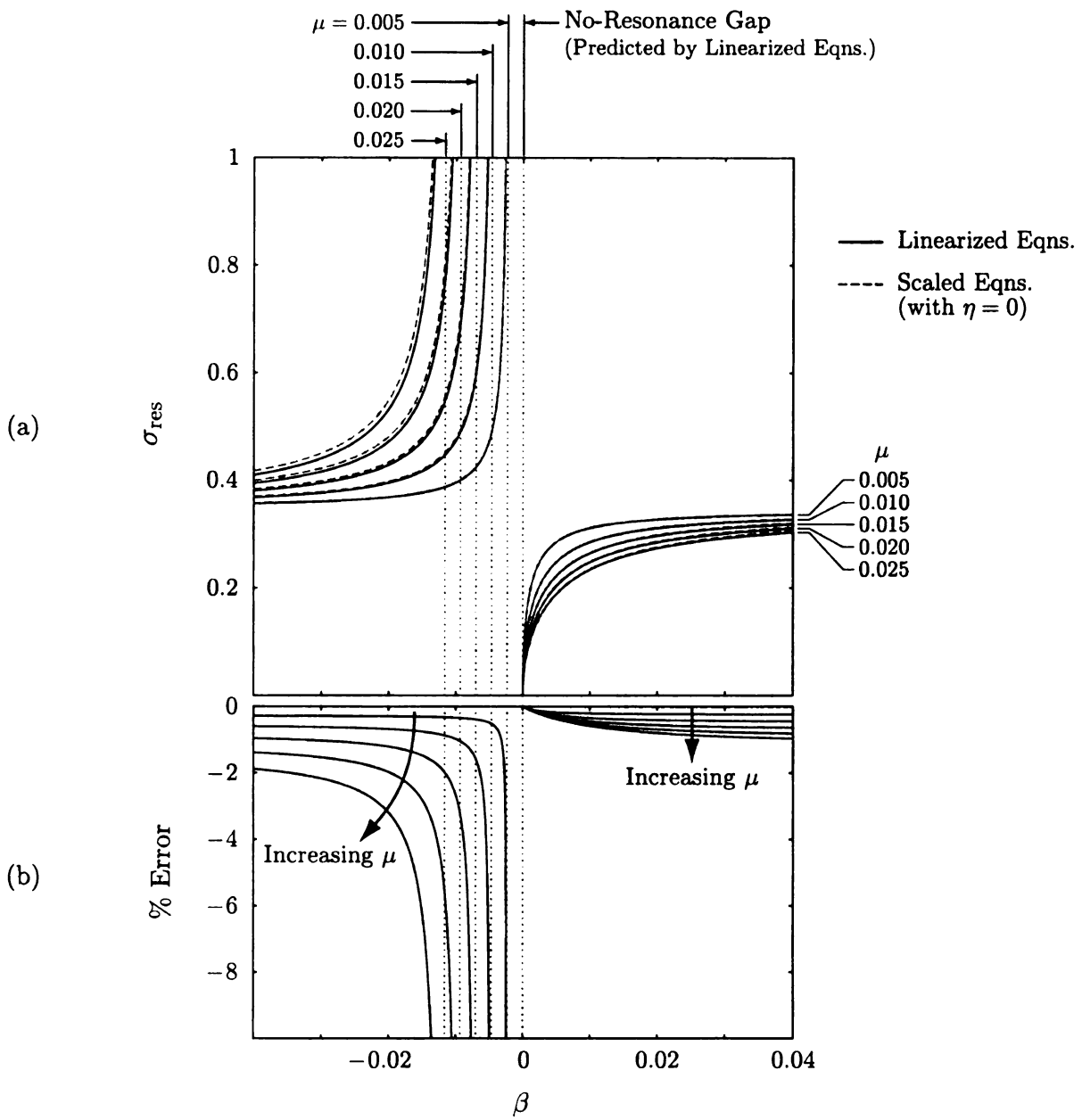

Figure 5.2. (a) The rotor speed σ_{res} corresponding to resonance for the linearized system of Chapter 4 and the scaled system formed by Equation (5.4) (with $\eta = 0$) versus the linear absorber detuning parameter β for a model with $N = 1$, $n = 3$, $\alpha = 0.84$, $\delta = 0.67$, $\nu = 0$, and for mass ratios $0.005 \leq \mu \leq 0.025$; (b) the corresponding percent error. The no-resonance gap (predicted by the linearized system of Chapter 4) is defined by $\beta_{\text{cr}} < \beta \leq 0$, where the values of the critical undertuning β_{cr} are given in Table 5.1 for the various mass ratios.

Polar Form

The weakly nonlinear set of oscillators defined by Equation (5.4) can be cast into a form that is suitable for averaging via the transformation[3]

$$\left.\begin{aligned}
\hat{\theta}_i(\tau) &= u_i(\tau)\cos\big(n\sigma\tau + \phi_i + \varrho_i(\tau)\big) \\
\hat{\theta}_i'(\tau) &= -n\sigma u_i(\tau)\sin\big(n\sigma\tau + \phi_i + \varrho_i(\tau)\big) \\
\hat{s}_i(\tau) &= v_i(\tau)\cos\big(n\sigma\tau + \phi_i + \varsigma_i(\tau)\big) \\
\hat{s}_i'(\tau) &= -n\sigma v_i(\tau)\sin\big(n\sigma\tau + \phi_i + \varsigma_i(\tau)\big)
\end{aligned}\right\}, \tag{5.5}$$

along with the usual constraint equations. Equation (5.5) represents a standard variation of parameters to transform the dependent variables from $\hat{\theta}_i$ (resp. $\hat{s}_i$) to u_i and ϱ_i (resp. v_i and ς_i), which allows for solutions with slowly-varying amplitudes and phases in individual sector responses, and it also serves to capture the desired traveling wave response among the sectors by including the inter-blade phase angle ϕ_i. In this way, the transformation additionally carries the *continuous time* and *discretized space* duality that was systematically described in Section 2.3.2 in the context of engine order excitation. Depending on the value n relative to N, it can therefore capture BTW, FTW, and SW responses. It should be noted from the onset, however, that there could be a multitude of other response types and that the averaged models to be developed based on Equation (5.5) are general enough to capture them. However, the desired and most basic response is that of a traveling wave, the existence, stability and bifurcation of which forms the main focus of this chapter.

Upon substitution of Equation (5.5) into Equation (5.4) and elimination of terms

[3]The notation ϱ_i and ς_i is recycled in this chapter for convenience, and should not be confused with Equation (B.15) or the circular-path absorber angle in Figure 3.6.

at $\mathcal{O}(\varepsilon^{3/2})$ and higher we obtain

$$\left.\begin{aligned}
u_i' &= \frac{1}{n\sigma}\Big((\bar{\omega}_{11}^2 - n^2\sigma^2)u_i\cos(n\sigma\tau + \phi_i + \varrho_i) + \varepsilon f_{11}^{(i)}\Big)\sin(n\sigma\tau + \phi_i + \varrho_i)\\
u_i\varrho_i' &= \frac{1}{n\sigma}\Big((\bar{\omega}_{11}^2 - n^2\sigma^2)u_i\cos(n\sigma\tau + \phi_i + \varrho_i) + \varepsilon f_{11}^{(i)}\Big)\cos(n\sigma\tau + \phi_i + \varrho_i)\\
v_i' &= \frac{1}{n\sigma}\Big((\bar{\omega}_{22}^2 - n^2\sigma^2)v_i\cos(n\sigma\tau + \phi_i + \varsigma_i) + \varepsilon f_{22}^{(i)}\Big)\sin(n\sigma\tau + \phi_i + \varsigma_i)\\
v_i\varsigma_i' &= \frac{1}{n\sigma}\Big((\bar{\omega}_{22}^2 - n^2\sigma^2)v_i\cos(n\sigma\tau + \phi_i + \varsigma_i) + \varepsilon f_{22}^{(i)}\Big)\cos(n\sigma\tau + \phi_i + \varsigma_i)
\end{aligned}\right\} \tag{5.6}$$

for each $i \in \mathcal{N}$, where the functions

$$\left.\begin{aligned}
f_{11}^{(i)} = &- n\sigma\hat{\xi}_b u_i\sin(n\sigma\tau + \phi_i + \varrho_i) - \hat{f}\cos(n\sigma\tau)\\
&- (r_o\bar{\omega}_{22}^2 - \delta\sigma^2)v_i\cos(n\sigma\tau + \phi_i + \varsigma_i)\\
&+ \hat{\nu}^2\left[\begin{aligned}&2\bar{u}_i\cos(n\sigma\tau + \phi_i + \varsigma_i) - \bar{u}_{i-1}\cos(n\sigma\tau + \phi_{i-1} + \varsigma_{i-1})\\ &\qquad - \bar{u}_{i+1}\cos(n\sigma\tau + \phi_{i+1} + \varsigma_{i+1})\end{aligned}\right]\\
f_{22}^{(i)} = &- n\sigma\hat{\xi}_{\bar{a}} v_i\sin(n\sigma\tau + \phi_i + \varsigma_i) + \eta\sigma^2 v_i^3\cos^3(n\sigma\tau + \phi_i + \varsigma_i)\\
&- (r_o\bar{\omega}_{11}^2 - \delta\sigma^2)u_i\cos(n\sigma\tau + \phi_i + \varrho_i)
\end{aligned}\right\} \tag{5.7}$$

capture all of the $\mathcal{O}(\varepsilon)$ terms in Equation (5.4). The differences

$$\bar{\omega}_{11}^2 - n^2\sigma^2 = -\frac{\sigma^2 - \sigma_r^2}{\sigma_r^2}, \tag{5.8a}$$

$$\bar{\omega}_{22}^2 - n^2\sigma^2 = (\tilde{n}^2 - n^2)\sigma^2, \tag{5.8b}$$

give a measure of proximity of the rotor speed relative to blade resonance and to the absorber design relative to ideal linear tuning, respectively, where $\bar{\omega}_{11}$ is the natural frequency of an isolated blade without an absorber, $\sigma_r = \sqrt{n^2 - \delta}$ is its resonant frequency,[4] and $\bar{\omega}_{22}$ is the natural frequency of each absorber if the blades are locked relative to the rotating hub. Equation (5.8) motivates the speed and order detunings

$$\sigma^2 = \sigma_r^2(1 + \varepsilon\Delta), \tag{5.9a}$$

$$\tilde{n}^2 - n^2 = \varepsilon\lambda, \tag{5.9b}$$

[4]This is not to be confused with σ_{res}, which corresponds to the intersection of $\bar{\omega}_{1,2}^{(n+1)}$ with the engine order line $n\sigma$.

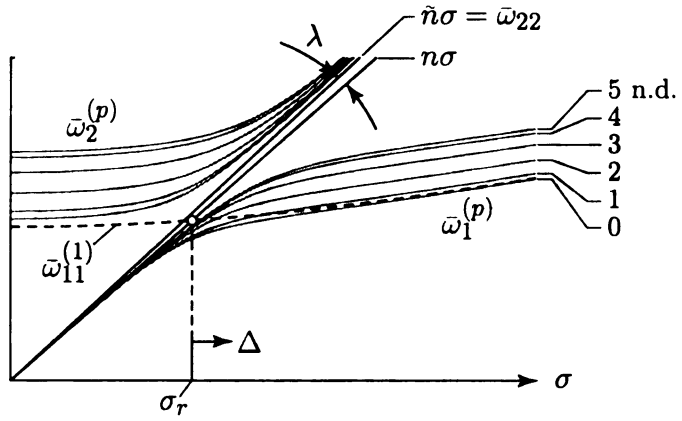

Figure 5.3. Example Campbell diagram showing the speed and order detuning parameters Δ and λ.

where Δ plays the role of the rotor speed and λ is the counterpart to the linear order detuning from Chapter 4. These can be visualized in Figure 5.3, where it is observed that $\bar{\omega}_{11} \cong \bar{\omega}_{11}^{(1)}$ for small mass ratios μ. (See Equation (4.26) on page 89.) Under the detuning scheme defined by Equation (5.9) the right hand side of Equation (5.8a) and Equation (5.8b) reduce to $-\varepsilon\Delta$ and $\varepsilon\lambda\sigma^2$, respectively, and Equation (5.6) becomes suitable for averaging. Finally, the two order detuning parameters λ and β are related by

$$\lambda = \frac{\beta n^2(\beta+2)}{\sqrt{\mu}}, \tag{5.10}$$

which follows from Equation (5.9b) and Equation (4.44). The no-resonance zone is such that $\beta_{\text{cr}} < \beta \leq 0$, to which there corresponds a range $\lambda_{\text{cr}} < \lambda \leq 0$ that can be computed using Equation (5.10).

After the appropriate substitutions are made Equation (5.6) is averaged over one period $T = 2\pi/n\sigma$. The result is partitioned into two vector functions, one that defines the stationary points of the i^{th} averaged sector model (this is discussed more fully in Section 5.3.1) and the other inherits any remaining terms. To $\mathcal{O}(\varepsilon^{3/2})$ and for each $i \in \mathcal{N}$, the desired form is

$$(\bar{u}_i', \bar{u}_i\bar{\varrho}_i', \bar{v}_i, \bar{v}_i\bar{\varsigma}_i')^T = \frac{\varepsilon}{2n\sigma}\mathbf{G}(\mathbf{v}_{i-1}, \mathbf{v}_i, \mathbf{v}_{i+1}) + \frac{\varepsilon}{2n\sigma}\mathbf{g}(\mathbf{v}_{i-1}, \mathbf{v}_i, \mathbf{v}_{i+1}), \tag{5.11}$$

where $\mathbf{v}_i = (\bar{u}_i, \bar{\varrho}_i, \bar{v}_i, \bar{\varsigma}_i)^T$. The elements of the 4×1 vector $\mathbf{G}$ are given by

$$\left.\begin{aligned}
G_1 &= -\alpha(n^2+1)\sigma^2\bar{v}_i \sin(\bar{\varrho}_i - \bar{\varsigma}_i) - n\sigma\hat{\xi}_b\bar{u}_i - \hat{f}\sin\bar{\varrho}_i \\
G_2 &= -\alpha(n^2+1)\sigma^2\bar{v}_i \cos(\bar{\varrho}_i - \bar{\varsigma}_i) - \Delta\bar{u}_i - \hat{f}\cos\bar{\varrho}_i \\
&\quad + \hat{\nu}^2\left[\begin{array}{l} 2\bar{u}_i - \bar{u}_{i-1}\cos(\bar{\varrho}_{i-1} - \bar{\varrho}_i - \varphi_{n+1}) \\ \qquad - \bar{u}_{i+1}\cos(\bar{\varrho}_{i+1} - \bar{\varrho}_i + \varphi_{n+1}) \end{array}\right] \\
G_3 &= +\alpha(n^2+1)\sigma^2\bar{u}_i \sin(\bar{\varrho}_i - \bar{\varsigma}_i) - n\sigma\hat{\xi}_{\bar{a}}\bar{v}_i \\
G_4 &= -\alpha(n^2+1)\sigma^2\bar{u}_i \cos(\bar{\varrho}_i - \bar{\varsigma}_i) + \lambda\sigma^2\bar{v}_i + \tfrac{3}{4}\eta\sigma^2\bar{v}_i^3
\end{aligned}\right\}, \quad i \in \mathcal{N} \tag{5.12}$$

where the identity $\phi_{i\pm1} - \phi_i = \pm 2\pi\frac{n}{N} = \pm\varphi_{n+1}$ has been employed, and the first element of $\mathbf{g}$ is

$$g_1 = \hat{\nu}^2\bar{u}_{i-1}\sin(\bar{\varrho}_{i-1} - \bar{\varrho}_i - \varphi_{n+1}) + \hat{\nu}^2\bar{u}_{i+1}\sin(\bar{\varrho}_{i+1} - \bar{\varrho}_i + \varphi_{n+1}), \qquad i \in \mathcal{N} \tag{5.13}$$

with the remaining entries being equal to zero.

As a final and important note, it is customary at this point to expand all appearances of σ according to Equation (5.9a) and to keep only $\mathcal{O}(\varepsilon)$ terms in Equation (5.11), which amounts to simply replacing σ with the *constant* σ_r. However, we opt instead to keep σ in the analysis which, as we shall see, gives much more satisfactory results.[5] Benchmark results in which the substitution *is* made are given in Appendix E; these are to be compared with the analysis and results to follow, particularly the blade and absorber frequency response curves of Section 5.4.

The averaged sector models defined by Equation (5.11) serve as the basis for the analysis in the rest of this chapter. The corresponding Cartesian form is also useful, which is given next.

[5]Note that Guckenheimer and Holmes take the same approach in their analysis of a simple Duffing oscillator in Chapter 4 of [96]. (In particular, see Equation (4.2.14) on page 174.)

CARTESIAN FORM

The averaged systems given by Equation (5.11) can be converted to Cartesian form via the transformation

$$\left.\begin{aligned} \bar{u}_i(\tau) &= \sqrt{A_i^2(\tau) + B_i^2(\tau)}, \qquad \tan\bar{\varrho}_i(\tau) = -B_i(\tau)/A_i(\tau) \\ \bar{v}_i(\tau) &= \sqrt{C_i^2(\tau) + D_i^2(\tau)}, \qquad \tan\bar{\varsigma}_i(\tau) = -D_i(\tau)/C_i(\tau) \end{aligned}\right\}, \qquad i \in \mathcal{N}.$$

Then if $\mathbf{w}_i = (A_i, B_i, C_i, D_i)^T$ it can be shown that

$$\mathbf{w}_i' = \frac{\varepsilon}{2n\sigma}\mathbf{P}(\mathbf{w}_{i-1}, \mathbf{w}_i, \mathbf{w}_{i+1}) + \frac{\varepsilon}{2n\sigma}\mathbf{p}(\mathbf{w}_{i-1}, \mathbf{w}_i, \mathbf{w}_{i+1}) + \mathcal{O}(\varepsilon^{3/2}), \qquad i \in \mathcal{N} \quad (5.14)$$

where the elements of $\mathbf{P}$ are given by

$$\left.\begin{aligned} P_1 &= -\alpha(n^2+1)\sigma^2 D_i - \Delta B_i - n\sigma\hat{\xi}_b A_i \\ &\qquad + \hat{\nu}^2\big(2B_i - (B_{i-1} + B_{i+1})\cos\varphi_{n+1}\big) \\ P_2 &= +\alpha(n^2+1)\sigma^2 C_i + \Delta A_i - n\sigma\hat{\xi}_b B_i + \hat{f} \\ &\qquad + \hat{\nu}^2\big(-2A_i + (A_{i-1} + A_{i+1})\cos\varphi_{n+1}\big) \\ P_3 &= -\alpha(n^2+1)\sigma^2 B_i + \lambda\sigma^2 D_i - n\sigma\hat{\xi}_{\bar{a}} C_i + \tfrac{3}{4}\eta\sigma^2(D_i^3 + C_i^2 D_i) \\ P_4 &= +\alpha(n^2+1)\sigma^2 A_i - \lambda\sigma^2 C_i - n\sigma\hat{\xi}_{\bar{a}} D_i - \tfrac{3}{4}\eta\sigma^2(C_i D_i^2 + C_i^3) \end{aligned}\right\}. \quad (5.15)$$

The first two elements of the vector $\mathbf{p}$ are

$$\left.\begin{aligned} p_1 &= -\hat{\nu}^2(A_{i-1} - A_{i+1})\sin\varphi_{n+1} \\ p_2 &= -\hat{\nu}^2(B_{i-1} - B_{i+1})\sin\varphi_{n+1} \end{aligned}\right\}, \qquad i \in \mathcal{N} \quad (5.16)$$

and the remaining two elements are zero.

Existence and local stability of the desired traveling wave response of the coupled system is discussed next.

5.3 Traveling Wave Response

The desired system response is that of a *traveling wave* (TW), where each sector behaves identically, except for a fixed phase difference among its nearest neighbors.

Such a response is characterized by the fullest degree of (cyclic) symmetry that is possible, which can be visualized in Figure 2.7 on page 35. Then the absorbers become entrained with the (discrete BTW, FTW, or SW) applied dynamic loading among the blades (see Section 2.3.2) and are hence most effective in addressing their attendant vibrations. This type of response is the counterpart to the desired *synchronous* motion in the CPVA work by Shaw and coworkers, where any other response type implies a degradation of absorber performance in which some of the absorbers work against the others [22, 23].

The averaged models described in Section 5.2.4 were formulated specifically to capture a TW response, but they are also general enough to identify other solution types (if they exist) that involve amplitude and phase modulations in individual sectors. Throughout the remainder of this chapter we focus on TW solutions, the existence, determination, and stability of which is considered next. Possible bifurcation to other response types is addressed in Section 5.5.

5.3.1 Existence

A TW response is characterized by *identical* dynamics of individual sectors together with a fixed phase difference in these dynamics among neighboring sectors. If $\mathbf{v} = (\bar{u}, \bar{\varrho}, \bar{v}, \bar{\varsigma})^T$ and $\mathbf{w} = (A, B, C, D)^T$, then such a response corresponds to

$$(\mathbf{v}_{i-1}, \mathbf{v}_i, \mathbf{v}_{i+1}) = (\mathbf{v}, \mathbf{v}, \mathbf{v}), \qquad \forall\, i \in \mathcal{N} \qquad \text{(Polar Form)} \tag{5.17a}$$

$$(\mathbf{w}_{i-1}, \mathbf{w}_i, \mathbf{w}_{i+1}) = (\mathbf{w}, \mathbf{w}, \mathbf{w}), \qquad \forall\, i \in \mathcal{N} \qquad \text{(Cartesian Form)} \tag{5.17b}$$

where the phase difference among adjacent sectors is built into the transformation defined by Equation (5.5) via the inter-blade phase angles ϕ_i. Since $\mathbf{g}(\mathbf{v}, \mathbf{v}, \mathbf{v}) = \mathbf{0}$ (resp. $\mathbf{h}(\mathbf{w}, \mathbf{w}, \mathbf{w}) = \mathbf{0}$), which can be verified from Equation (5.13) (resp. Equation (5.16)) by setting $\bar{\varrho}_{i-1} = \bar{\varrho}_{i+1} = \bar{\varrho}$ (resp. $A_{i-1} = A_{i+1} = A$ and $B_{i-1} = B_{i+1} = B$), it thus

follows that

$$\mathbf{0} = \mathbf{G}(\mathbf{v}, \mathbf{v}, \mathbf{v}), \qquad \text{(Polar Form)} \tag{5.18a}$$

$$\mathbf{0} = \mathbf{P}(\mathbf{w}, \mathbf{w}, \mathbf{w}), \qquad \text{(Cartesian Form)} \tag{5.18b}$$

defines a TW response when the averaged models are in polar (resp. Cartesian) form. That is, if a *stationary point* $\mathbf{v}$ (or $\mathbf{w}$) can be found that satisfies Equation (5.18a) (or Equation (5.18b)), then there exists a corresponding TW response. Existence, therefore, follows from the equilibria of an *individual* averaged sector model, a simplification that follows from the assumption of identical, identically-coupled sectors, and expressions for their determination are derived in the next section. In contrast, local stability of a stationary point involves *all* N averaged sector models, which is discussed in Section 5.3.3.

5.3.2 Stationary Points

To each stationary point $\mathbf{v}$ (or $\mathbf{w}$) that satisfies Equation (5.18) (when it exists) corresponds a TW solution. In general, the determination of these equilibrium points is too formidable to be carried out analytically, but some important insight can be gleaned from their defining equations. If damping is ignored, however, a simplified set of implicit expressions can be obtained, from which blade and absorber amplitudes $|\bar{u}|$ and $|\bar{v}|$ easily follow. These expressions are used to generate representative frequency response curves in Section 5.4 for the isolated nonlinear system and in Section 5.5 for the fully coupled nonlinear system. Finally, in all of what follows it is assumed that $n \in \mathbb{Z}_+$, $\sigma > 0$, $\hat{f} \neq 0$, $0 < \alpha < 1$, and $n^2 - \delta > 0$. Physically, the last two conditions imply that the absorber is attached along the length of the blade and, essentially, that the rotor radius is comparable to the blade length if the engine order is very small—a restriction that will generally be satisfied for the engine orders of interest and for practical rotor/blade geometries.

We begin by considering the fully damped system and focus on general insight; the special undamped case is considered subsequently.

The Damped System

When they exist, the stationary points can be obtained from either Equation (5.18a) or Equation (5.18b). The former is slightly less cumbersome to work with analytically and hence it is employed throughout the remainder of this section. It can be written as

$$0 = -\alpha(n^2+1)\sigma^2\bar{v}\sin(\bar{\varrho}-\bar{\varsigma}) - n\sigma\hat{\xi}_b\bar{u} - \hat{f}\sin\bar{\varrho}, \tag{5.19a}$$

$$0 = -\alpha(n^2+1)\sigma^2\bar{v}\cos(\bar{\varrho}-\bar{\varsigma}) - \big(\Delta - 2\hat{\nu}^2(1-\cos\varphi_{n+1})\big)\bar{u} - \hat{f}\cos\bar{\varrho}, \tag{5.19b}$$

$$0 = +\alpha(n^2+1)\sigma^2\bar{u}\sin(\bar{\varrho}-\bar{\varsigma}) - n\sigma\hat{\xi}_a\bar{v}, \tag{5.19c}$$

$$0 = -\alpha(n^2+1)\sigma^2\bar{u}\cos(\bar{\varrho}-\bar{\varsigma}) + \lambda\sigma^2\bar{v} + \tfrac{3}{4}\eta\sigma^2\bar{v}^3, \tag{5.19d}$$

from which a number of general insights can be gleaned.

In the absence of nonlinearity, which appears only in Equation (5.19d) via the cubic absorber path term, Equation (5.19) approximates the amplitudes of the exact linearized response defined by Equation (4.34) as σ is swept from zero. Moreover, the inter-sector coupling appears only in Equation (5.19b) in combination with the speed detuning parameter Δ, and it therefore reflects the same shift in the linear resonance (associated with coupling) that was observed in Chapter 4. In this way, the fundamental effects of nonlinearity on the TW response amplitudes, and bifurcations to other *traveling wave* responses, can be qualitatively captured in the absence of coupling—that is, for an *isolated* sector. This is the focus of Section 5.4. The frequency response amplitudes for the fully coupled nonlinear system are essentially the same as those of the uncoupled case, except for a shift in the primary resonance by an amount that is directly proportional to ν^2; when the coupling is small, this shift is nearly undetectable. However, there may also be potentially rich instabilities

to response types other than the desired TW (i.e., those with a reduced degree of symmetry) when coupling is present. This possibility is discussed in Section 5.5.

The presence of damping renders Equation (5.19) essentially intractable since there is no clear way to eliminate phases and solve for the desired amplitudes $\bar{u}$ and $\bar{v}$. Even the corresponding Cartesian form poses much difficulty. Thus when damping is included the equilibrium points are obtained numerically.

The special case of zero damping is considered next. In this instance, an implicit pair of expressions for the blade and absorber amplitudes can be derived.

The Undamped System

For zero damping, and when the stationary points exist, they are defined implicitly by Equation (5.19) with $\hat{\xi}_b = \hat{\xi}_{\bar{a}} = 0$, that is,

$$0 = -\alpha(n^2+1)\sigma^2\bar{v}\sin\big(\bar{\varrho}-\bar{\varsigma}\big) - \hat{f}\sin\bar{\varrho}, \tag{5.20a}$$

$$0 = -\alpha(n^2+1)\sigma^2\bar{v}\cos\big(\bar{\varrho}-\bar{\varsigma}\big) - \big(\Delta - 2\hat{\nu}^2(1-\cos\varphi_{n+1})\big)\bar{u} - \hat{f}\cos\bar{\varrho}, \tag{5.20b}$$

$$0 = +\alpha(n^2+1)\sigma^2\bar{u}\sin\big(\bar{\varrho}-\bar{\varsigma}\big), \tag{5.20c}$$

$$0 = -\alpha(n^2+1)\sigma^2\bar{u}\cos\big(\bar{\varrho}-\bar{\varsigma}\big) + \lambda\sigma^2\bar{v} + \tfrac{3}{4}\eta\sigma^2\bar{v}^3, \tag{5.20d}$$

from which a simple pair of implicit expressions for the blade and absorber amplitudes can be distilled. However, the case of zero damping is highly degenerate and this system gives rise to nonhyperbolic equilibria. Nonetheless, an arbitrarily small level of damping removes the degeneracy, which is shown in Section (5.3.3), and thus the expressions in Equation (5.20) collectively give a good approximation to the blade and absorber amplitudes in the presence of light damping. Local stability is obtained accordingly.

It should be pointed out from the onset that, due to the appearance of $\sin\bar{\varrho}$ and $\cos\bar{\varrho}$ in the forcing terms of Equation (5.20a) and Equation (5.20b), the usual approach to eliminate phases cannot be employed and, correspondingly, the analysis

is somewhat more cumbersome. Equation (5.20c) is used as a guide on how to proceed. Under the assumptions indicated above, it is satisfied only if $\sin(\bar{\varrho}-\bar{\varsigma}) = 0$, $\bar{u} = 0$, or both. The first condition gives rise to the most general form of the equilibria and it is described in detail below. The second condition gives rise to the desired motions in which the blades remain stationary relative to the spinning rotor. It is simply a special case of the first and is described in Section 5.4.2. Finally, the third condition can be obtained from the first two, and it does not give rise to any additional equilibria.

If $\sin(\bar{\varrho} - \bar{\varsigma}) = 0$ then Equation (5.20c) is trivial and it follows from Equation (5.20a) that $\sin\bar{\varrho} = 0$, and together these expressions imply $\sin\bar{\varsigma} = 0$. The phases must therefore satisfy

$$\bar{\varrho} = k\pi \quad \text{and} \quad \bar{\varsigma} = l\pi, \qquad k, l \in \mathbb{Z} \tag{5.21}$$

and the system given by Equation (5.20) reduces to

$$\begin{aligned} 0 = &-\alpha(n^2+1)\sigma^2\bar{v}\cos(k\pi)\cos(l\pi) \\ &- \big(\Delta - 2\hat{\nu}^2(1-\cos\varphi_{n+1})\big)\bar{u} - \hat{f}\cos(k\pi), \end{aligned} \tag{5.22a}$$

$$0 = -\alpha(n^2+1)\sigma^2\bar{u}\cos(k\pi)\cos(l\pi) + \lambda\sigma^2\bar{v} + \tfrac{3}{4}\eta\sigma^2\bar{v}^3, \tag{5.22b}$$

for $k, l \in \mathbb{Z}$. There are at most four integer pairs (k, l) that yield distinct blade/absorber amplitudes $(\bar{u}, \bar{v})$, and one such choice is summarized in Table 5.2. Physically, when $(k, l) = (0, 0)$ (resp. $(1, 1)$) each blade and its attendant absorber oscillate with the same phase and their motions are in phase (resp. out of phase) with respect to the applied dynamic loading. For the case of $(k, l) = (0, 1)$ (resp. $(1, 0)$) their motions are out of phase and the blades (resp. absorbers) responds out of phase (resp. in phase) relative to the excitation. (Of course, some of these motions may be unstable.) These details are not belabored, however, since in the absence of damping *every* stationary point is nonhyperbolic, which is shown in Section 5.3.3.

The (k, l)-dependence in Equation (5.22) can be eliminated by multiplying Equation (5.22a) by $\cos(k\pi)$ and Equation (5.22b) by $\cos^3(l\pi) = \cos(l\pi)$. Then by defining

Table 5.2. Example integer pairs (k, l) that yield distinct stationary points $\bar{u}$ and $\bar{v}$ of the averaged system. Also indicated are the corresponding values of $\bar{\varrho}$ and $\bar{\varsigma}$ and whether the resulting blade/absorber motions are in phase (IP) or out of phase (OP).

k	l	$\cos(k\pi)$	$\cos(l\pi)$	$\cos(k\pi)\cos(l\pi)$	$\bar{\varrho} = k\pi$	$\bar{\varsigma} = l\pi$	Phase
0	0	1	1	1	0	0	IP
1	1	−1	−1	1	π	π	IP
0	1	1	−1	−1	0	π	OP
1	0	−1	1	−1	π	0	OP

$\tilde{u} = \bar{u}\cos(k\pi)$ and $\tilde{v} = \bar{v}\cos(l\pi)$ and simplifying the result it follows that

$$0 = \alpha(n^2+1)\sigma^2\tilde{v} + \big(\Delta - 2\hat{\nu}^2(1-\cos\varphi_{n+1})\big)\tilde{u} + \hat{f}, \tag{5.23a}$$

$$0 = \alpha(n^2+1)\tilde{u} - \lambda\tilde{v} - \tfrac{3}{4}\eta\tilde{v}^3, \tag{5.23b}$$

from which the steady-state blade/absorber amplitudes $|\tilde{u}| = |\bar{u}|$ and $|\tilde{v}| = |\bar{v}|$ can easily be computed.

There are at most three roots for $\tilde{v}$, and these can be obtained by eliminating $\tilde{u}$ in Equation (5.23). They follow implicitly from

$$\frac{3}{4}\eta\tilde{v}^3 + \left(\frac{\alpha^2(n^2+1)^2\sigma^2}{\Delta - 2\hat{\nu}^2(1-\cos\varphi_{n+1})} + \lambda\right)\tilde{v} + \frac{\alpha(n^2+1)\hat{f}}{\Delta - 2\hat{\nu}^2(1-\cos\varphi_{n+1})} = 0, \tag{5.24}$$

where the corresponding values

$$\tilde{u} = -\frac{\alpha(n^2+1)\sigma^2}{\Delta - 2\hat{\nu}^2(1-\cos\varphi_{n+1})}\tilde{v} - \frac{\hat{f}}{\Delta - 2\hat{\nu}^2(1-\cos\varphi_{n+1})} \tag{5.25}$$

follow from Equation (5.23a). Given the geometry of the bladed disk assembly, the strength and order of the excitation, a particular linear tuning, the coupling level, and the strength of the absorber path nonlinearity, one can construct the blade and absorber amplitude frequency response curves in terms of the rotor speed using Equation (5.24) and Equation (5.25). In doing so, the reader is reminded that the dimensionless rotor speed σ and its detuning parameter Δ are related by Equation (5.9a), where $\varepsilon = \sqrt{\mu}$.

Local stability of the TW response is considered next.

5.3.3 Local Stability

A hyperbolic fixed point $\mathbf{v}$ (or $\mathbf{w}$) implies a unique hyperbolic periodic orbit in the i^{th} nonlinear sector and together all such orbits form a TW response among the sectors with the same stability type [96, 109]. Local stability of $\mathbf{v}$ is considered next for the fully coupled system. The results are subsequently stated for the corresponding Cartesian form and also for the special case of a single isolated sector.

THE COUPLED NONLINEAR SYSTEM

Local stability of a stationary point $\mathbf{v} = (\bar{u}, \bar{\varrho}, \bar{v}, \bar{\varsigma})^T$, the elements of which are defined implicitly by Equation (5.19), can be obtained by considering the small perturbations

$$\boldsymbol{\eta}_i = \mathbf{v}_i - \mathbf{v}, \qquad i \in \mathcal{N}$$

away from $\mathbf{v}_i = (\bar{u}_i, \bar{\varrho}_i, \bar{v}_i, \bar{\varsigma}_i)^T$. Then for each $i \in \mathcal{N}$, Equation (5.11) can be locally approximated to leading order by the linearized equation

$$\boldsymbol{\eta}_i' = \frac{\varepsilon}{2n\sigma}\Big[(\mathbf{A}-\mathbf{B})\boldsymbol{\eta}_{i-1} + \mathbf{U}\boldsymbol{\eta}_i + (\mathbf{A}+\mathbf{B})\boldsymbol{\eta}_{i+1}\Big] + \text{HOT}, \qquad i \in \mathcal{N}. \tag{5.26}$$

In Equation (5.26) the subscripts are taken mod N such that $\boldsymbol{\eta}_0 = \boldsymbol{\eta}_N$ and $\boldsymbol{\eta}_{N+1} = \boldsymbol{\eta}_1$ and

$$\mathbf{U} = \begin{bmatrix} -n\sigma\hat{\xi}_b & -\bar{\alpha}\bar{v}C_{(\bar{\varrho}-\bar{\varsigma})} - \hat{f}C_{(\bar{\varrho})} - 2\hat{\nu}^2\bar{u}C_{(\varphi_{n+1})} & -\bar{\alpha}S_{(\bar{\varrho}-\bar{\varsigma})} & \bar{\alpha}\bar{v}C_{(\bar{\varrho}-\bar{\varsigma})} \\ -\Delta + 2\hat{\nu}^2 & \bar{\alpha}\bar{v}S_{(\bar{\varrho}-\bar{\varsigma})} + \hat{f}S_{(\bar{\varrho})} & -\bar{\alpha}C_{(\bar{\varrho}-\bar{\varsigma})} & -\bar{\alpha}\bar{v}S_{(\bar{\varrho}-\bar{\varsigma})} \\ \bar{\alpha}S_{(\bar{\varrho}-\bar{\varsigma})} & \bar{\alpha}\bar{u}C_{(\bar{\varrho}-\bar{\varsigma})} & -n\sigma\hat{\xi}_{\bar{a}} & -\bar{\alpha}\bar{u}C_{(\bar{\varrho}-\bar{\varsigma})} \\ -\bar{\alpha}C_{(\bar{\varrho}-\bar{\varsigma})} & \bar{\alpha}\bar{u}S_{(\bar{\varrho}-\bar{\varsigma})} & \lambda\sigma^2 + \frac{9}{4}\eta\sigma^2\bar{v}^2 & -\bar{\alpha}\bar{u}S_{(\bar{\varrho}-\bar{\varsigma})} \end{bmatrix},$$

where the shorthand notation $\bar{\alpha} = \alpha(n^2+1)\sigma^2$, $S_{(\chi)} = \sin(\chi)$ and $C_{(\chi)} = \cos(\chi)$ has been introduced. If the matrices $\mathbf{A}$ and $\mathbf{B}$ are partitioned into four 2×2 blocks then the $(1,1)$ blocks are given by

$$\mathbf{A}_{11} = \begin{bmatrix} 0 & \hat{\nu}^2\bar{u}\cos\varphi_{n+1} \\ -\hat{\nu}^2\cos\varphi_{n+1} & 0 \end{bmatrix}, \qquad \mathbf{B}_{11} = \begin{bmatrix} \hat{\nu}^2\sin\varphi_{n+1} & 0 \\ 0 & \hat{\nu}^2\bar{u}\sin\varphi_{n+1} \end{bmatrix},$$

and all other entries are zero.

The N linear systems defined by Equation (5.26) can be handled in the same way as the sector models in Section 4.3.2. By stacking each 4×1 vector $\boldsymbol{\eta}_i$ into the configuration vector $\boldsymbol{\eta} = (\boldsymbol{\eta}_1, \boldsymbol{\eta}_2, \ldots, \boldsymbol{\eta}_N)^T$ it follows that $\boldsymbol{\eta}' = \varepsilon \mathbf{J}_{\mathrm{CS}}^{(\mathrm{P})} \boldsymbol{\eta}$, where

$$\mathbf{J}_{\mathrm{CS}}^{(\mathrm{P})} = \frac{1}{2n\sigma} \mathrm{circ}\,(\mathbf{U}, \mathbf{A}+\mathbf{B}, \mathbf{0}, \ldots, \mathbf{0}, \mathbf{A}-\mathbf{B}) \tag{5.27}$$

is the $4N \times 4N$ Jacobian matrix, which belongs to $\mathscr{BCBS}_{4,N}$. That is, $\mathbf{J}_{\mathrm{CS}}^{(\mathrm{P})}$ is a block circulant, block symmetric matrix of type $(4, N)$ and can thus be block diagonalized via the unitary transformation defined by Equation (2.11) on page 15. This gives rise to the set of N, 4×4 matrices

$$\mathbf{J}_k^{(\mathrm{P})} = \frac{1}{2n\sigma}\Big(\mathbf{U} + 2\mathbf{A}\cos\varphi_k + 2j\mathbf{B}\sin\varphi_k\Big), \qquad k \in \mathcal{N} \tag{5.28}$$

where, recall, $\varphi_k = \frac{2\pi}{N}(k-1)$. The $4N$ system eigenvalues are preserved under this transformation and hence they can be obtained by solving N reduced-order eigensystems involving 4×4 matrices instead of just one potentially formidable eigenvalue problem involving a $4N \times 4N$ matrix. However, the transformation renders the reduced Jacobians *complex*, which makes their interpretation more difficult. This is discussed more fully in Section 5.5.

A similar analysis can be carried out for the averaged sector models in Cartesian form. In this case the Jacobian matrix $\mathbf{J}_{\mathrm{CS}}^{(\mathrm{C})}$ (the counterpart to $\mathbf{J}_{\mathrm{CS}}^{(\mathrm{P})}$ when Cartesian coordinates are used) has generating matrices $\mathbf{P}, \mathbf{Q}+\mathbf{R}, \mathbf{0}, \ldots, \mathbf{0}, \mathbf{Q}-\mathbf{R}$, where

$$\mathbf{P} = \begin{bmatrix} -n\sigma\hat{\xi}_b & -\Delta + 2\hat{\nu}^2 & 0 & -\bar{\alpha}\sigma^2 \\ \Delta - 2\hat{\nu}^2 & -n\sigma\hat{\xi}_b & \bar{\alpha}\sigma^2 & 0 \\ 0 & -\bar{\alpha}\sigma^2 & \frac{3}{2}\eta\sigma^2 CD - n\sigma\hat{\xi}_{\bar{a}} & \frac{3}{4}\eta\sigma^2(C^2+3D^2) + \lambda\sigma^2 \\ \bar{\alpha}\sigma^2 & 0 & -\frac{3}{4}\eta\sigma^2(3C^2+D^2) - \lambda\sigma^2 & -\frac{3}{2}\eta\sigma^2 CD - n\sigma\hat{\xi}_{\bar{a}} \end{bmatrix},$$

and the $(1,1)$ blocks of $\mathbf{Q}$ and $\mathbf{R}$ are given by

$$\mathbf{Q}_{11} = \begin{bmatrix} 0 & -\hat{\nu}^2\cos\varphi_{n+1} \\ \hat{\nu}^2\cos\varphi_{n+1} & 0 \end{bmatrix}, \qquad \mathbf{R}_{11} = \begin{bmatrix} \hat{\nu}^2\sin\varphi_{n+1} & 0 \\ 0 & \hat{\nu}^2\sin\varphi_{n+1} \end{bmatrix},$$

with all other elements being equal to zero. This gives rise to the set of N, 4×4 block decoupled Jacobian matrices

$$\mathbf{J}_k^{(\mathrm{C})} = \frac{1}{2n\sigma}\Big(\mathbf{P} + 2\mathbf{Q}\cos\varphi_k + 2j\mathbf{R}\sin\varphi_k\Big), \qquad k \in \mathcal{N} \tag{5.29}$$

which are the Cartesian counterparts to the matrices defined by Equation (5.28).

Some local stability results are given next for the special case of an isolated sector, including a polynomial expression for the eigenvalues of its Jacobian matrix.

The Isolated Nonlinear System

The Jacobian matrix corresponding to an isolated sector can be obtained from Equation (5.28) or Equation (5.29) by setting $\hat{\nu} = 0$, in which case the matrices **A**, **B**, **Q**, and **R** (and hence the k-dependence) all vanish. In polar and Cartesian forms, the Jacobians are

$$\mathbf{J}_{\mathrm{IS}}^{(\mathrm{P})} = \frac{1}{2n\sigma}\begin{bmatrix} -n\sigma\hat{\xi}_b & -\bar{\alpha}\bar{v}C_{(\bar{\varrho}-\bar{\varsigma})} - \hat{f}C_{(\bar{\varrho})} & -\bar{\alpha}S_{(\bar{\varrho}-\bar{\varsigma})} & \bar{\alpha}\bar{v}C_{(\bar{\varrho}-\bar{\varsigma})} \\ -\Delta & \bar{\alpha}\bar{v}S_{(\bar{\varrho}-\bar{\varsigma})} + \hat{f}S_{(\bar{\varrho})} & -\bar{\alpha}C_{(\bar{\varrho}-\bar{\varsigma})} & -\bar{\alpha}\bar{v}S_{(\bar{\varrho}-\bar{\varsigma})} \\ \bar{\alpha}S_{(\bar{\varrho}-\bar{\varsigma})} & \bar{\alpha}\bar{u}C_{(\bar{\varrho}-\bar{\varsigma})} & -n\sigma\hat{\xi}_{\bar{a}} & -\bar{\alpha}\bar{u}C_{(\bar{\varrho}-\bar{\varsigma})} \\ -\bar{\alpha}C_{(\bar{\varrho}-\bar{\varsigma})} & \bar{\alpha}\bar{u}S_{(\bar{\varrho}-\bar{\varsigma})} & \lambda\sigma^2 + \frac{9}{4}\eta\sigma^2\bar{v}^2 & -\bar{\alpha}\bar{u}S_{(\bar{\varrho}-\bar{\varsigma})} \end{bmatrix}, \tag{5.30a}$$

$$\mathbf{J}_{\mathrm{IS}}^{(\mathrm{C})} = \frac{1}{2n\sigma}\begin{bmatrix} -n\sigma\hat{\xi}_b & -\Delta & 0 & -\bar{\alpha}\sigma^2 \\ \Delta & -n\sigma\hat{\xi}_b & \bar{\alpha}\sigma^2 & 0 \\ 0 & -\bar{\alpha}\sigma^2 & \frac{3}{2}\eta\sigma^2 CD - n\sigma\hat{\xi}_{\bar{a}} & \frac{3}{4}\eta\sigma^2(C^2+3D^2) + \lambda\sigma^2 \\ \bar{\alpha}\sigma^2 & 0 & -\frac{3}{4}\eta\sigma^2(3C^2+D^2) - \lambda\sigma^2 & -\frac{3}{2}\eta\sigma^2 CD - n\sigma\hat{\xi}_{\bar{a}} \end{bmatrix}, \tag{5.30b}$$

which have the same elements as the matrices $\mathbf{U}/2n\sigma$ and $\mathbf{P}/2n\sigma$, respectively, in the absence of inter-sector coupling.

Stability results are more transparent and tractable for the isolated sector case, especially in Cartesian form. The eigenvalues ζ of $\mathbf{J}_{\mathrm{IS}}^{(\mathrm{C})}$ follow implicitly from the fourth-order polynomial $\det\left(\mathbf{J}_{\mathrm{IS}}^{(\mathrm{C})} - \zeta\mathbf{I}\right) = 0$, which can be written as

$$s^4 + d_3 s^3 + (a_2 + d_2)s^2 + d_1 s + (a_0 + d_0) = 0, \tag{5.31}$$

where $s = 2n\sigma\zeta$. The coefficients are

$$\left.\begin{aligned}
a_2 &= \Delta^2 + \tfrac{1}{16}\Big(32\alpha^2(n^2+1)^2 + \big(3\eta(C^2+D^2)+4\lambda\big)\big(9\eta(C^2+D^2)+4\lambda\big)\Big)\sigma^4 \\
a_0 &= \tfrac{1}{16}\big(4\alpha^2(n^2+1)^2\sigma^2 + 3\eta(C^2+D^2)\Delta + 4\lambda\Delta\big) \\
&\quad \times \big(4\alpha^2(n^2+1)^2\sigma^2 + 9\eta(C^2+D^2)\Delta + 4\lambda\Delta\big)\sigma^4 \\
d_3 &= 2n\sigma\big(\hat{\xi}_{\bar{a}} + \hat{\xi}_b\big) \\
d_2 &= n^2\sigma^2\big(\hat{\xi}_{\bar{a}}^2 + 4\hat{\xi}_{\bar{a}}\hat{\xi}_b + \hat{\xi}_b^2\big) \\
d_1 &= 2n\sigma^5\Big(\alpha^2(n^2+1)^2(\hat{\xi}_{\bar{a}} + \hat{\xi}_b) + \tfrac{1}{16}\big(3\eta(C^2+D^2)+4\lambda\big)\big(9\eta(C^2+D^2)+4\lambda\big)\hat{\xi}_b\Big) \\
&\quad + 2n\sigma\Delta^2\hat{\xi}_{\bar{a}} + 2n^3\sigma^3\hat{\xi}_{\bar{a}}\hat{\xi}_b(\hat{\xi}_{\bar{a}} + \hat{\xi}_b) \\
d_0 &= \tfrac{1}{16}n^2\sigma^6\hat{\xi}_b\Big(32\alpha^2(n^2+1)^2\hat{\xi}_{\bar{a}} + \big(3\eta(C^2+D^2)+4\lambda\big)\big(9\eta(C^2+D^2)+4\lambda\big)\hat{\xi}_b\Big) \\
&\quad + n^2\sigma^2\hat{\xi}_{\bar{a}}^2\big(\Delta^2 + n^2\sigma^2\hat{\xi}_b^2\big)
\end{aligned}\right\},$$

where each d_k $(k = 1, 2, 3, 4)$ vanishes when $\hat{\xi}_{\bar{a}} = \hat{\xi}_b = 0$. In the absence of damping Equation (5.31) is quadratic in s^2 and it thus features quadrantal symmetry in the complex plane. This in turn implies nonhyperbolic or otherwise unstable stationary points $\mathbf{v}$, depending on the details of a_2 and a_0. An arbitrarily small level of blade and/or absorber damping destroys the quadrantal symmetry, thus removing the possibility of nonhyperbolicity.

Next the averaged sector equations are employed to detail some global features of the forced response. This is done first for the isolated nonlinear system in Section 5.4 and subsequently for the fully coupled nonlinear system in Section 5.5. For convenience, and where appropriate, the analysis is carried out using both polar and cartesian forms.

5.4 Forced Response of the Isolated Nonlinear System

In order to focus on the nonlinear dynamic performance of the absorbers without the potentially complicating effects of inter-sector coupling (in particular, the possibility of additional symmetry-breaking instabilities) we focus on an *isolated* sector in this

section, which consists of a single blade and nonlinear absorber. (A treatment of the fully coupled nonlinear system is postponed to Section 5.5.) The results are presented in Section 5.4.1 in terms of blade and absorber (amplitude) frequency response curves. A criterion that guarantees a branch corresponding to zero blade amplitudes is subsequently derived in Section 5.4.2, which is the nonlinear counterpart to the ideal, or exact linear tuning.

5.4.1 Frequency Response

Example plots of the blade and absorber TW amplitudes $|\bar{u}|$ and $|\bar{v}|$ are shown in Figure 5.4 versus the rotor speed σ for a hardening absorber path ($\eta > 0$), zero damping, and for various levels of the order detuning β, and a corresponding set of plots is shown in Figure 5.5 for a softening path ($\eta < 0$). In these figures, the undamped absorber and blade amplitudes were generated using Equation (5.24) and Equation (5.25) with $\hat{\nu} = 0$, and stability results were numerically determined according to Equation (5.30) with the addition of very light damping (approximately 0.01% absorber damping relative to critical and zero blade damping). For comparison, the linearized frequency response curves of Chapter 4 are also included. Figure 5.6 features the same frequency response loci shown in Figure 5.5 for softening absorbers, but with nonzero blade and absorber damping $\hat{\xi}_b = 2 \times 10^{-3}$ and $\xi_{\bar{a}} = 2 \times 10^{-6}$. These curves were obtained numerically according to Equation (5.19) (stationary points) and Equation (5.30a) (local stability). A set of frequency response curves showing more resolution with respect to β within and near the no-resonance zone is shown in Figure 5.7 for a hardening absorber path and in Figure 5.8 for a softening absorber path; these are meant to accompany Figure 5.4 and Figure 5.5, respectively. Finally, it was shown in Section 5.2.2 that the linear resonance structure described in Chapter 4 is preserved under the scaling (see Figure 5.2 on page 125), and it is clear from Figures 5.4-5.8 that this structure qualitatively persists in the averaged system as well. However, the

nonlinearity gives rise to some additional features, and we describe them first for the case of hardening absorber paths.

In Figure 5.4 either one or two nonlinear resonances can be observed, depending on the order detuning β, and there is interplay/duality — between the two. For convenience, these are defined as *primary* and *auxiliary* (nonlinear) resonances and are denoted by $\mathcal{R}_{\mathrm{p}}^{\mathrm{NL}}$ and $\mathcal{R}_{\mathrm{a}}^{\mathrm{NL}}$, respectively. The primary resonance is simply the nonlinear counterpart to the *linear* resonance (denoted by $\mathcal{R}^{\mathrm{L}}$) and, for a hardening absorber path, it bends toward the direction of increasing rotor speed. When it exists, $\mathcal{R}_{\mathrm{a}}^{\mathrm{NL}}$ is a secondary resonance that arises due to the presence of the nonlinearity.

For large undertuning values, $\mathcal{R}_{\mathrm{p}}^{\mathrm{NL}}$ and $\mathcal{R}^{\mathrm{L}}$ are nearly coincident close to $\sigma = \sigma_r = 0.346$, which is shown in Figure 5.4a, but the hardening nonlinearity sharply bends the primary resonance in the direction of increasing σ. In this figure, the nonlinearity gives rise to an additional resonance $\mathcal{R}_{\mathrm{a}}^{\mathrm{NL}}$, which appears from zero rotor speed. For the blade, it increases gradually for increasing σ, whereas for the absorber it begins at nearly constant amplitude. For both, the auxiliary resonant amplitudes increase sharply at $\sigma = \sigma_r$ which, recall, is the resonant speed of an isolated blade without an absorber and it also corresponds to zero speed detuning, i.e., $\Delta = 0$.

As β is increased $\mathcal{R}_{\mathrm{p}}^{\mathrm{NL}}$ and $\mathcal{R}^{\mathrm{L}}$ move together to the right[6] (Figure 5.4b) toward infinite σ, leaving behind the same set of linear amplitude branches that were observed in Chapter 4. This situation, which is shown in Figure 5.4c, corresponds to the no-resonance zone predicted by the linear theory. However, the auxiliary resonance $\mathcal{R}_{\mathrm{a}}^{\mathrm{NL}}$ persists, which is an artifact of the absorber path nonlinearity. The case of perfect linear tuning ($\beta = 0$) is similar, except that the linear amplitude branch for the blade vanishes (this is shown in Figure 5.4d) and $\mathcal{R}_{\mathrm{a}}^{\mathrm{NL}}$ and $\mathcal{R}_{\mathrm{p}}^{\mathrm{NL}}$ become coincident—that is to say, as β is swept through exact linear tuning $\mathcal{R}_{\mathrm{a}}^{\mathrm{NL}}$ essentially switches roles to become the primary resonance. By further increasing the linear detuning (that is, for

[6]The error between the location of these resonances can be approximated by the curves in Figure 5.2b on page 125.

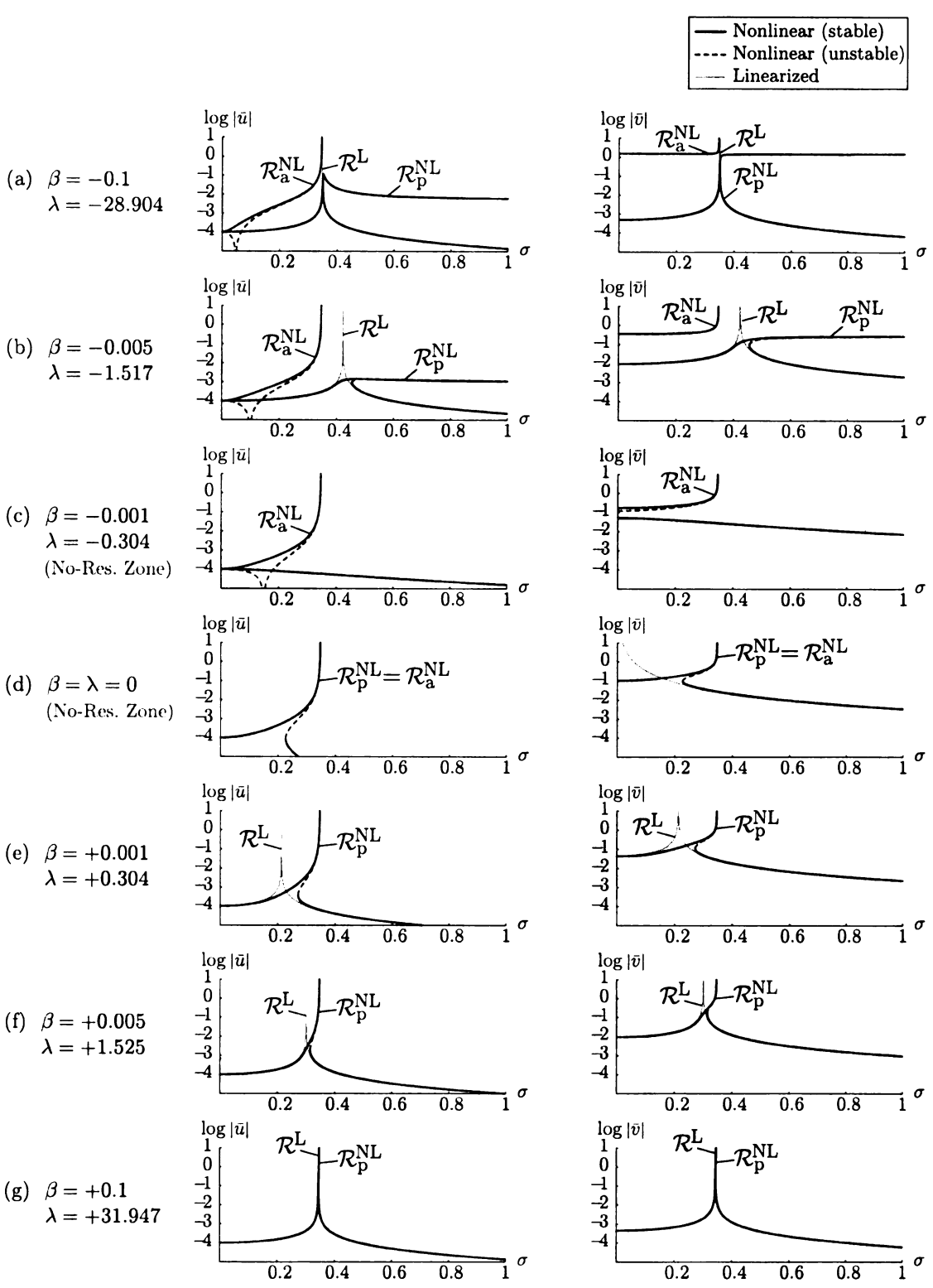

Figure 5.4. Blade/absorber frequency response curves for the essentially undamped isolated nonlinear system with a *hardening* absorber path ($\eta = 1$), for various detuning values β, and for $n = 3$, $\alpha = 0.84$, $\delta = 0.67$, $\mu = 0.0035$ ($\varepsilon = 0.0592$), and $F = 0.0001$ ($\hat{f} = 0.117$).

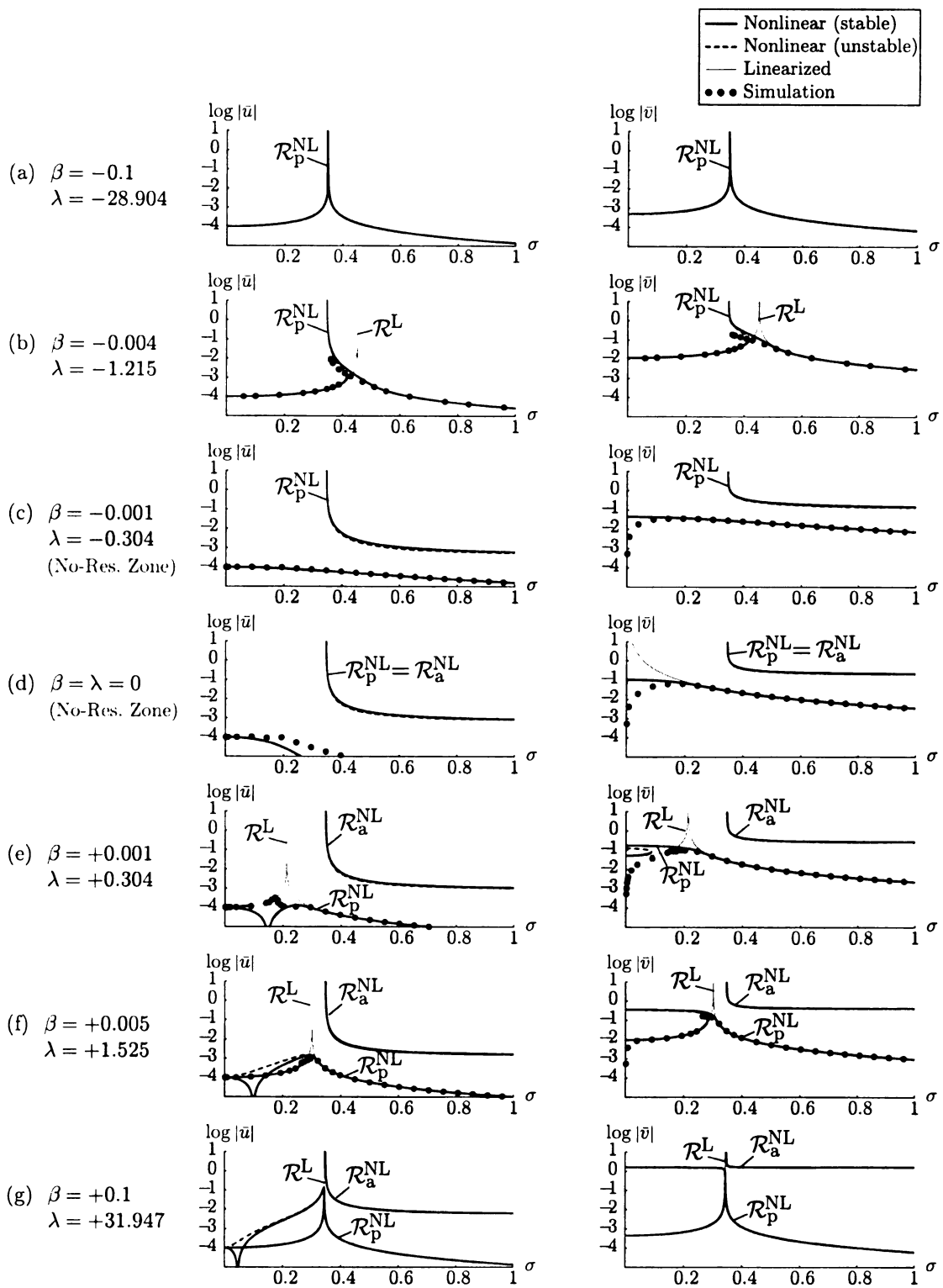

Figure 5.5. Blade/absorber frequency response curves for the essentially undamped isolated nonlinear system with a *softening* absorber path ($\eta = -1$), for various detuning values β, and for $n = 3$, $\alpha = 0.84$, $\delta = 0.67$, $\mu = 0.0035$ ($\varepsilon = 0.0592$), and $F = 0.0001$ ($\hat{f} = 0.117$).

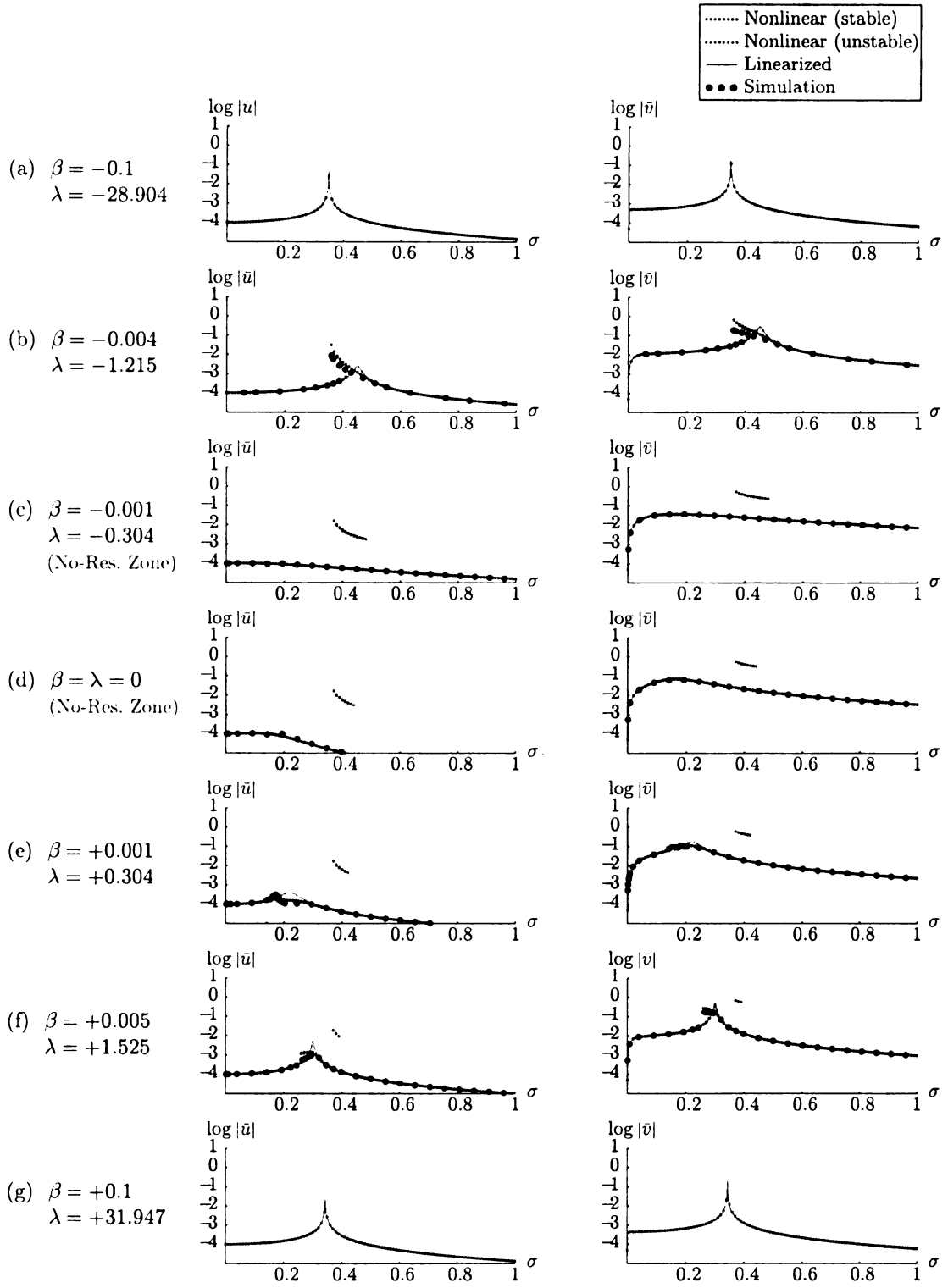

Figure 5.6. Blade and absorber frequency response curves for the same conditions in Figure 5.5 except with nonzero damping: $\hat{\xi}_b = 2 \times 10^{-3}$ and $\xi_{\bar{a}} = 2 \times 10^{-6}$.

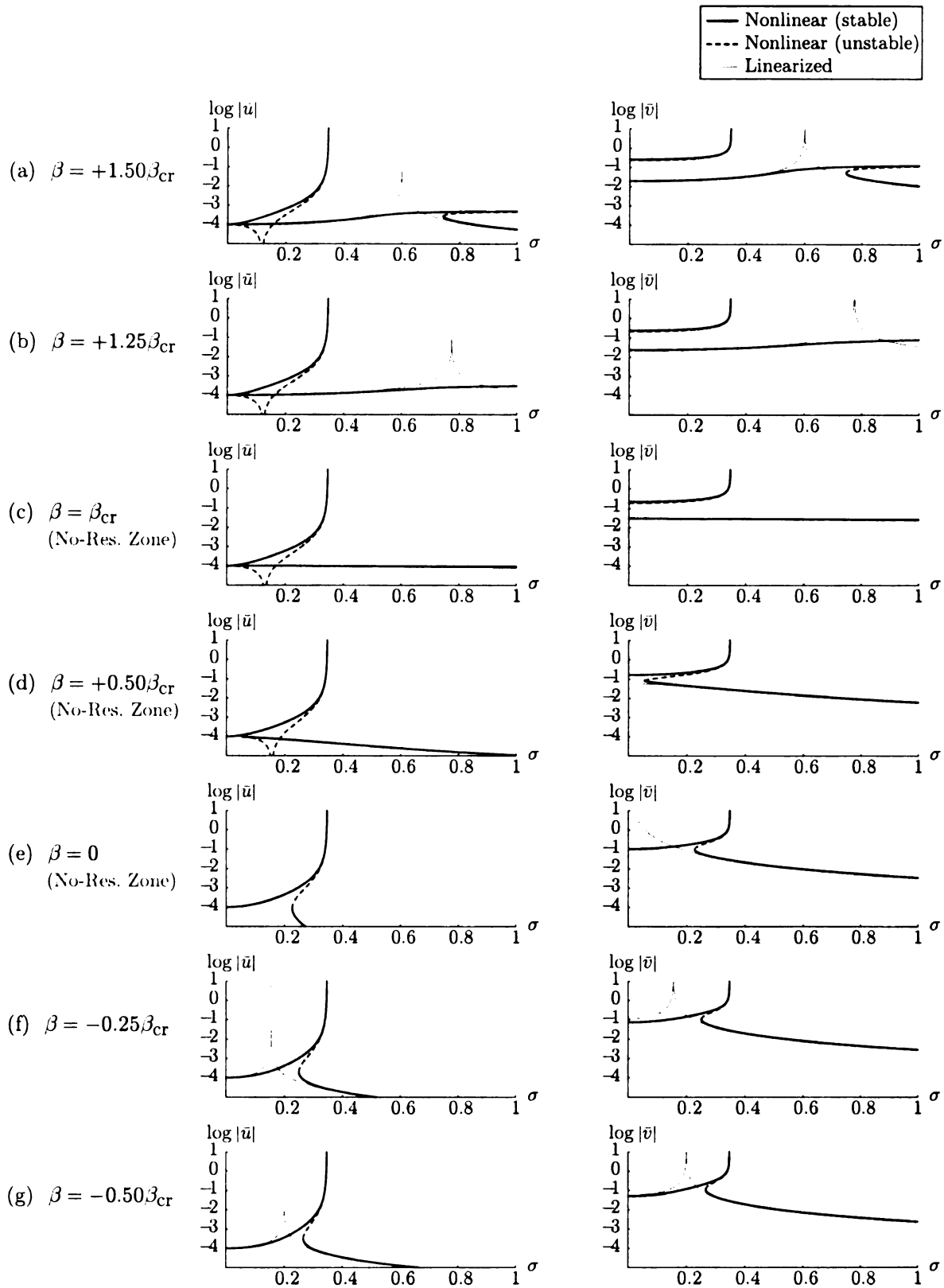

Figure 5.7. Blade and absorber frequency response curves to accompany those shown in Figure 5.4 for a *hardening* absorber path showing various levels of the order detuning β relative to $\beta_{cr} = -0.00164$ inside and near the no-resonance zone.

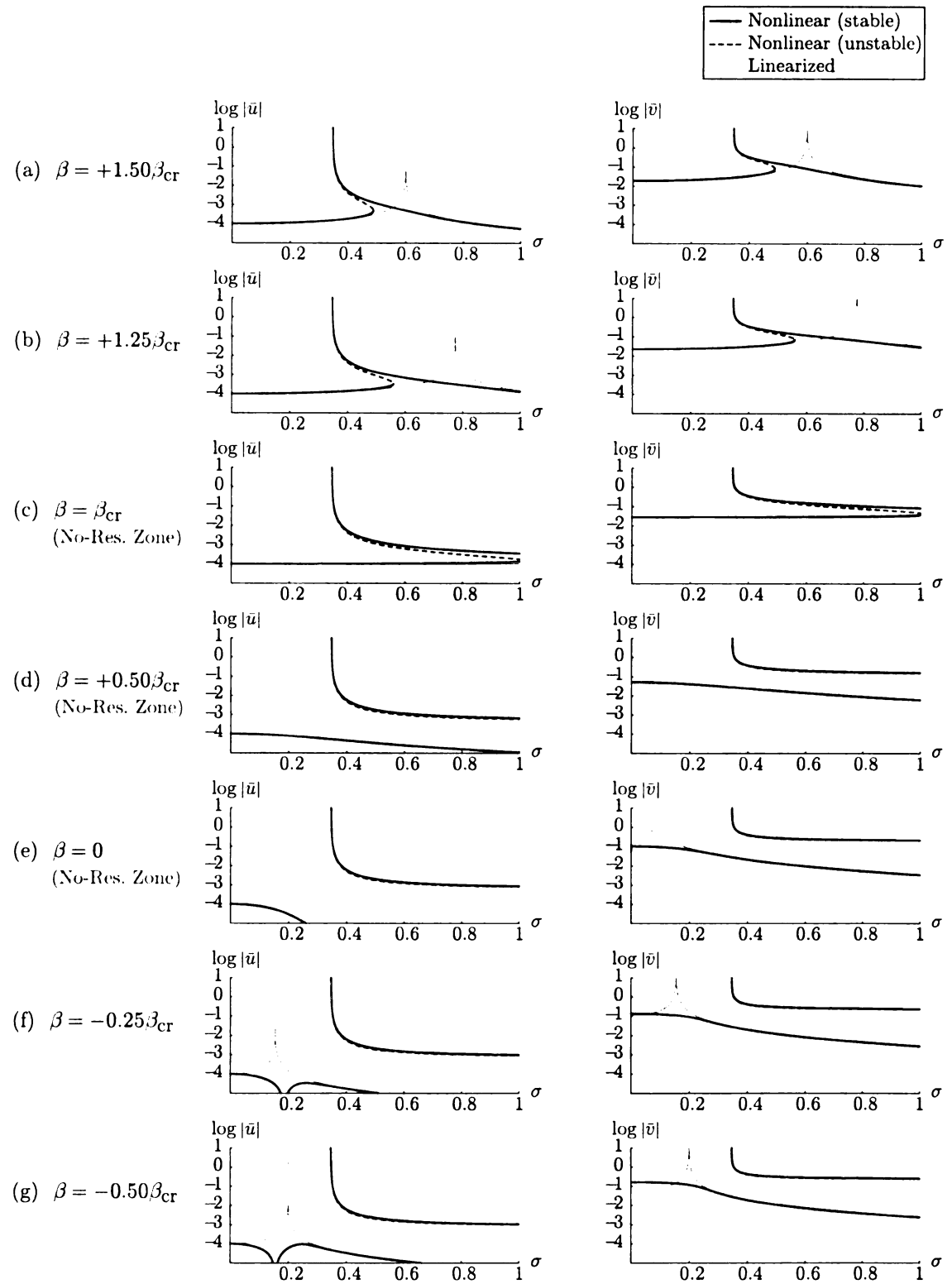

Figure 5.8. Blade and absorber frequency response curves to accompany those shown in Figure 5.5 for a *softening* absorber path showing various levels of the order detuning β relative to $\beta_{cr} = -0.00164$ inside and near the no-resonance zone.

$\beta > 0$) the linear resonance appears from the left at zero rotor speed and $\mathcal{R}_{\mathrm{p}}^{\mathrm{NL}}$ moves with it to the right, which is shown in Figure 5.4e-f. As β becomes large the primary and linear resonances become nearly identical. This is shown in Figure 5.4g.

In summary, the primary nonlinear resonance behaves in the same way as the linearized resonance when the linear detuning is swept from negative to positive, and it observes the no-resonance zone by vanishing when $\beta_{\mathrm{cr}} < \beta < 0$. It also features a hardening bend in the direction of increasing σ that extends out to infinite rotor speed. Finally, the nonlinearity gives rise to an additional auxiliary resonance that exists for all undertuning values, that is, for any $\beta < 0$.

A similar trend can be observed in Figure 5.5 for the case of a softening absorber path, except that the auxiliary resonance exists when the absorber is *overtuned* and, of course, the primary and auxiliary resonances bend in the direction of decreasing rotor speed. The primary nonlinear resonance does exist for detuning values within the no-resonance zone, but its effective location corresponds to large rotor speeds and it approaches infinite σ as the linear order tuning approaches zero (ideal tuning). In this way, the no-resonance zone essentially persists, where the primary nonlinear resonance simply places an upper limit on the effective range of permissible rotor speeds. As $\mathcal{R}_{\mathrm{p}}^{\mathrm{NL}}$ moves with $\mathcal{R}^{\mathrm{L}}$ toward infinite σ for increasing β, it leaves its remnants behind which, when the tuning such that $\beta > 0$, is regarded as the auxiliary resonance $\mathcal{R}_{\mathrm{a}}^{\mathrm{NL}}$. A key difference for the softening case is that the linear branches within the no-resonance zone are (for sufficiently small forcing levels and absorber path nonlinearity) *isolated* from nonlinear response branches for rotor speeds to the left of primary resonance. (Compare Figure 5.5c-d with Figure 5.4c-d.) For a softening absorber path, it is therefore possible to spin the rotor up from zero speed to some (sufficiently small) steady operating point without passing through resonance. This is generally not possible for a hardening path, in which case there are potentially unavoidable auxiliary or primary resonances for *all* order detuning values—including

those within the no-resonance zone. It can thus be said that absorber designs involving hardening paths are generally not acceptable. Softening absorber paths are clearly desired, but they do set an upper limit on the rotor speed, the value of which depends to a large extent on the excitation strength and the strength of the absorber path nonlinearity.

Figure 5.5 also shows simulation data corresponding to the full nonlinear model for blade and absorber damping levels of $\xi_b = 2\times10^{-3}$ and $\xi_{\tilde{a}} = 2\times10^{-6}$, respectively. The predicted frequency response amplitudes (which correspond to *zero* damping) are seen to be in reasonably good agreement with these data. A corresponding set of frequency response loci were numerically generated with the same damping levels used in the simulations. These follow from Equation (5.19) (stationary points) with $\hat{\nu} = 0$ and Equation (5.30a) (stability) and are shown in Figure 5.6. The results are seen to be in very good agreement with the simulation data, thus validating the accuracy of the averaged sector models. If only qualitative features of the forced response are desired, however—response amplitudes in particular—the simple analytical expressions defined by Equation (5.24) and Equation (5.25) are quite sufficient.

In both Figure 5.5 and Figure 5.6, simulation data could not be obtained for the nonlinear auxiliary resonance branches (for the particular parameter values used) due to their small domains of attraction. However, when the excitation strength is increased, these domains widen and the branches of $\mathcal{R}_{\mathrm{a}}^{\mathrm{NL}}$ can be captured. This is shown in Figure 5.9, which depicts the blade and absorber frequency response loci for a softening absorber path, linear tuning within the no-resonance zone, and for various levels of the dimensionless force amplitude F. The figure also indicates an upper limit on the excitation strength, where a bifurcation destroys the no-resonance structure.

The frequency response results described above are in overall good agreement with the actual nonlinear response (based on the full nonlinear equations and indicated

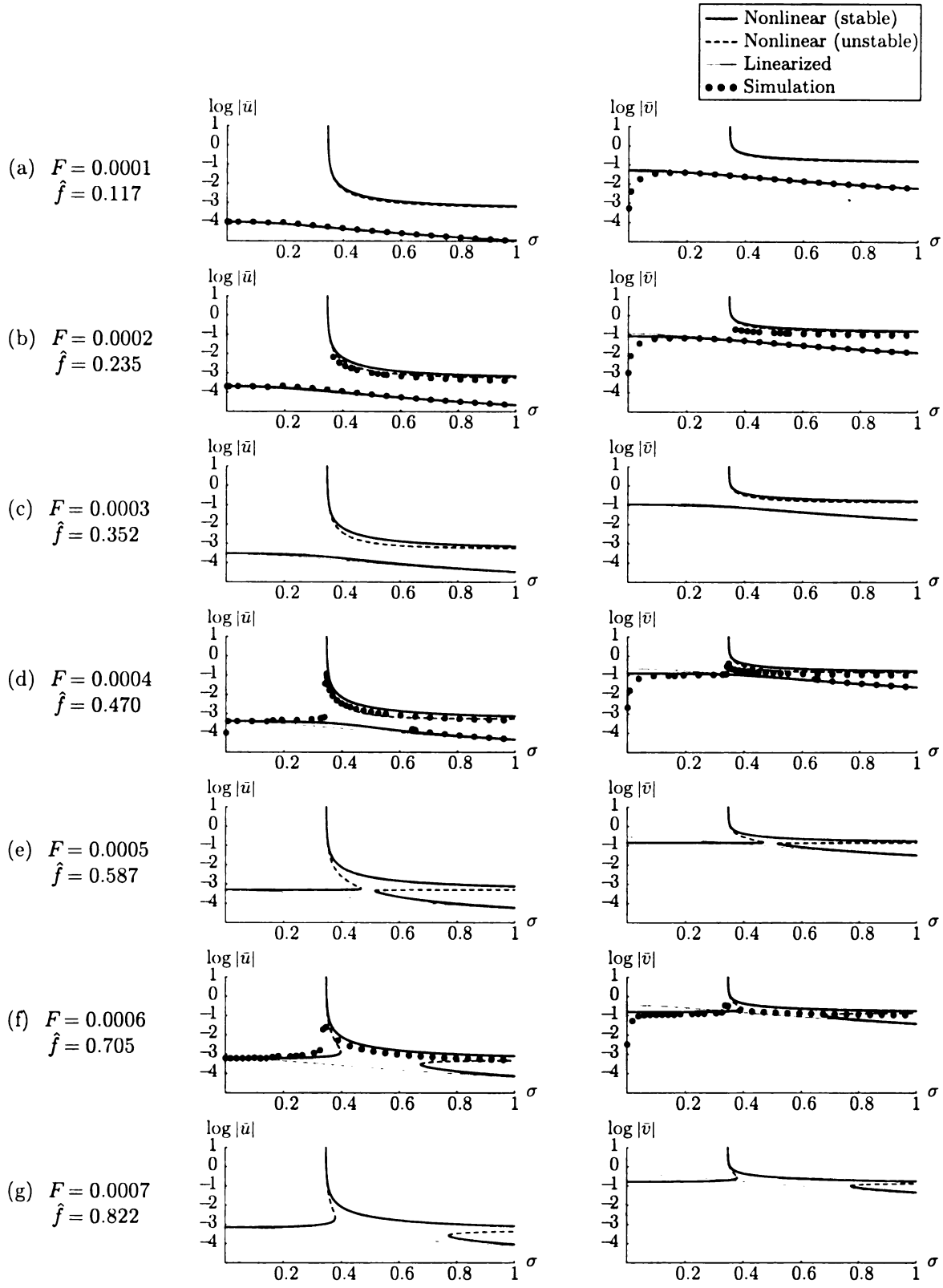

Figure 5.9. Blade and absorber frequency response curves for the essentially undamped isolated nonlinear system with a softening absorber path, for linear tuning within the no-resonance zone ($\beta = \beta_{cr}/2 = -0.822 \times 10^{-3}$), for various levels of the force amplitude F, and for $n = 3$, $\alpha = 0.84$, $\delta = 0.67$, and $\mu = 0.0035$ ($\varepsilon = 0.0592$).

by the simulation data), particularly when damping is included and if the parameter values are reasonable. The representative examples depicted in Figure 5.6 show that the averaged sector models can be very accurate, even for very large positive or negative order detuning β (values of $\tilde{n}$ relative to n) or speed detuning Δ (rotor speed σ relative to σ_r). The same cannot be said, however, had the usual approach to averaging been carried out. Recall from Section 5.2.4 that an alternative approach was adopted in which σ is retained in the averaged equations, essentially keeping key higher-order terms in the model. This is a crucial observation in the methodology since the usual approach to averaging (which amounts to simply replacing σ with the *constant* σ_r) gives at best mediocre results, and it fails completely to capture the no-resonance zone. The reader can verify these claims by comparing the analysis and results presented thus far with those given in Appendix E, where the usual approach to averaging is employed.

A criterion for zero blade motions relative to the rotating hub is derived next, which is the nonlinear counterpart to the ideal, or exact linear tuning described in Section 4.4.1.

5.4.2 Criteria for Zero Blade Amplitudes

The desired system response is one in which the blades remain stationary relative to the spinning rotor and the absorbers move accordingly in a TW configuration. Such a response can be achieved for a linear system (in the absence of damping) by the exact linear tuning described in Section 4.4.1. However, a more realistic linear tuning strategy is one in which the absorbers are detuned within the no-resonance zone, which offers robustness to parameter uncertainties but it comes at the expense of residual blade vibrations. The aim of this section is to possibly exploit the absorber path nonlinearity to address these vibrations and further improve the absorber performance.

The desired response is, in fact, possible (but not necessarily stable) for zero

damping and the corresponding requirements on the system parameters follow from Equation (5.20) by setting $\bar{u} = 0$. Then

$$0 = -\alpha(n^2+1)\sigma^2\bar{v}\sin\big(\bar{\varrho}-\bar{\varsigma}\big) - \hat{f}\sin\bar{\varrho}, \tag{5.32a}$$

$$0 = -\alpha(n^2+1)\sigma^2\bar{v}\cos\big(\bar{\varrho}-\bar{\varsigma}\big) - \hat{f}\cos\bar{\varrho}, \tag{5.32b}$$

$$0 = \lambda\sigma^2\bar{v} + \tfrac{3}{4}\eta\sigma^2\bar{v}^3. \tag{5.32c}$$

However, the phase $\bar{\varrho}$ is *undefined* if $\bar{u} = 0$ and hence Equations (5.32a) and Equation (5.32b) should be *independent* of $\bar{\varrho}$. To see this, the latter is solved for $\bar{v}$ and is introduced to the first. Upon simplification the result is

$$0 = \hat{f}\sin\bar{\varsigma},$$

which is indeed $\bar{\varrho}$-independent and it implies $\bar{\varsigma} = l\pi$ for $l \in \mathbb{Z}$. Then Equation (5.32a) and Equation (5.32b) both reduce to a single expression and, together with Equation (5.32c), the required conditions become

$$0 = \alpha(n^2+1)\sigma^2\bar{v}\cos(l\pi) + \hat{f}, \tag{5.33a}$$

$$0 = \Big(\lambda + \tfrac{3}{4}\eta\bar{v}^2\Big)\sigma^2\bar{v}. \tag{5.33b}$$

Since $\bar{u} = 0$ by assumption, the case of $\bar{v} = 0$ gives rise to the trivial response $(\bar{u}, \bar{v}) = (0, 0)$ and mathematically it corresponds to a nonhyperbolic stationary point. By restricting $\bar{v} > 0$ (meaning that the absorber must assume nonzero motions in order to achieve zero blade vibrations) and eliminating the absorber amplitude in Equation (5.33), one can solve for the critical nonlinear tuning parameter. The result is

$$\eta_{\mathrm{cr}} = -\frac{4\lambda\alpha^2(n^2+1)^2\sigma^4}{3\hat{f}^2}, \tag{5.34}$$

which is seen to depend on the engine order, the placement of the absorber relative to the blade, and the linear tuning order. However, it also depends on both the excitation strength and the rotor speed, which implies that the critical nonlinear

tuning is valid only for a *single* set of operating conditions. While it may be possible to design an *active* absorber, where the nonlinear tuning is adjusted on-the-fly for varying $\hat{f}$ and σ, effective implementation in the harsh operating environments (e.g., rotation, extreme temperatures, and so on) is likely to by impractical, if not entirely impossible. Moreover, since proper linear tuning is negative ($\lambda_{\text{cr}} < \lambda \leq 0$) and all other parameters in the right hand side of Equation (5.34) are positive, the nonlinear tuning requires *hardening* absorber paths ($\eta > 0$). As discussed in Section 5.4.1 this is an undesirable path type, one that gives rise to potentially problematic resonances—even for proper linear tuning.

These findings clearly show that the nonlinear tuning defined by Equation (5.34) is unsatisfactory for the *passive* absorbers under consideration. More generally, they also suggest that nonlinearity cannot be exploited to improve the absorber performance. However, we do offer some general recommendations for the critical nonlinear tuning next with the understanding that they are feasible only for an *active* absorber implementation, which may have applications in other settings.

Example plots of blade and absorber frequency response curves are shown in Figure 5.10 for linear tuning within the no-resonance zone, for perfect nonlinear tuning according to $\eta = \eta_{\text{cr}}$, and also for slight over- and undertuning with respect to η_{cr}. In addition to the host of other issues described above, this figure highlights sensitivity to parameter uncertainties. As shown in Figure 5.10c, *any* level of nonlinear overtuning is accompanied by a jump instability to the nonlinear auxiliary resonance. Slight nonlinear undertuning relative to η_{cr} is therefore desirable. However, it is again stressed that this is feasible *only* for an active absorber implementation, and there still remains a potentially problematic auxiliary resonance.

Finally, while the nonlinear tuning scheme described above is not acceptable for applications involving passive absorbers, all is not lost; some insight can be gleaned and reinforced from the analysis. Equation (5.33a) implies that the absorber ampli-

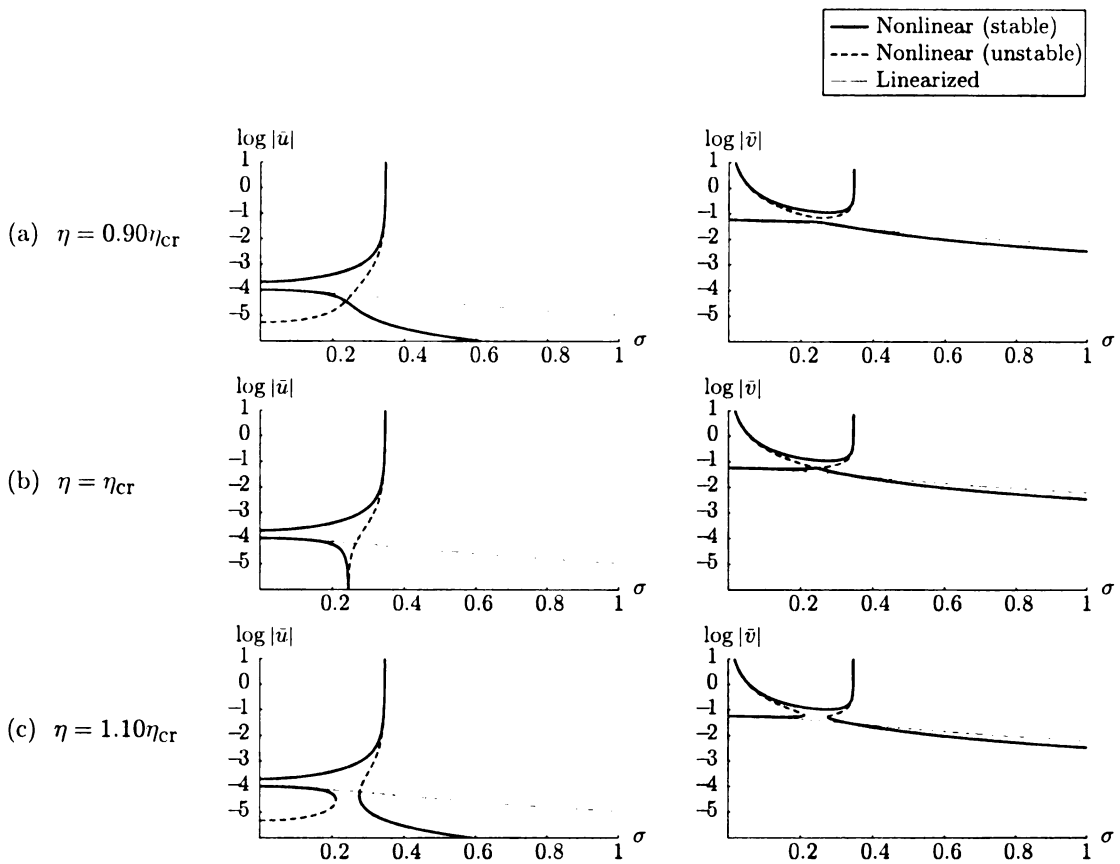

Figure 5.10. Example blade and absorber frequency response curves for linear tuning within the no-resonance zone ($\beta = \beta_{cr}/2$), for several nonlinear tuning values relative to η_{cr}, and for a model with $n = 3$, $\alpha = 0.84$, $\delta = 0.67$, $\mu = 0.0035$ ($\varepsilon = 0.0592$), $f = 0.0001$ ($\hat{f} = 0.117$), and $\hat{\xi}_b = \hat{\xi}_{\bar{a}} = 0$.

tude increases linearly with the strength of the excitation in a way that depends on the engine order and placement of the absorber along the extent of the blade. Consistent with intuition, the absorber should be placed as close to the end of the blade as possible to achieve the smallest absorber motions given a specific excitation strength. Equation (5.33a) also indicates that, for a given forcing level, higher engine order excitations will give rise to lower absorber amplitudes.

The nonlinear results discussed up to this point for the special case of an isolated sector qualitatively embody all of the fundamental features of the fully coupled system, except for the possibility of additional instabilities to response types other than the desired TW variety. The existence of such bifurcations is considered next.

5.5 Forced Response of the Coupled Nonlinear System

The forced response of the isolated nonlinear system, which consists of a single linear blade and nonlinear absorber, were described in detail in Section 5.4. These fundamental results can be used to qualitatively predict many of the corresponding features of the fully coupled nonlinear system, including its TW response amplitudes and jump bifurcations to other traveling wave solutions. The frequency response amplitudes of the coupled system qualitatively match those of the uncoupled case, except for a shift in the primary resonance (when it exists) according to the third term on the right hand side of Equation (5.19b), that is,

$$\Delta - 2\hat{\nu}^2(1 - \cos\varphi_{n+1}) \equiv \bar{\Delta}, \tag{5.35}$$

by an amount that is directly proportional to $\nu^2 = \varepsilon\hat{\nu}^2$. Hence the shift will be small if the inter-sector elastic coupling is weak, in which case amplitude predictions for the fully coupled system based on the isolated sector model are quite accurate. In what follows, it will be shown that stability results associated with the isolated nonlinear system qualitatively apply to the coupled system as well, where any bifurcation iden-

tified in the former simply corresponds to a jump in blade/absorber amplitudes in the latter to *another traveling wave response.* These bifurcations are said to preserve the symmetry of the response. However, the coupled nonlinear system may feature additional symmetry-breaking instabilities that the isolated system cannot predict, which involve bifurcation to response types other than the desired TW. These possible instabilities are addressed in the next section, where the findings strongly suggest that symmetry-breaking bifurcations do not occur.

It should be noted that, while closed form analytical expressions are available for the prediction of response amplitudes, determination of local stability in the presence of coupling is quite a bit more formidable. The set of block decoupled Jacobian matrices from Section 5.3.3 (for the coupled case) do offer a substantial savings in computation (which is quite useful for numerical studies), but even these 4×4 reduced matrices are analytically unaccommodating and hence essentially intractable. (Stability results for the simplified case of zero coupling follow from Equation (5.31), which features complicated coefficients. The addition of coupling gives rise to N polynomials of the same form with coefficients that are many times more complicated.) At least some insight can be gleaned from the reduced Jacobians, however, and this is done in Section 5.5.1, but they are otherwise handled numerically. In what follows we offer a sampling of results based on extensive case studies and numerical investigations. These are briefly summarized in Section 5.5.2 using examples of models with $N = 5$ (odd) and $N = 6$ (even) sectors.

5.5.1 Local Stability of the Traveling Wave Response

For the special case of zero coupling ($\hat{\nu} = 0$), local stability of a stationary point $\mathbf{v}$ follows from the 4×4 Jacobian matrix $\mathbf{J}_{\text{IS}}^{(\text{C})}$, which is defined by Equation (5.30b).[7] For a particular equilibrium point, and if this matrix is Hurwitz (meaning that all

[7] In what follows, we restrict the discussion to Cartesian forms for convenience, where it is understood that the same arguments hold for the corresponding polar forms as well.

four of its eigenvalues lie in the open left-half complex plane), there corresponds a stable periodic orbit in the isolated nonlinear system [96, 97, 109]. If any eigenvalue of $\mathbf{J}_{\mathrm{IS}}^{(\mathrm{C})}$ crosses the imaginary axis into the right-half complex plane as the rotor speed (or any other parameter) is varied, a jump bifurcation occurs in which *all* of the blade and absorber amplitudes spontaneously assume different values, and the TW symmetry is preserved.

A similar type of (symmetry-preserving) instability can be observed in the fully coupled nonlinear system in which there is a jump in blade and absorber amplitudes *and the response maintains its TW configuration.* This is found to occur when an eigenvalue of *one* particular reduced Jacobian crosses the imaginary axis. Thus any crossings by an eigenvalue of any *other* reduced Jacobian matrix generically corresponds to a symmetry-breaking bifurcation in the coupled nonlinear system to a response type other than the desired TW. However, based on extensive numerical investigations, no such instabilities could be identified.

To see these features more clearly, we consider in more detail the reduced Jacobian matrices that were derived in Section 5.3.3, which are stated again here (in Cartesian form) for convenience. They are

$$2n\sigma\mathbf{J}_{k}^{(\mathrm{C})} = \mathbf{P} + 2\mathbf{Q}\cos\varphi_k + 2j\mathbf{R}\sin\varphi_k, \qquad k \in \mathcal{N} \tag{5.36}$$

where the factor $2n\sigma$ has been moved to the left of the equality for convenience. The matrices $\mathbf{Q}$ and $\mathbf{R}$ vanish when $\hat{\nu} = 0$ and the matrix $\mathbf{P}$ is the same as $\mathbf{J}_{\mathrm{IS}}^{(\mathrm{C})}$ (isolated sector), except for the addition of $2\hat{\nu}^2$ (resp. $-2\hat{\nu}^2$) in the $(1,2)$ (resp. $(2,1)$) element. Since Equation (5.36) was obtained by way of a *unitary* transformation of the full Jacobian matrix $\mathbf{J}_{\mathrm{CS}}^{(\mathrm{C})} \in \mathscr{BCBS}_{4,N}$ (coupled sector), the eigenvalues persist in these N, 4×4 reduced matrices. Note that they feature a cyclic structure with respect to the index $k \in \mathcal{N}$, which arises from the sine and cosine terms involving φ_k. Since $\cos\varphi_{N+2-k} = \cos\varphi_k$ and $\sin\varphi_{N+2-k} = -\sin\varphi_k$ the reduced Jacobians generally

appear as complex conjugates of the form

$$\mathbf{P} + 2\mathbf{Q}\cos\varphi_k \pm 2j\mathbf{R}\sin\varphi_k, \tag{5.37}$$

except for $k = 1$ when the form is $\mathbf{P} + 2\mathbf{Q}$ or if N is odd, in which the $k = (N+2)/2$ case gives rise to $\mathbf{P} - 2\mathbf{Q}$ in addition.[8]

Based on extensive numerical evidence it is found that the real matrix

$$\mathbf{J}_{\text{EFF}}^{(\text{C})} \equiv \mathbf{J}_1^{(\text{C})} = \frac{1}{2n\sigma}(\mathbf{P} + 2\mathbf{Q}) \tag{5.38}$$

is the *only* one of the N reduced Jacobians that gives rise to instabilities. It corresponds to Equation (5.36) with $k = 1$ and is such that

$$\mathbf{P} + 2\mathbf{Q} = \begin{bmatrix} -n\sigma\hat{\xi}_b & -\bar{\Delta} & 0 & -\bar{\alpha}\sigma^2 \\ \bar{\Delta} & -n\sigma\hat{\xi}_b & \bar{\alpha}\sigma^2 & 0 \\ 0 & -\bar{\alpha}\sigma^2 & \frac{3}{2}\eta\sigma^2 CD - n\sigma\hat{\xi}_{\bar{a}} & \frac{3}{4}\eta\sigma^2(C^2+3D^2) + \lambda\sigma^2 \\ \bar{\alpha}\sigma^2 & 0 & -\frac{3}{4}\eta\sigma^2(3C^2+D^2) - \lambda\sigma^2 & -\frac{3}{2}\eta\sigma^2 CD - n\sigma\hat{\xi}_{\bar{a}} \end{bmatrix},$$

where $\bar{\Delta}$ is the effective resonance shift defined by Equation (5.35) and, recall, $\bar{\alpha} = \alpha(n^2+1)\sigma^2$. Equation (5.38) is the same as the Jacobian matrix $\mathbf{J}_{\text{IS}}^{(\text{C})}$ of the isolated nonlinear system, but it additionally incorporates the resonance shift associated with coupling, which is reflected in $\bar{\Delta}$. In fact, it is the Jacobian matrix of an *effective* isolated nonlinear system consisting of a single blade, a nonlinear absorber, plus a single elastic coupling element, which follows from the averaged sector model corresponding to $i = 1$ rather than the model obtained by setting $\hat{\nu} = 0$. In this way, instabilities observed in $\mathbf{J}_{\text{EFF}}^{(\text{C})}$ directly correspond to those predicted by $\mathbf{J}_{\text{IS}}^{(\text{C})}$. Moreover, since instabilities were detected *only* by the effective Jacobian matrix $\mathbf{J}_{\text{EFF}}^{(\text{C})} = \mathbf{J}_1^{(\text{C})}$ and none of the other reduced Jacobians, it thus follows (based on numerical evidence) that there are no symmetry-breaking bifurcations to response types other than the desired TW. Again, this observation is based on extensive numerical

[8]Analogous features that arise due to cyclicity can be observed in the multiplicity of eigenfrequencies and normal modes of a generic cyclic system (Figure 2.5) and also in the BTW, FTW, and SW characteristics of engine order excitation (Figure 2.3).

evidence and case studies. Therefore, while it cannot be said with certainty that such bifurcations absolutely *cannot* occur, these findings *strongly suggest* that they do not.

A sampling of results is given next for specific values of N and with an emphasis on blade/absorber frequency response and traveling wave characteristics of the coupled system.

5.5.2 Case Studies

In this section we briefly highlight some case studies for models with a specific number of sectors. It is clear that $N = 1$ is a trivial case since it features only one sector. The next simplest systems with $N = 2$ and $N = 3$ sectors are special cases where, in addition to *nearest-neighbor* coupling, they also feature *all-to-all* coupling in which each sector is coupled to *all* other sectors. Moreover, it is well-known that the case of $N = 4$ sectors gives rise to additional rich dynamics that are not generically observed for general N [106–108]. Finally, it is recalled from Section 2.4 that the traveling wave nature (BTW, FTW, or SW) of the system can be different for an odd or even number of sectors. The case studies are thus summarized for models with $N = 5$ (odd) and $N = 6$ (even) sectors. We begin with the case of $N = 5$.

A representative set of blade and absorber frequency response curves are is shown in Figure 5.11 for softening absorber paths, undertuned absorbers, and for a number of coupling levels that increase from zero. In fact, Figure 5.11a corresponds to the blade and absorber amplitude responses shown in in Figure 5.5b and Figure 5.6b for the isolated (zero coupling) nonlinear system, and Figures 5.11b-g simiply show how this picture changes as the coupling in increased from zero. For small coupling the frequency response loci are nearly the same as the isolated sector case, where the resonance shift associated with coupling is essentially imperceptible. As the coupling is increased the primary nonlinear resonance (linear resonance) moves to the right. This resonance shift is expected, and is manifested by the term defined by Equa-

tion (5.35). Finally, simulation data is included near primary resonance in several of the plots, which indicates that the results are valid even for large coupling strengths. The sparsity of data points can be attributed to very long simulation run times; even with today's computers it can take many hours for a numerical solver to settle into a steady-state.

Figure 5.12 shows the blade and absorber time responses for the same parameters used in Figure 5.11e and for a rotor speed of $\sigma = 0.55$. Since the absorbers are *undertuned* outside of the no-resonance zone, the mode shape associated with an individual sector is $(1, -1)$ and hence the blade and its attendant absorber feature out-of-phase motions with respect to one another. This can be confirmed, for example, by comparing the dashed line in Figure 5.12a to that in Figure 5.12b. Finally, the engine order $n = 3$ excites mode $p = n + 1 = 4$ which, according to Table 2.2 on page 32, is of the FTW variety. This can also be identified in the figure, where the periodic motions of, for example, blade 1 are followed by the same motions in blade 2, 3, and so on until the pattern repeats itself.

A corresponding set of blade and absorber frequency response curves are shown in Figure 5.13 for the same parameters use in Figure 5.11, except with $N = 6$ sectors. Nothing qualitatively different is expected nor observed in these figures. However, in this case the engine order $n = 3$ excites a SW mode corresponding to $p = n + 1 = 4$, which can be verified by Table 2.2 and clearly observed in the blade and absorber time responses depicted in Figure 5.14, which corresponds to Figure 5.13e with $\sigma = 0.55$.

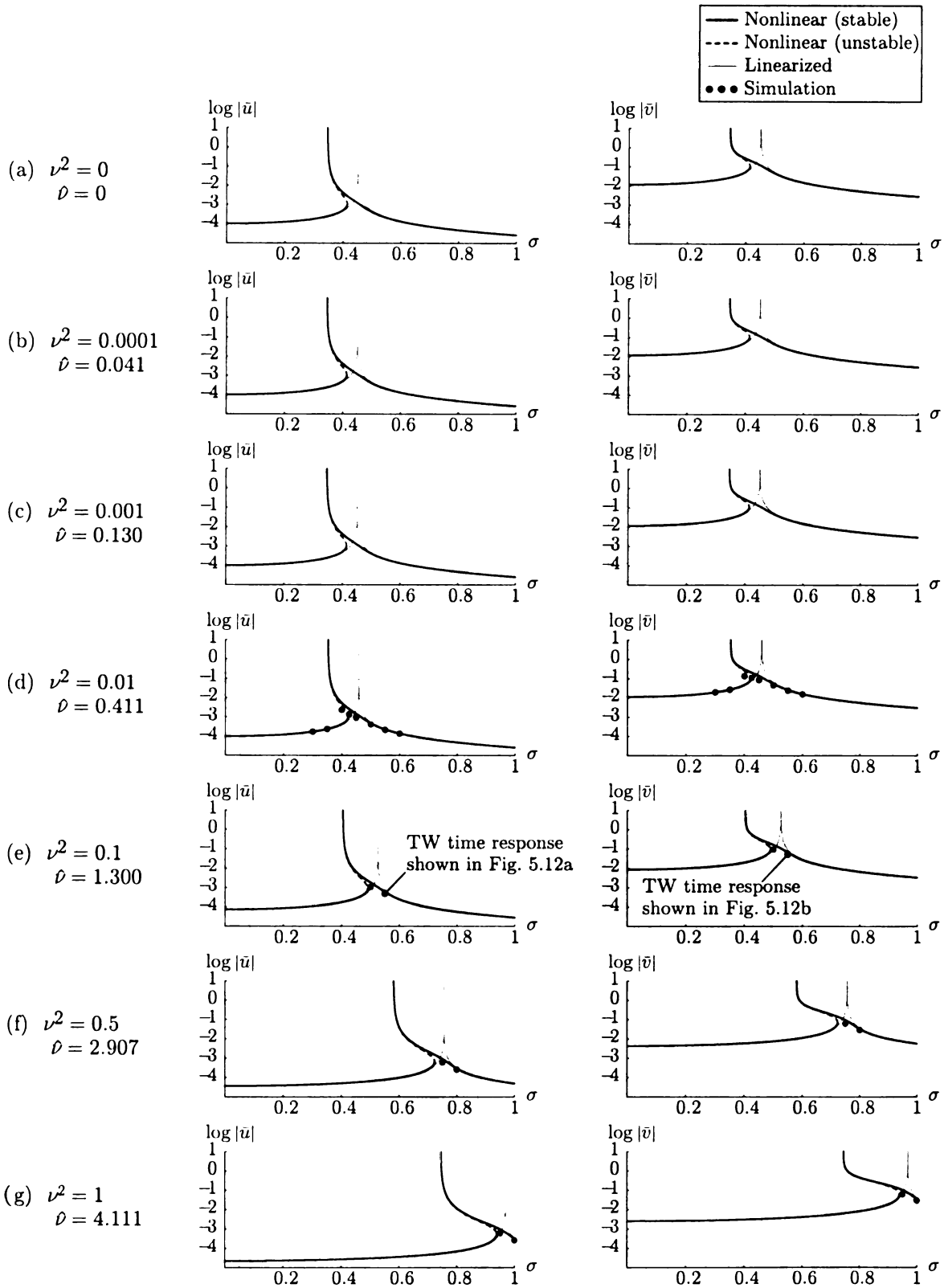

Figure 5.11. Blade/absorber frequency response curves for the essentially undamped coupled nonlinear system with $N = 5$ (odd) sectors, softening absorber paths ($\eta = -1$), linear undertuning $\beta = -0.004$, various coupling levels ν, and for $n = 3$, $\alpha = 0.84$, $\delta = 0.67$, $\mu = 0.0035$ ($\varepsilon = 0.0592$), and $F = 0.0001$ ($\hat{f} = 0.117$).

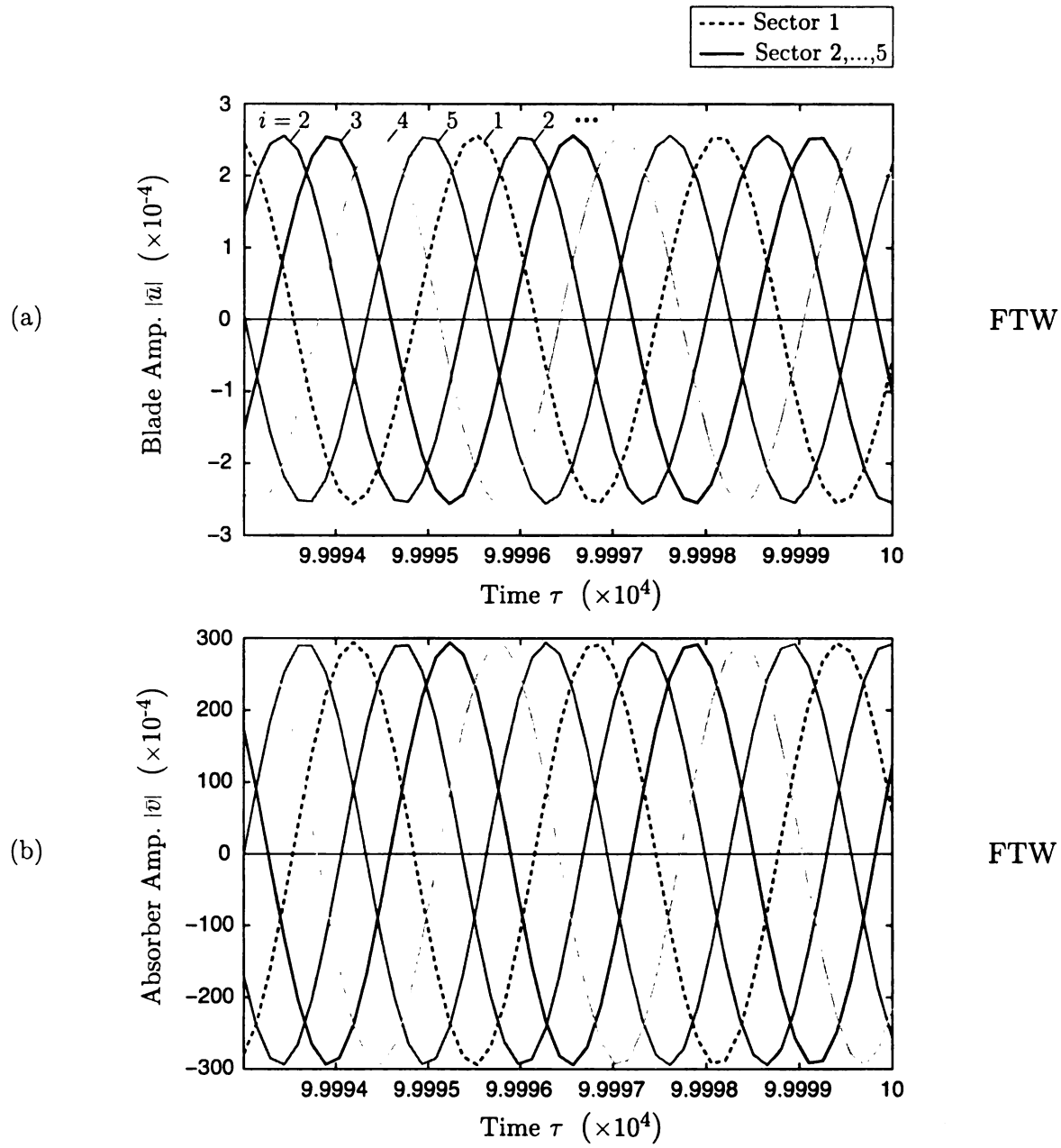

Figure 5.12. (a) Blade and (b) absorber backward traveling wave (BTW) time responses for the essentially undamped coupled nonlinear system with $N = 5$ (odd) sectors, softening absorber paths ($\eta = -1$), linear undertuning $\beta = -0.004$, coupling strength $\nu = 0.1$, and for $n = 3$, $\alpha = 0.84$, $\delta = 0.67$, $\mu = 0.0035$ ($\varepsilon = 0.0592$), $F = 0.0001$ ($\hat{f} = 0.117$), and $\sigma = 0.55$.

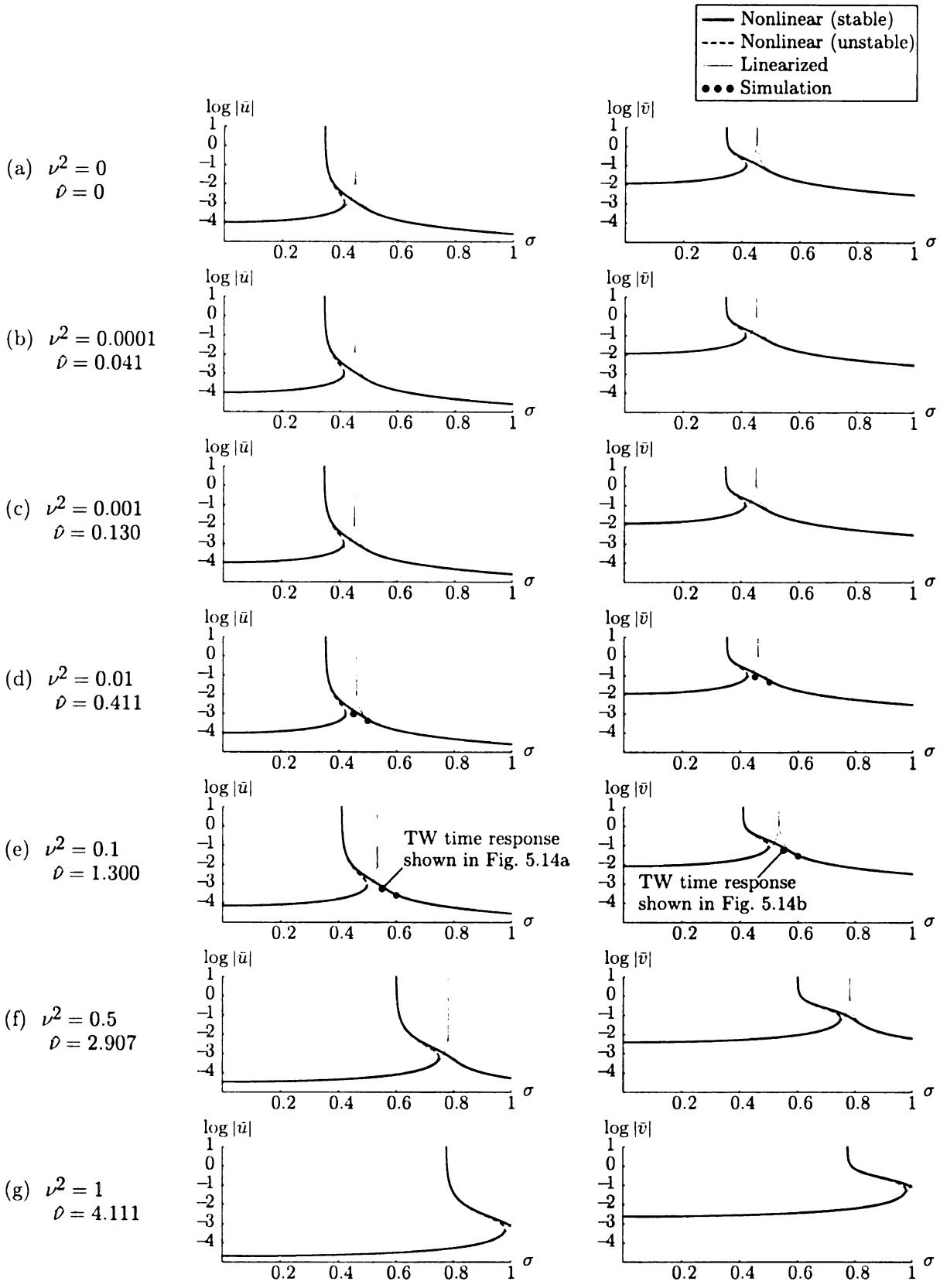

Figure 5.13. Blade/absorber frequency response curves for the essentially undamped coupled nonlinear system with $N = 6$ (even) sectors, softening absorber paths ($\eta = -1$), linear undertuning $\beta = -0.004$, various coupling levels ν, and for $n = 3$, $\alpha = 0.84$, $\delta = 0.67$, $\mu = 0.0035$ ($\varepsilon = 0.0592$), and $F = 0.0001$ ($\hat{f} = 0.117$).

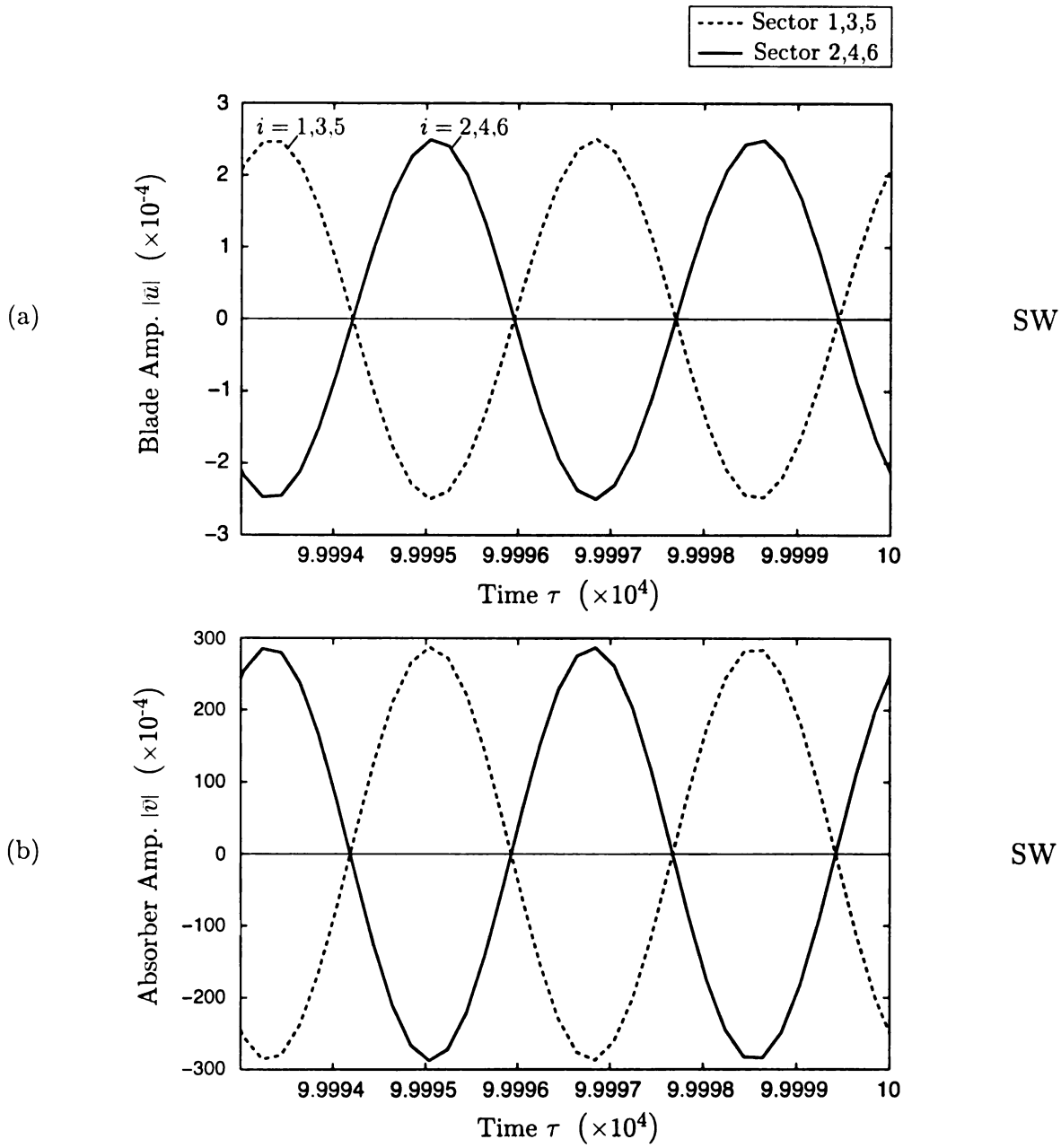

Figure 5.14. (a) Blade and (b) absorber standing wave (SW) time responses for the essentially undamped coupled nonlinear system with $N = 6$ (odd) sectors, softening absorber paths ($\eta = -1$), linear undertuning $\beta = -0.004$, coupling strength $\nu = 0.1$, and for $n = 3$, $\alpha = 0.84$, $\delta = 0.67$, $\mu = 0.0035$ ($\varepsilon = 0.0592$), $F = 0.0001$ ($\hat{f} = 0.117$), and $\sigma = 0.55$.

5.6 Concluding Remarks

This chapter has extended the linear design, theory, and methodology of Chapter 4 to include the basic, first-order effects of nonlinearity, which was introduced via the absorber path geometry. A key finding is that, for the passive order-tuned absorbers of interest, one cannot exploit nonlinearity via the path design to improve absorber performance. However, general conclusions on the effects of system nonlinearity can be gleaned from the analysis. The results show that hardening characteristics are undesirable since they give rise to a primary resonance, a potentially troublesome auxiliary resonances at low rotor speeds, or both. If system nonlinearity is unavoidable, it was shown that softening characteristics are acceptable and that they essentially set an upper limit on permissible rotor speeds. Finally, for the weakly coupled and lightly damped system under consideration, no symmetry-breaking instabilities of the desired TW type solution could be identified. These results, together with the linear absorber tuning strategy given in Chapter 4, give rise to a final recommendations for absorber design, which are summarized in the next chapter.

CHAPTER 6

Conclusions

This thesis has investigated the use of centrifugally-driven, order-tuned vibration absorbers to suppress the steady-state motions of a rotating bladed disk assembly under engine order excitation. For this purpose a simplified, lumped parameter model was employed. Each sector was assumed to be identical and identically coupled, consisting of a single-DOF pendulum-like blade model together with a general path, lumped-mass absorber. At the time of writing, this work reports the first systematic analytical treatment of systems of order-tuned absorbers applied to cyclic rotating flexible structures under engine order excitation, and thus such a simplified model is justified. Just as the generic single-DOF harmonic oscillator can be employed in the theory of elementary vibrations to capture and understand fundamental properties such as natural frequency and resonance, so can the model employed in this work to quantify the rich linear resonance structure, the basic effects of system nonlinearity, and to clearly motivate both a linear and nonlinear absorber design strategy in terms of the system and absorber path parameters. The results of this work are fundamental to future studies of its kind, both analytical and experimental.

The major contributions of this investigation are briefly reviewed in Section 6.1. These have given rise to a number of detailed recommendations for absorber design, which are summarized in Section 6.2. Finally, directions for future work are highlighted in Section 6.3.

6.1 Summary of Contributions

The main results of this study follow from Chapter 4, where the linearized dynamics of the cyclically-coupled system fitted with order-tuned absorbers were investigated, and in Chapter 5, where these basic results were generalized to include the first-order effects of nonlinearity.

According to the linear theory of Chapter 4 there exists an ideal (exact) absorber design such that, in the absence of damping, a complete elimination of blade vibrations (relative to the rotating hub) is possible. The design is accomplished by setting the (isolated) absorber natural frequency equal to the excitation frequency, just as it is done with the classical frequency-tuned dynamic vibration absorber due to Den Hartog [99]. However, since both frequencies scale directly with the rotor speed, this amounts to an *order tuning* in which the absorber tuning order identically matches the order of the excitation. In this way, the linear order tuning is valid *independent of the rotor speed.* While exact tuning offers the best possible (linear) absorber performance, it is susceptible to the effects of parameter uncertainties. Any level of unintentional absorber overtuning or sufficiently large undertuning gives rise to a linear system resonance. The most significant finding of Chapter 4, and arguably of this entire study, is the existence of a *no-resonance zone.* It consists of a finite range of absorber undertuning values for which there are no system resonances over the full range of possible rotor speeds. The upper bound of this spectrum of feasible designs consists of exact tuning and it is bounded from the bottom by a critical linear detuning. Proper absorber design involves intentional *under*tuning within this generally small, but finite gap. The absorbers profit from such a design in terms of robustness to parameter uncertainties, but this is accompanied by slightly reduced performance in the form of residual blade vibrations.

The fundamental linear results described above were generalized in Chapter 5 to include the basic first-order effects of nonlinearity, which was introduced via the ab-

sorber path geometry, and the possibility of exploiting this nonlinearity to improve the absorber performance was investigated. It was shown that the underlying linear resonance structure (and hence the no-resonance zone) qualitatively persists, provided that both the path nonlinearity and excitation levels are sufficiently small. In this way, the linear tuning from Chapter 4 remains effective. There does exist a critical nonlinear tuning that guarantees a branch of solutions corresponding to zero blade motions (which is, in fact, valid for *any* linear tuning). However, it was shown to depend on the rotor speed and excitation strength, and is thus effective for only a *single* operating condition—much like the classical frequency-tuned dynamic vibration absorber. It is therefore impossible to exploit nonlinearity to further improve the performance of the passive order-tuned absorbers of interest. However, the analysis does highlight some general conclusions on the effects of nonlinearity (in the absorbers or otherwise) that can aid in the absorber design process. First, it was shown that softening characteristics are acceptable, and that they essentially place an upper limit on permissible rotor speeds. In contrast, hardening characteristics should be avoided altogether, since they give rise to problematic auxiliary and/or primary resonances. Finally, for the weakly coupled and lightly damped system under consideration, no symmetry-breaking instabilities of the desired TW response could be identified.

6.2 Recommendations for Absorber Design

In what follows the major results of this thesis pertaining to absorber design are consolidated for quick reference. In Section 6.2.1 the linear tuning strategy described above, together with conclusions based on the nonlinear analysis, are summarized in a parameter space that involves the linear order detuning and nonlinear tuning parameters. Section 6.2.2 comments on system damping, and suggestions for the absorber sizing and placement are give in Section 6.2.3. Finally, a particular class of absorber path types is recommended in Section 6.2.4.

6.2.1 Linear and Nonlinear Tuning

Proper absorber design can be summarized in the parameter space depicted in Figure 6.1. This design chart indicates ideal (exact) absorber tuning and also qualitative regions of desired, acceptable, possibly poor, and poor absorber performance due to primary resonance (prim. res.) and/or auxiliary resonance (aux. res.) in terms of the linear and nonlinear tuning parameters β and η, the values of which span the range from (linear) under- to overtuning and (nonlinear) softening to hardening, respectively. A nonlinear absorber tuning scheme with $\eta > 0$, that is, if the absorber paths are hardening, involves a potentially problematic auxiliary resonance at low rotor speeds, an unavoidable primary resonance, or both. Thus any design in quadrants I and region II of the (β, η) parameter space gives rise to poor absorber performance. Designs in region II_u are generally undesirable, especially for light damping, in which case the auxiliary resonance is more problematic. Similar statements can be made for any linear overtuning ($\beta > 0$) or for sufficiently large linear undertuning ($\beta < \beta_{\text{cr}}$), in which case a linear (primary nonlinear) resonance is guaranteed. Hence any design in quadrant IV of Figure 6.1 yields poor absorber performance, as do all designs in quadrant III to the left of β_{cr}. This leaves only the shaded region in quadrant three (denoted by III_d) where absorber designs are feasible, though the performance degrades as the paths are made more softening. (This has the effect of moving the primary resonance in the direction of lower rotor speeds, thus limiting the effective operating range of the bladed assembly.) Ideal absorber tuning corresponds to $(\beta, \eta) = (0, 0)$, but in order to incorporate robustness to parameter uncertainty, a tuning scheme in which the absorbers are slightly softening and tuned within the no-resonance zone is recommended, that is, in the region indicated by "Acceptable" in Figure 6.1.

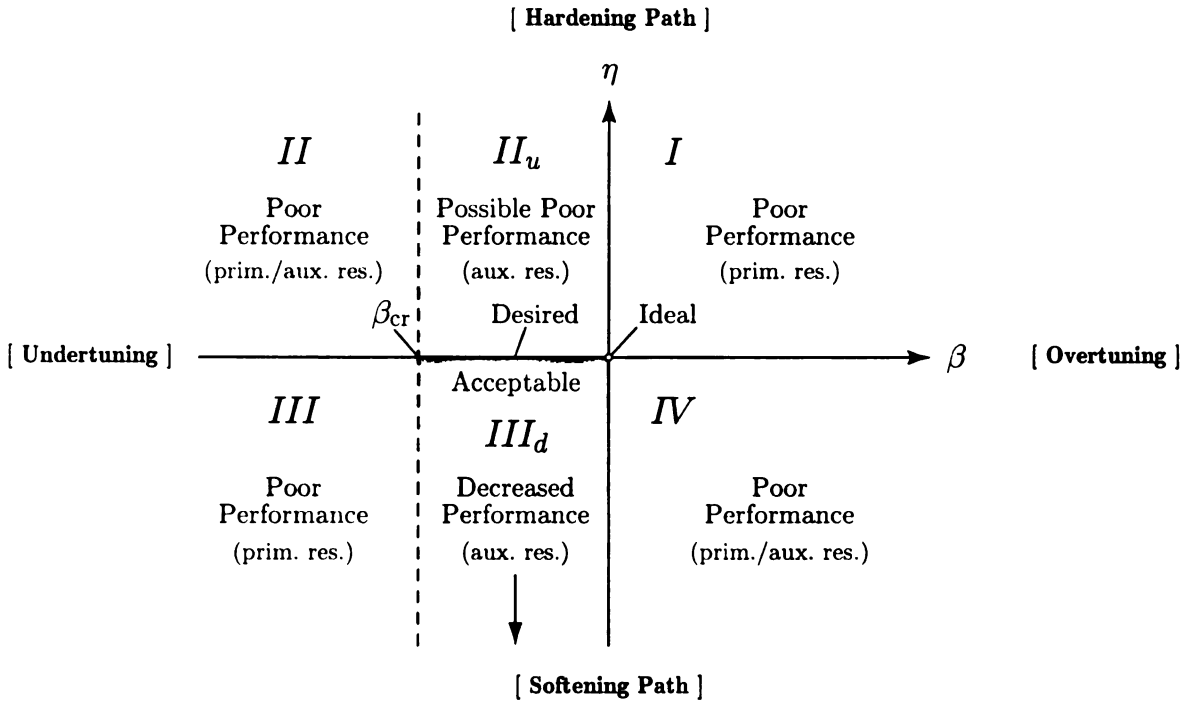

Figure 6.1. Absorber design chart showing ideal tuning and qualitative regions of desired, acceptable, possibly poor, and poor absorber performance due to primary resonance (prim. res.) and/or auxiliary resonance (aux. res.) in terms of the linear and nonlinear tuning parameters β and η, the values of which span the range from under- to overtuning and softening to hardening paths, respectively.

6.2.2 Damping

The basic effects of absorber, blade, and inter-blade, damping were discussed in Section 4.5, where it was indicated that the latter two forms of damping actually *help* the absorbers address blade vibrations. However, the presence of absorber damping essentially weakens their action on the blades and hence lessens their ability to operate properly. For sufficiently large absorber damping, this can lead to a system resonance—even for proper linear undertuning—thereby destroying the no-resonance zone. Thus in addition to the linear and nonlinear design recommendations given in Section 6.2.1, the absorber damping should be kept sufficiently small so that the no-resonance zone persists. The response plots shown in Figure 4.12 on page 112 can be used to estimate maximum permissible absorber damping levels.

6.2.3 Absorber Sizing and Placement

Throughout this work the results have shown that large absorber inertia (relative to the blades) is highly desirable. This is quite clear in physical terms since a larger absorber mass is able to exert increased dynamic loads on its attendant blade and is hence more effective (if properly tuned) in addressing blade vibrations. It was also shown in Section 4.4.2 that the extent of the no-resonance gap depends (nearly linearly) on the absorber-to-blade mass ratio and (nearly quadratically) on the absorber placement along the blade length. By increasing either, the gap can be widened. Thus the absorber mass should be made as large as possible, where it is understood that this is limited fundamentally by the blade geometry, and it should be placed close to the end of the blade.

6.2.4 Path Type

A key result from Chapter 5 is that nonlinearity cannot be exploited to improve the absorber performance, and it is therefore desirable for the absorber motions to be lin-

ear. This can be achieved by selecting a *tautochronic* path, the geometry of which has been systematically described by Denman [17] for a bifilar pendulum absorber configuration. Such a path could be implemented by restricting $\eta = 0$ in Equation (3.20) on page 66 and then backing out the appropriate expansion coefficients b_0, b_2 and b_4 in Equation (3.19).

6.3 Directions for Future Work

This investigation has laid the fundamental groundwork for future analytical and experimental studies involving order-tuned vibration absorbers applied to nominally cyclic rotating flexible structures under engine order excitation. This is essentially a new line of study, one that unites the individually mature bodies of research on *absorber systems* and *cyclic systems*, and hence there is considerable work left to be done. Some major topics that remain to be addressed are briefly considered below. Many of the individual subtopics could form the basis of an M.S. or Ph.D. level thesis.

Mistuning Studies

The models considered for this study were perfectly cyclic, consisting of identical, identically-coupled sectors. However, there will always exist *mistuning* among the sectors, that is, small random uncertainties in system parameters (due to in-service wear, machine tolerances, and so on) that break the cyclic symmetry [37–40]. This can lead to *localization* of vibration energy to a subgroup of sectors, giving rise to higher vibration amplitudes than what is predicted by the perfectly cyclic system [41–45]. With our current knowledge of localization in nominally cyclical systems, it is expected that their responses will also exhibit localized behavior when absorbers are attached to the substructures. There are many questions pertaining to absorber design that must be addressed in this context, which include the following.

- Will the response be localized in the blades, in the absorbers, or both? If so, to what degree?
- How is the response affected by system parameters, in particular by key parameters that govern localization?
- In the presence of mistuning, how does one account for nonlinearity (including impacts) that become unavoidable for the small absorber masses required by the blade geometry?
- How does localization affect the linear and nonlinear absorber design? Does the no-resonance zone persist? Is it possible to exploit nonlinearity when mistuning is present?
- Can intentional patters of mistuning of the blades and/or absorbers be employed to enhance the operation of the overall system?

The answers to these questions are crucial if absorbers are to be implemented in practical systems.

Higher-Fidelity Models

Future analytical studies should consider higher-fidelity blade models, including those with lumped parameters and many degrees of freedom [36], continuous beam and shell-type elements [9], and full finite element representations [3]. It may also be possible to employ *systems* of vibration absorbers, including multiple absorbers applied to a single structural element or multiple absorber implementations in a single system, each tuned to address a specific problematic resonance.

Methodology

The desired traveling wave response exhibits the highest possible degree of symmetry and it is said to belong to the *cyclic group* $\mathbf{Z}_N$ [110–112]. In addition to the usual jump bifurcations that preserve this symmetry (these are predicted by the isolated sector model), there could be a host of other instabilities when coupling is present, including those with reduced symmetry (the so-called *isotropy subgroups* of $\mathbf{Z}_N$) or

no symmetry at all [106–108]. In this work, however, numerical evidence has strongly suggested that no such symmetry-breaking bifurcations occur. The mathematical machinery of group theory, which offers a tremendously powerful and systematic way to catalogue these bifurcations, could possibly be used to *prove* this claim [113, 114]. The theory of groups has also been employed in mistuning studies [57, 115, 116], and is likely to be very useful to investigate the effects of mistuning on absorber performance.

Experiments

Lastly, experimental validation of the results of this thesis (and of future analytical studies) is critical. In the context of this work, it must be verified that the small, but finite no-resonance zone is physically realizable in order for the tuning recommendations to be of use. Moreover, even if it can be analytically proved that there exist no symmetry-breaking bifurcations, this must be also be observed in a carefully-controlled experimental setting before the results can be seriously considered for practical implementation.

APPENDIX A

Selected Topics from Linear Algebra

A.1 Introduction

In what follows some selected topics from linear algebra are reviewed. Most of the basic results are included either as a quick reference or to support theoretical developments elsewhere in this thesis. Two matrix operations are introduced in Section A.2 and some special matrices are described in Section A.3. Similarity transformations and their basic properties are discussed in Section A.4.

A.2 The Direct Sum and Direct Product

Definition A.1 (Direct Sum) *For $i = 1, \ldots, N$ let $\mathbf{A}_i \in \mathbb{C}^{p_i \times p_i}$ with each $p_i \in \mathbb{Z}_+$. Then the direct sum of $\mathbf{A}_i$ is denoted by*

$$\mathbf{A}_1 \oplus \mathbf{A}_2 \oplus \ldots \oplus \mathbf{A}_N = \oplus_{i=1}^{N} \mathbf{A}_i$$

and results in the block diagonal square matrix

$$\mathbf{A} = \begin{bmatrix} \mathbf{A}_1 & \mathbf{0} & \ldots & \mathbf{0} \\ \mathbf{0} & \mathbf{A}_2 & \ldots & \mathbf{0} \\ \vdots & \vdots & \ddots & \vdots \\ \mathbf{0} & \mathbf{0} & \ldots & \mathbf{A}_N \end{bmatrix}$$

of order $p_1 + p_2 + \ldots + p_N$, where each zero matrix $\mathbf{0}$ has the appropriate dimension. Δ

In this work the direct sum of N matrices $\mathbf{A}_i$ is denoted by the block diagonal matrix

$$\operatorname{diag}(\mathbf{A}_1, \mathbf{A}_2, \ldots, \mathbf{A}_N) = \operatorname*{diag}_{i=1,\ldots,N}(\mathbf{A}_i).$$

For the case when each $\mathbf{A}_i = a_i$ is a scalar (1×1), the direct sum of a_i will be denoted by the diagonal matrix

$$\operatorname{diag}(a_1, a_2, \ldots, a_N) = \operatorname*{diag}_{i=1,\ldots,N}(a_i).$$

The direct, or Kronecker product is defined next.

Definition A.2 (Kronecker Product) *Let* $\mathbf{a}, \mathbf{b} \in \mathbb{C}^n$. *Then the direct product (or Kronecker product) of* $\mathbf{a}$ *and* $\mathbf{b}^T$ *is the square matrix*

$$\mathbf{a} \otimes \mathbf{b}^T = \begin{bmatrix} a_1 b_1 & a_1 b_2 & \cdots & a_1 b_n \\ a_2 b_1 & a_2 b_2 & \cdots & a_2 b_n \\ \vdots & \vdots & \ddots & \vdots \\ a_n b_1 & a_n b_2 & \cdots & a_n b_n \end{bmatrix}.$$

Let the matrices $\mathbf{A} \in \mathbb{C}^{m \times n}$ *and* $\mathbf{B} \in \mathbb{C}^{p \times q}$. *Then the direct product of* $\mathbf{A}$ *and* $\mathbf{B}$ *is the* $mp \times nq$ *matrix*

$$\mathbf{A} \otimes \mathbf{B} = \begin{bmatrix} a_{11}\mathbf{B} & a_{12}\mathbf{B} & \cdots & a_{1n}\mathbf{B} \\ a_{21}\mathbf{B} & a_{22}\mathbf{B} & \cdots & a_{2n}\mathbf{B} \\ \vdots & \vdots & \ddots & \vdots \\ a_{m1}\mathbf{B} & a_{m2}\mathbf{B} & \cdots & a_{mn}\mathbf{B} \end{bmatrix}. \qquad \Delta$$

Some important properties of the direct product are as follows.

1. The direct product is a bilinear operator. If α is a scalar and $\mathbf{A}$, $\mathbf{B}$ are square matrices, then
$$\alpha(\mathbf{A} \otimes \mathbf{B}) = (\alpha\mathbf{A}) \otimes \mathbf{B} = \mathbf{A} \otimes (\alpha\mathbf{B}). \tag{A.1}$$

2. The direct product distributes over addition. If $\mathbf{A}$, $\mathbf{B}$ and $\mathbf{C}$ are square matrices, such that $\mathbf{A}$ and $\mathbf{B}$ (resp. $\mathbf{B}$ and $\mathbf{C}$) are of the same dimension, then
$$(\mathbf{A} + \mathbf{B}) \otimes \mathbf{C} = \mathbf{A} \otimes \mathbf{C} + \mathbf{B} \otimes \mathbf{C}, \tag{A.2a}$$
$$\mathbf{A} \otimes (\mathbf{B} + \mathbf{C}) = \mathbf{A} \otimes \mathbf{B} + \mathbf{A} \otimes \mathbf{C}. \tag{A.2b}$$

3. The direct product is associative. If $\mathbf{A}$, $\mathbf{B}$, and $\mathbf{C}$ are square matrices, then

$$\mathbf{A} \otimes (\mathbf{B} \otimes \mathbf{C}) = (\mathbf{A} \otimes \mathbf{B}) \otimes \mathbf{C}. \tag{A.3}$$

4. If $\mathbf{A}$, $\mathbf{B}$, $\mathbf{C}$, and $\mathbf{D}$ are square matrices such that $\mathbf{AC}$ and $\mathbf{BD}$ exist, then

$$(\mathbf{A} \otimes \mathbf{B})(\mathbf{C} \otimes \mathbf{D}) = (\mathbf{AC}) \otimes (\mathbf{BD}). \tag{A.4}$$

5. If $\mathbf{A}$ and $\mathbf{B}$ are invertible matrices, then

$$(\mathbf{A} \otimes \mathbf{B})^{-1} = \mathbf{A}^{-1} \otimes \mathbf{B}^{-1}. \tag{A.5}$$

6. If $\mathbf{A}$ and $\mathbf{B}$ are square matrices, then

$$(\mathbf{A} \otimes \mathbf{B})^T = \mathbf{A}^T \otimes \mathbf{B}^T, \tag{A.6a}$$
$$(\mathbf{A} \otimes \mathbf{B})^{\mathcal{H}} = \mathbf{A}^{\mathcal{H}} \otimes \mathbf{B}^{\mathcal{H}}, \tag{A.6b}$$

   where $(\,\cdot\,)^T$ denotes transposition and $(\,\cdot\,)^{\mathcal{H}}$ is the conjugate transpose.

7. If $\mathbf{A}$ and $\mathbf{B}$ are square matrices with dimensions n and m, respectively, then

$$\det(\mathbf{A} \otimes \mathbf{B}) = (\det \mathbf{A})^m (\det \mathbf{B})^n, \tag{A.7a}$$
$$\mathrm{tr}(\mathbf{A} \otimes \mathbf{B}) = \mathrm{tr}\mathbf{A}\,\mathrm{tr}\mathbf{B}. \tag{A.7b}$$

A.3 Special Matrices

There are a number of special matrices employed in this work, and their definitions and pertinent properties are outlined here. Hermitian, and unitary matrices are defined first (a summary of these special matrices is given in Table A.1), followed by a brief treatment of two important permutation matrices. The details of the Fourier matrix and circulant matrices, which are employed throughout this work, are deferred to Appendix B.

Table A.1. Some types of special matrices.

Type	Condition		
Symmetric	$\mathbf{A} = \mathbf{A}^T$		
Hermitian	$\mathbf{A} = \mathbf{A}^{\mathcal{H}}$		
Orthogonal	$\mathbf{A}^T\mathbf{A} = \mathbf{I}$	or	$\mathbf{A}^T = \mathbf{A}^{-1}$
Unitary	$\mathbf{A}^{\mathcal{H}}\mathbf{A} = \mathbf{I}$	or	$\mathbf{A}^{\mathcal{H}} = \mathbf{A}^{-1}$

A.3.1 Hermitian and Unitary Matrices

Definition A.3 (Hermitian Matrix) *A matrix* $\mathbf{H} \in \mathbb{C}^{N\times N}$ *is said to be Hermitian if* $\mathbf{H} = \mathbf{H}^{\mathcal{H}}$. Δ

The elements of a Hermitian matrix $\mathbf{H}$ satisfy $h_{ik} = \bar{h}_{ki}$ for all $1 \leq i, k \leq N$. Thus the diagonal elements h_{ii} of a Hermitian matrix must be real, while the off-diagonal elements may be complex. If $\mathbf{H} = \mathbf{H}^T$ then $\mathbf{H}$ is said to be *symmetric.*

Definition A.4 (Unitary Matrix) *A matrix* $\mathbf{U} \in \mathbb{C}^{N\times N}$ *is said to be unitary if* $\mathbf{U}^{\mathcal{H}}\mathbf{U} = \mathbf{I}$. Δ

Real unitary matrices are *orthogonal* matrices. If a matrix $\mathbf{U}$ is unitary then so too is $\mathbf{U}^{\mathcal{H}}$. If in addition it is nonsingular then $\mathbf{U}^{\mathcal{H}} = \mathbf{U}^{-1}$.

A.3.2 Permutation Matrices

A general permutation matrix is formed from the identity matrix by reordering its columns or its rows. Here we introduce two such matrices: the cyclic forward shift matrix and the flip matrix.

The Cyclic Forward Shift Matrix

The $N \times N$ *cyclic forward shift matrix* plays an important role in the theory of circulants. It is populated with one's along its superdiagonal and in the $(N, 1)$ position

and its remaining elements are set to zero, that is,

$$\boldsymbol{\sigma}_N = \begin{bmatrix} 0 & 1 & 0 & \cdots & 0 & 0 \\ 0 & 0 & 1 & \cdots & 0 & 0 \\ \vdots & \vdots & \vdots & \ddots & \vdots & \vdots \\ 0 & 0 & 0 & \cdots & 1 & 0 \\ 0 & 0 & 0 & \cdots & 0 & 1 \\ 1 & 0 & 0 & \cdots & 0 & 0 \end{bmatrix}_{N \times N} . \tag{A.8}$$

It will be shown subsequently that Equation (A.8) is a *circulant* matrix, and hence we defer a treatment of its properties to Appendix B.

The Flip Matrix

The $N \times N$ *flip matrix* has one's in the $(1,1)$ position and along the subantidiagonal, with all other elements equal to zero. It is given by

$$\boldsymbol{\kappa}_N = \begin{bmatrix} 1 & 0 & 0 & \cdots & 0 & 0 \\ 0 & 0 & 0 & \cdots & 0 & 1 \\ 0 & 0 & 0 & \cdots & 1 & 0 \\ \vdots & \vdots & \vdots & \iddots & \vdots & \vdots \\ 0 & 0 & 1 & \cdots & 0 & 0 \\ 0 & 1 & 0 & \cdots & 0 & 0 \end{bmatrix}_{N \times N} \tag{A.9}$$

and is such that

$$\boldsymbol{\kappa}_N^2 = \mathbf{I}_N, \tag{A.10a}$$

$$\boldsymbol{\kappa}_N^{\mathcal{H}} = \boldsymbol{\kappa}_N^T = \boldsymbol{\kappa}_N = \boldsymbol{\kappa}_N^{-1}, \tag{A.10b}$$

where $\mathbf{I}_N$ is the $N \times N$ identity matrix.

A.4 Similarity Transformations

Definition A.5 (Similarity Transformation) *Let* $\mathbf{Q}$ *be an arbitrary nonsingular matrix. Then* $\mathbf{B} = \mathbf{Q}^{-1}\mathbf{A}\mathbf{Q}$ *is a similarity transformation and* $\mathbf{B}$ *is said to be similar to* $\mathbf{A}$. Δ

Table A.2. Some types of linear transformations.

Type	Condition	Transformation
Equivalence	$\mathbf{P}$, $\mathbf{Q}$ are nonsingular	$\mathbf{B} = \mathbf{PAQ}$
Congruence	$\mathbf{Q}$ is nonsingular	$\mathbf{B} = \mathbf{Q}^T\mathbf{AQ}$
Similarity	$\mathbf{Q}$ is nonsingular	$\mathbf{B} = \mathbf{Q}^{-1}\mathbf{AQ}$
Orthogonal	$\mathbf{Q}$ is nonsingular and orthogonal	$\mathbf{B} = \mathbf{Q}^T\mathbf{AQ} = \mathbf{Q}^{-1}\mathbf{AQ}$
Unitary	$\mathbf{Q}$ is nonsingular and unitary	$\mathbf{B} = \mathbf{Q}^{\mathcal{H}}\mathbf{AQ} = \mathbf{Q}^{-1}\mathbf{AQ}$

If $\mathbf{B}$ is similar to $\mathbf{A}$, then $\mathbf{A} = \left(\mathbf{Q}^{-1}\right)^{-1}\mathbf{B}\left(\mathbf{Q}^{-1}\right)$ is similar to $\mathbf{B}$. It therefore suffices to say that $\mathbf{A}$ and $\mathbf{B}$ are *similar matrices.* A summary of some other linear transformations is given in Table A.2. By inspection of this table, it also follows that if $\mathbf{B}$ is orthogonally (resp. unitarily) similar to $\mathbf{A}$, then $\mathbf{A}$ and $\mathbf{B}$ are orthogonally (resp. unitarily) similar matrices.

Theorem A.1 *If* $\mathbf{A}$ *and* $\mathbf{B}$ *are similar matrices, then they have the same characteristic equation and hence the same eigenvalues.* □

PROOF. Let p_A and p_B denote the characteristic polynomials of $\mathbf{A}$ and $\mathbf{B}$, respectively, and let $\mathbf{B}$ be similar to $\mathbf{A}$. That is, let $\mathbf{B}$ be any matrix such that $\mathbf{B} = \mathbf{Q}^{-1}\mathbf{AQ}$ for some nonsingular matrix $\mathbf{Q}$. Then the characteristic polynomial of $\mathbf{B}$ is

$$\begin{aligned} p_B(\lambda) &= \det(\mathbf{B} - \lambda\mathbf{I}) \\ &= \det(\mathbf{Q}^{-1}\mathbf{AQ} - \lambda\mathbf{Q}^{-1}\mathbf{IQ}) \\ &= \det(\mathbf{Q}^{-1}(\mathbf{A} - \lambda\mathbf{I})\mathbf{Q}) \\ &= \det(\mathbf{Q}^{-1})\det(\mathbf{A} - \lambda\mathbf{I})\det(\mathbf{Q}) \\ &= p_A(\lambda), \end{aligned}$$

where we have used the fact that $\det(\mathbf{Q}^{-1})\det(\mathbf{Q}) = \det(\mathbf{Q}^{-1}\mathbf{Q}) = \det(\mathbf{I}) = 1$. Thus $\mathbf{A}$ and $\mathbf{B}$ have the same characteristic polynomial and share the same eigenvalues. ■

Theorem A.1 guarantees that the eigenvalues of a matrix are preserved under a similarity transformation; the same is true for orthogonal and unitary transformations.

Next we show that if $\mathbf{A}$ and $\mathbf{B}$ are similar matrices, and if p is an arbitrary finite polynomial, then $p(\mathbf{A})$ is similar to $p(\mathbf{B})$.

Theorem A.2 *Let p be an arbitrary finite polynomial and $\mathbf{B} = \mathbf{Q}^{-1}\mathbf{A}\mathbf{Q}$. Then $p(\mathbf{B}) = \mathbf{Q}^{-1}p(\mathbf{A})\mathbf{Q}$.* □

PROOF. Let $\mathbf{Q}$ be an arbitrary nonsingular matrix and let

$$p(t) = \sum_{k=0}^{N} c_k t^k$$

be a polynomial of degree N with arbitrary constant coefficients c_k. Then

$$\begin{aligned}
p(\mathbf{B}) &= p(\mathbf{Q}^{-1}\mathbf{A}\mathbf{Q}) \\
&= \sum_{k=0}^{N} c_k(\mathbf{Q}^{-1}\mathbf{A}\mathbf{Q})^k \\
&= c_0\mathbf{I} + c_1\mathbf{Q}^{-1}\mathbf{A}\mathbf{Q} + c_2\mathbf{Q}^{-1}\mathbf{A}\mathbf{Q}\mathbf{Q}^{-1}\mathbf{A}\mathbf{Q} + \ldots + c_N\mathbf{Q}^{-1}\mathbf{A}\mathbf{Q}\cdots\mathbf{Q}^{-1}\mathbf{A}\mathbf{Q} \\
&= c_0\mathbf{I} + c_1\mathbf{Q}^{-1}\mathbf{A}\mathbf{Q} + c_2\mathbf{Q}^{-1}\mathbf{A}^2\mathbf{Q} + \ldots + c_N\mathbf{Q}^{-1}\mathbf{A}^N\mathbf{Q} \\
&= \mathbf{Q}^{-1}\left(c_0\mathbf{I} + c_1\mathbf{A} + c_2\mathbf{A}^2 + \ldots + c_N\mathbf{A}^N\right)\mathbf{Q} \\
&= \mathbf{Q}^{-1}p(\mathbf{A})\mathbf{Q},
\end{aligned}$$

which completes the proof. ■

If one chooses $p(t) = t^k$ with $k > 0$, then we have the following.

Corollary A.1 *If $\mathbf{B} = \mathbf{Q}^{-1}\mathbf{A}\mathbf{Q}$, then $\mathbf{B}^k = \mathbf{Q}^{-1}\mathbf{A}^k\mathbf{Q}$ for any $k \in \mathbb{Z}_+$.* □

Diagonalizability of a matrix is defined next.

Definition A.6 (Diagonalizable Matrix) *A square matrix $\mathbf{A}$ is diagonalizable if there exists a nonsigular matrix $\mathbf{Q}$ and a diagonal matrix $\mathbf{D}$ such that $\mathbf{Q}^{-1}\mathbf{A}\mathbf{Q} = \mathbf{D}$.*△

Thus a matrix is diagonalizable if it is similar to a diagonal matrix. If $\mathbf{A}$ is diagonalizable by $\mathbf{Q}$, we say that $\mathbf{Q}$ *diagonalizes* $\mathbf{A}$ and that $\mathbf{Q}$ is the *diagonalizing matrix.*

Theorem A.3 *An $N \times N$ matrix $\mathbf{A}$ is diagonalizable if it has N linearly independent eigenvectors.* □

PROOF. Suppose $\mathbf{A}$ has N linearly independent eigenvectors and denoted them by $\mathbf{q}_1, \mathbf{q}_2, \ldots, \mathbf{q}_N$. Let λ_i be the eigenvalue of $\mathbf{A}$ corresponding to $\mathbf{q}_i$ for each $i = 1, \ldots, N$. Then if $\mathbf{Q}$ is the matrix that has as its i^{th} column the vector $\mathbf{q}_i$, it follows that

$$\begin{aligned}
\mathbf{AQ} &= (\mathbf{Aq}_1, \mathbf{Aq}_2, \ldots, \mathbf{Aq}_N) \\
&= (\mathbf{q}_1\lambda_1, \mathbf{q}_2\lambda_2, \ldots, \mathbf{q}_N\lambda_N) \\
&= (\mathbf{q}_1, \mathbf{q}_2, \ldots, \mathbf{q}_N) \operatorname*{diag}_{i=1,\ldots,N} (\lambda_i) \\
&\equiv \mathbf{QD}.
\end{aligned}$$

Since $\mathbf{Q}$ is nonsingular by hypothesis, $\mathbf{D} = \mathbf{Q}^{-1}\mathbf{AQ}$. ■

APPENDIX B

The Theory of Circulants

B.1 Introduction

This appendix gives a more exhaustive treatment of the theory of circulants and is meant to complement the overview given in Section 2.2. It is distilled from the seminal work by Davis [62] and follows the presentation style of Óttarsson [36], one that should be familiar to the vibrations engineer. The sections that follow act simultaneously as a detailed reference *and* tutorial. Thus, in addition to a detailed treatment of the theory (including many of the proofs), some worked examples are also included.

The appendix is organized as follows. Circulant and block circulant matrices are defined in Section B.2 and Section B.3, respectively, and some of their more relevant properties are given. Diagonalization of (block) circulants is discussed at length in Section B.4, which begins with a treatment of the N^{th} roots of unity in Section B.4.1 and the Fourier matrix in Section B.4.2. It is subsequently shown how to diagonalize the cyclic forward shift matrix in Section B.4.3, a circulant in Section B.4.4, and a block circulant in Section B.4.5. The appendix closes in Section B.4.6 with some generalizations of the theory, including the diagonalization of block circulants with circulant blocks.

B.2 Circulant Matrices

We begin with a definition.

Definition B.1 (Circulant Matrix) *An $N \times N$ circulant matrix (or circulant) is formed from an N-vector by cyclically permuting its entries and is of the form*

$$\mathbf{C} = \begin{bmatrix} c_1 & c_2 & \cdots & c_N \\ c_N & c_1 & \cdots & c_{N-1} \\ \vdots & \vdots & \ddots & \vdots \\ c_2 & c_3 & \cdots & c_1 \end{bmatrix}. \qquad \Delta$$

Thus a circulant matrix is defined completely by an ordered set of *generating elements* $c_1, c_2, \ldots, c_N$ in its first row. These are cyclically shifted to the right by one position per row to form the subsequent rows. The set of all such matrices will be designated by $\mathscr{C}_N$, and are said to be circulant matrices of type N.

It is convenient to define the *circulant operator* circ $(\cdot)$ that takes as its argument the generating elements $c_1, c_2, \ldots, c_N$ and results in the array given in Definition B.1, that is,

$$\mathbf{C} = \text{circ}\,(c_1, c_2, \ldots, c_N)\,. \tag{B.1}$$

An $N \times N$ circulant can also be characterized in terms of its (i,k) entry by $(\mathbf{C})_{ik} = c_{k-i+1(\text{mod}\,N)}$ with $1 \leq i, k \leq N$.

Example B.1

$$\text{circ}\,(a,b,c,d) = \begin{bmatrix} a & b & c & d \\ d & a & b & c \\ c & d & a & b \\ b & c & d & a \end{bmatrix} \in \mathscr{C}_4. \qquad \square$$

If a matrix is both circulant and symmetric it can be written as

$$\mathbf{C} = \begin{cases} \text{circ}\left(c_1, c_2, \ldots, c_{\frac{N}{2}}, c_{\frac{N+2}{2}}, c_{\frac{N}{2}}, \ldots, c_3, c_2\right), & N \text{ even} \\ \text{circ}\left(c_1, c_2, \ldots, c_{\frac{N-1}{2}}, c_{\frac{N+1}{2}}, c_{\frac{N+1}{2}}, c_{\frac{N-1}{2}}, \ldots, c_3, c_2\right), & N \text{ odd} \end{cases} \tag{B.2}$$

and necessarily has repeated generating elements; only $(N+2)/2$ are distinct if N is even and $(N+1)/2$ are distinct if N is odd. The set of all $N \times N$ *symmetric circulants* will be denoted by $\mathscr{SC}_N$.

Example B.2

$$N = 4: \qquad \text{circ}\,(a,b,c,b) = \begin{bmatrix} a & b & c & b \\ b & a & b & c \\ c & b & a & b \\ b & c & b & a \end{bmatrix} \in \mathscr{SC}_4$$

$$N = 5: \qquad \text{circ}\,(a,b,c,c,b) = \begin{bmatrix} a & b & c & c & b \\ b & a & b & c & c \\ c & b & a & b & c \\ c & c & b & a & b \\ b & c & c & b & a \end{bmatrix} \in \mathscr{SC}_5$$

□

It is clear from Equation (A.8) of Section A.3.2 that the cyclic forward shift matrix is a circulant with generating elements $0, 1, 0, \ldots, 0, 0$. Hence the integer powers of $\boldsymbol{\sigma}_N$ can be written as

$$\left.\begin{aligned} \boldsymbol{\sigma}_N^0 &= \text{circ}\,(1,0,0,0,0,\ldots,0,0) = \mathbf{I}_N \\ \boldsymbol{\sigma}_N^1 &= \text{circ}\,(0,1,0,0,0,\ldots,0,0) \\ \boldsymbol{\sigma}_N^2 &= \text{circ}\,(0,0,1,0,0,\ldots,0,0) \\ &\vdots \\ \boldsymbol{\sigma}_N^{N-1} &= \text{circ}\,(0,0,0,0,0,\ldots,0,1) \\ \boldsymbol{\sigma}_N^N &= \text{circ}\,(1,0,0,0,0,\ldots,0,0) = \boldsymbol{\sigma}_N^0 = \mathbf{I}_N \end{aligned}\right\}. \tag{B.3}$$

Next we give (without proof) a necessary and sufficient condition for a square matrix to be circulant.

Theorem B.1 *Let $\boldsymbol{\sigma}_N$ be the cyclic forward shift matrix. Then a $N \times N$ matrix $\mathbf{C}$ is circulant if and only if $\mathbf{C}\boldsymbol{\sigma}_N = \boldsymbol{\sigma}_N\mathbf{C}$.* □

Any matrix that commutes with the cyclic forward shift matrix is, therefore, a circulant. Theorem B.1 also says that circulant matrices are invariant under similarity transformations involving the cyclic forward shift matrix.

Example B.3 *Consider the* 3×3 *matrix*

$$\mathbf{A} = \begin{bmatrix} a & b & c \\ c & a & b \\ b & c & a \end{bmatrix}.$$

Since

$$\begin{bmatrix} a & b & c \\ c & a & b \\ b & c & a \end{bmatrix}\begin{bmatrix} 0 & 1 & 0 \\ 0 & 0 & 1 \\ 1 & 0 & 0 \end{bmatrix} = \begin{bmatrix} c & a & b \\ b & c & a \\ a & b & c \end{bmatrix} = \begin{bmatrix} 0 & 1 & 0 \\ 0 & 0 & 1 \\ 1 & 0 & 0 \end{bmatrix}\begin{bmatrix} a & b & c \\ c & a & b \\ b & c & a \end{bmatrix},$$

it follows that $\mathbf{A} = \text{circ}\,(a, b, c) \in \mathscr{C}_3$. ◻

An important feature of circulants is that they can be represented by a finite matrix polynomial involving the cyclic forward shift matrix and its powers. In particular, by inspection of the structure of the matrices $\boldsymbol{\sigma}_N^k$ in Equation (B.3), it is clear that a circulant matrix with generating elements $c_1, c_2, \ldots, c_N$ can be represented by the matrix sum

$$\begin{aligned} \text{circ}\,(c_1, c_2, \ldots, c_N) &= c_1\mathbf{I}_N + c_2\boldsymbol{\sigma}_N + c_3\boldsymbol{\sigma}_N^2 + \ldots + c_N\boldsymbol{\sigma}_N^{N-1} \\ &= \sum_{k=1}^{N} c_k\boldsymbol{\sigma}_N^{k-1}. \end{aligned} \tag{B.4}$$

This property is exploited in Section B.4.4 to diagonalize a general circulant matrix.

Example B.4 *The matrix* $\mathbf{A} = \text{circ}\,(a, b, c)$ *from Example B.3 can be represented by the matrix sum*

$$\begin{aligned} \mathbf{A} &= a\mathbf{I}_3 + b\boldsymbol{\sigma}_3 + c\boldsymbol{\sigma}_3^2 \\ &= a\begin{bmatrix} 1 & 0 & 0 \\ 0 & 1 & 0 \\ 0 & 0 & 1 \end{bmatrix} + b\begin{bmatrix} 0 & 1 & 0 \\ 0 & 0 & 1 \\ 1 & 0 & 0 \end{bmatrix} + c\begin{bmatrix} 0 & 0 & 1 \\ 1 & 0 & 0 \\ 0 & 1 & 0 \end{bmatrix} = \begin{bmatrix} a & b & c \\ c & a & b \\ b & c & a \end{bmatrix}. \end{aligned}$$ ◻

Next we introduce block circulant matrices, which is a natural generalization of ordinary circulants.

B.3 Block Circulant Matrices

Suppose each entry c_k of the circulant array in Definition B.1 is replaced by the $M \times M$ matrix $\mathbf{C}_k$ for $k = 1, \ldots, N$. Then the resulting $NM \times NM$ array is a *block circulant* matrix of type (M, N) and is written as

$$\mathbf{C} = \operatorname{circ}(\mathbf{C}_1, \mathbf{C}_2, \ldots, \mathbf{C}_N), \tag{B.5}$$

where $\mathbf{C}_1, \mathbf{C}_2, \ldots, \mathbf{C}_N$ are its *generating matrices*. The set of all such matrices will be denoted by $\mathscr{BC}_{M,N}$. A matrix $\mathbf{C} \in \mathscr{BC}_{M,N}$ is not necessarily a circulant, as the following example demonstrates.

Example B.5 *Let*

$$\mathbf{A} = \begin{bmatrix} 2 & -1 \\ -1 & 2 \end{bmatrix}, \qquad \mathbf{B} = \begin{bmatrix} -1 & 0 \\ 0 & -1 \end{bmatrix}.$$

Then

$$\mathbf{C} = \begin{bmatrix} \mathbf{A} & \mathbf{B} & \mathbf{0} & \mathbf{B} \\ \mathbf{B} & \mathbf{A} & \mathbf{B} & \mathbf{0} \\ \mathbf{0} & \mathbf{B} & \mathbf{A} & \mathbf{B} \\ \mathbf{B} & \mathbf{0} & \mathbf{B} & \mathbf{A} \end{bmatrix} = \left[\begin{array}{cc:cc:cc:cc} 2 & -1 & -1 & 0 & 0 & 0 & -1 & 0 \\ -1 & 2 & 0 & -1 & 0 & 0 & 0 & -1 \\ \hdashline -1 & 0 & 2 & -1 & -1 & 0 & 0 & 0 \\ 0 & -1 & -1 & 2 & 0 & -1 & 0 & 0 \\ \hdashline 0 & 0 & -1 & 0 & 2 & -1 & -1 & 0 \\ 0 & 0 & 0 & -1 & -1 & 2 & 0 & -1 \\ \hdashline -1 & 0 & 0 & 0 & -1 & 0 & 2 & -1 \\ 0 & -1 & 0 & 0 & 0 & -1 & -1 & 2 \end{array}\right]$$

is a block circulant of type $(2, 4)$*, but it is not a circulant.* ◻

Next we give (without proof) a necessary and sufficient condition for a matrix to be a block circulant.

Theorem B.2 *Let* $\boldsymbol{\sigma}_N$ *be the cyclic forward shift matrix of dimension* N *and* $\mathbf{I}_M$ *be the identity matrix of dimension* M*. Then a* $NM \times NM$ *matrix* $\mathbf{C}$ *is a block circulant of type* (M, N) *if and only if* $\mathbf{C}(\boldsymbol{\sigma}_N \otimes \mathbf{I}_M) = (\boldsymbol{\sigma}_N \otimes \mathbf{I}_M)\mathbf{C}$. ◻

The reader can verify that the matrix $\mathbf{C}$ in Example B.5 satisfies the condition in Theorem B.2, but not that in Theorem B.1.

A *block circulant, block symmetric* matrix of type (M, N) has the same form as Equation (B.2), and is obtained by replacing each entry c_k by the $M \times M$ matrix $\mathbf{C}_k$ for $k = 1, \ldots, N$. The set of all such matrices will be denoted by $\mathscr{BCBS}_{M,N}$. The matrix $\mathbf{C}$ in Example B.5 is recognized to be a block symmetric, block circulant matrix of type $(2, 4)$, that is, it is contained in $\mathscr{BCBS}_{2,4}$.

A block circulant with generating matrices $\mathbf{C}_1, \mathbf{C}_2, \ldots, \mathbf{C}_N$ can be represented by the marix sum

$$\begin{aligned} \text{circ}\,(\mathbf{C}_1, \mathbf{C}_2, \ldots, \mathbf{C}_N) &= \mathbf{I}_N \otimes \mathbf{C}_1 + \boldsymbol{\sigma}_N \otimes \mathbf{C}_2 + \ldots + \boldsymbol{\sigma}_N^{N-1} \otimes \mathbf{C}_N \\ &= \sum_{k=1}^{N} \boldsymbol{\sigma}_N^{k-1} \otimes \mathbf{C}_k, \end{aligned} \tag{B.6}$$

where the integer powers of the cyclic forward shift matrix are given by Equation (B.3).

B.4 Diagonalization of Circulants

Any circulant matrix can be represented in terms of the cyclic forward shift matrix, which is clear from Equation (B.4). The diagonalization of a general circulant begins, therefore, by finding a matrix that diagonalizes $\boldsymbol{\sigma}_N$. Together with some basic results from linear algebra (these are summarized in Appendix A) this leads naturally to the diagonalization of an *arbitrary* circulant. Regarding a suitable diagonalizing matrix, there are a number of candidates [91, 92, 94, 100, 102, 117], but all seem to feature powers of the N^{th} roots of unity or their real/imaginary parts. In this work we employ the complex Fourier matrix, which has as its elements the distinct N^{th} roots of unity and their integer powers; these are defined in Section B.4.1. The Fourier matrix is introduced in Section B.4.2, whereupon its relevant features are detailed. The diagonalization of the cyclic forward shift matrix is carried out in Section B.4.3

via a unitary transformation involving the Fourier matrix, and the diagonalization of a general circulant matrix is subsequently described in Section B.4.4. These results are generalized to handle general block circulant matrices in Section B.4.5 and some special block circulants in Section B.4.6.

B.4.1 N^{th} Roots of Unity

Here we follow the presentation in [118]. The N^{th} roots of a complex number $z_o = r_o e^{j\theta_o}$ are given by a nonzero number $z = re^{j\theta}$ such that $z^N = z_o$ with $N \in \mathbb{Z}_+$, or upon substitution, $r^N e^{jN\theta} = r_o e^{j\theta_o}$. This equality holds if and only if $r^N = r_o$ and $N\theta = \theta_o + 2\pi k$ with $k \in \mathbb{Z}$. Therefore,

$$\left.\begin{aligned} r &= \sqrt[N]{r_o} \\ \theta &= \frac{\theta_o + 2\pi k}{N} \end{aligned}\right\}, \qquad k \in \mathbb{Z} \tag{B.7}$$

and the N^{th} roots are

$$z = \sqrt[N]{r_o}\exp\left(j\frac{\theta_o + 2\pi k}{N}\right), \qquad k \in \mathbb{Z}. \tag{B.8}$$

It is clear from this exponential form that the roots all lie on a circle of radius $\sqrt[N]{r_o}$ centered at the origin in the complex plane, and that they are equally distributed every $2\pi/N$ radians. Hence all of the *distinct* roots correspond to $k = 0, 1, 2, \ldots, N-1$. The *distinct* N^{th} *roots of unity* follow from Equation (B.8) by setting $r_o = 1$ and $\theta_o = 0$ and are given by

$$w_N^{(k)} = \exp\left(\frac{2j\pi}{N}k\right), \qquad k = 0, 1, 2, \ldots, N-1. \tag{B.9}$$

The *primitive* N^{th} root of unity corresponds to $k = 1$ and is denoted by

$$w_N = e^{\frac{2j\pi}{N}}. \tag{B.10}$$

Note that the integer powers $w_N^k = \left(e^{\frac{2j\pi}{N}}\right)^k = e^{\frac{2j\pi}{N}k}$ of the primitive N^{th} root of unity are equivalent to the distinct N^{th} roots of unity, i.e., those given by Equation (B.9).

They are

$$1, w_N, w_N^2, \ldots, w_N^{N-1},$$

example plots of which are shown in Figure B.1 for $N = 1, 2, \ldots, 9$.

B.4.2 The Fourier Matrix

Definition B.2 *Let* $w_N = e^{\frac{2j\pi}{N}}$ *be the primitive* N^{th} *root of unity with* $N \in \mathbb{Z}_+$ *and* $j = \sqrt{-1}$. *Then the* $N \times N$ *complex* Fourier matrix *is defined as*

$$\mathbf{E}_N = \frac{1}{\sqrt{N}} \begin{bmatrix} 1 & 1 & 1 & \cdots & 1 \\ 1 & w_N & w_N^2 & \cdots & w_N^{N-1} \\ 1 & w_N^2 & w_N^4 & \cdots & w_N^{2(N-1)} \\ \vdots & \vdots & \vdots & \ddots & \vdots \\ 1 & w_N^{N-1} & w_N^{2(N-1)} & \cdots & w_N^{(N-1)(N-1)} \end{bmatrix}_{N \times N} . \qquad \Delta$$

Clearly the Fourier matrix is symmetric, but generally it is not Hermitian. It can be written element-wise as

$$\begin{aligned} (\mathbf{E}_N)_{ik} &= \frac{1}{\sqrt{N}} w_N^{(i-1)(k-1)} \\ &= \frac{1}{\sqrt{N}} e^{j(i-1)\varphi_k} \\ &= \frac{1}{\sqrt{N}} e^{j(k-1)\varphi_i}, \qquad i, k = 1, \ldots, N \end{aligned} \tag{B.11}$$

where φ_i is the angle subtended from the positive real axis in the complex plane to the i^{th} power of w_N. It will be shown in Section B.4.4 that all circulant matrices share the same linearly independent eigenvectors, the elements of which compose the N columns (or rows) of $\mathbf{E}_N$. They are denoted by the column vectors

$$\left.\begin{aligned} \mathbf{e}_i &= \frac{1}{\sqrt{N}} \left(1, w_N^{(i-1)}, w_N^{2(i-1)}, \ldots, w_N^{(N-1)(i-1)}\right)^T \\ &= \frac{1}{\sqrt{N}} \left(1, e^{j\varphi_i}, e^{j2\varphi_i}, \ldots, e^{j(N-1)\varphi_i}\right)^T \end{aligned}\right\}, \qquad i = 1, \ldots, N. \tag{B.12}$$

A very important feature of $\mathbf{E}_N$ is that it is unitary. To see this, we first consider the finite geometric series identity and subsequently a result involving a summation on powers of the primitive N^{th} roots of unity.

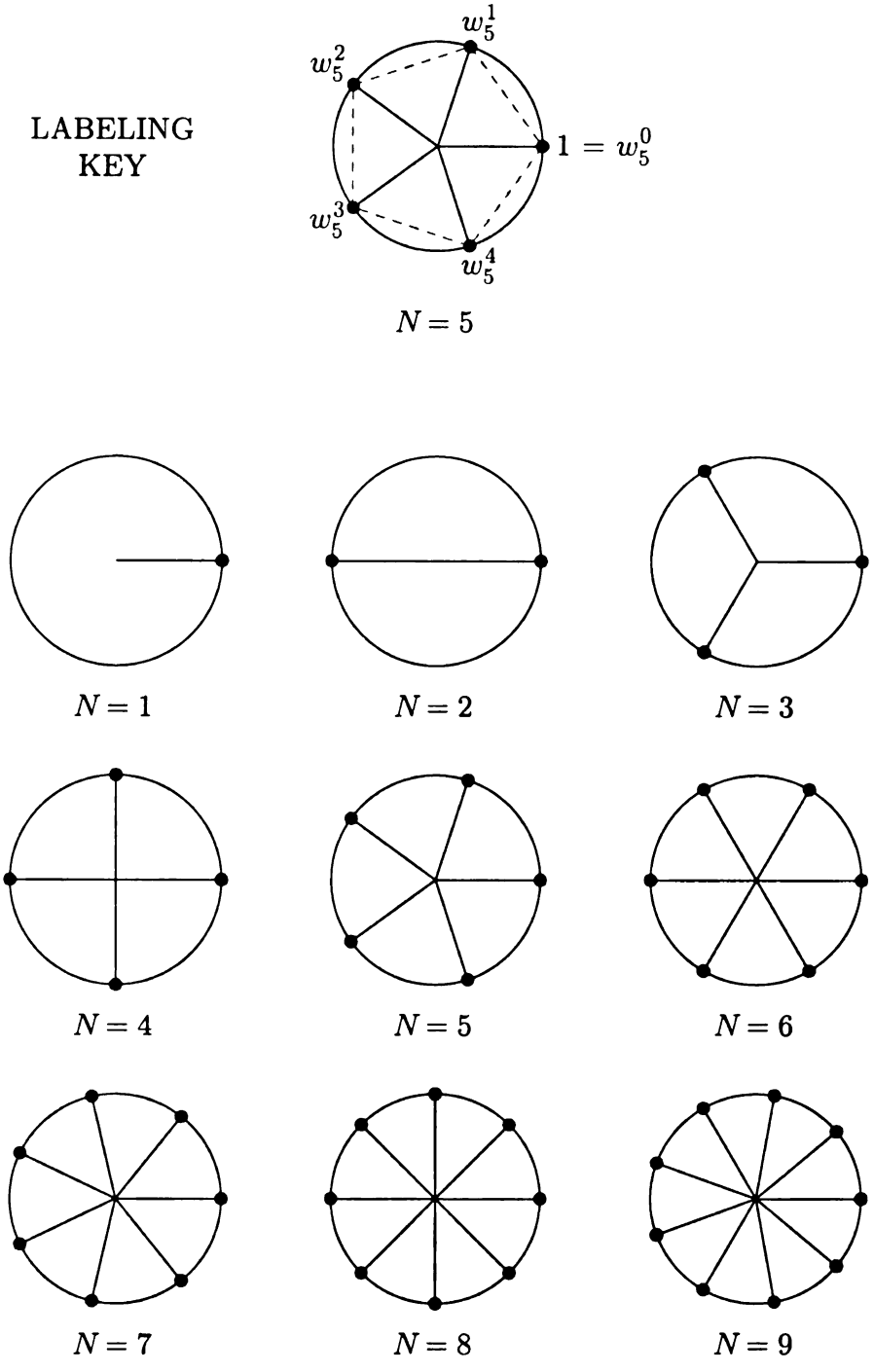

Figure B.1. The distinct N^{th} roots of unity w_N^k $(k = 0, 1, 2, \ldots, N-1)$ arranged on the unit circle in the complex plane (centered at the origin) for $N = 1, 2, \ldots, 9$. Note that $w_N^0 = 1$ is real, as is $w_N^{N/2} = -1$ if N is even. The remaining roots appear in complex conjugate pairs.

Lemma B.1 (Finite Geometric Series Identity) *Let $N \in \mathbb{Z}_+$ and $q \in \mathbb{C}$. Then for any $s \in \mathbb{Z}$ and $q \neq 1$,*

$$\sum_{r=s}^{s+N-1} q^r = \frac{q^s(1-q^N)}{1-q}.$$ □

PROOF. Consider the finite geometric series

$$\begin{aligned}\sum_{r=s}^{s+N-1} q^r &= q^s + q^{s+1} + q^{s+2} + \ldots q^{s+N-1} \\ &= q^s(1 + q + q^2 + \ldots + q^{N-1}).\end{aligned}$$

Multiplying from the left by q yields

$$q\sum_{r=s}^{s+N-1} q^r = q^s(q + q^2 + q^3 + \ldots + q^N).$$

Subtraction of the second equation from the first results in

$$(1-q)\sum_{r=s}^{s+N-1} q^r = q^s(1-q^N),$$

from which the proof is established since $q \neq 1$ by restriction. ■

Lemma B.1 is now used to establish the following theorem, which is needed to show that the Fourier matrix is unitary. The result will also aid in the diagonalization of circulants in subsequent sections.

Theorem B.3 *Let $i, k \in \mathbb{Z}$ and $w_N = e^{\frac{2j\pi}{N}}$ be the primitive N^{th} root of unity with $N \in \mathbb{Z}_+$. Then for any $s, m \in \mathbb{Z}$,*

$$\sum_{r=s}^{s+N-1} w_N^{r(i-k)} = \begin{cases} N, & i-k = mN \\ 0, & \text{otherwise} \end{cases}$$ □

PROOF. Let $q = w_N^{(i-k)} = e^{\frac{2j\pi}{N}(i-k)}$ and note that $q^N = 1$. If $i - k = mN$, then $q = e^{2j\pi m} = 1$ for any integer m and it follows that

$$\sum_{r=s}^{s+N-1} w_N^{r(i-k)} = \sum_{r=s}^{s+N-1} q^r = \underbrace{(1)^s + (1)^{s+1} + (1)^{s+2} + \ldots + (1)^{s+N-1}}_{N \text{ terms}} = N.$$

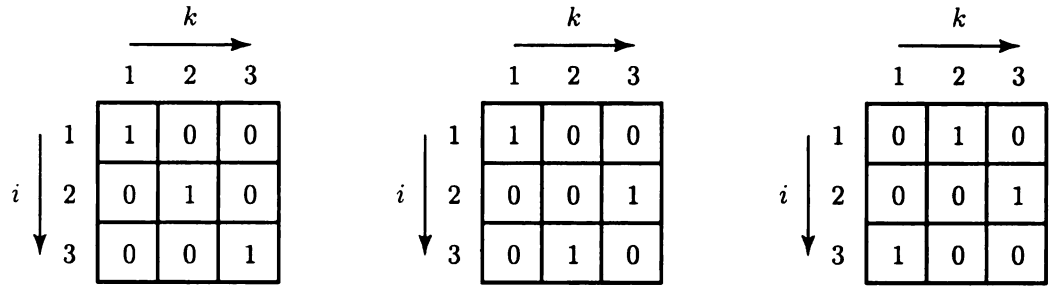

(a) $(\mathbf{I}_3)_{ik}$ (b) $(\boldsymbol{\kappa}_3)_{ik}$ (c) $(\boldsymbol{\sigma}_3)_{ik}$

Figure B.2. Arrays showing the (i,k) elements of the (a) identity, (b) flip, and (c) cyclic forward shift matrices of dimension $N = 3$ for $i, k = 1, 2, 3$.

For the case when $i - k \neq mN$ it follows from Lemma B.1 that

$$\sum_{r=s}^{s+N-1} q^r = \frac{q^s(1-1)}{1-q} = 0,$$

which completes the proof. ■

Theorem B.3 allows for a representation of the $N \times N$ identity, flip, and cyclic forward shift matrices in terms of certain conditions on their indices relative to N. For $i, k = 1, \ldots, N$ and for any integer m the (i,k) element of these matrices is given by

$$(\mathbf{I}_N)_{ik} = \frac{1}{N}\sum_{r=0}^{N-1} w_N^{r(i-k)} = \begin{cases} 1, & i-k = mN \\ 0, & \text{otherwise} \end{cases} \tag{B.13a}$$

$$(\boldsymbol{\kappa}_N)_{ik} = \frac{1}{N}\sum_{r=0}^{N-1} w_N^{r(i+k-2)} = \begin{cases} 1, & i+k-2 = mN \\ 0, & \text{otherwise} \end{cases} \tag{B.13b}$$

$$(\boldsymbol{\sigma}_N)_{ik} = \frac{1}{N}\sum_{r=0}^{N-1} w_N^{r(i-k+1)} = \begin{cases} 1, & i-k+1 = mN \\ 0, & \text{otherwise} \end{cases} \tag{B.13c}$$

respectively. The reader can check these by verifying the arrays in Figure B.2 for the special case of $N = 3$.

We are now ready to state the main result of this section, and indeed one of the most important results of this appendix.

Theorem B.4 *The Fourier matrix* $\mathbf{E}_N$ *is unitary.* □

PROOF. For $1 \leq i,k \leq N$ the (i,k) entry of $\mathbf{E}_N\mathbf{E}_N^{\mathcal{H}}$ is given by

$$\begin{aligned}
\left(\mathbf{E}_N\mathbf{E}_N^{\mathcal{H}}\right)_{ik} &= \sum_{r=1}^{N}(\mathbf{E}_N)_{ir}(\mathbf{E}_N^{\mathcal{H}})_{rk} \\
&= \sum_{r=1}^{N}\frac{1}{\sqrt{N}}w_N^{(i-1)(r-1)}\frac{1}{\sqrt{N}}w_N^{-(r-1)(k-1)} \qquad \text{(from Eqn. (B.11))} \\
&= \frac{1}{N}\sum_{r=1}^{N}w_N^{(r-1)(i-k)} \\
&= \frac{1}{N}\sum_{r=0}^{N-1}w_N^{r(i-k)} \\
&= (\mathbf{I}_N)_{ik}\,, \qquad \text{(from Eqn. (B.13a))}
\end{aligned}$$

from which it follows that $\mathbf{E}_N\mathbf{E}_N^{\mathcal{H}} = \mathbf{I}_N$. ■

Remarks

1. The column vectors of $\mathbf{E}_N$ are orthonormal, that is, $\mathbf{e}_i^{\mathcal{H}}\mathbf{e}_k = \delta_{ik}$, where δ_{ik} is the Kronecker delta.
2. Since $\mathbf{E}_N$ is unitary so too is the $NM \times NM$ matrix $\mathbf{E}_N \otimes \mathbf{I}_M$.
3. The $NM \times M$ matrices $\mathbf{e}_i \otimes \mathbf{I}_M$ are such that $(\mathbf{e}_i \otimes \mathbf{I}_M)^{\mathcal{H}}(\mathbf{e}_k \otimes \mathbf{I}_M) = \delta_{ik}\mathbf{I}_M$.

Next we derive a relationship between the Fourier and flip matrices.

Theorem B.5 $\mathbf{E}_N^2 = \boldsymbol{\kappa}_N = \left(\mathbf{E}_N^{\mathcal{H}}\right)^2$. □

PROOF. First we show that $\mathbf{E}_N^2 = \mathbf{E}_N\mathbf{E}_N = \boldsymbol{\kappa}_N$ using the same approach as the proof of Theorem B.4. For $1 \leq i,k \leq N$ and for any integer m the (i,k) entry of

$\mathbf{E}_N\mathbf{E}_N$ is given by

$$\begin{aligned}
(\mathbf{E}_N\mathbf{E}_N)_{ik} &= \sum_{r=1}^{N}(\mathbf{E}_N)_{ir}(\mathbf{E}_N)_{rk} \\
&= \sum_{r=1}^{N}\frac{1}{\sqrt{N}}w_N^{(i-1)(r-1)}\frac{1}{\sqrt{N}}w_N^{(r-1)(k-1)} && \text{(from Eqn. (B.11))} \\
&= \frac{1}{N}\sum_{r=0}^{N-1}w_N^{r(i+k-2)} \\
&= (\boldsymbol{\kappa}_N)_{ik}\,, && \text{(from Eqn. (B.13b))}
\end{aligned}$$

from which it follows that $\mathbf{E}_N^2 = \boldsymbol{\kappa}_N$. Finally, the result $\boldsymbol{\kappa}_N = \left(\mathbf{E}_N^{\mathcal{H}}\right)^2$ follows from conjugation and transposition of $\boldsymbol{\kappa}_N = \mathbf{E}_N\mathbf{E}_N$, and by invoking the properties $\boldsymbol{\kappa}_N^{\mathcal{H}} = \boldsymbol{\kappa}_N$ and $\left(\mathbf{E}_N^2\right)^{\mathcal{H}} = \left(\mathbf{E}_N^{\mathcal{H}}\right)^2$. ■

A number of properties follow directly from Theorem B.5.

Corollary B.1 *Let* $\mathbf{E}_N$, $\boldsymbol{\kappa}_N$, *and* $\mathbf{I}_N$ *be the* $N \times N$ *Fourier, flip, and identity matrices. Then*

i. $\mathbf{E}_N\boldsymbol{\kappa}_N = \boldsymbol{\kappa}_N\mathbf{E}_N$;

ii. $\boldsymbol{\kappa}_N^2 = \mathbf{I}_N \quad \text{or} \quad \boldsymbol{\kappa}_N = \sqrt{\mathbf{I}_N}$;

iii. $\mathbf{E}_N^4 = \mathbf{I}_N \quad \text{or} \quad \mathbf{E}_N = \sqrt[4]{\mathbf{I}_N}$. □

Propterty (i) says that the flip and Fourier matrices commute or, since $\mathbf{E}_N$ is unitary, that $\boldsymbol{\kappa}_N$ is invariant under a unitary transformation with respect to $\mathbf{E}_N$. Hence $\boldsymbol{\kappa}_N$ is not diagonalizable by $\mathbf{E}_N$. Properties (ii) and (iii) give alternative definitions of the flip and Fourier matrices, respectively. Moreover, since the (possibly fractional) power of a diagonal matrix can be obtained by raising each diagonal element of that matrix to the power in question, if follows that the eigenvalues of $\boldsymbol{\kappa}_N$ are ± 1 and those of $\mathbf{E}_N$ are ± 1 and $\pm j$, each with the appropriate multiplicities.

B.4.3 Diagonalization of the Cyclic Forward Shift Matrix

In this section it is shown that the Fourier matrix diagonalizes the cyclic forward shift matrix. For this purpose, it is convenient to introduce diagonal matrix

$$\boldsymbol{\Omega}_N = \text{diag}\left(1, w_N, w_N^2, \ldots, w_N^{N-1}\right), \tag{B.14}$$

which has as its diagonal elements the distinct N^{th} roots of unity.

Theorem B.6 $\mathbf{E}_N^{\mathcal{H}} \boldsymbol{\sigma}_N \mathbf{E}_N = \boldsymbol{\Omega}_N$. □

PROOF. For $1 \leq i, k \leq N$ the (i,k) entry of $\mathbf{E}_N \boldsymbol{\Omega}_N \mathbf{E}_N^{\mathcal{H}}$ is given by

$$\begin{aligned}
\left(\mathbf{E}_N \boldsymbol{\Omega}_N \mathbf{E}_N^{\mathcal{H}}\right)_{ik} &= \sum_{r=1}^{N}\sum_{p=1}^{N} (\mathbf{E}_N)_{ip} (\boldsymbol{\Omega}_N)_{pr} (\mathbf{E}_N^{\mathcal{H}})_{rk} \\
&= \sum_{r=1}^{N}\sum_{p=1}^{N} \frac{1}{\sqrt{N}} w_N^{(i-1)(p-1)} \delta_{pr} w_N^{(r-1)} \frac{1}{\sqrt{N}} w_N^{-(r-1)(k-1)} \\
&= \frac{1}{N} \sum_{r=1}^{N} w_N^{(i-1)(r-1)} w_N^{(r-1)} w^{-(r-1)(k-1)} \\
&= \frac{1}{N} \sum_{r=1}^{N} w_N^{(r-1)(i-k+1)} \\
&= \frac{1}{N} \sum_{r=0}^{N-1} w_N^{r(i-k+1)} \\
&= (\boldsymbol{\sigma}_N)_{ik}, \qquad \text{(from Eqn. (B.13c))}
\end{aligned}$$

from which it follows that $\mathbf{E}_N \boldsymbol{\Omega}_N \mathbf{E}_N^{\mathcal{H}} = \boldsymbol{\sigma}_N$. The desired result follows by multiplying from the right by $\mathbf{E}_N$ and multiplying from the left by $\mathbf{E}_N^{\mathcal{H}}$. ■

Theorem B.6 implies that $\boldsymbol{\sigma}_N$ is unitarily similar to a diagonal matrix whose diagonal elements are the nonnegative integer powers of the primitive N^{th} root of unity. Since the eigenvalues of a matrix are preserved under such a transformation (this is guaranteed by Theorem A.1), it follows that

$$\lambda(\boldsymbol{\sigma}_N) = \{1, w_N, w_N^2, \ldots, w_N^{N-1}\},$$

where $\lambda(\cdot)$ denotes the matrix spectrum. The eigenvectors of $\boldsymbol{\sigma}_N$ are the linearly independent columns of $\mathbf{E}_N = [\mathbf{e}_1, \mathbf{e}_2, \ldots, \mathbf{e}_N]$, which are given by Equation (B.12).[1] In light of Corollary A.1, we have the following result.

Corollary B.2 $\mathbf{E}_N^{\mathcal{H}} \boldsymbol{\sigma}_N^k \mathbf{E}_N = \boldsymbol{\Omega}_N^k$ *for any* $k \in \mathbb{Z}_+$. □

B.4.4 Diagonalization of a Circulant

It will be convenient to define

$$\varrho(\mathbf{t}, \boldsymbol{\tau}) = \sum_{k=1}^{N} \mathbf{t}^{k-1} \otimes \boldsymbol{\tau}, \tag{B.15}$$

where $\mathbf{t}$ and $\boldsymbol{\tau}$ are arbitrary square matrices. Then the general circulant and block circulant matrices given by Equation (B.4) and Equation (B.6) can be represented by

$$\varrho(\boldsymbol{\sigma}_N, c_k) = \sum_{k=1}^{N} \boldsymbol{\sigma}_N^{k-1} c_k = \operatorname{circ}(c_1, c_2, \ldots, c_N), \tag{B.16a}$$

$$\varrho(\boldsymbol{\sigma}_N, \mathbf{C}_k) = \sum_{k=1}^{N} \boldsymbol{\sigma}_N^{k-1} \otimes \mathbf{C}_k = \operatorname{circ}(\mathbf{C}_1, \mathbf{C}_2, \ldots, \mathbf{C}_N), \tag{B.16b}$$

respectively. What is meant by the notation $\varrho(\boldsymbol{\sigma}_N, c_k)$, for example, is to substitute $\mathbf{t}$ with $\boldsymbol{\sigma}_N$ and $\boldsymbol{\tau}$ with c_k in Equation (B.15) and then perform the summation *observing any indices* k *introduced by the substitution.* Note also that

$$\varrho(\boldsymbol{\Omega}_N, \boldsymbol{\tau}) = \operatorname*{diag}_{i=1,\ldots,N} \left(\varrho\left(w_N^{i-1}, \boldsymbol{\tau} \right) \right) = \operatorname*{diag}_{i=1,\ldots,N} \left(\sum_{k=1}^{N} \boldsymbol{\tau} w_N^{(k-1)(i-1)} \right), \tag{B.17}$$

which is diagonal (resp. block diagonal) when $\boldsymbol{\tau}$ is a scalar (resp. matrix).

Theorem B.7 *Let* $\mathbf{C} \in \mathscr{C}_N$ *have generating elements* $c_1, c_2, \ldots, c_N$. *Then*

$$\mathbf{E}_N^{\mathcal{H}} \mathbf{C} \mathbf{E}_N = \begin{bmatrix} \lambda_1 & & & 0 \\ & \lambda_2 & & \\ & & \ddots & \\ 0 & & & \lambda_N \end{bmatrix}$$

[1] In fact, *all* circulant matrices share the same eigenvectors $\mathbf{e}_k$, which is shown in the next section.

is a diagonal matrix, where

$$\lambda_i = \varrho\Big(w_N^{i-1}, c_k\Big) = \sum_{k=1}^{N} c_k w_N^{(k-1)(i-1)}, \qquad i = 1, \ldots, N$$

are its diagonal elements. □

PROOF. Consider the representation

$$\begin{aligned}
\mathbf{C} &= \varrho(\boldsymbol{\sigma}_N, c_k) && \text{(from Eqn. B.16a)} \\
&= \varrho\Big(\mathbf{E}_N \boldsymbol{\Omega}_N \mathbf{E}_N^{\mathcal{H}}, c_k\Big) && \text{(from Thm. B.6)} \\
&= \mathbf{E}_N \varrho(\boldsymbol{\Omega}_N, c_k)\, \mathbf{E}_N^{\mathcal{H}}. && \text{(from Thm. A.2, Thm. B.4)}
\end{aligned}$$

Thus $\mathbf{E}_N^{\mathcal{H}} \mathbf{C} \mathbf{E}_N = \varrho(\boldsymbol{\Omega}_N, c_k)$, where the diagonal matrix $\varrho(\boldsymbol{\Omega}_N, c_k) = \underset{i=1,\ldots,N}{\text{diag}}\,(\lambda_i)$ follows from Equation (B.17). ■

Remarks

1. The Fourier matrix $\mathbf{E}_N$ diagonalizes *any* circulant matrix.
2. $\mathbf{E}_N^{\mathcal{H}} \mathbf{C} \mathbf{E}_N$ is a unitary transformation, and hence preserves the eigenvalues of $\mathbf{C}$. Thus λ_i $(i = 1, \ldots, N)$ are the eigenvalues of $\mathbf{C}$.
3. All cirulants share the same linearly independent eigenvectors (the columns of the Fourier matrix $\mathbf{E}_N$), which are given by Equation (B.12).

The eigenvalues of a matrix $\mathbf{C} \in \mathscr{SC}_N$ with generating elements $c_1, c_2, \ldots, c_N$ are given by

$$\lambda_i = \begin{cases} c_1 + 2\displaystyle\sum_{k=2}^{N/2} c_k \cos\Big(\frac{2\pi(k-1)(i-1)}{N}\Big) + (-1)^{i-1} c_{\frac{N+2}{2}}, & N \text{ even} \\ c_1 + 2\displaystyle\sum_{k=2}^{(N+1)/2} c_k \cos\Big(\frac{2\pi(k-1)(i-1)}{N}\Big), & N \text{ odd} \end{cases} \tag{B.18}$$

a result that is proved in [36]. In this case there are repeated eigenvalues due to the presence of the cosine term. The eigenvalue λ_1 is distinct, but the remaining eigenvalues $\lambda_i = \lambda_{N+2-i}$ appear in repeated pairs. However, when N is even $\lambda_{\frac{N+2}{2}}$ is also distinct.

Example B.6 *Let* $\mathbf{C} = \operatorname{circ}(4, -1, 0, -1)$. *Then*

$$\begin{aligned}
\mathbf{E}_4^{\mathcal{H}}\mathbf{C}\mathbf{E}_4 &= \frac{1}{\sqrt{4}}\begin{bmatrix} 1 & 1 & 1 & 1 \\ 1 & -j & -1 & j \\ 1 & -1 & 1 & -1 \\ 1 & j & -1 & -j \end{bmatrix}\begin{bmatrix} 4 & -1 & 0 & -1 \\ -1 & 4 & -1 & 0 \\ 0 & -1 & 4 & -1 \\ -1 & 0 & -1 & 4 \end{bmatrix}\frac{1}{\sqrt{4}}\begin{bmatrix} 1 & 1 & 1 & 1 \\ 1 & j & -1 & -j \\ 1 & -1 & 1 & -1 \\ 1 & -j & -1 & j \end{bmatrix} \\
&= \frac{1}{\sqrt{4}}\begin{bmatrix} 1 & 1 & 1 & 1 \\ 1 & -j & -1 & j \\ 1 & -1 & 1 & -1 \\ 1 & j & -1 & -j \end{bmatrix}\begin{bmatrix} 1 & 2 & 3 & 2 \\ 1 & 2j & -3 & -2j \\ 1 & -2 & 3 & -2 \\ 1 & -2j & -3 & 2j \end{bmatrix} \\
&= \operatorname{diag}(2, 4, 6, 4).
\end{aligned}$$

Hence the eigenvalues of $\mathbf{C}$ *are* $2, 4, 6, 4$. *Since* $\mathbf{C} \in \mathscr{SC}_4$, *these can be verified using Equation* (B.18) *for* $N = 4$, *which yields*

$$\lambda_i = 4 - 2\cos\frac{\pi}{2}(i-1)$$

for $i = 1, \ldots, 4$. ∎

The determinant of a circulant matrix $\mathbf{C} = \operatorname{circ}(c_1, c_2, \ldots, c_N)$ is simply the product of its eigenvalues and is given by

$$\det \mathbf{C} = \prod_{i=1}^{N} \lambda_i = \prod_{i=1}^{N} \sum_{k=1}^{N} c_k w_N^{(k-1)(i-1)}, \tag{B.19}$$

where the eigenvalues λ_i are defined in Theorem B.7 or by Equation (B.18) if $\mathbf{C}$ is also symmetric.

B.4.5 Block Diagonalization of a Block Circulant

Theorem B.7 can be generalized to handle block circulants.

Theorem B.8 *Let* $\mathbf{C} \in \mathscr{BC}_{M,N}$ *and denote its* $M \times M$ *generating matrices by* $\mathbf{C}_1, \mathbf{C}_2, \ldots, \mathbf{C}_N$. *Then*

$$(\mathbf{E}_N^{\mathcal{H}} \otimes \mathbf{I}_M)\mathbf{C}(\mathbf{E}_N \otimes \mathbf{I}_M) = \begin{bmatrix} \mathbf{\Lambda}_1 & & & \mathbf{0} \\ & \mathbf{\Lambda}_2 & & \\ & & \ddots & \\ \mathbf{0} & & & \mathbf{\Lambda}_N \end{bmatrix}$$

is a block diagonal matrix, where

$$\mathbf{\Lambda}_i = \varrho\Big(w_N^{i-1}, \mathbf{C}_k\Big) = \sum_{k=1}^{N} \mathbf{C}_k w_N^{(k-1)(i-1)}, \qquad i = 1, \ldots, N$$

are its $M \times M$ diagonal blocks. □

PROOF. Consider the representation

$$\begin{aligned}
\mathbf{C} &= \sum_{k=1}^{N} \boldsymbol{\sigma}_N^{k-1} \otimes \mathbf{C}_k && \text{(from Eqn. B.16b)} \\
&= \sum_{k=1}^{N} (\mathbf{E}_N \mathbf{\Omega}_N^{k-1} \mathbf{E}_N^{\mathcal{H}}) \otimes \mathbf{C}_k && \text{(from Cor. B.2)} \\
&= \sum_{k=1}^{N} (\mathbf{E}_N \otimes \mathbf{I}_M) \left(\mathbf{\Omega}_N^{k-1} \otimes \mathbf{C}_k\right) (\mathbf{E}_N^{\mathcal{H}} \otimes \mathbf{I}_M) && \text{(from Eqn. A.4)} \\
&= (\mathbf{E}_N \otimes \mathbf{I}_M) \varrho(\mathbf{\Omega}_N, \mathbf{C}_k) (\mathbf{E}_N^{\mathcal{H}} \otimes \mathbf{I}_M), && \text{(from Eqn. B.15)}
\end{aligned}$$

where the block diagonal matrix

$$\varrho(\mathbf{\Omega}_N, \mathbf{C}_k) = \operatorname*{diag}_{i=1,\ldots,N} (\mathbf{\Lambda}_i)$$

follows from Equation (B.17). Since $(\mathbf{E}_N \otimes \mathbf{I}_M)$ is unitary the desired result follows by multiplying from the right by $(\mathbf{E}_N \otimes \mathbf{I}_M)$ and from the left by $(\mathbf{E}_N^{\mathcal{H}} \otimes \mathbf{I}_M) = (\mathbf{E}_N \otimes \mathbf{I}_M)^{\mathcal{H}}$. ■

Remarks

1. The unitary matrix $\mathbf{E}_N \otimes \mathbf{I}_M$ can reduce *any* $NM \times NM$ block circulant matrix with $M \times M$ blocks to a block diagonal matrix with $M \times M$ diagonal blocks.

2. $(\mathbf{E}_N^{\mathcal{H}} \otimes \mathbf{I}_M)\mathbf{C}(\mathbf{E}_N \otimes \mathbf{I}_M)$ is a unitary transformation, and hence preserves the eigenvalues of $\mathbf{C}$, which are the eigenvalues of the N, $M \times M$ matrices $\mathbf{\Lambda}_i$.

3. If $\mathbf{v}_i$ is an eigenvector of the i^{th} eigensystem $\mathbf{\Lambda}_i$, then the corresponding eigenvector of $\mathbf{C}$ is $\mathbf{u}_i = \mathbf{e}_i \otimes \mathbf{v}_i$.

Example B.7 *Consider the matrix* $\mathbf{C} = \text{circ}(\mathbf{A}, \mathbf{B}, \mathbf{0}, \mathbf{B})$ *from Example B.5. It can be block diagonalized via the transformation*

$$(\mathbf{E}_4^{\mathcal{H}} \otimes \mathbf{I}_2)\mathbf{C}(\mathbf{E}_4 \otimes \mathbf{I}_2) = \left[\begin{array}{cc:cc:cc:cc} 0 & -1 & 0 & 0 & 0 & 0 & 0 & 0 \\ -1 & 0 & 0 & 0 & 0 & 0 & 0 & 0 \\ \hdashline 0 & 0 & 2 & -1 & 0 & 0 & 0 & 0 \\ 0 & 0 & -1 & 2 & 0 & 0 & 0 & 0 \\ \hdashline 0 & 0 & 0 & 0 & 4 & -1 & 0 & 0 \\ 0 & 0 & 0 & 0 & -1 & 4 & 0 & 0 \\ \hdashline 0 & 0 & 0 & 0 & 0 & 0 & 2 & -1 \\ 0 & 0 & 0 & 0 & 0 & 0 & -1 & 2 \end{array}\right]$$

$$= \text{diag}(\mathbf{\Lambda}_1, \mathbf{\Lambda}_2, \mathbf{\Lambda}_3, \mathbf{\Lambda}_4),$$

from which the eigenvalues can be obtained from the 2×2 *matrices* $\mathbf{\Lambda}_i$ *for* $i = 1, \ldots, 4$. *In particular,* $\lambda(\mathbf{\Lambda}_1) = \{-1, 1\}$, $\lambda(\mathbf{\Lambda}_3) = \{3, 5\}$, *and* $\lambda(\mathbf{\Lambda}_2) = \lambda(\mathbf{\Lambda}_4) = \{1, 3\}$. ◻

B.4.6 Some Generalizations

Let $\mathbf{C} \in \mathscr{BC}_{M,N}$ and denote its generating matrices by $\mathbf{C}_1, \mathbf{C}_2, \ldots, \mathbf{C}_N$. Then if $(\cdot)^*$ and $(\cdot)^{\#}$ denote arbitrary matrix operations and for any matrices $\mathbf{A} \in \mathbb{C}^{N \times N}$ and $\mathbf{B} \in \mathbb{C}^{M \times M}$,

$$\begin{aligned}(\mathbf{A}^* \otimes \mathbf{B}^{\#})\mathbf{C}(\mathbf{A} \otimes \mathbf{B}) &= (\mathbf{A}^* \otimes \mathbf{B}^{\#}) \left[\sum_{k=1}^{N} \boldsymbol{\sigma}_N^{k-1} \otimes \mathbf{C}_k\right] (\mathbf{A} \otimes \mathbf{B}) \\ &= \sum_{k=1}^{N} \left[(\mathbf{A}^* \boldsymbol{\sigma}_N^{k-1}) \otimes (\mathbf{B}^{\#} \mathbf{C}_k)\right] (\mathbf{A} \otimes \mathbf{B}) \\ &= \sum_{k=1}^{N} (\mathbf{A}^* \boldsymbol{\sigma}_N^{k-1} \mathbf{A}) \otimes (\mathbf{B}^{\#} \mathbf{C}_k \mathbf{B}), \end{aligned} \tag{B.20}$$

where Equation (A.4) has been employed. The importance of this result is that $\mathbf{C}$ can be decomposed into a summation of direct products of two separate equivalence transformations, one that operates on $\boldsymbol{\sigma}_N^{k-1}$ and the other on $\mathbf{C}_k$. This decomposition justifies the diagonalizing matrix employed in Theorem B.8 and it also motivates some generalizations.

In light of Theorem B.6 together with Corollary A.1, it is clear that the choice of $\mathbf{A} = \mathbf{E}_N$ and $(\cdot)^* = (\cdot)^{\mathcal{H}}$ accomplishes block diagonaliztion of a matrix $\mathbf{C} \in \mathscr{BC}_{M,N}$.

Then if one chooses $\mathbf{B} = \mathbf{I}_M$, the appropriate diagonalizing matrix to block decouple $\mathbf{C}$ *without operating on its generating matrices* is $\mathbf{E}_N \otimes \mathbf{I}_M$. However, if $\mathbf{B}$ and $(\cdot)^{\#}$ are kept general, we have the following result.

Theorem B.9 *Let $\mathbf{C} \in \mathscr{BC}_{M,N}$ have $M \times M$ generating matrices $\mathbf{C}_1, \mathbf{C}_2, \ldots, \mathbf{C}_N$. Then for an arbitrary matrix $\mathbf{B} \in \mathbb{C}^{M \times M}$ and operator $(\cdot)^{\#}$*

$$(\mathbf{E}_N^{\mathcal{H}} \otimes \mathbf{B}^{\#})\mathbf{C}(\mathbf{E}_N \otimes \mathbf{B}) = \begin{bmatrix} \boldsymbol{\Psi}_1 & & & \mathbf{0} \\ & \boldsymbol{\Psi}_2 & & \\ & & \ddots & \\ \mathbf{0} & & & \boldsymbol{\Psi}_N \end{bmatrix}$$

is a block diagonal matrix, where

$$\boldsymbol{\Psi}_i = \varrho\left(w_N^{i-1}, \mathbf{B}^{\#}\mathbf{C}_k\mathbf{B}\right) = \sum_{k=1}^{N} \mathbf{B}^{\#}\mathbf{C}_k\mathbf{B}w_N^{(k-1)(i-1)}, \qquad i = 1, \ldots, N$$

are its $M \times M$ diagonal blocks. □

This result is useful if there exists an equivalence transformation $\mathbf{B}^{\#}\mathbf{C}_k\mathbf{B}$ that simplifies each of the generating matrices. For example, if each $\mathbf{C}_k$ is a circulant of type M then the additional choice of $\mathbf{B} = \mathbf{E}_M$ and $(\cdot)^{\#} = (\cdot)^{\mathcal{H}}$ fully diagonalizes a block circulant matrix $\mathbf{C} \in \mathscr{BC}_{N,M}$ with circulant blocks.

Corollary B.3 *Let $\mathbf{C} \in \mathscr{BC}_{M,N}$ have generating matrices $\mathbf{C}_1, \mathbf{C}_2, \ldots, \mathbf{C}_N \in \mathscr{C}_M$ and denote the generating elements of each $\mathbf{C}_i$ by $c_1^{(i)}, c_2^{(i)}, \ldots, c_M^{(i)}$. Then*

$$(\mathbf{E}_N^{\mathcal{H}} \otimes \mathbf{E}_M^{\mathcal{H}})\mathbf{C}(\mathbf{E}_N \otimes \mathbf{E}_M) = \underset{i=1,\ldots,N}{\operatorname{diag}} \begin{bmatrix} \lambda_1^{(i)} & & & 0 \\ & \lambda_2^{(i)} & & \\ & & \ddots & \\ 0 & & & \lambda_M^{(i)} \end{bmatrix}$$

is a diagonal matrix, where

$$\lambda_p^{(i)} = \sum_{k=1}^{N} \sum_{l=1}^{M} c_l^{(k)} w_M^{(l-1)(p-1)} w_N^{(k-1)(i-1)}$$

is the p^{th} diagonal element of the i^{th} diagonal block. □

Example B.8 *Reconsider the matrix* $\mathbf{C} = \text{circ}\,(\mathbf{A}, \mathbf{B}, \mathbf{0}, \mathbf{B})$ *from Example B.5. Since* $\mathbf{A}, \mathbf{B} \in \mathscr{C}_2$ *it can be diagonalized via the transformation*

$$(\mathbf{E}_4^{\mathcal{H}} \otimes \mathbf{E}_2^{\mathcal{H}})\mathbf{C}(\mathbf{E}_4 \otimes \mathbf{E}_2) = \left[\begin{array}{cc:cc:cc:cc} -1 & 0 & 0 & 0 & 0 & 0 & 0 & 0 \\ 0 & 1 & 0 & 0 & 0 & 0 & 0 & 0 \\ \hdashline 0 & 0 & 1 & 0 & 0 & 0 & 0 & 0 \\ 0 & 0 & 0 & 3 & 0 & 0 & 0 & 0 \\ \hdashline 0 & 0 & 0 & 0 & 3 & 0 & 0 & 0 \\ 0 & 0 & 0 & 0 & 0 & 5 & 0 & 0 \\ \hdashline 0 & 0 & 0 & 0 & 0 & 0 & 1 & 0 \\ 0 & 0 & 0 & 0 & 0 & 0 & 0 & 3 \end{array}\right],$$

from which is follows that $\lambda(\mathbf{C}) = \{-1, 1, 1, 3, 3, 5, 1, 3\}$. ∎

APPENDIX C

Noninteger Engine Order Excitation

It is well-known that a perfectly cyclic system (i.e., one without parameter uncertainty, or mistuning) under engine order excitation will respond in one and *only* one mode corresponding to $p = n \bmod N + 1$, where n is the order of the excitation. For a bladed disk assembly in a jet engine the excitation order corresponds to a problematic harmonic in an expansion of the axial gas pressure field, and is therefore a positive integer. However, *noninteger* engine order may occur in other applications and in what follows we briefly consider the general case of $n \in \mathbb{R}_+$. Then orthogonality between the normal modes and system forcing vector generically breaks down and this gives rise to additional system resonances.

Consider the prototypical cyclic system of Section 2.4 under engine order excitation. In the steady-state it responds according to Equation (2.34), which indicates that the total forced response is simply a superposition of modal responses. For the case of $n \in \mathbb{Z}_+$ only mode $p = n \bmod N + 1$ survives, which follows from the orthogonality condition given by Equation (2.35), that is,[1]

$$\mathbf{e}_p^{\mathcal{H}} \mathbf{f} = \frac{f}{\sqrt{N}} \sum_{k=1}^{N} w_N^{(k-1)(n+1-p)} \qquad (n \in \mathbb{R}_+) \qquad \text{(C.1)}$$

$$= \begin{cases} \sqrt{N} f, & n + 1 - p = mN \\ 0, & \text{otherwise} \end{cases} \qquad (n \in \mathbb{Z}_+) \qquad \text{(C.2)}$$

[1]The result holds even for $n \leq 0$, but physically we restrict $n > 0$.

where m is an arbitrary integer. (This result follows from Theorem B.3 on page 192.) However, if the engine order is noninteger such that $n \in \mathbb{R}_+/\mathbb{Z}_+$ Equation (C.2) does not hold and therefore *every* system mode contributes to the total response, which is given by Equation (2.34) by replacing the p^{th} model forcing term $\mathbf{e}_p^{\mathcal{H}}\mathbf{f}$ with the right hand side Equation (C.1). Correspondingly, for a given engine order there are N system resonances and these occur whenever the excitation frequency matches a natural frequency, that is, when $n\sigma = \bar{\omega}_p$, where the p^{th} eigenfrequency is defined by Equation (2.38). Thus in addition to the "principle resonance" corresponding to $p = n \bmod N + 1$, there are $(N-1)/2$ (resp. $N/2$) resonances due to the noninteger excitation if N is odd (resp. even). An example is shown in Figure C.1 for a system with $N = 10$ sectors and for various engine orders $n \in \mathbb{R}_+$. The additional resonances can be clearly observed, and they become more pronounced for larger deviations of the engine order away from the integer value $n = 3$.

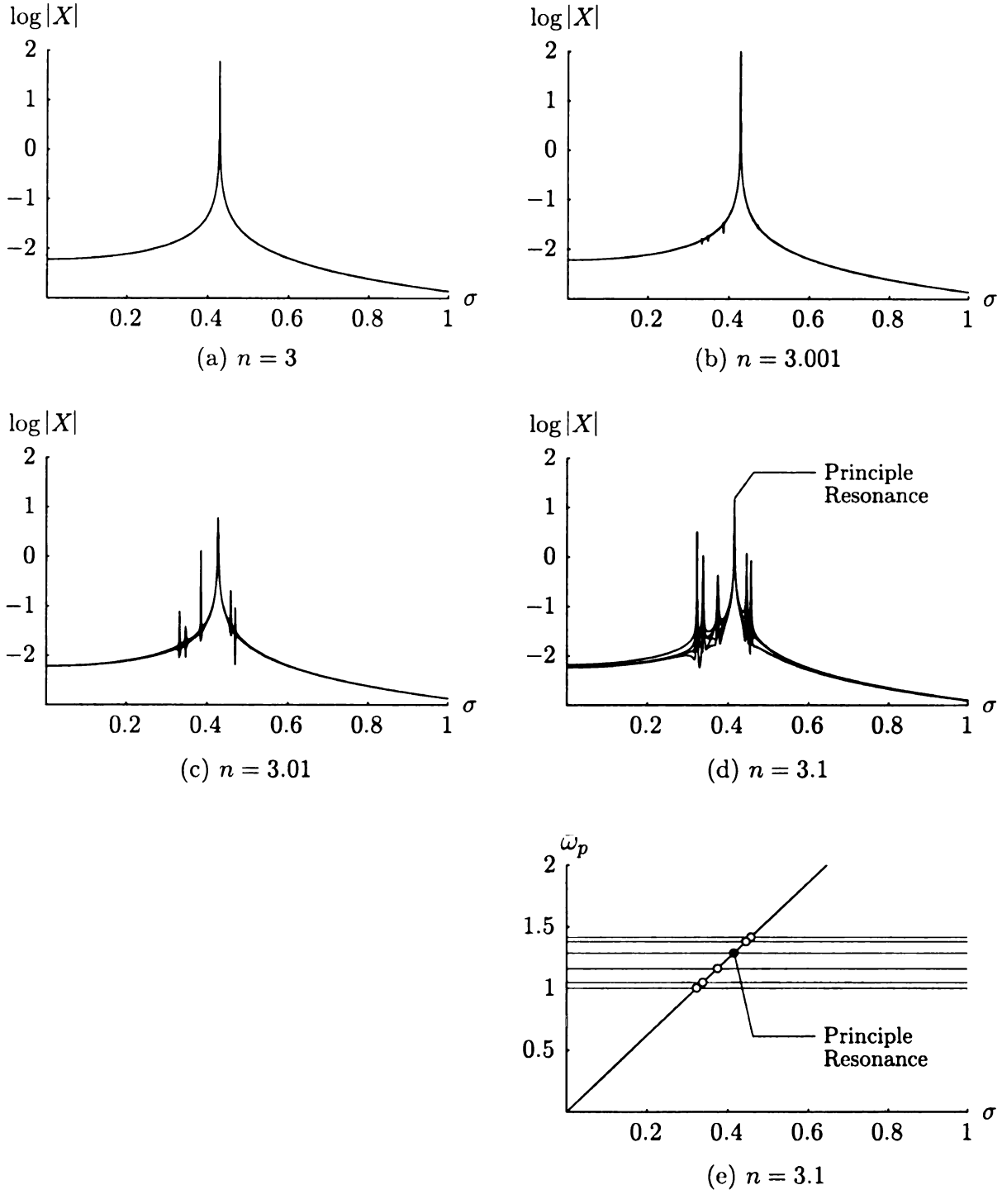

Figure C.1. Frequency response curves for the system shown in Figure 2.4 on page 23 for $N = 10$, $\nu = 0.5$, and $f = 0.01$: (a) $n = 3$; (b) $n = 3.001$; (c) $n = 3.01$; and (d) $n = 3.1$; and (e) corresponding Campbell diagram for $n = 3.1$. In (d) and (e) the principle resonance corresponding to $n + 1 = 4.1$ is indicated by the black circle.

APPENDIX D

The Critical Linear Detuning and Tuning Order

The critical linear absorber tuning order $\hat{n}$ is defined implicitly by Equation (4.36) and represents the limiting slope of the natural frequencies $\bar{\omega}_2^{(i)}$ in the frequency versus σ curves of Figure 4.5. It is convenient to express $\hat{n}$ in terms of the absorber tuning order $\tilde{n}$, which is introduced via Equation (4.39). Then

$$\hat{n}(\tilde{n}) = \sqrt{\frac{\hat{a}_1\mu + \hat{a}_0 + \sqrt{\hat{a}_1^2\mu^2 + \hat{b}_1\mu + \hat{b}_0^2}}{2\tilde{n}^2}}, \tag{D.1}$$

where

$$\left.\begin{aligned}
\hat{a}_0 &= \tilde{n}^2(\tilde{n}^2 + \delta) \\
\hat{b}_0 &= \tilde{n}^2(\tilde{n}^2 - \delta) \\
\hat{a}_1 &= \alpha^2(\tilde{n}^2 + 1)\left(\tilde{n}^2 + \tfrac{\delta}{\alpha} + 1\right) \\
\hat{b}_1 &= 2\alpha^2\tilde{n}^2(\tilde{n}^2 + 1)\left((\tilde{n}^2 + 1)(\tilde{n}^2 + \delta) - \tfrac{\delta}{\alpha}(\tilde{n}^2 - \delta)\right)
\end{aligned}\right\}.$$

The critical absorber undertuning can be obtained by replacing $\tilde{n}$ with $n(1 + \beta)$ in Equation (D.1), setting $\hat{n} = n$, and then solving for $\beta = \beta_{\mathrm{cr}}$. Then β_{cr} is given implicitly by

$$(1 + \beta_{\mathrm{cr}})^2 = \frac{a_1\mu + c_0 + \sqrt{b_2\mu^2 + b_1\mu + c_0^2}}{c_1\mu + 2c_0}, \tag{D.2}$$

where

$$\left.\begin{aligned} a_1 &= \alpha^2\left(\tfrac{\delta}{\alpha} - n^2\left(2 + \tfrac{\delta}{\alpha}\right)\right) \\ b_1 &= -2\alpha^2 n^2(n^2 - \delta)(n^2 + 1)\left(2 + \tfrac{\delta}{\alpha}\right) \\ b_2 &= \alpha^2\delta^2(n^2 + 1)^2 \\ c_0 &= n^2(n^2 - \delta) \\ c_1 &= 2\alpha^2 n^2\left(n^2 - \tfrac{\delta}{\alpha}\right) \end{aligned}\right\}.$$

Note that when $\mu = 0$, the right hand side of Equation (D.2) is unity, which implies $\beta_{\text{cr}} = 0$ (i.e., the no-resonance gap vanishes), and the same is true when $\alpha = 0$ (in which case $a_1 = b_1 = b_2 = c_1 \equiv 0$, but $c_0 \neq 0$).

It is clear from Figure 4.9 that changes in β_{cr} due to parameter variations decrease for increasing engine order. In the limit as $n \to \infty$ Equation (D.2) reduces to

$$(1 + \beta_{\text{cr}})^2 = \frac{1}{1 + \alpha^2\mu}, \qquad (n \to \infty) \tag{D.3}$$

which is shown by the dashed line in Figure 4.9d. It depends only on α and μ and approximates β_{cr} to within 3% of its limiting large-n value for $n \geq 10$.

APPENDIX E

Averaging: The Usual Approach

E.1 Introduction

In the process of averaging it is customary to expand all parameters involving ε and to keep only $\mathcal{O}(\varepsilon)$ terms in the resulting expressions. This amounts to replacing $\tilde{n}$ with n and also σ with the *constant* $\sigma_r = 1/\sqrt{n^2 - \delta}$, which is the resonant rotor speed of an isolated blade without an absorber. In what follows, we carry out the averaging for the *isolated* nonlinear system of Chapter 5 in this way and show that the results are adequate for large linear under- or overtuning of the absorbers but they are completely unsatisfactory within the no-resonance zone (precisely where the results are of the most interest) due to the latter substitution. The aim of this appendix is to document the rather significant difference in the averaged models obtained via the usual approach employed below and by means of the slightly modified approach employed in the nonlinear analysis in Chapter 5.

We begin by defining a detuning scheme (different from that employed in Chapter 5) and then present the averaged equations in both polar and Cartesian forms. The appendix closes with some representative frequency response curves and a short discussion.

E.2 Detuning Scheme

In order to investigate the nonlinear dynamics near perfect linear tuning and close to the rotor speeds of interest, we take

$$\tilde{n} = n(1 + \varepsilon\lambda), \tag{E.1a}$$

$$\sigma = \sigma_r(1 + \varepsilon\Delta), \tag{E.1b}$$

where λ serves as the linear order detuning parameter and Δ plays the role of the rotor speed. Then the order detuning parameters are related by $\beta = \varepsilon\lambda$, which is clear by comparing Equation (E.1a) to Equation (4.44). It should be pointed out that the detuning scheme adopted here is slightly different than the one employed in Chapter 5, that is, Equation (5.9). (Equation (E.1) was the original detuning used by the author before the improved method of averaging was adopted.) This does not, however, preclude qualitative comparisons between the results of the two approaches.

Next the averaged equations are derived in polar and Cartesian forms.

E.3 The Averaged Equations

The nonlinear analysis is carried out exactly as it was done in Section 5.2.4 except that all appearances of σ are replaced by the constant σ_r and, as we shall see, this gives rise to a significantly less accurate model, one that serves as a benchmark for the modeling approach employed in Chapter 5.

Under the detuning scheme defined in Section E.2, Equation (5.8) on page 127 reduces to[1]

$$\left.\begin{aligned} \bar{\omega}_{11}^2 - n^2\sigma^2 &= -\varepsilon 2\Delta + \mathcal{O}(\varepsilon^2) \\ \bar{\omega}_{22}^2 - n^2\sigma^2 &= \varepsilon\frac{2\lambda n^2}{n^2 - \delta} + \mathcal{O}(\varepsilon^2) \end{aligned}\right\}. \tag{E.2}$$

[1]For the detuning employed in Chapter 5 the $\mathcal{O}(\varepsilon)$ terms are $-\varepsilon\Delta$ and $\varepsilon\lambda\sigma^2$.

Table E.1. Shorthand notation.

$\bar{\varepsilon} = \varepsilon/2n\sqrt{n^2-\delta}$	$\bar{\Delta} = 2(n^2-\delta)\Delta$	$\bar{\xi}_b = n\sqrt{n^2-\delta}\,\hat{\xi}_b$	$\bar{f} = (n^2-\delta)\hat{f}$
$\bar{\alpha} = (n^2+1)\alpha$	$\bar{\lambda} = 2n^2\lambda$	$\bar{\xi}_{\bar{a}} = n\sqrt{n^2-\delta}\,\hat{\xi}_{\bar{a}}$	

After the appropriate substitutions are made, Equation (5.6) is averaged over one period $T = 2\pi/n\sigma$ and the shorthand notation given in Table E.1 is introduced.[2] Then if $\mathbf{v} = (\bar{u}, \bar{\varrho}, \bar{v}, \bar{\varsigma})^T$ the result is

$$(\bar{u}', \bar{u}\bar{\varrho}', \bar{v}', \bar{v}\bar{\varsigma}')^T = \bar{\varepsilon}\,\mathbf{G}(\mathbf{v}) + \mathcal{O}(\bar{\varepsilon}^{3/2}), \tag{E.3}$$

where

$$\left.\begin{aligned} G_1(\mathbf{v}) &= -\bar{\alpha}\bar{v}\sin(\bar{\varrho}-\bar{\varsigma}) - \bar{\xi}_b\bar{u} - \bar{f}\sin\bar{\varrho} \\ G_2(\mathbf{v}) &= -\bar{\alpha}\bar{v}\cos(\bar{\varrho}-\bar{\varsigma}) - \bar{\Delta}\bar{u} - \bar{f}\cos\bar{\varrho} \\ G_3(\mathbf{v}) &= +\bar{\alpha}\bar{u}\sin(\bar{\varrho}-\bar{\varsigma}) - \bar{\xi}_{\bar{a}}\bar{v} \\ G_4(\mathbf{v}) &= -\bar{\alpha}\bar{u}\cos(\bar{\varrho}-\bar{\varsigma}) + \bar{\lambda}\bar{v} + \tfrac{3}{4}\eta\bar{v}^3 \end{aligned}\right\} \tag{E.4}$$

are the elements of the vector $\mathbf{G}$. In Equation (E.4), note that the rotor speed appears in $G_2(\mathbf{v})$ only (implicitly via the shorthand detuning parameter $\bar{\Delta}$). However, in the model employed in Chapter 5, the rotor speed appears in each $G_p(\mathbf{v})$ $(p = 1, \ldots, 4)$. It is this absence of the rotor speed that gives rise to less accurate results.

The corresponding Cartesian form of the averaged equations is

$$\mathbf{w}' = \bar{\varepsilon}\,\mathbf{P}(\mathbf{w}) + \mathcal{O}(\bar{\varepsilon}^{3/2}), \tag{E.5}$$

where $\mathbf{w} = (A, B, C, D)^T$ and the functions

$$\left.\begin{aligned} P_1(\mathbf{w}) &= -\bar{\alpha}D - \bar{\Delta}B - \bar{\xi}_b A \\ P_2(\mathbf{w}) &= +\bar{\alpha}C + \bar{\Delta}A - \bar{\xi}_b B + \bar{f} \\ P_3(\mathbf{w}) &= -\bar{\alpha}B + \bar{\lambda}D - \bar{\xi}_{\bar{a}}C + \tfrac{3}{4}\eta(D^3 + C^2D) \\ P_4(\mathbf{w}) &= +\bar{\alpha}A - \bar{\lambda}C - \bar{\xi}_{\bar{a}}D - \tfrac{3}{4}\eta(CD^2 + C^3) \end{aligned}\right\} \tag{E.6}$$

[2]The shorthand notation in Table E.1 applies to this appendix only; some of these symbols are defined differently elsewhere in the thesis.

compose the elements of the vector $\mathbf{P}$.

Some representative frequency response results are given next, and we briefly point out their reduced accuracy.

E.4 Forced Response of the Undamped System

For the purpose of comparison we consider the forced response of the undamped averaged model corresponding to the isolated nonlinear system, that is, Equation (E.3) with $\bar{\xi}_{\bar{a}} = \bar{\xi}_b = 0$. Figure E.1 summarizes the results in terms of the speed detuning parameter Δ (which is related to the dimensionless rotor speed σ via Equation (E.1b)), for several order detuning values β, and for a hardening absorber path; a representative set of softening frequency response curves is shown in Figure E.2. In these figures, the nonlinear frequency response loci are indicated by thick solid (stable) and dashed (unstable) lines and the corresponding linear frequency response is given by the thin gray line. The simulation data from Chapter 5 is superimposed in Figure E.2, which corresponds to the full nonlinear model, i.e., Equation (3.14) together with the generalized absorber path described in Section 3.4.4, with representative damping levels $\xi_b = 2 \times 10^{-3}$ and $\xi_{\bar{a}} = 2 \times 10^{-6}$.

For large under- or overtuning values β the approximate averaged results given above are, in fact, quite satisfactory. This is clear from the hardening (resp. softening) frequency response curves shown in Figure E.1a-b (resp. E.2a-b) and Figure E.1e-g (resp. E.1e-g), which correspond to absorber detuning values *outside* the no-resonance zone. In these regions, the averaged model captures the essence of the linearized resonance $\mathcal{R}^{\mathrm{L}}$ in addition to the first-order nonlinear effects of the absorber, which are manifested in the additional auxiliary resonance $\mathcal{R}_{\mathrm{a}}^{\mathrm{NL}}$ and the hardening/softening bends in the primary resonance $\mathcal{R}_{\mathrm{p}}^{\mathrm{NL}}$.[3]

[3]The linearized, nonlinear auxiliary, and nonlinear primary resonances $\mathcal{R}^{\mathrm{L}}$, $\mathcal{R}_{\mathrm{a}}^{\mathrm{NL}}$, $\mathcal{R}_{\mathrm{p}}^{\mathrm{NL}}$ are discussed more fully in Section 5.4.

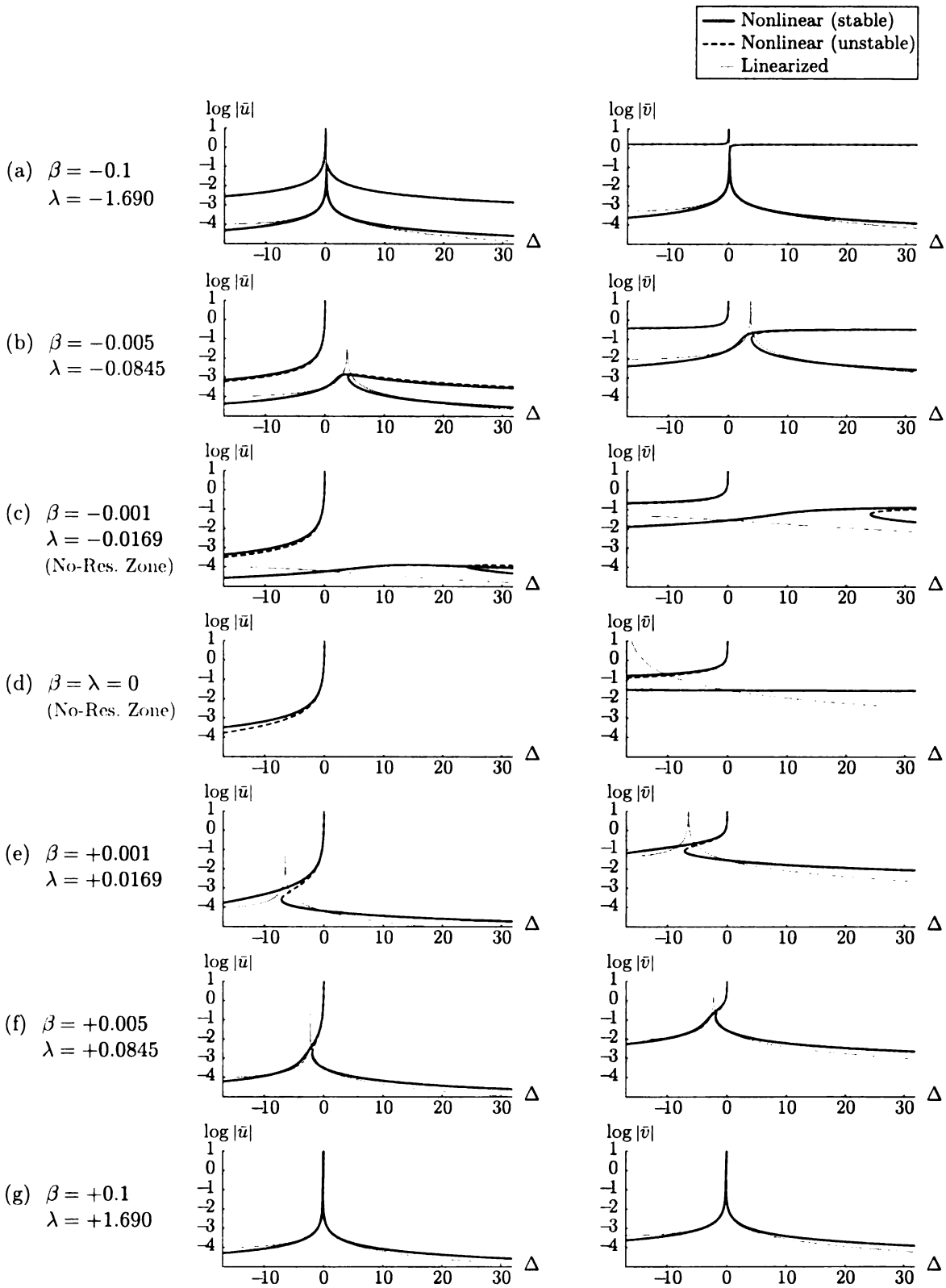

Figure E.1. Blade and absorber frequency response curves for the same conditions in Figure 5.4 on page 143 (*hardening* absorber path) based on the less accurate model defined by Equation (E.3).

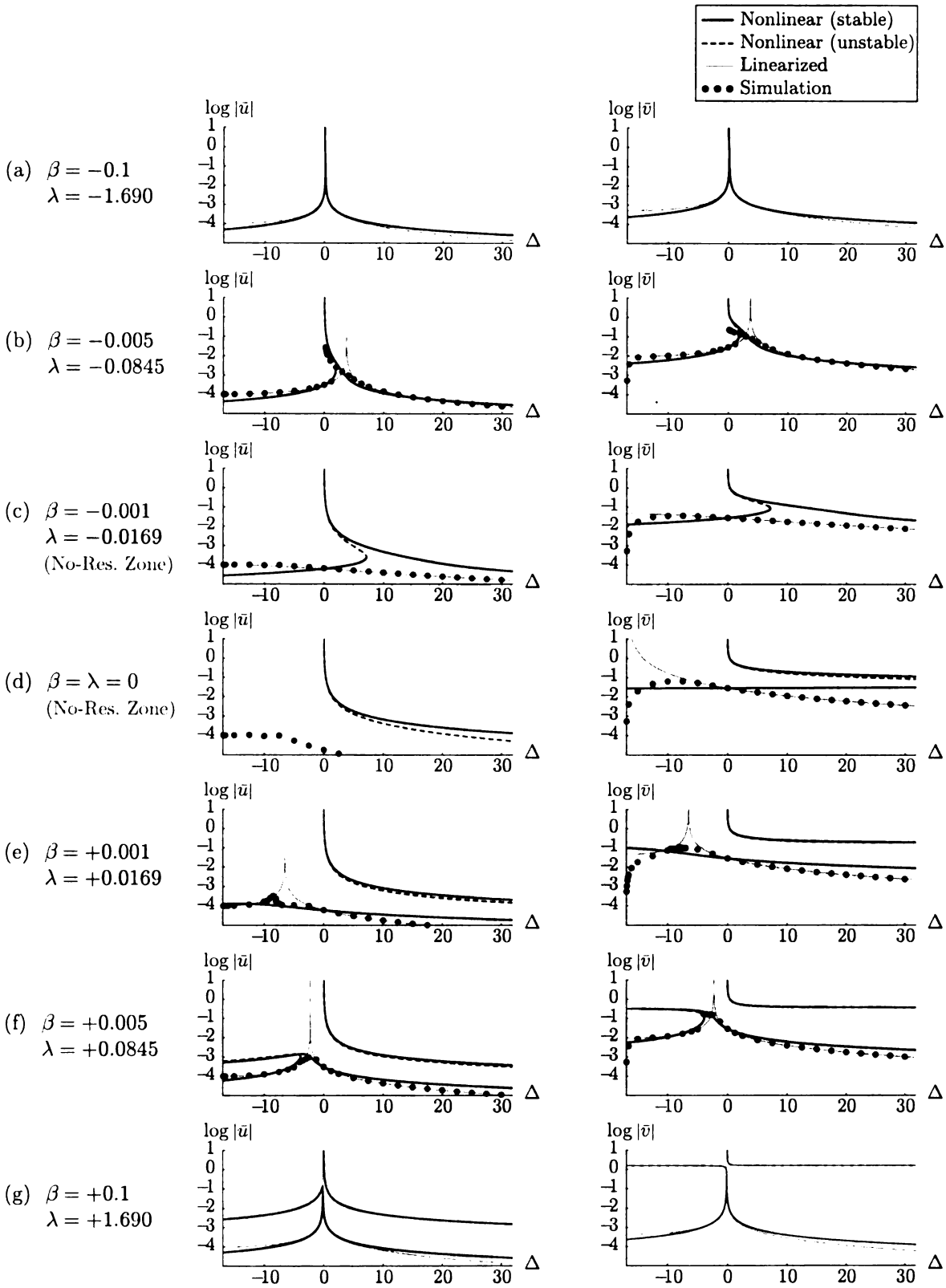

Figure E.2. Blade and absorber frequency response curves for the same conditions in Figure 5.5 on page 144 (*softening* absorber path) based on the less accurate model defined by Equation (E.3).

In contrast, for order detunings $\beta_{cr} \leq \beta < 0$ *inside* the no-resonance-zone the results are poor at best or completely erroneous. This is shown in Figure E.1c-d (resp. E.2c-d) for a hardening (resp. softening) absorber path. For example, in Figure E.2c the linear theory predicts no resonances over the full range of rotor speeds, and this is verified by the simulation data, yet the nonlinear theory gives rise to a primary resonance. As another example, the nonlinear auxiliary resonance in Figure E.2d is expected, as it also appears in the improved model employed in Chapter 5 (compare with Figure 5.5d and Figure 5.6d), but the nonlinear theory does not adequately capture the linear branch of absorber motions.

Since the no-resonance zone is where the results are of the most interest, and since that is precisely where they are *least* accurate (or completely erroneous), the averaged model described above is not at all satisfactory.

BIBLIOGRAPHY

[1] D. E. Knuth, *Computers & Typesetting*, vol. A: The TEXbook. Boston: Addison-Wesley, 1986.

[2] L. Lamport, *LaTeX A Document Preparation System.* Reading: Addison-Wesley, 2 ed., 1994.

[3] R. Bladh, C. Pierre, M. P. Castanier, and M. J. Kruse, "Dynamic Response Predictions for a Mistuned Industrial Turbomachinery Rotor Using Reduced-Order Modeling," *Journal of Engineering for Gas Turbines and Power*, vol. 124, no. 2, pp. 311–324, 2002.

[4] H. Frahm, "Device for Damping of Bodies." United States Patent No. 989958, 1911.

[5] J. Ormondroyd and J. P. Den Hartog, "The Theory of Dynamic Vibration Absorbers," *Transactions of the ASME*, vol. 50, pp. A9–A22, 1928.

[6] J. P. Den Hartog, *Mechanical Vibrations.* New York: Dover Publications, 1985. (First published in 1934 by McGraw-Hill, Inc., New York).

[7] J. P. Den Hartog, "Tuned Pendulums as Torsional Vibration Eliminators," in *Stephen Timoshenko 60th Anniversary Volume*, pp. 17–26, New York: The Macmillan Company, 1938.

[8] D. E. Bently, *Fundamentals of Rotating Machinery Diagnostics.* ASME, 2003.

[9] D. J. Ewins, "Vibration Characteristics of Bladed Disc Assemblies," *Journal of Mechanical Engineering Science*, vol. 15, no. 3, pp. 165–186, 1973.

[10] W. Ker Wilson, *Practical Solutions of Torsional Vibration Problems*, vol. IV, ch. XXX. London: Champman and Hall Ltd, 3rd ed., 1968.

[11] M. Wachs, "The Main Rotor Bifilar Absorber and its Effect on Helicopter Reliability/Maintainability," *SAE Technical Paper Series 730894*, 1973.

[12] M. Cook, "Absolute Absorbtion," *Car Craft Magazine*, p. 75, August 1994.

[13] T. M. Nester, A. G. Haddow, S. W. Shaw, J. E. Brevick, and V. J. Borowski., "Vibration Reduction in Variable Displacement Engines Using Pendulum Absorbers," in *Proceedings of the SAE Noise and Vibration Conference and Exhibition*, no. 2003-01-1484, (Traverse City, Michigan), 2003.

[14] A. S. Alsuwaiyan and S. W. Shaw, "Performance and Dynamic Stability of General-Path Centrifugal Pendulum Vibration Absorbers," *Journal of Sound and Vibration*, vol. 252, no. 5, pp. 791–815, 2002.

[15] D. E. Newland, "Nonlinear Aspects of the Performance of Centrifugal Pendulum Vibration Absorbers," *Journal of Engineering for Industry*, vol. 86, pp. 257–263, 1964.

[16] J. F. Madden, "Constant Frequency Bifilar Vibration Absorber." United States Patent No. 4218187.

[17] H. H. Denman, "Tautochronic Bifilar Pendulum Torsion Absorbers for Reciprocating Engines," *Journal of Sound and Vibration*, vol. 159, no. 2, pp. 251–277, 1992.

[18] C. T. Lee and S. W. Shaw, "On the Counteraction of Periodic Torques in Rotating Systems Using Centrifugally Driven Vibration Absorbers," *Journal of Sound and Vibration*, vol. 191, no. 5, pp. 695–719, 1996.

[19] C. T. Lee, S. W. Shaw, and V. T. Coppola, "A Subharmonic Vibration Absorber for Rotating Machinery," *Journal of Vibration and Acoustics*, vol. 119, pp. 590–595, 1997.

[20] C. T. Lee and S. W. Shaw, "The Nonlinear Dynamic Response of Paired Centrifugal Pendulum Vibration Absorbers," *Journal of Sound and Vibration*, vol. 203, no. 5, pp. 731–743, 1997.

[21] C. P. Chao and S. W. Shaw, "The Effects of Imperfections on the Performance of the Subharmonic Vibration Absorber System," *Journal of Sound and Vibration*, vol. 115, no. 5, pp. 1065–1099, 1998.

[22] C. P. Chao, S. W. Shaw, and C. T. Lee, "Stability of the Unison Response for a Rotating System with Multiple Tautochronic Pendulum Vibration Absorbers," *Journal of Applied Mechanics*, vol. 64, pp. 149–156, 1997.

[23] C. P. Chao, C. T. Lee, and S. W. Shaw, "Non-Unison Dynamics of Multiple Centrifugal Pendulum Vibration Absorbers," *Journal of Sound and Vibration*, vol. 204, no. 5, pp. 769–794, 1997.

[24] A. Alsuwaiyan and S. W. Shaw, "Steady-State Synchronous and Localized Responses of Tuned Pendulum Vibration Absorbers," in *Proceedings-ASME Design Engineering Technical Conferences*, no. DETC99/VIB-8014, (Las Vegas, Nevada), 1999.

[25] C. P. Chao and S. W. Shaw, "The Dynamic Response of Multiple Pairs of Subharmonic Pendulum Vibration Absorbers," *Journal of Sound and Vibration*, vol. 231, no. 2, pp. 411–431, 2000.

[26] A. S. Alsuwaiyan and S. W. Shaw, "Localization of Free Vibration Modes in Systems of Nearly-Identical Vibration Absorbers," *Journal of Sound and Vibration*, vol. 228, no. 3, pp. 703–711, 1999.

[27] A. S. Alsuwaiyan and S. W. Shaw, "Steady-State Response of Systems of Nearly-Identical Torsional Vibration Absorbers," *Journal of Vibration and Acoustics*, vol. 125, no. 1, pp. 80–87, 2003.

[28] A. G. Haddow and S. W. Shaw, "Centrifugal Pendulum Vibration Absorbers: An Experimental and Theoretical Investigation," *Nonlinear Dynamics*, vol. 34, pp. 293–307, 2003.

[29] T. Nester, "Experimental Investigation of Circular Path Centrifugal Pendulum Vibration Absorbers," M.S. thesis, Michigan State University, East Lansing, MI, 2002.

[30] P. M. Schmitz, "Experimental Investigation into Epicycloidal Centrifugal Pendulum Vibration Absorbers," M.S. thesis, Michigan State University, East Lansing, MI, 2003.

[31] T. Nester, A. G. Haddow, and S. W. Shaw, "Experimental Investigation of a System with Nearly Identical Centrifugal Pendulum Vibration Absorbers," in *Proceedings of the ASME 19th Biennial Conference on Mechanical Vibration and Noise*, (Chicago, Illinois), 2003.

[32] K. P. Duffy, R. L. Bagley, and O. Mehmed, "On a Self-Tuning Impact Vibration Damper for Rotating Turbomachinery," in *36th AIAA/ASME/SAE/ASEE Joint Propulsion Conference and Exhibit*, no. AIAA-2000-3100, (Huntsville, Alabama), 2000.

[33] K. Duffy, O. Mehmed, and D. Johnson, "Self-Tuning Impact Dampers for Fan and Turbine Blades," in *Proceedings of the 6th National Turbine Engine High Cycle Fatigue (HCF) Conference*, (Wright-Patterson AFB, Ohio), 2001.

[34] S. W. Shaw and C. Pierre, "The Dynamic Response of Tuned Impact Absorbers for Rotating Flexible Structures," *Journal of Computational and Nonlinear Dynamics*, vol. 1, pp. 13–24, 2006.

[35] R. Kielb, F. Macri, D. Oeth, A. Nashif, P. Macioce, H. Panossian, and F. Lieghley, "Advanced Damping Systems for Fan and Compressor Blisks," in *Proceedings of the 34th AIAA/ASME/SAE/ASEE Joint Propulsion Conference and Exhibit*, no. AIAA Paper 98-35599, (Cleveland, Ohio), 1998.

[36] G. S. Óttarsson, *Dynamic Modeling and Vibration Analysis of Mistuned Bladed Disks.* Ph.D. dissertation, University of Michigan, Ann Arbor, MI, 1994.

[37] P. W. Anderson, "Absence of Diffusion in Certain Random Lattices," *Physical Review*, vol. 109, no. 5, pp. 1492–1505, 1958.

[38] C. H. Hodges, "Confinement of Vibration by Structural Irregularity," *Journal of Sound and Vibration*, vol. 82, no. 3, pp. 411–424, 1982.

[39] S. T. Wei and C. Pierre, "Localization Phenomena in Mistuned Assemblies with Cyclic Symmetry Part I: Free Vibrations," *Journal of Vibration, Acoustics, Stress, and Reliability in Design*, vol. 110, pp. 429–438, 1988.

[40] S. T. Wei and C. Pierre, "Localization Phenomena in Mistuned Assemblies with Cyclic Symmetry Part II: Forced Vibrations," *Journal of Vibration, Acoustics, Stress, and Reliability in Design*, vol. 110, pp. 439–449, 1988.

[41] D. S. Whitehead, "Effect of Mistuning on the Vibration of Turbomachine Blades Induced by Wakes," *Journal of Mechanical Engineering Science*, vol. 8, no. 1, pp. 15–21, 1966.

[42] D. J. Ewins, "The Effect of Detuning upon the Forced Vibrations of Bladed Disks," *Journal of Sound and Vibration*, vol. 9, no. 1, pp. 65–79, 1969.

[43] R. C. F. Dye and T. A. Henry, "Vibration Amplitudes of Compressor Blades Resulting From Scatter in Blade Natural Frequencies," *Journal of Engineering for Power*, vol. 91, pp. 182–188, 1969.

[44] J. C. MacBain and P. W. Whaley, "Maximum Resonant Response of Mistuned Bladed Disks," *Journal of Vibration, Acoustics, Stress, and Reliability in Design*, vol. 106, no. 2, pp. 218–223, 1984.

[45] D. S. Whitehead, "The Maximum Factor by Which Forced Vibration of Blades Can Increase Due to Mistuning," *Journal of Engineering for Gas Turbines and Power*, vol. 120, no. 1, pp. 115–119, 1998.

[46] D. E. Thomson, "The National Turbine Engine High Cycle Fatigue (HCF) Program," in *Proceedings of the 3rd National Turbine Engine High Cycle Fatigue Conference*, (San Antonio, Texas), 1998.

[47] A. F. Vakakis, "Dynamics of a Nonlinear Periodic Structure with Cyclic Symmetry," *Acta Mechanica*, vol. 95, pp. 197–226, 1992.

[48] S. Samaranayake, A. K. Bajaj, and O. D. I. Nwokah, "Amplitude Modulated Dynamics and Bifurcations in the Resonant Response of a Structure with Cyclic Symmetry," *Acta Mechanica*, vol. 109, pp. 101–125, 1995.

[49] M. E. King and A. F. Vakakis, "A Very Complicated Structure of Resonances in a Nonlinear System with Cyclic Symmetry: Nonlinear Forced Linearization," *Nonlinear Dynamics*, vol. 7, pp. 85–104, 1995.

[50] S. Samaranayake and A. K. Bajaj, "Subharmonic Oscillations in Harmonically Excited Mechanical Systems With Cyclic Symmetry," *Journal of Sound and Vibration*, vol. 206, no. 1, pp. 39–60, 1997.

[51] C. Pierre and S. W. Shaw, "Mode Localization due to Symmetry-Breaking Nonlinearities," *International Journal of Bifurcation and Chaos*, vol. 1, pp. 471–475, 1991.

[52] A. F. Vakakis, T. Nayfeh, and M. King, "A Multiple-Scales Analysis of Nonlinear Localized Modes in a Cyclic Periodic System," *Journal of Applied Mechanics*, vol. 60, pp. 388–397, June 1993.

[53] A. F. Vakakis and C. Cetinkaya, "Mode Localization in a Class of Multi-Degree-of-Freedom Nonlinear Systems with Cyclic Symmetry," *SIAM Journal of Applied Mathematics*, vol. 53, pp. 265–282, 1993.

[54] M. E. King and P. A. Layne, "Dynamics of Nonlinear Cyclic Systems with Structural Irregularity," *Nonlinear Dynamics*, vol. 15, pp. 225–244, 1998.

[55] M. P. Castanier and C. Pierre, "Consideration on the Benefits of Intentional Blade Mistuning for the Forced Response of Turbomachinery Rotors," in *Proceedings of the 1997 ASME International Mechanical Engineering Congress and Exposition*, (Dallas, Texas), pp. 419–425, AD-Vol. 55, American Society of Mechanical Engineers, 1997.

[56] M. P. Castanier and C. Pierre, "Investigation of the Combined Effects of Intentional and Random Mistuning on the Forced Response of Bladed Disks," in *Proceedings of the 34th AIAA/ASME/SAE/ASEE Joint Propulsion Conference and Exhibit*, no. 98-3720, (Cleveland, Ohio), 1998.

[57] B. Shapiro, "Solving for Mistuned Forced Response by Symmetry," *Journal of Propulsion and Power*, vol. 15, no. 2, pp. 310–325, 1999.

[58] M. P. Castanier and C. Pierre, "Using Intentional Mistuning in the Design of Turbomachinery Rotors," *AIAA Journal*, vol. 40, no. 10, pp. 2077–2086, 2002.

[59] M. Hamouda and G. Pierce, "Helicopter Vibration Suppression Using Simple Pendulum Absorbers on the Rotor Blade," *Journal of the American Helicopter Society*, vol. 29, pp. 19–29, 1984.

[60] Y. Wang, C. P. Chao, and S. W. Shaw, "Design of Pendulum Vibration Absorbers for the Attenuation of Transverse Vibrations in Rotating Beams," in *Proceedings of the ASME 17th Biennial Conference on Mechanical Vibration and Noise*, no. DETC97/VIB-4182, (Sacramento, California), 1997.

[61] J. J. Hollkamp, R. L. Bagley, and R. W. Gordon, "A Centrifugal Pendulum Absorber for Rotating, Hollow Engine Blades," *Journal of Sound and Vibration*, vol. 219, no. 3, pp. 539–549, 1999.

[62] P. J. Davis, *Circulant Matrices.* New York: John Wiley & Sons, 2nd ed., 1979.

[63] J. G. Proakis and D. G. Manolakis, *Introduction to Digital Signal Processing.* New York: Macmillan, 1988.

[64] C. S. Williams, *Designing Digital Filters.* Englewood Cliffs: Prentice-Hall, 1986.

[65] L. Meirovitch, *Principles and Techniques of Vibrations.* Upper Saddle River: Prentice Hall, 1997.

[66] S. S. Rao, *Mechanical Vibrations.* Upper Saddle River: Prentice Hall, 4th ed., 2004.

[67] H. Puksand, "Optimum Conditions for Dynamic Vibration Absorbers for Variable Speed Systems with Rotating and Reciprocating Unbalance," vol. 3, pp. 145–152, 1975.

[68] A. Soom and M. S. Lee, "Optimal Design of Linear and Nonlinear Absorbers for Damped Systems," *Journal of Vibration, Acoustics, Stress, and Reliability in Design*, vol. 105, pp. 112–119, 1983.

[69] J. B. Hunt, *Dynamic Vibration Absorbers.* London: Mechanical Engineering Publications, 1979.

[70] A. S. Alsuwaiyan, *Performance Stability and Localization of Systems of Vibration Absorbers.* Ph.D. dissertation, Michigan State University, East Lansing, MI, 1999.

[71] M. Sharif-Bakhtiar and S. W. Shaw, "Effects of Nonlinearities and Damping on the Dynamic Response of a Centrifugal Pendulum Vibration Absorber," *Journal of Vibration and Acoustics*, vol. 114, pp. 305–311, 1992.

[72] M. Sharif-Bakhtiar and S. W. Shaw, "The Dynamic Response of a Centrifugal Pendulum Vibration Absorber with Motion-Limiting Stops," *Journal of Sound and Vibration*, vol. 126, no. 2, pp. 221–235, 1988.

[73] A. G. Haddow and S. W. Shaw, "Torsional Vibration Absorbers: A Testing and Evaluation Apparatus," in *Proceedings of SAE Noise and Vibration Conference*, no. 01NVC1577, 2001.

[74] A. G. Haddow and S. W. Shaw, "An Experimental Study of Torsional Vibration Absorbers," in *Proceedings of the 18th Biennial Conference on Mechanical Vibration and Noise*, no. DET2001/VIB-21754, (Pittsburgh, Pennsylvania), 2001.

[75] T. M. Nester, P. M. Schmitz, A. G. Haddow, and S. W. Shaw, "Experimental Observations of Centrifugal Pendulum Vibration Absorbers," in *10th International Symposium on Transport Phenomena and Dynamics of Rotating Machinery*, no. ISROMAC10-2004-043, (Honolulu, Hawaii), 2004.

[76] K. P. Duffy, "Durability of the Self-Tuning Impact Damper in Rotating Turbine Blades,"

[77] A. Leissa, "Vibrational aspects of rotating turbomachinery blades," *Applied Mechanics Review*, vol. 34, no. 5, pp. 629–635, 1981.

[78] G. Genta, "On the stability of rotating blade arrays," *Journal of Sound and Vibration*, vol. 273, pp. 805–836, 2004.

[79] S. Baik, M. P. Castanier, and C. Pierre, "Mistuning Sensitivity Prediction of Bladed Disks Using Eigenvalue Curve Veerings," in *9th National Turbine Engine High Cycle Fatigue Conference*, (Pinehurst, North Carolina), 2004.

[80] J. A. Kenyon and J. H. Griffin, "Forced Response of Turbine Engine Bladed Disks and Sensitivity to Harmonic Mistuning," *Journal of Engineering for Gas Turbines and Power*, vol. 125, pp. 113–120, 2003.

[81] S. K. Sinha, "Dynamic characteristics of a flexible bladed-rotor with Coulomb damping due to tip-rub," *Journal of Sound and Vibration*, vol. 273, pp. 875–919, 2004.

[82] K. R. V. Kaza and R. E. Kielb, "Effects of structural coupling on mistuned cascade flutter and response," *Journal of Engineering for Gas Turbines and Power*, vol. 106, no. 1, pp. 17–24, 1984.

[83] E. P. Petrov and D. J. Ewins, "Analysis of the Worst Mistuning Patters in Bladed Disk Assemblies," *Journal of Turbomachinery*, vol. 125, pp. 623–631, October 2003.

[84] E. P. Petrov, K. Y. Sanliturk, and D. J. Ewins, "A New Method for Dynamic Analysis of Mistuned Bladed Disks Based on the Exact Relationship Between Tuned and Mistuned Systems," *Journal of Engineering for Gas Turbines and Power*, vol. 124, pp. 586–597, 2002.

[85] R. Bladh, M. P. Castanier, and C. Pierre, "Component-Mode-Based Reduced Order Modeling Techniques for Mistuned Bladed Disks, Part II: Application," *Journal of Engineering for Gas Turbines and Power*, vol. 123, no. 1, pp. 100–108, 2001.

[86] R. Bladh, M. P. Castanier, and C. Pierre, "Component-Mode-Based Reduced Order Modeling Techniques for Mistuned Bladed Disks, Part I: Theoretical Models," *Journal of Engineering for Gas Turbines and Power*, vol. 123, no. 1, pp. 89–99, 2001.

[87] M. P. Castanier, G. Óttarsson, and C. Pierre, "A Reduced Order Modeling Technique for Mistuned Bladed Disks," *Journal of Vibration and Acoustics*, vol. 119, no. 3, pp. 439–447, 1997.

[88] M. T. Yang and J. H. Griffin, "A Reduced-Order Model of Mistuning Using a Subset of Nominal System Modes," *Journal of Engineering for Gas Turbines and Power*, vol. 123, no. 4, pp. 893–900, 2001.

[89] S. H. Lim, R. Bladh, M. P. Castanier, and C. Pierre, "A Compact, Generalized Component Mode Mistuning Representation for Modeling Bladed Disk Vibration," in *Proceedings of the 44th AIAA/ASME/ASCE/AHS Structures, Structural Dynamics, and Materials Conference*, (Norfolk, Virginia), 2003.

[90] B. S. Grewal, *Higher Engineering Mathematics*. Sai Sarak: Khanna Publishers, 36th ed., 2001.

[91] J. Wildheim, "Excitation of Rotating Circumferentially Periodic Structures," *Journal of Sound and Vibration*, vol. 75, no. 3, pp. 397–416, 1981.

[92] L. F. Wagner and J. H. Griffin, "Forced Harmonic Response of Grouped Blade Systems: Part I–Discrete Theory," *Journal of Engineering for Gas Turbines and Power*, vol. 118, pp. 130–136, 1996.

[93] L. F. Wagner and J. H. Griffin, "Forced Harmonic Response of Grouped Blade Systems: Part II–Application," *Journal of Engineering for Gas Turbines and Power*, vol. 118, pp. 137–145, 1996.

[94] D. L. Thomas, "Dynamics of Rotationally Periodic Structures," *International Journal for Numerical Methods in Engineering*, vol. 14, pp. 81–102, 1979.

[95] A. H. Nayfey and D. T. Mook, *Nonlinear Oscillations.* New York: John Wiley & Sons, 1979.

[96] J. Guckenheimer and P. Holmes, *Nonlinear Oscillations, Dynamical Systems, and Bifurcations of Vector Fields*, vol. 42 of *Applied Mathematical Sciences.* Springer-Verlag, 1983.

[97] H. K. Khalil, *Nonlinear Systems.* New Jersey: Prentice Hall, third ed., 2002.

[98] S. W. Shaw, B. J. Olson, and C. Pierre, "Order-Tuned and Impact Vibration Absorbers for Rotating Flexible Structures," in *Proceedings of the 11th International Symposium on Transport Phenomena and Dynamics of Rotating Machinery*, 2006.

[99] J. P. Den Hartog, *Mechanical Vibrations.* New York: McGraw-Hill, 1956.

[100] C. W. Cai, Y. K. Cheung, and H. C. Chan, "Uncoupling of Dynamic Equations for Periodic Structures," *Journal of Sound and Vibration*, vol. 139, no. 2, pp. 253–263, 1990.

[101] C. W. Cai, Y. K. Cheung, and H. C. Chan, "Dynamic Response of Infinite Continuous Beams subjected to a Moving Force—An Exact Method," *Journal of Sound and Vibration*, vol. 123, no. 3, pp. 461–472, 1988.

[102] I. Y. Shen, "Vibration of Rotationally Periodic Structures," *Journal of Sound and Vibration*, vol. 172, no. 4, pp. 459–470, 1994.

[103] D. J. Ewins, "A Study of Resonance Coincidence in Bladed Discs," *Journal of Mechanical Engineering Science*, vol. 12, no. 5, pp. 305–312, 1970.

[104] N. C. Perkins and J. C. D. Mode, "Comments on Curve Veering in Eigenvalue Problems," *Journal of Sound and Vibration*, vol. 106, no. 3, pp. 451–463, 1986.

[105] C. Pierre, "Mode Localization and Eigenvalue Loci Veering Phenomena in Disordered Structures," *Journal of Sound and Vibration*, vol. 126, no. 3, pp. 485–502, 1988.

[106] C. N. Folley, *Bifurcation and Symmetry in Cyclic Structures.* Ph.D. dissertation, Purdue University, 1999.

[107] C. Folley and A. Bajaj, "The Dynamics of a Cyclic Ring of Coupled Duffing Oscillators," in *ASME International Design Engineering Technical Conferences & Computers and Information in Engineering Conference*, 2005.

[108] P. Ashwin and J. W. Swift, "The Dynamics of n Weakly Coupled Identical Oscillators," *Journal of Nonlinear Science*, vol. 2, pp. 69–108, 1992.

[109] S. Wiggins, "Introduction to applied nonlinear dynamical systems and chaos," in *Texts in Applied Mathematics*, Springer, 2cd ed., 2003.

[110] R. McWeeny, "Topic 1: Mathematical Techniques," in *Symmetry: An Introduction to Group Theory and its Applications* (H. Jones, ed.), vol. 3 of *The International Encyclopedia of Physical Chemistry and Chemical Physics*, New York: Macmillan, 1963.

[111] A. Fässler and E. Stiefel, *Group Theoretical Methods and their Applications.* Boston: Birkhäuser, 1992.

[112] B. E. Sagan, "The Symmetric Group: Representations, Combinatorial Algorithms, and Symmetric Functions," vol. 203 of *Graduate Texts in Mathematics*, New York: Springer, 2 ed., 2001.

[113] M. Golubitsky and D. G. Schaeffer, "Singularities and Groups in Bifurcation Theory, Volume I," vol. 51 of *Applied Mathematical Sciences*, New York: Springer-Verlag, 1988.

[114] M. Golubitsky, I. Stewart, and D. G. Schaeffer, "Singularities and Groups in Bifurcation Theory, Volume II," vol. 69 of *Applied Mathematical Sciences*, New York: Springer-Verlag, 1988.

[115] B. Shapiro, *Passive Control of Flutter and Forced Response in Bladed Disks via Mistuning.* Ph.D. dissertation, California Institute of Technology, Pasadena, CA, May 1999.

[116] B. Shapiro, "A Symmetry Approach to Extension of Flutter Boundaries via Mistuning," *Journal of Propulsion and Power*, vol. 14, no. 3, pp. 354–366, 1998.

[117] J. Wildheim, "Vibrations of Rotating Circumferentially Periodic Structures," *Quarterly Journal of Mechanics and Applied Mathematics*, vol. 34, no. 2, pp. 213–229, 1981.

[118] J. W. Brown and R. V. Churchill, *Complex Variables and Applications.* New York: McGraw-Hill, 6th ed., 1996.